Translational Control of Autophagy Rejuvenates Immune Responses



Hanlin Zhang

St Cross College

University of Oxford

Thesis submitted for the degree of

Doctor of Philosophy

Hilary 2018

Abstract

As our body's guardian, the immune system maintains systemic health through removal of pathogens, damage and cancer. Ageing of the immune system is associated with compromised immune responses as well as decreased tumour surveillance and is therefore a key risk factor for major diseases in the elderly. Adaptive immune responses are mediated by T and B lymphocytes, and failure in adaptive immunity is a particular hallmark of the ageing organism. Here we show that autophagy is impaired in aged murine B lymphocytes, and loss of autophagy causes severely reduced B cell responses. Our data demonstrate that B cell senescence can be reversed in an autophagy-dependent manner by spermidine, a naturally occurring polyamine metabolite. Mechanistically, our study reveals that the translation factor eIF5A, that requires spermidine for its activation, regulates the expression of the master autophagy/lysosomal transcription factor TFEB. Importantly, we show in humans that spermidine, eIF5A and TFEB levels decrease with age and may serve as ageing biomarkers. Taken together our results indicate that the translational control of autophagy by eIF5A is dysregulated with ageing, and identify a novel pathway with therapeutic implications.

Declaration

This thesis is submitted to the University of Oxford in support of my application for the degree of Doctor of Philosophy. The work described herein was performed when I was a graduate student at the Weatherall Institute of Molecular Medicine and the Kennedy Institute of Rheumatology, under the supervision of Professor Katja Simon. All the work presented in this thesis is the result of my own work unless otherwise stated. No part of my thesis has been accepted or is currently being submitted for any degree, diploma or certificate or other qualification in the University of Oxford or elsewhere.

Author's Publications

Zhang H, Puleston DJ, Simon AK. 2016. Autophagy and Immune Senescence. *Trends Mol Med* 22: 671-86.

Zhang H, Alsaleh G, Feltham J, Sun Y, Riffelmacher T, Charles P, Frau L, Yu Z, Mohammed S, Balabanov S, Mellor J, Simon AK. Translational control of TFEB and autophagy via eIF5A rejuvenates B cell immunity. *In submission.*

Puleston DJ, **Zhang H**, Powell TJ, Lipina E, Sims S, Panse I, Watson AS, Cerundolo V, Townsend AR, Klenerman P, Simon AK. 2014. Autophagy is a critical regulator of memory CD8(+) T cell formation. *Elife* 3.

Yu Z, **Zhang H**, Huang H, Kessler BM. A simpler method for polyamine analysis by GCXGC-MS. *In submission*.

Acknowledgements

Numerous brilliant minds have been thriving in Oxford since 800 years ago to push human civilization forward. I feel very lucky to have a chance to come here, meet them and follow their footsteps.

The first English book I successfully read from start to finish was called *Who Wants to be a Scientist?* It was a gift from my supervisor Professor Katja Simon in the beginning of my first year of DPhil study. The book introduces a wide range of topics of academic career development, which initiated a thorough DPhil training delivered by Katja. In the following 4 years, Katja set a close example how to be an energetic scientist and an enlightening supervisor. I would like to express my most grateful appreciation to Katja for her valuable encouragement and trust on me by giving me sufficient freedom to chase my own ideas, for those illuminating conversations about the project and science, for her great generosity in supporting me to develop my own career, and for the large amount of time she spent on improving my scientific skills.

I wish to acknowledge my current and previous colleagues for their help in lab. My 4-year DPhil study was accompanied by another gifted student Thomas Riffelmacher, from whom I gained a lot of help and learned a lot. Lisa Frau and Yizhe Sun are hardworking students taking their internships with me. I hope they enjoyed their experience here and the credit goes to them for helping me with my project. I would like to thank Ghada Alsaleh, Daniel Puleston, Alexander Clarke, Sandrine Obba, Isabel Panse, Sharon Sanderson, Ghadeer Almuhaini, Dingxi Zhou, and Felix Richter for their general help and advice.

I am particularly grateful for the guidance given by my thesis committee members and project advisors Dr Consuelo Anzilotti, Dr Alfredo Castello Palomares, Professor Claus Nerlov, and Dr Giorgio Napolitani. Being the

experts in immunology, haematology, and protein translation, they provided valuable suggestions to push my project forward.

Thanks are extended to my lovely friends, who share the memory of these 4 years with me. It is a great pleasure to meet my undergraduate classmates Xijin Xu, Xiao Qin, and Chi Zhang again in the same DPhil program, where we firmly support each other to overcome difficulties and pursue a scientific career. Yiyan Zheng, Yingjie Wang, and Houfu Leng provided me with generous help in experiments and daily life. Genuine thanks also go to Yuan (Oliver) Lui, Ran Li, Jiahe Yang, Peng Hua, Yanchun Peng, Lei Zhang, Lina Guo, Jun Guan, Wei Wu, Linyi Zhu and all other friends for their technical assistance and the enjoyable time we spent together.

This thesis was carefully read and corrected by Professor Xin Lu (internal examiner) and Professor Malene Hansen (external examiner). Their valuable input is greatly appreciated.

I would like to offer my special thanks to my parents and other family members for their unfailing support, inspiration and love throughout my life.

Finally, I wish to thank the professional and efficient facilities of the Weatherall Institute of Molecular Medicine, the Kennedy Institute of Rheumatology, St Cross College, and other facilities in the university. The China Scholarship Council, the Nuffield Department of Medicine, and the Elysium Health are gratefully acknowledged for their generous stipend and fees to support my study in Oxford, and the Wellcome Trust for providing general support.

List of Abbreviations

Abbreviation	Full name
ACS	Antibody secreting cells
ADP	Adenosine diphosphate
AID	Activation-induced cytidine deaminase
AMP	Adenosine monophosphate
AMPK	AMP-activated protein kinase
AP	Alkaline phosphatase
ATF4	Activating transcription factor 4
ATG	Autophagy-related gene
ATP	Adenosine triphosphate
BafA1	Bafilomycin A1
BCR	B-cell receptor
bHLH	Basic helix-loop-helix
C domain	Constant domain
C. elegans	Caenorhabditis elegans
cAMP	Cyclic adenosine monophosphate
Cd40lg	CD40 ligand
CDC	Centers for Disease Control and Prevention
ChIP	Chromatin immunoprecipitation
CHOP	CCAAT-enhancer-binding protein homologous protein
CHX	Cycloheximide

CLEAR	Coordinated lysosomal expression and regulation
CLP	Common lymphoid progenitor
CMV	Cytomegalovirus
COPII	Coat protein complex II
DFCP1	Double FYVE-containing protein 1
DFMO	Difluoromethylornithine
DHS	Deoxyhypusine synthase
DMH	1,2-dimethylhydrazine
DOHH	Deoxyhypusine hydroxylase
DTT	Dithiothreitol
EBV	Epstein-Barr virus
EDTA	Ethylenediaminetetraacetic acid
EF-P	Elongation factor P
eIF2	Eukaryotic initiation factor 2
eIF5A	Eukaryotic translation initiation factor 5A
ELISpot	Enzyme-linked immunoSpot
ER	Endoplasmic reticulum
FASP	Filter aided sample preparation
FDA	Food and Drug Administration
FDC	Follicular dendritic cell
FDR	False discovery rate
FOXO	Forkhead box O protein
FOXP3	Forkhead box P3

GAPDH	Glyceraldehyde 3-phosphate dehydrogenase
GC	Germinal centre
GC-MS	Gas chromatography–mass spectrometry
GC7	N1-guanyl-1,7-diaminoheptane
GFP	Green fluorescent protein
GH	Growth hormone
GMP	Granulocyte-macrophage progenitor
H chain	Heavy chain
H&E	Haemotoxylin and eosin
HAT	Histone acetyltransferase
HDAC6	Histone deacetylase 6
HIV	Human immunodeficiency virus
HSC	Haematopoietic stem cell
IFN	Interferon
IGF-1	Insulin-like growth factor 1
IKK	IκB kinase
IL	Interleukin
ip	Intraperitoneal
IP	Immunoprecipitation
IRGM1	Immunity-related GTPase family M protein 1
IκB	Inhibitor of κB
L chain	Light chain
LAMP2A	Lysosome-associated membrane protein type 2a

LC3 (MAP1LC3)	Microtubule-associated proteins 1A/1B light chain 3B
LCMV	Lymphocytic choriomeningitis virus
LMPP	Lymphoid-biased multipotent progenitor cell
LPS	Lipopolysaccharide
LSK	$Lineage^{-}Sca1^{+}cKit^{+}$ cells
MHC	Major histocompatibility complex
MiT	Microphthalmia transcription factor
MITF	Microphthalmia-associated transcription factor
MkP	Megakaryocyte progenitor
MMWR	Morbidity and mortality weekly report
MPP	Multipotent progenitor cell
MS	mass spectrometry
mTORC1	Mammalian target of rapamycin complex 1/Mechanistic target of rapamycin complex 1
NAC	N-acetylcysteine
NAD	Nicotinamide adenine dinucleotide
NBR1	Next to BRCA1 gene 1 protein
NCOA4	Nuclear receptor coactivator 4
NDP52	Nuclear dot protein 52
NF-κB	Nuclear factor kappa-light-chain-enhancer of activated B cells
NLS	Nuclear localization signal
NOD	Nucleotide-binding oligomerization domain

NP-CGG	4-Hydroxy-3-nitrophenylacetyl-Chicken gamma globulin
NP-KLH	4-Hydroxy-3-nitrophenylacetyl-Keyhole limpet hemocyanin
Nrf	Nuclear respiratory factor
ODC	Ornithine decarboxylase
OPP	O-propargyl-puromycin
OPTN	Optineurin
PAMP	Pathogen-associated molecular pattern
PBMC	Peripheral blood mononuclear cell
PDE	Phosphodiesterases
PE	Phosphatidylethanolamine
PERK	Protein kinase R (PKR)-like endoplasmic reticulum kinase
PFA	Paraformaldehyde
PGC-1α	Peroxisome proliferator-activated receptor gamma coactivator 1-alpha
PHA	Phytohaemagglutinin
PI3K	Phosphatidylinositol 3-kinase
PI3P	Phosphatidylinositol 3-phosphate
PIK3C3	Phosphatidylinositol 3-kinase catalytic subunit type 3
PINK1	PTEN-induced putative kinase 1
Poly IC	Polyinosinic-polycytidylic acid
PPI (II) helix	Polyproline I (II) helix
PPL	Procedure Project Licence

Pre-B cell	Precursor B cell
Pre-GM	Pre-granulocyte/macrophage
Pre-MegE	Pre-megakaryocytes/erythrocyte
Pre-pro-B cell	Germline progenitor B cell
Pro (P)	Proline
Pro-B cell	Progenitor B cell
Pro-Ery	Pro-erythroblast cell
PSM	Peptide-spectrum matches
PTD	Protein transduction domain
PTEN	Phosphatase and tensin homolog
RBC	Red blood cell
ROS	Reactive oxygen species
SAM3	S-adenosylmethionine metabolism protein 3
DUR3	Urea active transporter
SASP	Senescence-associated secretory phenotype
SEM	Standard error of the mean
Ser (S)	Serine
SHM	Somatic hypermutation
SILAC	Stable isotope labeling with amino acids in cell culture
Sir2	Silent information regulator 2/NAD-dependent histone deacetylase SIR2
SIRT1	SIR2-like protein 1/NAD-dependent protein deacetylase sirtuin-1

SL chain	Surrogate light chain
SNAP29	Synaptosomal-associated protein 29
SOD2	Superoxide dismutase 2
Spd	Spermidine
SQSTM1 (p62)	Sequestosome-1
TBC1D17	TBC1 domain family member 17
TCEP	Tris (2-carboxyethyl) phosphine
TCR	T-cell receptor
TEAB	Triethylammonium bicarbonate buffer
TFE3	Transcription factor E3
TFEB	Transcription factor EB
TFEC	Transcription factor EC
T_{FH}	Follicular helper T cell
Th1	Type 1 T helper
Th17	T helper 17
Th2	Type 2 T helper
Thr (T)	Threonine
TIV	Trivalent inactivated influenza vaccine
TLR	Toll-like receptor
TNF	Tumor necrosis factor
Treg	Regulatory T cell
TSC	Tuberous sclerosis protein
UHPLC	Ultra-high performance liquid chromatography

ULK	Unc-51-like kinase
uORF	Upstream open reading frame
V domain	Variable domain
Val (V)	Valine
Vps34	Vacuolar protein sorting-associated protein 34
WIPI2	WD repeat domain phosphoinositide-interacting protein 2
Zip	Leucine zipper

Contents

Abstract I

Declaration II

Author's Publications III

Acknowledgements IV

List of Abbreviations VI

List of Figures XIX

Chapter 1. General Introduction: 1

Autophagy and Adaptive Immune Senescence 1

1.1 Autophagy and autophagy signaling pathways 2

1.1.1 Autophagy process 2

1.1.2 Autophagy cargo specificity 5

1.1.3 Autophagy signaling pathways 5

1.1.3.1 Insulin/IGF-1-mTOR signaling pathway 7

1.1.3.2 AMPK signaling pathway 7

1.1.3.3 SIRT1 8

1.1.3.4 Innate immune signals 8

1.1.4 Age-related changes/manipulations of autophagy signaling pathways 9

1.1.4.1 Insulin/IGF-1 9

1.1.4.2 mTORC1 10

1.1.4.3 AMPK 10

1.1.4.4 FOXOs 11

1.1.4.5 SIRT1 11

1.1.4.6 Inflammageing 12

1.1.4.7 Lysosome 13

1.2 Autophagy controls cellular senescence 14

1.2.1 Mitochondria and ROS 14

1.2.2 Genome stability 16

1.2.3 Proteostasis 17

1.2.4 Inflammation 19

1.3 Adaptive immune senescence 20

1.3.1 T cells 23

1.3.1.1 Reduced TCR repertoire diversity during ageing 23

1.3.1.2 Functional changes with age 24
1.3.1.3 Autophagy controls T cell development and functions 26
1.3.1.4 Autophagy and T cell senescence 27
1.3.2 B cells 28
1.3.2.1 Reduced BCR repertoire diversity during ageing 28
1.3.2.2 Compromised humoral responses with age 29
1.3.2.3 Autophagy controls B cell responses 30
1.3.2.4 B-1 B cells 31
1.4 Spermidine as an autophagy inducer 32
1.5 Thesis summary 33
Chapter 2. Materials and Methods 35
2.1 Mice 36
2.1.1 Strains 36
2.1.2 Drug administration 36
2.1.3 Tissue and serum processing 36
2.1.4 Bone marrow chimera 37
2.2 Cell culture and drug treatments 38
2.3 List of antibodies 39
2.4 Flow cytometry (FACS) 44
2.4.1 Surface marker staining and analysis 44
2.4.2 LC3-II FACS staining 45
2.4.3 CytoID staining 45
2.4.4 OPP-Click Assay 45
2.5 Western blot 46
2.6 Immunoprecipitation 48
2.7 Quantitative PCR 49
2.8 siRNA transfection 50
2.9 HAT activity assays 50
2.10 NP-CGG immunization and analysis 51
2.10.1 Immunization 51
2.10.2 NP-IgM/IgG1 ELISA 51
2.10.3 NP-IgG1 ELISpot 53
2.11 Mouse B cell purification and stimulation 53
2.12 Confocal microscopy 54
2.13 Cell fractionation 54
2.14 Proteomics mass spectrometry 55

2.15 Spermidine measurement by gas chromatography mass spectrometry (GC-MS) ... **58**
2.16 Ribosome profiling ... **58**
2.17 Human samples ... **60**
2.18 Statistical analyses ... **61**
Chapter 3. The Autophagy Inducer Spermidine Rejuvenates Humoral Immunity in Aged Mice ... **63**
3.1 Introduction ... **63**
3.1.1 Murine B cell development ... 64
3.1.2 B cell activation ... 66
3.2 Results ... **70**
3.2.1 Phenotypic changes of the haematopoiesis in old mice ... 71
3.2.2 Bone marrow cells from old mice reconstitute well into recipients ... 80
3.2.3 Autophagy is impaired in lymphocytes from old mice ... 87
3.2.4 Autophagic flux is blocked in B cells from old mice ... 89
3.2.5 Spermidine improves the humoral responses in old mice ... 92
3.2.6 Spermidine improves the humoral responses in an autophagy-dependent manner ... 96
3.2.7 Spermidine does not improve humoral responses in young mice ... 99
3.3 Discussion ... **100**
3.3.1 Can we target HSCs to improve haematopoiesis/immunity in old individuals? ... 101
3.3.2 How does autophagy modulation contribute to the aged haematopoietic system? ... 103
3.3.3 Does spermidine improve humoral responses in old mice via autophagy? ... 105
3.3.4 Potential side effects of spermidine ... 107
3.3.5 Conclusions ... 108
Chapter 4. Spermidine Regulates Autophagy via eIF5A Hypusination ... **110**
4.1 Introduction ... **110**
4.1.1 Molecular functions of spermidine ... 111
4.1.2 Hypusination of eIF5A and its molecular functions ... 112
4.1.3 Cellular functions of polyamines and eIF5A ... 114
4.1.4 Physiological functions of polyamines and eIF5A ... 115
4.2. Results ... **117**
4.2.1 Spermidine is required for autophagy ... **118**

4.2.2 Spermidine does not inhibit HAT activity in Jurkat cells 122
4.2.3 High dose spermidine induces ER stress in Jurkat cells 127
4.2.4 Hypusinated eIF5A is required for autophagy 129
4.2.5 Autophagy and the expression of eIF5A are induced during primary B cell activation 133
4.2.6 Hypusinated eIF5A is required for autophagy in primary B cells 133
4.2.7 Hypusinated eIF5A is required for optimal protein synthesis 136
4.2.8 Hypusinated eIF5A is required for translation initiation and termination in primary B cells 138
4.2.9 Polyproline causes translation stalls in primary B cells 138
4.3 Discussion 141
4.3.1 Can we induce eIF5A hypusination? 142
4.3.2 Why is PPP stalling reduced upon GC7 treatment in primary B cells? 143
4.3.3 Conclusions 144
Chapter 5. eIF5A Controls TFEB Expression 146
5.1 Introduction 146
5.1.1 MiT transcription factors 147
5.1.2 TFEB is a key autophagy/lysosome transcription factor 147
5.1.3 Molecular mechanisms of TFEB activation 149
5.1.4 TFEB functions *in vivo* 150
5.1.4.1 TFEB knockout is embryonic lethal 150
5.1.4.2 TFEB in liver 151
5.1.4.3 TFEB in muscle 151
5.1.4.4 TFEB in immune cells 152
5.1.4.5 TFEB in ageing 152
5.2 Results 154
5.2.1 Identify the targets of eIF5A using protein mass spectrometry 155
5.2.2 eIF5A controls the expression of TFEB 157
5.2.3 GC7 promotes the decay of *Tfeb* mRNA 162
5.2.4 Reduced expression of TFEB in mice during ageing 169
5.2.5 The spermidine-eIF5A-TFEB pathway is affected in old people 169
5.3 Discussion 173
5.3.1 Why does mammalian TFEB require polyproline motifs? 174
5.3.2 How can we improve TFEB functions during ageing? 176
5.3.3 Conclusions 177
Chapter 6. General Discussion 179

6.1 Changes of protein translation during ageing 180
6.2 The potential regulatory role of proline in protein translation 182
6.3 Protein translation and autophagy are coordinated with each other 185
6.4 Therapeutic prospects 186
6.5 Thesis summary 189

Bibliography 193

List of Figures

Chapter 1. General Introduction 1

Fig1.1 The core autophagy machinery. 4

Fig 1.2 Autophagy signaling pathways and their changes with age. 6

Fig 1.3 Autophagy protects cells from senescence. 18

Fig 1.4 Schematic overview of the mammalian haematopoiesis. 21

Fig 1.5 Schematic overview of the polyamine synthesis pathway. 32

Chapter 2. Materials and Methods 35

Chapter 3. The Autophagy Inducer Spermidine Rejuvenates Humoral Immunity in Aged Mice 63

Fig 3.1 Schematic overview of B cell development. 65

Fig 3.2 Schematic overview of T-dependent B cell activation, focusing on germinal centre reactions. 67

Fig 3.3 Expanded HSCs in bone marrow from old mice. 72

Fig 3.4 Expanded myeloid progenitors in bone marrow from old mice. 74

Fig 3.5 Accumulated B cell progenitors in bone marrow from old mice. 75

Fig 3.6 Spleen lineages are myeloid-biased in old mice. 77

Fig 3.7 Peripheral blood lineages are myeloid-biased in old mice. 78

Fig 3.8 $CD44^{hi}$ memory-like T cells are accumulated in old mice. 78

Fig 3.9 Bone marrow and spleen cellularity in young, old, and old mice administered with spermidine. 79

Fig 3.10 Use competitive bone marrow chimera to assess HSCs reconstitution ability. 80

Fig 3.11 Old bone marrow cells have a higher reconstitution ability of HSCs. 81

Fig 3.12 Comparable reconstitution ability of myeloid progenitors between young and old bone marrow. 83

Fig 3.13 Comparable reconstitution ability of T cell progenitors between young and old bone marrow 84

Fig 3.14 Comparable reconstitution ability of B cell progenitors between young and old bone marrow. 86

Fig 3.15 Autophagic flux is significantly reduced in lymphocytes from old mice, and spermidine increases autophagic flux *in vivo*. 88

Fig 3.16 Purity check of magnetic-activated cell sorting (MACS) of murine B cells. 90

Fig 3.17 Autophagy is impaired at the lysosomal degradation level in B cells from old mice, which is ameliorated by spermidine administration. 91
Fig 3.18 Spermidine improves humoral responses in old mice. 93
Fig 3.19 Spermidine increases the number of long-term NP-IgG1-secreting cells in old mice. 95
Fig 3.20 Reduced autophagy in Atg7-/- B cells. 97
Fig 3.21 Spermidine fails to improve the humoral responses in B cell-specific autophagy-deficient mice. 98
Fig 3.22 Spermidine does not improve humoral responses in young mice. 99

Chapter 4. Spermidine Regulates Autophagy via eIF5A Hypusination 110

Fig 4.1 Schematic overview of the polyamine synthesis and the eIF5A hypusination pathway. 112
Fig 4.2 Schematic overview of the tri-proline structure. 113
Fig 4.3 Spermidine induces autophagy. 119
Fig 4.4 Spermidine does not affect mTOR and AMPK activity. 121
Fig 4.5 Spermidine is required for autophagy. 121
Fig 4.6 Selected autophagy gene expression changes caused by spermidine treatment. 123
Fig 4.7 Spermidine does not reduce the acetylation of H3 or ATG7. 124
Fig 4.8 Spermidine does not inhibit HAT activity. 126
Fig 4.9 High-dose spermidine induces ER stress. 128
Fig 4.10 Spermidine is required for the hypusination of eIF5A. 129
Fig 4.11 eIF5A is required for autophagy. 130
Fig 4.12 Hypusination of eIF5A is required for autophagy. 132
Fig 4.13 Autophagy and the expression of hypusinated eIF5A are induced during primary B cell activation. 134
Fig 4.14 eIF5A hypusination is required for autophagy in B cells. 135
Fig 4.15 Hypusinated eIF5A regulates autophagy in an mTOR-independent manner. 136
Fig 4.16 Hypusinated eIF5A is required for optimal protein synthesis. 137
Fig 4.17 Hypusinated eIF5A controls translation initiation and termination. 139
Fig 4.18 Polyproline stalls translation. 140

Chapter 5. eIF5A Controls TFEB Expression 146

Fig 5.1 Human TFEB protein structure. 149
Fig 5.2 GC7 does not affect the expression of the chosen polyproline-containing autophagy proteins. 155

Fig 5.3 Label-free quantitative protein MS to identify autophagy proteins regulated by eIF5A. 158
Fig 5.4 SILAC protein MS to identify autophagy proteins regulated by eIF5A. 159
Fig 5.5 eIF5A controls the expression of TFEB. 160
Fig 5.6 Nuclear TFEB is reduced by GC7 treatment. 160
Fig 5.7 The expression of TFEB target genes is reduced by GC7 treatment. 161
Fig 5.8 TFEB protein sequence alignment across species. 164
Fig 5.9 Ribosome occupancy of *Tfeb* mRNA. 165
Fig 5.10 *Tfeb* mRNA has a short half life of less than 2 hours. 166
Fig 5.11 GC7 induces the decay of *Tfeb* mRNA. 168
Fig 5.12 Reduced TFEB expression in B cells from old mice. 169
Fig 5.13 Reduced expression of TFEB and eIF5A in PBMCs from old people. 171
Fig 5.14 Spermidine levels in human PBMCs are reduced with age. 172

Chapter 6. General Discussion ..... Error! Bookmark not defined.

Fig 6.1 Proposed model for the potential regulatory role of proline in protein synthesis and cell growth. 184
Fig 6.2 Proposed working model of a novel autophagy signaling pathway and its involvement in ageing. 191

Chapter 1. General Introduction:

Autophagy and Adaptive Immune Senescence

1.1 Autophagy and autophagy signaling pathways

Autophagy is a highly conserved homeostatic cellular process in which cells degrade their own components through lysosomal degradation. There are three types of autophagy identified in eukaryotic cells: macroautophagy, microautophagy, and chaperone-mediated autophagy (higher eukaryotes). Macroautophagy involves the formation of a double-membrane structure called autophagosome, which carries bulk cellular materials to the lysosome for degradation. Microautophagy is mediated by the direct invagination or membrane extension of vacuoles like lysosome and endosome (3-5). Chaperone-mediated autophagy relies on chaperones to recognize specific protein substrates, and then unfolds and translocates them into the lysosome (6-8). Macroautophagy is the most thoroughly studied type of autophagy, and autophagy hereafter used in this review all refers to macroautophagy.

1.1.1 Autophagy process

The basic autophagy process is well characterized in eukaryotic cells (Fig 1.1) (9). Upon autophagy induction, the activated ULK protein kinase complex forms in proximal to ER, mitochondria or other membrane structures (10-12), initiating the formation of the autophagosome. Class III PI3-kinase complex is then recruited by the ULK complex and produces the autophagosomal membrane-specific lipid phosphatidylinositol 3-phosphate (PI3P). PI3P-enriched membranes are Ω-like, therefore termed omegasome (13). Omegasome is the platform where the isolation membrane (autophagophore) expands to engulf cytoplasmic materials including organelles and soluble

components (14). Enrichment of PI3P on omegasomes facilitates the recruitment of PI3P-binding proteins such as DFCP1 that may carry ER and Golgi membranes for autophagosomal membranes expansion (13), and WIPI2 that interacts with the ATG12-ATG5-ATG16L complex for the phagophore membrane expansion (15). Moreover, according to a proteomic analysis, Atg1 kinase complex (yeast homolog of ULK) and PI3-kinase complexes also direct interacts with COPII transport vesicles, guiding ER vesicles to fuse with autophagophore membranes (16).

The autophagophore expansion is also associated with two ubiquitin-like reactions, ATG12-ATG5-ATG16L and LC3-phosphatidylethanolamine (LC3-PE) (Fig 1.1). ATG12 is activated by ATG7 (E1-like) and then transferred to ATG5 by ATG10 (E2-like). ATG12-ATG5 forms a complex with ATG16L later. LC3 is activated by ATG7 (E1-like) and conjugated to PE by ATG3 (E2 like). The ATG12-ATG5-ATG16L complex functions as an E3-like ligase to carry PE for LC3 lipidation (17, 18). Although the lipidated form of LC3 (LC3-PE, or LC3-II) is not essential for the formation of autophagosomes (19), it controls cargo specificity via interacting with multiple adaptors such as p62, NBR1, NDP52, and NCOA4 (20).

Eventually, the elongated membrane closes to form mature autophagosome and fuse with the lysosome for degradation.

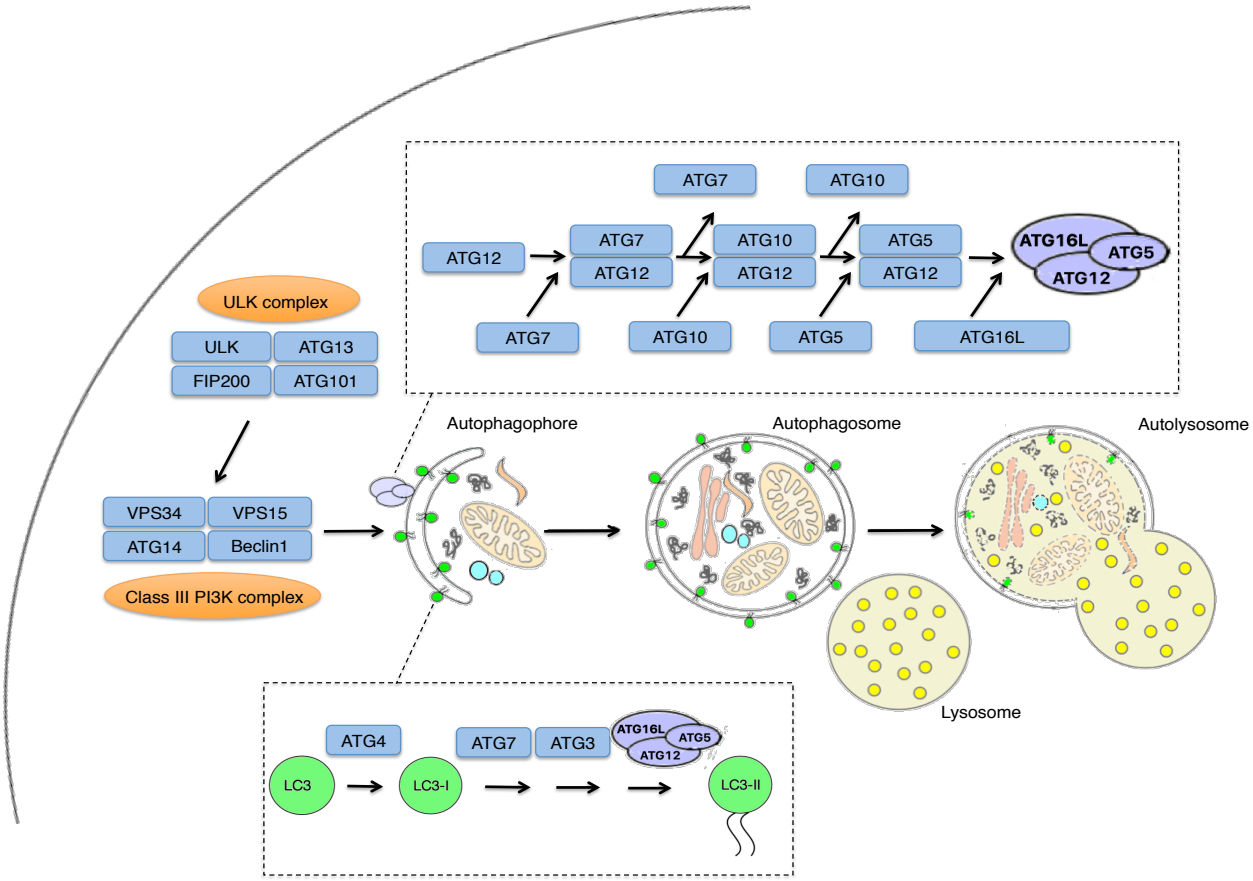


Fig 1.1 The core autophagy machinery. Upon starvation or other autophagy-inducing signals, the ULK complex is activated to recruit and stimulate the class III PI3K complex, which then initiates the formation of autophagophores. The elongation of autophagophores involves two ubiquitin-like reactions for the formation of the ATG12-ATG5-ATG16L complex and the lipidated LC3-II (LC3-PE). Autophagophores close to form autophagosomes, which eventually fuse with lysosomes for cargo degradation.

1.1.2 Autophagy cargo specificity

Starvation-induced bulk autophagy degradation is thought to be a non-selective process in which autophagosomes engulf bulk cytoplasmic components for degradation and nutrient supply. Meanwhile, damaged or surplus organelles, protein aggregates, and invading intracellular pathogens are specifically targeted to autophagophores for autophagic degradation. Such cargo specificity is usually determined by adaptor proteins, which interact with both cargos and autophagy proteins including ULK (21) and ATG8 family proteins. For example, p62 was the first adaptor protein found to bind to both LC3-PE and polyubiquitin-labelled targets, thereby targeting polyubiquitinated substrates to autophagy (22). Another adaptor protein NBR1 functions together with p62 or independently to target ubiquitinated substrates to autophagy (23). Besides ubiquitination-mediated substrate recognition, certain types of direct protein-protein interaction are also used for cargo-specific autophagy. For example, NCOA4 interacts with ferritin and targets iron stock to autophagy to maintain intracellular iron levels (ferritinophagy) (20), which is essential for erythroid differentiation shown in zebra fish and human K562 erythroid cell line (24).

1.1.3 Autophagy signaling pathways

As the only bulk-degradation mechanism in cells identified so far, autophagy is tightly regulated to maintain the homeostasis or remodel the cells in response to various signaling inputs. Various autophagy signaling pathways

are altered during ageing (Fig 1.2), which affects cellular autophagy and imposes an impact on the progress of cellular senescence.

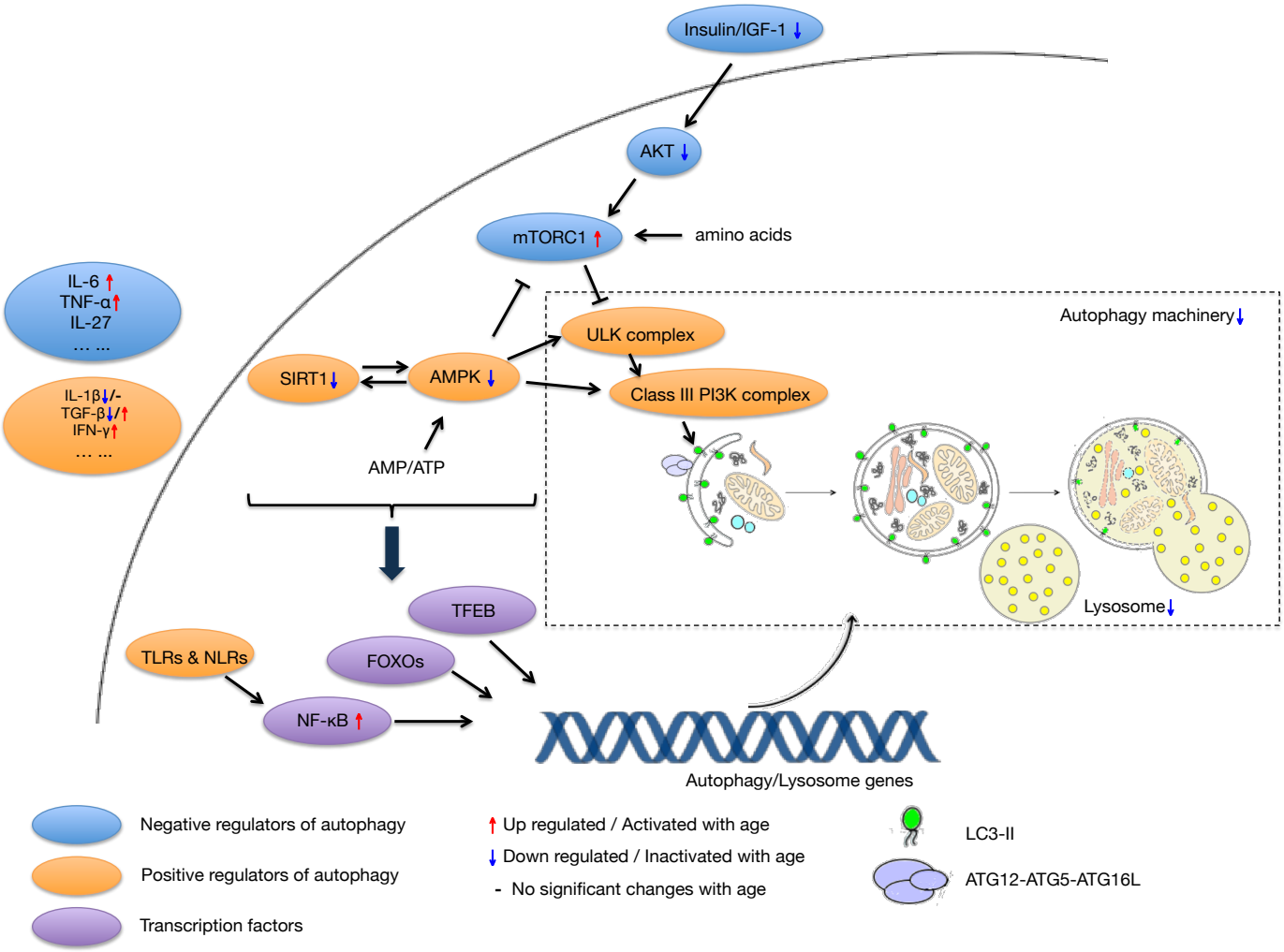


Fig 1.2 Autophagy signaling pathways and their changes with age. Autophagy is controlled by multiple nutrient- and stress-related signals including growth factors, energy supply and cytokines. Particular transcription factors integrate stress signals to regulate autophagy. Age-related changes of autophagy signaling pathway components are labeled out with arrows. Modified from (2).

1.1.3.1 Insulin/IGF-1-mTOR signaling pathway

Cells turn on autophagy as a stress response to maintain nutrient supply under starvation, and autophagy is suppressed by nutrient signals. When environmental nutrient supply is optimum, the conserved insulin/IGF-1 signalling pathway is activated to promote cell growth. Insulin/IGF-1 activates AKT, which further activates mTORC1 and inhibits forkhead box O proteins (FOXOs) to promote anabolism and inhibits autophagy (Fig 1.2) (25). mTORC1 translocates to lysosomal surface and is activated by the Rag-Ragulator complex that senses amino acids in the lysosomal lumen (26, 27). Activated mTORC1 inhibits autophagy induction via phosphorylation of ULK. mTORC1 also phosphorylates and thus inhibits the function of TFEB, which is a key transcription factor for autophagosome and lysosome biogenesis (28-30). FOXOs are transcription factors downstream of insulin/IGF-1 pathway and promote the expression of multiple stress response genes including autophagy, apoptosis and cell cycle arrest (31, 32).

1.1.3.2 AMPK signaling pathway

Nutrient starvation usually leads to reduced energy supply. AMP-activated protein kinase (AMPK) senses the cellular energy status and gets activated by accumulated ADP and AMP (concomitant with a depletion of ATP) (33). AMPK induces autophagy directly via phosphorylation of autophagy machinery components including ULK and class III PI3K (34, 35), and also indirectly via activation of TSC1/2 to turn off the mTOR pathway (Fig 1.2) (36).

1.1.3.3 SIRT1

Mammalian SIRT1 is a conserved protein deacetylase that uses NAD^+ as a coenzyme (37). It plays a key regulatory role in multiple cellular processes including metabolism, DNA repair, inflammation, and ageing (38). NAD^+ is an indicator of the cellular metabolic status and increased NAD^+ activates SIRT1. Several autophagy-related proteins such as ATG5, ATG7 and LC3 are de-acetylated and activated by SIRT1 (39). SIRT1 also stimulates the activity of FOXO3 and AMPK to induce autophagy (40-42). Interestingly AMPK also enhances SIRT1 activity by increasing cellular NAD^+ levels (43). Therefore there is a positive feedback loop between AMPK and SIRT1 to induce autophagy in response to cellular stress (Fig 1.2) (44).

1.1.3.4 Innate immune signals

Besides the shortage of nutrient or growth factors, autophagy can also be induced by multiple immune signals (45, 46). Inflammatory cytokines and pattern recognition receptors trigger the activation of IκB kinase (IKK), which triggers the phosphorylation and degradation of the inhibitory protein IκB and releases NF-κB proteins for their nuclear translocation (47, 48). NF-κB comprises a transcription factor family with five members regulating pro-inflammatory and cell survival responses (47, 48). NF-κB induces the expression of certain autophagy-related genes such as *p62* and *Beclin1* (49, 50), and is shown to be required for autophagy induction under heat shock stress (Fig 1.2) (51). On the other hand, IKK induces autophagy in an NF-κB-independent manner (52, 53).

Certain immune signaling pathways also directly modify autophagy proteins to activate autophagy. For example, Toll-like receptor 4 (TLR4) signaling triggers Beclin1 ubiquitination, which is required for autophagy induction (54). The intracellular bacterial sensor NOD1 and NOD2 directly recruit ATG16L1 to bacteria entry sites on plasma membrane to facilitate the elongation of autophagosomes for xenophagy (55).

1.1.4 Age-related changes/manipulations of autophagy signaling pathways

Autophagy has been found reduced with age in multiple tissues including murine lungs (56), murine skeletal muscle (57), murine degenerated neurons (58), and human lymphocytes (59). A variety of age-related changes of autophagy signaling pathways contribute to altered autophagy levels as discussed below (Fig 1.2).

1.1.4.1 Insulin/IGF-1

The suppression of insulin/IGF-1 pathway by genetic modification or calorie restriction delays ageing from yeast to mammals (60-64). Conversely, mice with over-activated IGF-1 signaling by growth hormone (GH) overexpression show accelerated ageing of multiple organs and have a shorter lifespan (65). Actually human GH and IGF-1 secretion has been found to decline with age (Fig 1.2) (66, 67). This age-related decline of GH/IGF-1 may not be a cause of ageing but instead an adaptive response, because mutants or genetic

polymorphisms with a suppressed GH/IGF-1 pathway are long-lived and have fewer age-related pathologies (68).

1.1.4.2 mTORC1

mTORC1 is over activated in HSCs and skeletal muscles from old mice (Fig 1.2) (69, 70). Phosphorylation of the ribosomal protein S6, a downstream indicator of mTORC1 activity, is also mildly increased in muscle biopsies from healthy elderly (69). Genetic or pharmaceutical (rapamycin) inhibition of mTORC1 activity increases the lifespan from yeast to mammals (70-73), and also rejuvenates the functions of HSCs from aged mice in terms of improving long-term lymphoid lineages reconstitution in HSC adoptively transferred recipient mice (70). These findings suggest that increased mTORC1 signaling plays a causal role in ageing and also might be a contributor to reduced autophagy during ageing.

1.1.4.3 AMPK

Both total AMPK and activated AMPK levels are reduced in heart and skeletal muscle of aged mammals (Fig 1.2) (74, 75). Mice lacking AMPK in muscles fail to induce muscle autophagy during prolonged fasting and show a severe myopathy as well as accumulation of dysfunctional mitochondria during ageing (76). Overexpression or activation of AMPK induces autophagy and prolongs the lifespan in model organisms including worms, flies and rodents (77, 78). The up-regulation of autophagy protein ATG1 is necessary and sufficient to mediate the anti-ageing effects of AMPK activation in flies (79),

indicating that AMPK delays ageing via autophagy induction.

1.1.4.4 FOXOs

The activation of the key stress response transcription factors FOXOs in model organisms promotes an anti-ageing effect (80). For example, dietary restriction in worms activates AMPK, which phosphorylates and activates DAF-16 (the worm homolog of FOXO) to induce stress response genes like *sod-3* (81). Both AMPK and DAF-16 are required for the dietary restriction-induced lifespan elongation effect (81). *FOXO3A* polymorphism is also strongly correlated with human ageing (82). There are two alleles of *FOXO3A* found in human, T (major allele) and G. People with one or two G alleles are more likely to be long-lived and have a lower incidence of age-related diseases including cancer and diabetes (81).

1.1.4.5 SIRT1

Overexpression or activation of SIRT1 in yeast, worms, flies and mice extends their lifespan in an autophagy-dependent manner (83-85). The polyphenol resveratrol prolongs the lifespan of yeast, worms, and flies in a Sir2 (homolog of mammalian SIRT1)-dependent manner (86-88). Resveratrol also improves mitochondria metabolism as well as insulin sensitivity in young or aged mice (42, 89) and obese people (90). SIRT1 is required for the beneficial effects of resveratrol on mitochondrial functions (42, 89). Mechanistically resveratrol directly inhibits the activity of cAMP-specific phosphodiesterases (PDE), which then activate AMPK, SIRT1 and PGC-1α to promote mitochondrial

functions (91). Therefore SIRT1 induces autophagy and maintains mitochondrial health to delay ageing, making it an efficient target for drug design.

1.1.4.6 Inflammageing

Inflammageing is a physiological status in which old mammals display chronic low-grade inflammation. In the elderly, the balance of pro-inflammatory cytokines (including IL-1β, IL-6, IL-12, TNF, IFN-γ) and anti-inflammatory cytokines (including IL-4, IL10, TGF-β, IFN-α/β) is disrupted and more pro-inflammatory cytokines are produced (Fig 1.2) (92). At the cellular level, senescent cells develop the senescence-associated secretory phenotype (SASP) which is characterized by increased secretion of multiple inflammatory cytokines, proteases, as well as small molecules like ROS (93). The effects of pro-inflammatory cytokines on autophagy is complex: IL-1β (94), TGF-β (95, 96), and IFN-γ (97) are autophagy inducers, whereas IL-6 (98), IL-27 (97), and TNF (99) inhibit autophagy. It is noteworthy that these autophagy-inducing or –inhibitory effects can be also cell type-, dose- and time-dependent. For example, IFN-α2 induces autophagy in Daudi and Hela cells after 24 to 48 hours of treatment (100), whereas in H4 and HepG2 cells IFN-α2 only transiently induces autophagy in the first 8 hours and then inhibits autophagy after 12 hours of treatment (101). The complex cytokine profile changes (inflammageing) and their relationship with autophagy and other age-related cellular processes will need to be addressed in future studies.

1.1.4.7 Lysosome

Autophagy degradation relies on lysosomes, which themselves undergo a series of changes during ageing. A significant increase of lysosomal content and the senescence-associated-β-galactosidase activities is observed in senescent cells (102). Age-pigment lipofuscin accumulates in lysosomes with age, which comprises undegradable oxidized materials and inhibits the activity of multiple lysosomal hydrolases and anti-oxidant enzymes (Fig 1.2). The lipofuscin-bound iron catalyzes the generation of ROS (103), which may further oxidize and impair other cellular components and initiate a vicious positive feedback loop to generate more lipofuscin materials. Moreover, the expression of lysosome-associated membrane protein type 2a (LAMP2A), a receptor of chaperone-mediated autophagy, is reduced in livers of old rodents (104, 105). Restoration of LAMP2A preserves chaperone-mediated autophagy activity and delays ageing in mouse liver (104). In addition to bulk degradation, lysosomes play a central role in storage of amino acids and ions and thus regulate cellular nutrient homeostasis (106), which may also be affected during ageing.

Next it would be interesting to genetically or pharmaceutically induce lysosomal biogenesis or degradation efficiency in aged organisms to see if autophagy efficiency and more importantly, age-related functional declines could be restored.

1.2 Autophagy controls cellular senescence

Multiple changes occur in senescent cells including accumulation of damaged organelles and protein aggregates, oxidative stress, DNA mutations and telomere dysfunctions. These changes interact with each other in a complex manner to cause cellular dysfunctions and senescence, which further leads to systemic inflammation and organismal ageing. The following part will discuss how autophagy controls ageing through different mechanisms (Fig 1.3).

1.2.1 Mitochondria and ROS

Mitochondria produce ATP by oxidative phosphorylation and regulate many important cellular processes including metabolism, cell cycle, inflammation, and apoptosis (107). Autophagy maintains mitochondrial homeostasis through removal of damaged mitochondria (mitophagy). During mitophagy, reduced mitochondrial membrane potential leads to the accumulation of PTEN-induced putative kinase 1 (PINK1) on mitochondrial outer membrane. PINK1 recruits and activates the ubiquitin ligase parkin to build polyubiquitin chains on mitochondria which are then recognized by autophagy adaptors NDP52 and OPTN for degradation (21, 108, 109). Autophagy deficiency leads to accumulation of damaged mitochondria and ROS in yeast and other cell types (110-112), while induction reduces ROS and improves cells survival (Fig 1.3) (113).

The mitochondria free radical theory of ageing proposes that free radicals such as $O_2^{\cdot-}$ generated by mitochondria electron transport cause oxidative

damage of cell constituents to impair cell functions (103, 114). In accordance with this theory, a higher ROS level is observed in aged organs and cells (115). Mitochondria in aged cells are less efficient in ATP production (116) and generate more ROS (117). The increased ROS can further oxidize proteins, DNA, RNA and other cellular components to cause oxidative stress (118, 119). Actually damaged mitochondria and accumulated ROS also contribute to progression of age-related diseases like neuron degeneration (120, 121). The anti-ageing treatment calorie restriction activates the superoxide dismutase 2 (SOD2) and reduces oxidative stress (122).

However the causal role of ROS in ageing has become more controversial in recent years, and may rather be 'dose'-dependent. Rather than simply acting as a 'troublemaker', ROS is also a stress signal initiating anti-ageing responses and delay ageing (123). For example, calorie restriction or catalase inactivation extends the chronological lifespan of yeast through elevated H_2O_2 levels, which activates superoxide dismutases to reduce oxidative stress (124). Mutations in mitochondrial respiratory chain components, *Sod-2*, or treatment with the pro-oxidant paraquat in worms induce ROS accumulation and prolong lifespan despite the increased protein oxidation (125, 126). The elevated ROS are taken as an anti-ageing signal in this setting because treatment together with antioxidants vitamin C or N-acetylcysteine (NAC) shortens the long lifespan (126). Actually autophagy can also be induced by ROS via transcriptional and post-transcriptional mechanisms (127), which may then remove dysfunctional mitochondria and oxidative damage.

Therefore, ROS directly causes oxidative stress while activating autophagy and other stress responses. Cellular homeostasis will be rescued if these protective responses are efficiently induced. Otherwise, ROS and oxidative damage will continue accumulating and eventually tip the balance and cause cellular senescence or cell death.

1.2.2 Genome stability

Autophagy maintains the homeostasis of mitochondria and prevents ROS accumulation, thus indirectly maintains genomic stability. According to the somatic mutation theory of ageing, the accumulation of DNA mutations in somatic cells is a cause of reduced function and senescence (128). It has been extensively studied that ROS can attack single nucleobases to introduce DNA point mutations and breaks (129). Antioxidants and the mitochondrial protectant α-lipoic acid improve the genome integrity via reducing chromosomal breaks in lymphocytes from Fanconi anemia patients (130), indicating that ROS is an endogenous cause of genomic instability in cells. More specifically, telomeres are especially vulnerable to DNA damage inducers and the majority of DNA damage foci accumulate at telomeres in stress-induced senescent cells (131, 132). Therefore telomere may also be a favored target of ROS attack, and autophagy indirectly contributes to the maintenance of telemere integrity (Fig 1.3).

1.2.3 Proteostasis

Cellular protein homeostasis, or proteostasis, is tightly controlled at multiple levels, including the rate of translation, chaperone-assisted protein folding and eventually protein degradation (133). Proteins to be degraded are usually tagged with polyubiquitin chains, which can be recognized by proteasomes or autophagosomes for degradation. Depending on the structure of the polyubiquitin tags, cargos are degraded via different mechanisms: K48-polyubiquitinated proteins tend to be degraded by proteasomes, while K63-polyubiquitinated protein aggregates are preferentially targeted to autophagosomes (134, 135). The recognition of polyubiquitin-tagged targets and the selectivity for K63-polyubiquitination are mediated by autophagy adaptors such as p62, NBR1 and HDAC6 (23, 136). These adaptors promote the aggregation of polyubiquitinated proteins for a more efficient sequestration and clearance (137-140).

Ageing is associated with the disruption of proteostasis. A large scale of protein aggregation is found in aged mice as well as age-related diseases (115, 141). Actually both protein folding capacity and protein degradation systems are found impaired with age (142). Meanwhile the formation of protein aggregates is accelerated by elevated ROS levels (115). Therefore, autophagy maintains cellular proteostasis via direct clearance of protein aggregates and indirect alleviation of oxidative stress and protein damage (Fig 1.3).

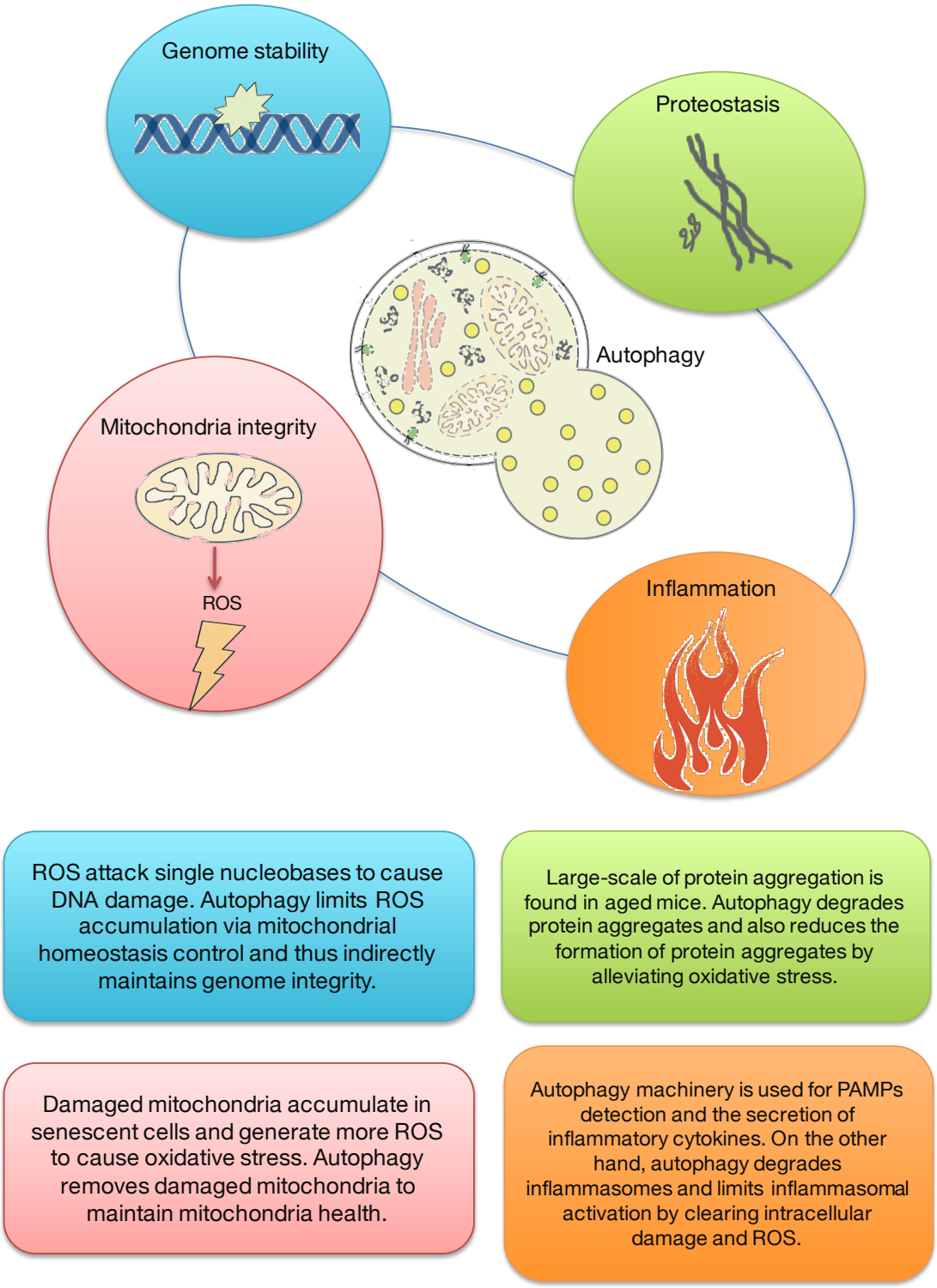


Fig 1.3 Autophagy protects cells from senescence. Modified from (2).

1.2.4 Inflammation

The effect of autophagy on inflammation is context-dependent. Pathogen-associated molecular patterns (PAMPs) in cytosol or endosomes are delivered by autophagy (xenophagy) to lysosomes, where they are recognized by TLRs to trigger innate immune responses (143). Genetic or pharmaceutical inhibition of autophagy suppresses PAMPs-induced TLRs activation in murine B cells and dendritic cells (144-146). Moreover, the autophagy machinery is also used for unconventional secretion of IL-1β and other proteins, and lysosomal hydrolases assist the activation of inflammasomes in murine bone marrow-derived macrophages (147).

On the other hand autophagy degrades intracellular pathogens and damage, thus relieves the overall damage burden and reduces inflammation responses (148). Inhibition of autophagy in cell lines or primary cells enhances the secretion of IL-1β and IL-18 (149, 150). Knock of the essential autophagy genes *Atg5* or *Atg7* in mouse myeloid cells results in increased pro-inflammatory cytokines levels in multiple tissues and exacerbated lung inflammation in response to drug stimulation (151). The increased inflammation without autophagy can be at least partially explained by loss of mitochondrial integrity. Autophagy deficiency promotes the release of mitochondrial DNA and ROS from damaged mitochondria, which triggers the activation of inflammasomes in bone marrow-derived macrophages (150, 152). Additionally, amyloid protein aggregates, which are also potential autophagy substrates, activate TLR2 and promote IL-1β production (153).

It is more likely that autophagy plays an overall suppressive role in inflammageing. When the balance between damage formation and autophagy clearance is disrupted and cellular damage accumulate, innate immune signaling pathways will be activated to secrete inflammatory cytokines. Consequently, cells will undergo senescence with excessive damage, further acquiring senescence-associated secretory phenotype and reinforcing the overall inflammation (Fig 1.3) (154).

1.3 Adaptive immune senescence

Being a key branch of the mammalian haematopoietic system (summarized in Fig 1.4 and Table 1.1), the adaptive immune system comprises two major cell types, T cells and B cells, which recognize specific antigens with diversified receptors and form long-term immune memory. T cells secrete cytokines and cytotoxins to regulate immune responses and directly destroy target cells, while B cells mainly secrete antibodies to mediate humoral responses. Severely compromised adaptive immune response is a key feature of mammalian ageing, and consequently a major cause of increased mobility and mortality due to infectious diseases in aged population. In the following part, age-related changes in development and responses of T cells and B cells will be summarized, and how autophagy controls their ageing will be discussed.

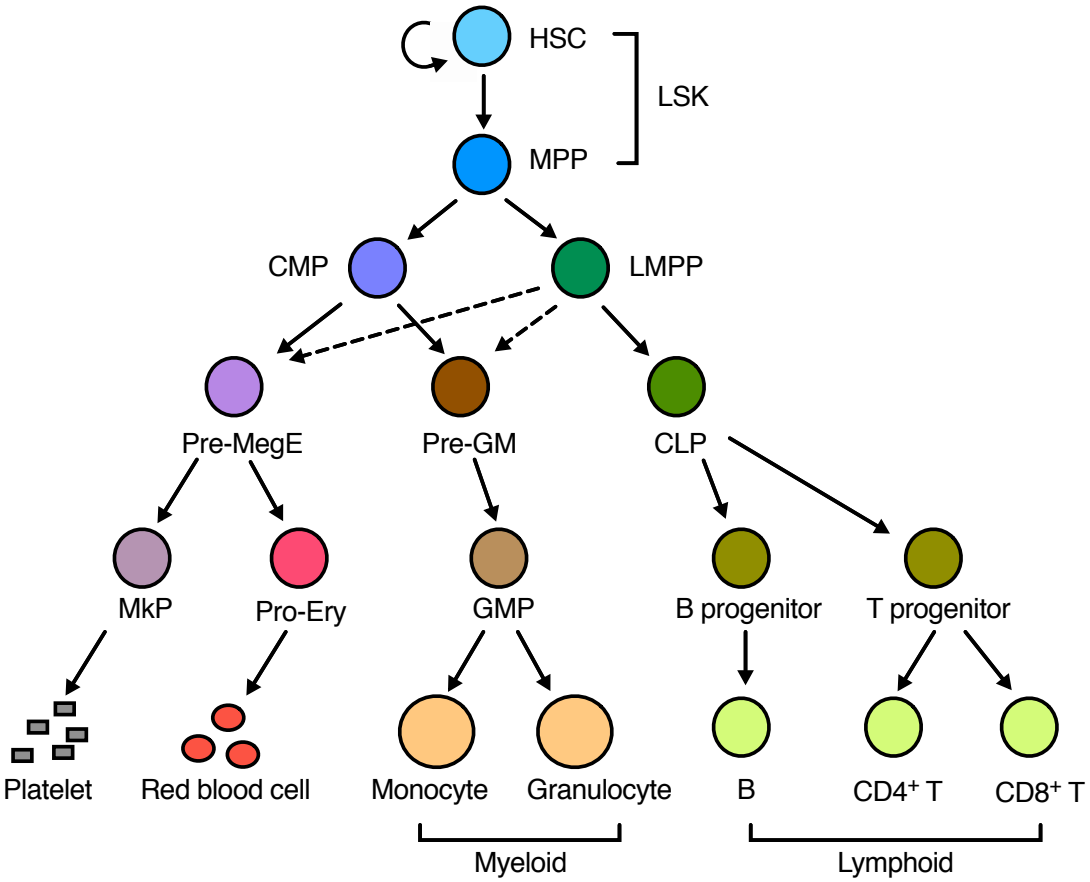


Fig 1.4 Schematic overview of the mammalian haematopoiesis. Haematopoietic stem cells (HSCs) give rise to the majority (if not all) of the cellular components in blood. Self-renewal HSCs differentiate into multipotent progenitors (MPPs), which then proliferate and differentiate into more lineage-restricted progenitors and eventually mature blood cells including red blood cells, myeloid and lymphoid cells, and blood cell-derived components such as platelets. Surface markers are commonly used for identification of different cell types, which are summarized in Table 1.1.

CMP, common myeloid progenitor; LMPP, lymphoid-primed multipotent progenitors; Pre-MegE, pre-megakaryocytes/erythrocyte; Pre-GM, pre-granulocytes/macrophage; CLP, common lymphoid progenitor; MkP, megakaryocyte progenitor; Pro-Ery, pro-erythroblast; GMP, granulocyte/macrophage progenitor.

Table 1.1 Murine haematopoietic cell surface markers used in this thesis

Cell type	Surface marker	Cell type	Surface marker
HSC	Lin1*$^-$Sca1$^+$cKit$^+$CD48$^-$ CD150$^+$	B progenitor (Fraction D)	B220$^+$CD43$^-$IgM$^-$IgD$^-$
MPP	Lin1$^-$Sca1$^+$cKit$^+$CD48$^-$ CD150$^-$	B progenitor (Fraction E)	B220$^+$CD43$^-$ IgM$^+$IgD$^-$
LSK	Lin1$^-$Sca1$^+$cKit$^+$	B progenitor (Fraction F)	B220$^+$CD43$^-$IgD$^+$
LMPP	Lin1$^-$Sca1$^+$cKit$^+$Flt3$^+$	T progenitor (DN§1)	Lin2**$^-$CD4$^-$CD8$^-$ CD44$^+$CD25$^-$
Pre-MegE	Lin1$^-$Sca1$^-$cKit$^+$CD41$^-$FcR II/III$^-$CD150$^+$CD105$^-$	T progenitor (DN2)	Lin2$^-$CD4$^-$CD8$^-$ CD44$^+$CD25$^+$
Pre-GM	Lin1$^-$Sca1$^-$cKit$^+$CD41$^-$FcR II/III$^-$CD150$^-$CD105$^-$	T progenitor (DN3)	Lin2$^-$CD4$^-$CD8$^-$ CD44$^-$CD25$^+$
MkP	Lin1$^-$Sca1$^-$ cKit$^+$CD41$^+$CD150$^+$	T progenitor (DN4)	Lin2$^-$CD4$^-$CD8$^-$ CD44$^-$CD25$^-$
Pro-Ery	Lin1$^-$Sca1$^-$cKit$^+$CD41$^-$FcR II/III$^-$CD150$^-$CD105$^+$	T progenitor (DP§)	Lin2$^-$CD4$^+$CD8$^+$
GMP	Lin1$^-$Sca1$^-$cKit$^+$CD41$^-$ CD150$^-$FcR II/III$^+$	Mature myeloid cell	CD11b$^+$Gr1$^+$
B progenitor (Fraction§ A)	B220$^+$CD43$^+$CD24$^-$BP1$^-$	Mature B cell	B220$^+$ or CD19$^+$
B progenitor (Fraction B)	B220$^+$CD43$^+$CD24$^+$BP1$^-$	Mature CD4$^+$ cell	CD4$^+$
B progenitor (Fraction C)	B220$^+$CD43$^+$CD24$^+$BP1$^+$	Mature CD8$^+$ cell	CD8$^+$

*Lineage mix 1: CD4, CD5, CD8a, CD11b, B220, Ter119, Gr1

**Lineage mix 2: CD3e, TCRg, TCRb, NK1.1, B220, Ter119, Gr1, CD11b, CD11c

§: Fraction A/B/C/D/E/F, DN (double negative) and DP (double positive) refer to different stages of B cell and T cell development, which will be discussed in detail in Chapter 3.

1.3.1 T cells

1.3.1.1 Reduced TCR repertoire diversity during ageing

Thymus is the main site of T cell development. It reaches the peak at childhood in size and functions, then shrinks and almost vanishes in old age (155). Thymic involution directly impairs the development and the output of naive T cells. Indeed, for both human $CD4^+$ and $CD8^+$ T cells, the absolute number of naïve cells (CD95-) significantly reduces with age, whereas the number of effector/memory cells ($CD95^+$) remains unchanged (156, 157). Different subpopulations of $CD4^+$ T cells have different kinetics with age. While the number of type 1 T helper (Th1) and type 2 T helper (Th2) cells is reduced with age (158), regulatory T cells (Tregs) increase in number (159).

In addition to reduced naïve T cells output, persistent exposure to foreign antigens further leads to a preponderance of effector/memory T cells in the elderly. Chronic virus infections such as cytomegalovirus (CMV) are a major cause of T cells oligoclonal expansions in human (160). Actually, the peripheral repertoire of $CD8^+$ T cells can be dominated by CMV-specific cells, with as much as 23% of the whole $CD8^+$ T cell population recognizing a single CMV epitope in healthy elderly individuals (160). In contrast, T cell clonal expansions in old mice are efficiently induced by adjuvant stimulations (161), indicating that the induced inflammatory responses might be an antigen-independent T cell clonal expansion mechanism in pathogen-free mice. Therefore inflammageing may contribute to nonspecific T cell clonal expansions in human.

Therefore, reduced output of naïve T cells due to thymic involution, together with increased clonal expansion due to chronic antigen stimulation and antigen-independent mechanisms, results in reduced diversity of TCR repertoire in peripheral (162), which severely impairs the ability of the T cell pool to respond to new antigens (163).

1.3.1.2 Functional changes with age

Besides the phenotypic alterations, senescent $CD4^+$ and $CD8^+$ T cells are less responsive to antigens. Senescent effector $CD4^+$ T cells express less CD28 and CD40L, which is accompanied by a reduced capacity of helping B cells for their proliferation and antibody production (164). Age is associated with an expansion of effector $CD8^+$ T cells in human, which are less proliferative *in vitro* in response to antigenic challenges than $CD28^+$ naïve/memory T cells (156). The production of cytokines and lytic granules such as TNF-α, IFN-γ, and granzyme B is reduced in $CD8^+$ T cells isolated from virus-infected old mice (165). $CD8^+$ T cells from old mice are also less proliferative *in vivo* when challenged with viruses or mitogens (166, 167). A significant correlation was observed between cytotoxicity and the amount of virus-specific $CD8^+$ T cells, which is similar in both young and old mice (167), indicating that the reduced $CD8^+$ T cytotoxicity is mostly due to a defect of the 'quantity' of expansion rather than the effector 'quality' per cell.

The memory T cell responses, and therefore long-term T cell immunity, are similarly affected during ageing. The recall expansion of $CD8^+$ T cells against

secondary challenge to lymphocytic choriomeningitis virus (LCMV) (168), *Listeria* (169), and influenza (170) is severely compromised in old mice. Interestingly, although memory $CD4^+$ T cells formed in old TCR-transgenic mice respond poorly to secondary immunizations, memory cells formed in young mice and then maintained to old age respond well (171), suggesting that it is the age at which memory T cells form that is the critical determinant of effective memory.

In contrast to functionally severely compromised $CD8^+$ and helper $CD4^+$ T cells, the response of Tregs is generally well maintained and in some cases augmented. An increase of $CD4^+$ Tregs in percentage (of $CD4^+$ T cells) and in absolute number is observed in old mice and human (159, 172-174). The ability to suppress the proliferation and IFN-γ production of $CD8^+$ T cells and the proliferation of $CD4^+CD25^{hi}$ non-Treg T cells is also well maintained in old mice in co-culture experiments (172, 173). Tregs from old human donors show increased FOXP3 expression (159, 174) and are functional in suppressing the proliferation of $CD4^+$ T cells (174). Although most functions of Tregs are well maintained, their ability to suppress Th17 cells *in vivo* is reduced (175). Th17 cells promote inflammation and are implicated in the pathogenesis of many autoimmune diseases. Therefore defect of aged Tregs in controlling autoimmune proliferation may contribute to increased susceptibility to autoimmunity in the elderly.

1.3.1.3 Autophagy controls T cell development and functions

Autophagy-deficient T cells develop normally in thymus, but show survival defects which cause T lymphopenia and homeostatic proliferation (170, 176-178). An increased content of mitochondria with accumulated ROS (179), as well as expanded ER (180) are found in autophagy-deficient $CD4^+$ and $CD8^+$ T cells, indicating that autophagy maintains the homeostasis of these organelles in T cells.

Cytokine production (181) and proliferation (176, 181, 182) of autophagy-deficient T cells are impaired after activation *ex vivo*. ATP generation of *ex vivo* activated Th1 cells is decreased when autophagy is blocked by lysosomal inhibitors, and the exogenous energy source methyl pyruvate partially rescues it (181). Therefore autophagy provides energy for T cell activation. The proliferation of $CD8^+$ T cells is not affected with autophagy deficiency *in vivo*, however their survival is reduced and less memory cells are formed/maintained (170, 183). Consistently, the memory responses of $CD8^+$ T cells are also severely impaired *in vivo* (170). The ROS scavenger NAC rescues the survival defect of autophagy-deficient $CD8^+$ T cells (184). Unpublished data in our lab show that NAC improves the memory responses of autophagy-deficient $CD8^+$ T cells. Therefore autophagy sustains T cell memory at least partially via maintaining mitochondrial homeostasis.

1.3.1.4 Autophagy and T cell senescence

A reduction of autophagy levels is found in $CD8^+$ T cells from aged mice (170) and human (59). Impaired mitochondrial function and elevated ROS levels are observed in T cells from the elderly (185). This correlation suggests that reduced autophagy may contribute to mitochondrial damage during ageing and autophagy induction may improve mitochondrial health to promote T cell function. Indeed, the mTOR-dependent autophagy inducer rapamycin improves memory $CD8^+$ T cell responses against LCMV infections in young mice and against Ankara vaccinations in monkey (186). Another autophagy inducer called spermidine which is mTOR-independent also restores $CD8^+$ T cell memory responses to influenza in old mice in an autophagy-dependent manner (170). Therefore, strategies to increase autophagy levels could be beneficial in attempts to improve vaccination efficacy and the immune responses against real infections in the elderly.

The survival of Tregs is significantly impaired with T cell-specific deletion of the essential autophagy genes such as *Atg7*, *Atg5*, *Vps34*, and *Atg16l1* (177, 187, 188), which leads to chronic intestinal inflammation (188). Therefore autophagy induction may also help restore the suppressive functions of Tregs (especially against Th17 cells) and control inflammageing and autoimmune diseases in the elderly.

1.3.2 B cells

Vaccination is probably our most powerful weapon in the war against pathogens. A robust humoral response mediated by B cells is a prerequisite of efficient vaccination. However, old people (aged 65 years or older) are poorly responsive to vaccinations and infections, which causes an increased hospitalization and even death rate due to infectious diseases in this age group. According to the Morbidity and Mortality Weekly Report (MMWR) by the Centers for Disease Control and Prevention (CDC) of USA, the cumulative hospitalization rate for influenza at the 2014-15 influenza season of ≥ 65 years is 322.8 per 100,000 population, comparing to 147.4 for the sum up of all other ages (189). Old people are also less responsive and thus less protected from vaccination. The frequency of the trivalent inactivated influenza vaccine- (TIV-) specific IgG antibody secreting cells (ACSs) on day 7 to 8 post vaccination in the elderly is about 100 per 0.1 million B cells, comparing to 1000 in the young (190). Therefore interventions improving the humoral immune responses against infections and vaccinations may significantly relieve the infectious disease burden on the ageing group.

1.3.2.1 Reduced BCR repertoire diversity during ageing

Extensive studies have been done to define aged-related changes of B cell development and responses. The production rate of bone marrow pre-B cells and peripheral mature B cells is lower in aged mice (191), leading to a slower turnover of peripheral B cell pools. However the number of peripheral B cells is well maintained or only slightly decreased in aged mice (192). High-

throughput DNA sequencing of immunoglobulin genes from peripheral B cells of young or old people show that chronic infections such as CMV and Epstein-Barr virus (EBV) correlate with B cell clonal expansion and reduction of overall BCR repertoire diversity (193, 194). Therefore, reduced naïve B cell production and the expansion of antigen-experienced B cells both lead to the overall reduction of the peripheral BCR repertoire, which might contribute to inefficient humoral responses against new antigens.

1.3.2.2 Compromised humoral responses with age

The antibody response is delayed (yellow fever vaccination (195)) or quantitatively reduced (influenza (190) and pneumococcal polysaccharide vaccination (196)) in the elderly within 28 days post vaccination. Germinal centre reactions are impaired in aged human B cells (197), to which reduced T cells and dendritic cells functions are extrinsic contributors (198). Meanwhile *ex vivo* activation experiments show that B cells from the elderly are less able to up-regulate AID expression in response to influenza vaccine (199), indicating their intrinsic defects of activation.

Interestingly, it is the quantity rather than the binding affinity of the vaccine-specific antibodies that declines with age (190), indicating that the reduced germinal centre reactions in the elderly are still competent to produce class-switched high-affinity plasma cells. Reduced BCR diversity and possibly the poor survival of newly formed long-lived plasma cells and memory B cells in the elderly might be responsible for reduced antibody quantities, which can be

considered as targets to develop novel interventions.

1.3.2.3 Autophagy controls B cell responses

Knockout of the essential autophagy gene *Atg5* or *Beclin1* in mice leads to the reduced number of bone marrow pre-B cells with the number of mature periphery B cells remaining unchanged (200, 201). Moreover, autophagy is induced during plasma cell differentiation (202), and required for persistent antibody production and the long-term survival of memory B cells (202-204). Mechanistically, *Atg5* knockout plasma cells exhibit increased ER stress and cell death, and fail to generate sufficient antibodies and form long-lived plasma cells *in vivo* (202), indicating that autophagy, or more specifically ER-phagy, maintains the homeostasis of ER of these professional antibody-secreting cells.

Memory B cells also have constitutively high autophagy levels (204). Memory B cells from mice with B cell-specific *Atg7* knockout are generated normally within 2 weeks post NP-KLH immunization, but then start to decline due to increased cell death (203, 204), indicating that the long-term maintenance rather than the formation of memory B cells relies on autophagy. Moreover, rapamycin, an autophagy inducer working via inhibiting mTOR, further enhances the survival and the immune responses of memory B cells in young adult mice against influenza infection (204).

It is still unknown how autophagy changes in B cells during ageing, or if autophagy inducers may rejuvenate B-cell development and responses in old individuals. However, considering that autophagy is indispensable for long-term humoral responses, autophagy induction might be a useful tool to improve humoral responses to infections and vaccinations in the elderly.

1.3.2.4 B-1 B cells

Conventional B cells mediate adaptive humoral responses with long-term memory and are known as B-2 B cells. In contrast, the other B cell subpopulation, called B-1 B cells is more involved in innate immune functions. B-1 B cells are maintained by self-renewal and secrete low-specificity autoantibodies against self- and bacterial antigens such as phosphatidylcholine, and do not give rise to robust memory responses (205). The number of B-1 B cells and their production of autoantibodies are both significantly increased with age (192, 206). Knockout of the essential autophagy genes *Atg7* or *Atg5* leads to reduced number of B-1 B cells (201, 202, 204), thus not concurring with the general hypothesis in adaptive immunity that decline in autophagy contributes to immune senescence. Further investigation is still required to identify the causes of age-related changes of B-1 B cells and their link to autophagy.

1.4 Spermidine as an autophagy inducer

Spermidine is a small polyamine in eukaryotic, archaea and eubacteria cells. In eukaryotic cells, the intracellular concentration of spermidine is at the millimolar level, for example 1.33 mM in bovine lymphocytes and 1.15 mM in rat livers (207). However, the majority of spermidine is bound to DNA, RNA and ATP, whereas only 10% of spermidine is free which can play an important regulatory role in cells (207). Cells can either synthesize spermidine themselves from ornithine with the key enzyme ornithine decarboxylase (ODC) (Fig 1.5), or directly take spermidine up from the environment (208). A series of transporters for spermidine have been reported in yeast such as DUR3 and SAM3 (209), but their functional counterparts in mammalian cells are still poorly defined.

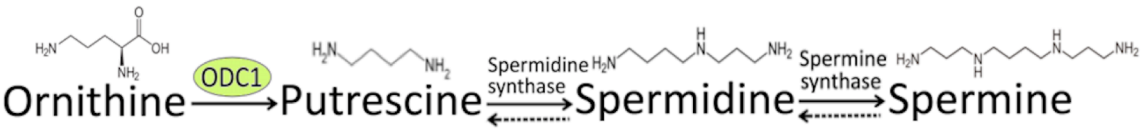


Fig 1.5 Schematic overview of the polyamine synthesis pathway. Ornithine decarboxylase 1 (ODC1) is the key enzyme for polyamine synthesis. Polyamines include putrescine, spermidine, and spermine.

Autophagy induction is a novel function downstream spermidine discovered in recent years. Eisenburg *et al.* first reported that spermidine is able to induce autophagy and increases the lifespan of the ageing yeast, worms, and flies

(210). Follow-up studies also showed that the memory of old flies (211), heart functions and lifespan of old mice (212, 213), and $CD8^+$ T cell responses in old mice (our lab) (170) are improved by spermidine in an autophagy-dependent manner. The mechanism of autophagy induction by spermidine is still unclear, which will be discussed in chapter 4.

1.5 Thesis summary

The role of autophagy in haematopoiesis has been extensively studied in recent years. Previous work in our lab revealed that autophagy is essential for the maintenance of HSCs (214), development of erythrocytes (112) and neutrophils (215), and functions of $CD8^+$ T cells (170) and macrophages (216). However if autophagy modulation is an effective way to improve immune health is still unknown. Severely compromised humoral responses are a feature of ageing, and also a cause of increased morbidity and mortality of multiple age-related diseases. Autophagy induction may help boost immune responses and improve the health status of the elderly.

Using aged mice as our research model, I started by assessing the age-related changes of haematopoiesis and humoral responses, and found that old lymphocytes had reduced autophagic flux. The autophagy inducer spermidine significantly improved the compromised humoral responses in old mice in an autophagy-dependent manner (Chapter 3). The following mechanistic studies using cell lines and *ex vivo* activated primary murine B

cells revealed that endogenous spermidine was required for cellular autophagy, and the target of spermidine in autophagy regulation was the protein translation factor eIF5A (Chapter 4). Proteomics were used to identify the target autophagy proteins downstream of eIF5A, and the master autophagy transcription factor TFEB was confirmed to be regulated by eIF5A. Interestingly, spermidine, eIF5A, and TFEB were all down regulated with age in human samples (Chapter 5). Therefore, we discovered a novel autophagy and ageing signaling pathway, which can be harnessed to rejuvenate adaptive immune responses.

Chapter 2. Materials and Methods

2.1 Mice

2.1.1 Strains

All mice are of C57BL/6J background except for B6.SJL used in chimera experiments. Both young (6-12 weeks) and old (22-24 months) wild type mice were purchased from Charles River UK. *Mb1-cre* mice were kind gift from M Reth, *Atg7*^{flox} mice were obtained from M Komatsu and GFP-LC3 mice from N Mizushima.

2.1.2 Drug administration

Spermidine (Cambridge Bioscience) was given in drinking water at the concentration of 5 mM to mice. Spermidine water was changed three times per week. All mice were held at the Biomedical Services, University of Oxford. Animal experiments were approved by the local ethical review committee and performed under UK project licenses PPL 30/2809, and PPL 30/3388.

2.1.3 Tissue and serum processing

Mouse spleens were crushed with a syringe plunger through 40 μm cell strainers (22363547, Fisherbrand) with PBS-0.1% BSA-2 mM EDTA for single-cell suspensions. After centrifugation at 300-400g, 4 °C, red blood cells (RBCs) were lysed with RBC Lysis Buffer (00-4333-57, eBioscience) for 4 minutes on ice. RBC-lysed splenocytes were washed once more with PBS-0.1% BSA- 2 mM EDTA and then used for experiments.

Mouse bone marrow cells were collected from femur and tibia. Bones were crushed with a pestle and mortar in PBS-0.1% BSA-2 mM EDTA and filtered through 40 μm cell strainers, then used directly for other experiments without RBC lysis.

For serum collection, mouse peripheral blood was collected from tail vein with capillary blood collection tubes (16.440, Microvette® CB 300 Z) and left at 4 °C for 1 hour to coagulate. Samples were centrifuged at full speed (16,000 g), 4 °C for 10 minutes and the supernatant (serum) was carefully aspirated and stored at -80 °C for long-term storage.

2.1.4 Bone marrow chimera

Competitive bone marrow chimeric mice were made to assess the reconstitution ability of HSCs. Bone marrow cells were collected from femur and tibia of the donor mice (young or old C57BL/6J CD45.2 mice, with young B6.SJL CD45.1 mice as competitors) and mixed at the ratio of 1:1 (CD45.1:CD45.2). The recipient B6.SJL mice were lethally irradiated (450 cGy twice with 4 hours apart) and rested for 1 hour prior to injection. A total of 10 million bone marrow cells were injected intravenously into recipient mice. Male recipient mice can receive bone marrow cells from both male and female donors, whereas female recipient mice can only receive bone marrow cells from female donors to avoid transplant rejection. The recipient mice were administrated with Baytril in drinking water during the first 2 weeks post

irradiation to avoid infections. After 16 weeks of long-term reconstitution, organs of recipient mice were collected for analysis.

2.2 Cell culture and drug treatments

Jurkat cells (TIB-152™, ATCC) were cultured in RPMI-1640 Medium (Sigma, R8758-500ML) supplemented with 10% FBS (Sigma), Penicillin-Streptomycin (P/S, Sigma, P0781, 1:100), and L-Glutamine (Sigma, G7513, 1:100) in 5% CO_2 at 37 °C.

NIH 3T3 cells (CRL-1658, ATCC) and HEK293T cells (CRL-3216, ATCC) were cultured in Dulbecco's Modified Eagle's Medium (DMEM) supplemented with 10% FBS, P/S, and L-Glutamine. The IPTG-inducible MISSION shRNA lentiviral vector pLKO-puro-IPTG-3xLacO was purchased either with a shRNA against the 3'-UTR of the murine eIF5A mRNA sequence (custom-made from #SHCLND-NM181582-TRCN0000125229, Sigma) or a corresponding non-target shRNA control (#SHC332-1EA, Sigma). Stable transduction of the lentiviral was performed as previously described (217) using HEK293T cells with the packaging plasmids pMDLg/pRRE (Gag/Pol), pRSV-Rev (Rev) and phCMV-VSV-G (envelope) as well as the ProFection Mammalian Transfection System Calcium Phosphate Kit (Promega). Positive cells were selected using puromycin. 100 μM IPTG (Thermo Fisher) was used to induce the expression of shRNA.

Immortalized *Dohh*$^{flox/flox}$ and *Dohh*$^{+/+}$ 3T3 cells were established from mouse embryonic fibroblasts as described before (218). 100 nM 4-OHT (Sigma) was used to induce the knock out of *Dohh*.

10 nM Bafilomycin A1 (Cayman Chemical) was added to cells for 2 hours for autophagic flux analysis. 10-100 μM GC7 (Millipore), 10 μg/ml cycloheximide (Sigma), 5 μg/ml Actinomycin D (Sigma), 100 nM Torin 1 (Cayman Chemical), 50 nM Rapamycin (Cayman Chemical, 10 μM Etoposide (Cayman Chemical), 1 mM Difluoromethylornithine (DFMO, Enzo Life Sciences), Spermidine (Cayman Chemical) of indicated concentrations were added to cells for indicated length of time.

2.3 List of antibodies

Table 2.1 Antibodies used in this thesis

Name/Target	Company	Clone	Cat #	Dilution (1:)
Western blot				
GAPDH	Millipore	6C5	MAB374	5000
LC3	Sigma	Poly	L8918	1000
eIF5A	BD Biosciences	26/eIF-5a	611976	3000
Hypusine	Millipore	Poly	ABS1064	1000
ATG7	Abcam	EPR6251	Ab133528	5000
H3	Cell Signaling	Poly	9715	1000
S6	Cell Signaling	54D2	2317	500
pS6 (Ser235/236)	Cell Signaling	D57.2.2E	4858	2500

AMPKα	Cell Signaling	F6	2793	1000
pAMPKα (T172)	Cell Signaling	40H9	2535	1000
AcK	Cell Signaling	Poly	9441	1000
ATF4	Santa Cruz	Poly	sc-200	200
eIF2α	Cell Signaling	L57A5	2103	1000
p-eIF2α (Ser51)	Cell Signaling	Poly	9721	1000
ATG3	Abcam	EPR4801	Ab108251	10000
PIK3C3	Cell Signaling	D4E2	3358	1000
IRDye 800CW Donkey Anti-Rabbit IgG (H+L)	LI-COR Biosciences	NA	926-32213	10000
IRDye 680RD Donkey Anti-Mouse IgG (H+L)	LI-COR Biosciences	NA	926-68022	20000
Flow cytometry				
CD16/CD32 Monoclonal Antibody (FcR Block)	Thermo Fisher	93	14-0161-85	400
Pacific Blue™ anti-mouse/human CD44 Antibody	BioLegend	IM7	103020	200
Pacific Blue™ anti-mouse TER-119/Erythroid Cells Antibody	BioLegend	TER-119	116232	100
Pacific Blue™ anti-mouse CD45.1 Antibody	BioLegend	A20	110722	100
Pacific Blue™ anti-mouse Ly-6G/Ly-6C (Gr-1) Antibody	BioLegend	RB6-8C5	108430	200
Pacific Blue™ anti-mouse Ly-6A/E (Sca-1) Antibody	BioLegend	E13-161.7	122520	200
Brilliant Violet 605™ anti-mouse CD41 Antibody	BioLegend	MWReg30	133921	200
Brilliant Violet 605™ anti-mouse CD4 Antibody	BioLegend	GK1.5	100451	800

Brilliant Violet 605™ anti-mouse/human CD45R/B220 Antibody	BioLegend	RA3-6B2	103244	200
Ly-6A/E (Sca-1) Monoclonal Antibody, PerCP-Cyanine5.5	Thermo Fisher	D7	45-5981-82	400
CD19 Monoclonal Antibody, PerCP-Cyanine5.5	Thermo Fisher	1D3	45-0193-82	400
FITC anti-mouse Ly-6A/E (Sca-1) Antibody	BioLegend	D7	108106	400
CD43 Monoclonal Antibody, FITC	Thermo Fisher	eBioR2/60	11-0431-81	200
FITC anti-mouse CD4 Antibody	BioLegend	GK1.5	100406	800
FITC anti-mouse IgM Antibody	BioLegend	RMM-1	406506	100
PE anti-mouse/human CD45R/B220 Antibody	BioLegend	RA3-6B2	103208	200
PE anti-mouse Ly-51 Antibody	BioLegend	6C3	108308	200
PE anti-mouse/human CD44 Antibody	BioLegend	IM7	103008	400
PE anti-mouse Ly-6G/Ly-6C (Gr-1) Antibody	BioLegend	RB6-8C5	108408	400
PE anti-mouse CD135 Antibody	BioLegend	A2F10	135306	50
PE anti-mouse CD19 Antibody	BioLegend	6D5	115508	800
PE anti-mouse/human CD11b Antibody	BioLegend	M1/70	101208	800
CD4 Monoclonal Antibody (GK1.5), PE-Cyanine5	Thermo Fisher	GK1.5	15-0041-82	800
PE/Cy5 anti-mouse CD5 Antibody	BioLegend	53-7.3	100610	800
PE/Cy5 anti-mouse CD8a Antibody	BioLegend	53-6.7	100710	800

PE/Cy5 anti-mouse/human CD11b Antibody	BioLegend	M1/70	101210	800
PE/Cy5 anti-mouse CD11c Antibody	BioLegend	N418	117316	400
PE/Cy5 anti-mouse/human CD45R/B220 Antibody	BioLegend	RA3-6B2	103210	200
PE/Cy5 anti-mouse CD3ε Antibody	BioLegend	145-2C11	100310	100
TCR beta Monoclonal Antibody, PE	Thermo Fisher	H57-597	12-5961-82	400
TCR gamma/delta Monoclonal Antibody, PE-Cyanine5	Thermo Fisher	GL3	15-5711-82	200
PE/Cy5 anti-mouse TER-119/Erythroid Cells Antibody	BioLegend	TER-119	116210	300
PE/Cy5 anti-mouse NK-1.1 Antibody	BioLegend	PK136	108716	300
PE/Cy5 anti-mouse Ly-6G/Ly-6C (Gr-1) Antibody	BioLegend	RB6-8C5	108410	400
PE/Cy7 anti-mouse CD43 Antibody	BioLegend	S11	143210	400
PE/Cy7 anti-mouse CD8a Antibody	BioLegend	53-6.7	100722	400
PE/Cy7 anti-mouse CD19 Antibody	BioLegend	6D5	115520	400
PE/Cy7 anti-mouse IgM Antibody	BioLegend	RMM-1	406514	200
PE/Cy7 anti-mouse CD150 (SLAM) Antibody	BioLegend	TC15-12F12.2	115914	100
APC anti-mouse CD105 Antibody	BioLegend	MJ7/18	120414	200
APC anti-mouse CD3ε Antibody	BioLegend	145-2C11	100312	100

TCR beta Monoclonal Antibody, APC	Thermo Fisher	H57-597	17-5961-81	400
TCR gamma/delta Monoclonal Antibody, APC	Thermo Fisher	GL3	17-5711-82	200
APC anti-mouse NK-1.1 Antibody	BioLegend	PK136	108710	200
APC anti-mouse/human CD45R/B220 Antibody	BioLegend	RA3-6B2	103212	200
APC anti-mouse/human CD11b Antibody	BioLegend	M1/70	101212	1600
APC anti-mouse Ly-6G/Ly-6C (Gr-1) Antibody	BioLegend	RB6-8C5	108412	800
APC anti-mouse CD24 Antibody	BioLegend	30-F1	138506	200
APC anti-mouse CD4 Antibody	BioLegend	GK1.5	100412	800
APC anti-mouse CD48 Antibody	BioLegend	HM48-1	103412	200
APC anti-human CD19	BioLegend	HIB19	302212	400
Alexa Fluor® 700 anti-mouse CD45.2 Antibody	BioLegend	104	109822	100
Alexa Fluor® 700 anti-mouse CD8a Antibody	BioLegend	53-6.7	100730	800
CD8a Monoclonal Antibody, APC-eFluor 780	Thermo Fisher	53-6.7	47-0081-82	200
APC/Cy7 anti-mouse/human CD11b Antibody	BioLegend	M1/70	101226	800
APC/Cy7 anti-mouse IgD Antibody	BioLegend	11-26c.2a	405716	400
APC/Cy7 anti-mouse CD19 Antibody	BioLegend	6D5	115530	200
CD117 (c-Kit) Monoclonal	Thermo Fisher	2B8	47-1171-	1200

Antibody (2B8), APC-eFluor 780			82	
Others				
Goat Anti-Mouse IgM, Human ads-AP	SouthernBiotech	Poly	1020-04	1000
Goat Anti-Mouse IgG1, Human ads-AP	SouthernBiotech	Poly	1070-04	2000
Rabbit IgG (IP)	Santa Cruz	Poly	sc-2027	500
ATG7 (IP)	Abcam	Poly	Ab58735	500
AcK (IP)	Cell Signaling	Poly	9441	100

2.4 Flow cytometry (FACS)

2.4.1 Surface marker staining and analysis

Cells were stained with fixable Live/Dead staining (Biolegend or Thermo Fisher), FcR block, and surface marker antibodies in PBS at 4 °C for 20 minutes, then washed once with PBS-0.1% BSA-2 mM EDTA. Unfixed cells were directly analyzed with four-laser LSR Fortessa X-20 and analyzed directly. If analyzed later, cells were first fixed with 2% paraformaldehyde (PFA) in PBS at room temperature for 10 minutes, then stored in PBS at 4 °C for up to 3 days. Acquired data were analyzed using FlowJo 10.2.

For Annexin V staining, cells were first washed with PBS and stained with Annexin V (1:50, Biolegend) and Live/Dead in Annexin V binding buffer at 4 °C for 20 minutes. Stained cells were then washed once with Annexin V binding buffer and analyzed in Annexin V binding buffer without fixation.

(10X Annexin V binding buffer: 0.1 M HEPES (pH 7.4), 1.4 M NaCl, and 25 mM $CaCl_2$)

2.4.2 LC3-II FACS staining

The FlowCellect™ Autophagy LC3 antibody based assay kit (FCCH100171, Millipore) was used according to the manufacturer's protocol. In brief, cells were stained with surface markers and washed with Assay Buffer and Reagent B. Then cells were stained with the LC3 antibody in Assay Buffer at 4°C for 30 minutes, and washed once with Assay Buffer. Stained cells were then fixed with 2% PFA before FACS analysis.

2.4.3 CytoID staining

Cells were stained with CytoID (ENZ-51031-K200, Enzo Life Sciences) according to the manufacturer's protocol. Briefly, cells were re-suspended in CytoID staining solution (1:4000 diluted in RPMI without phenol red (R1780, Sigma) supplemented with 5% FBS) and incubated at 37°C for 30 minutes in dark. Then cells were washed once by topping up with PBS, followed with the surface marker staining and FACS analysis without fixation.

2.4.4 OPP-Click Assay

Protein translation rate was measured using the Click-iT Plus OPP Protein Synthesis Assay (C10456, Thermo Fisher) according to the manufacturer's protocol. In brief, 20 μM O-propargyl-puromycin (OPP) was added to cell culture for 30 minutes. After surface marker staining, cells were fixed with 4%

PFA at room temperature for 10 minutes, permeabilized with 0.1% Triton X-100 at room temperature for 10 minutes, and re-suspended in the Click-iT Plus OPP reaction cocktail at room temperature for 30 minutes. Fluorescence-labeled cells were analyzed by FACS.

2.5 Western blot

Cells were washed once with PBS and lysed using NP-40 lysis buffer with proteinase inhibitors (Sigma) and phosphatase inhibitors (Sigma) on ice. After spinning down the debris, protein concentration in the supernatant was quantified by BCA Assay (23227, Thermo Fisher). Reducing Laemmli Sample Buffer was then added to the supernatant and heated at 100 °C for 5 minutes. 5-20 μg proteins were loaded for SDS-PAGE analysis. For LC3 western blot, 15% Tris-HCl gel and SDS running buffer was used to separate LC3-I and LC3-II. For non-LC3 western blot, NuPAGE Novex 4-12% Bis-Tris gradient gel (Thermo Fisher) with MES running buffer (Thermo Fisher) was used. Proteins were transferred to the PVDF membrane (IPFL00010, Millipore) and blocked with 5% skimmed milk-TBST (TBS+0.1% Tween 20). Membranes were incubated with primary antibodies dissolved in 1% milk over night and secondary antibodies dissolved in 1% milk with 0.01% SDS for imaging using the Odyssey CLx Imaging System. Data were analyzed using Image Studio Lite.

Table 2.2 Reducing Laemmli Sample Buffer (4X)

Component	Weight/Volume	Conc.
SDS	3.2g	8%
2-Mercaptoethanol	8 ml	20%
Glycerol	16 ml	40%
1M Tris (pH6.8)	8 ml	20%

Note: Add 0.03 g of bromophenol blue and bring to 40 ml with water.

Table 2.3 15% Tris-HCl polyacrylamide gels

For 2 gels	5% (Stacking)	15% (Separating)
H_2O /ml	4.8	4.6
30% Acr-Bis /ml	1.2	10
Buffer /ml	0.875	5
10% SDS /µl	70	200
10% Ammonium persulfate /µl	70	200
TEMED /µl	7	8
Total /ml	7	20

Buffer: 1M Tris (pH6.8) for Stacking, 1.5M Tris (pH8.8) for Separating.

Table 2.4 NP-40 lysis buffer (2X)

Compound	M.W.	Conc. (mM)	g/200 ml	g/500 ml
NaCl	58.4	300	3.5	8.75
Tris base	121.1	20	0.48	1.2
EGTA	380.4	2	0.154	0.385
EDTA	372.2	2	0.149	0.373

Notes:

1. pH to 7.5.
2. Add 4 ml (for 200 ml) or 10 ml (for 500 ml) of NP-40 detergent or NP-40 alternative.
3. Adjust total volume to 200 ml or 500 ml.

2.6 Immunoprecipitation

An equal number of cells from different treatments were collected, washed once with cold PBS and lysed using NP-40 lysis buffer with proteinase and phosphatase inhibitors on a rotator at 4 °C for 20 minutes. For 25 million Jurkat cells, 950 μl lysis buffer was used. Cell debris was centrifuged down at 13000 rpm for 15 minutes at 4 °C. 50 μl supernatant was collected as whole cell lysate (In put control), and the protein concentration was measured by BCA Assay. The remaining supernatant was transferred to another tube and mixed with 15 μl Protein A Agarose beads (Thermo Fisher) in PBS, then rotated at 4 °C for 15 minutes to pre-clear the lysate. The beads were removed by centrifugation at 6000 rpm for 1 minute. Immunoprecipitation (IP) Antibody (AcK, ATG7, or rabbit IgG) and 20 μl Protein A Agarose beads were

added to the lysate (about 900 μl) and then rotated at 4 °C over night. The beads were washed twice with NP-40 lysis buffer containing proteinase and phosphatase inhibitors and the supernatant discarded. 35 μl 2X Reducing Laemmli Sample Buffer was added to the beads and heated at 100 °C for 5 minutes. The supernatant was used for Western blot analysis.

2.7 Quantitative PCR

Cells were washed once with PBS and RNA was extracted using the RNeasy Plus Mini Kit (74134, Qiagen). The concentration of RNA was measured using NanoDrop1000 (Thermo Fisher). RNA was reverse transcribed to cDNA using the High Capacity RNA-to-cDNA Kit (4387406, Thermo Fisher). Taqman probes (Thermo Fisher), TaqMan Gene Expression Master Mix (Thermo Fisher, 4369016), and the ViiA 7 Real-Time PCR System (Thermo Fisher) were used for quantitative PCR. ΔΔCt method was used for the quantification of target mRNAs expression using B2m as the reference gene.

Table 2.5 TaqMan® probes for quantitative PCR

Gene	Assay ID
B2m	Mm00437762_m1
Atg9b	Mm01157883_g1
Ctsd	Mm00515586_m1
Gla	Mm00516323_m1
Neu1	Mm00456846_m1
Psap	Mm00478338_m1
Tfeb	Mm00448968_m1
Wipi1	Mm00461219_m1

GAPDH	Hs02758991_g1
ATG5	Hs00169468_m1
BECLIN1	Hs00186838_m1
ATG7	Hs00893770_m1
ATG10	Hs00919721_m1
GABARAPL1	Hs00740588_mH
SQSTM1	Hs01061917_g1
CHOP	Hs00358796_g1

2.8 siRNA transfection

NIH 3T3 cells were grown to about 50% confluency for transfection according to the protocol from Thermo Fisher (13778075, Lipofectamine® RNAiMAX Reagent). In brief, siRNA diluted in Opti-MEM® Medium (51985-026, Thermo Fisher) was mixed with the Lipofectamine® RNAiMAX Reagent and added to cells. Cells were collected on day 4 post transfection for western blot analysis.

Table 2.6 siRNAs used in this thesis

Target gene	Target sequence	Manufacturer
***Eif5a* #1**	GGACUUCGAGACAGGAGAU	Dharmacon
***Eif5a* #2**	UUACUGGGAAGAAAUAUGA	Dharmacon
Ctrl	NA	Dharmacon (D-001220-01-20)

2.9 HAT activity assays

Nuclei from Jurkat cells treated with or without spermidine were isolated using the Nuclear/Cytosol Fractionation Kit (K266, BioVision) without adding

dithiothreitol (DTT) according to the manufacturer's protocol. The activity of histone acetyltransferases (HATs) of the nuclear extract was measured using the HAT Activity Colorimetric Assay Kit (K332, BioVision). Briefly, 50 μg nuclear extract (quantified by BCA assay) in 40 μl Nuclear Extraction Buffer was mixed with the Assay Mix and added in a 96-well U-bottom plate and incubated at 37 °C for up to 3 hours. Spermidine was added 15 minutes after assay initiation. The absorbance at 440 nm was recorded every half an hour with a plate reader. The background absorbance was acquired using empty Nuclear Extraction Buffer mixed with the Assay Mix and subtracted from the readings of samples.

2.10 NP-CGG immunization and analysis

2.10.1 Immunization

Mice were injected intraperitoneally (ip) with 50 μg NP-CGG (N-5055D-5, Biosearch Technologies, dissolved in PBS) in Imject Alum adjuvant (Thermo Fisher) on day 0. Imject Alum was added dropwise to NP-CGG solution at 1:1 ratio (v/v) and mixed on a rotator at room temperature for 30 minutes. Secondary immunization was performed on or after day 42 by injecting ip with 50 μg NP-CGG in PBS. Peripheral blood samples were collected from tail vein on indicated days.

2.10.2 NP-IgM/IgG1 ELISA

ELISA plates (675061, Greiner Bio-One) were coated with 5 μg/ml NP-BSA (N-5050H-10, Biosearch Technologies) in biocarbonate/carbonate buffer at 4

°C over night. After three washes with PBS, plates were blocked with 5% skimmed milk (Sigma) in PBS at 37 °C for 1 hour, followed by 3 times of PBS wash. Serum samples diluted in 1% milk were added and incubate at 37 °C for 1 hour. For relative quantification, standard serum sample was made by pooling samples on day 7 post secondary immunization (peak response for both IgM and IgG1) from a prior experiment, then aliquoted for all following experiments.

Serum samples of various days were serially diluted first to determine the proper dilution rate. Eventually 1:500 was chosen for IgM ELISA, and 1:1000 (before boost)/5000 (after boost) was chosen for IgG1 ELISA. Standard serum was diluted at 1:400/800/1600/3200/6400/12800 for IgM ELISA, and 1:4000/8000/16000/32000/64000/128000 for IgG1 ELISA.

After serum sample incubation, plates were washed 6 times with PBS-0.05% Tween 20 followed with detection antibody incubation at 37 °C for 1 hour. The alkaline phosphatase- (AP-) conjugated goat-anti mouse IgM (SouthernBiotech) detection antibody was 1:1000 diluted in 1% milk-PBS, and the AP-conjugated goat-anti mouse IgG1(SouthernBiotech) diluted in 1:2000. After washing with PBS-0.05% Tween 20 for 5 times and PBS once, AP substrate (S0942, Sigma) dissolved in pNPP buffer was added for 15-20 min and absorbance was measured at 405 nm by ELISA plate reader (FLUOstar Omega, BMG Labtech).

2.10.3 NP-IgG1 ELISpot

Live cells were counted using count beads (424902, Biolegend) and 7-AAD (00-6993-50. eBioscience) with LSR Fortessa X-20. MultiScreenHTS-HA filter plates (MSHAS4510) were rinsed first with 35% ethanol for 30 seconds and washed 3 times with PBS. Plates were coated with 20 μg/ml NP-BSA in PBS at 4 °C over night. After three washes with PBS, plates were blocked with RPMI-1640 medium supplemented with 10% FBS at 37 °C for 30 minutes. Then bone marrow cells were added in duplicates in culture medium at the density of $3X10^5$ /100 μl each well and cultured at 37 °C over night. Plates were then washed 3 times with PBS and 3 times with PBS-0.05% Tween 20. AP-conjugated anti-mouse IgG1 detection antibody diluted in 1% FBS was added to plates for 1 hour incubation at 37 °C. After 5 times wash with PBS-0.05% Tween 20 and once with PBS, AP substrate (170-6432, Bio-Rad) was added for spot developing. Plates with clear spots and clean background were washed with water to stop development, dried, and counted with the AID EliSpot Reader System (ELR078IFL, AID GmbH).

2.11 Mouse B cell purification and stimulation

RBC-lysed mouse splenocytes were washed once with MACS buffer (PBS+0.5% BSA+2 mM EDTA). B cells were purified using the Pan B Cell Isolation Kit II (130-104-443, Miltenyi) and LS columns (Miltenyi). Cells were cultured at the density of 1 million/ml in the culture medium (RPMI-1640 + 10% FBS + P/S +L-Glutamine+ 50 μM 2-Mercaptoethanol + 20 mM HEPES) supplemented with 10 μg/ml LPS (Santa Cruz) for stimulation. Medium was

refreshed on day 3 of culture by replacing half volume with fresh culture medium containing LPS for analyses on day 4 and day 5.

2.12 Confocal microscopy

B cells from GFP-LC3 mice were MACS-purified and fixed with 4% PFA at room temperature for 10 min. After nuclear staining with DAPI (Sigma), cells were transferred to slides using Cytospin 3 cytocentrifuge (Shandon) and imaged with the Olympus FV1200 Laser Scanning Microscope. CellProfiler software was used for automatic autophagosome quantification. Nuclei were defined in DAPI channel with a diameter of 45-100 pixel units, whereas autophagosomes were defined in GFP channel with a diameter of 3-15 pixel units (1 pixel unit =100 nm). A threshold of 1-10 cellular GFP spots was used for analysis.

2.13 Cell fractionation

Cells in a 1.5 mL Eppendorf tube were washed once with cold PBS and re-suspended in HLB buffer (10 mM Tris-HCl pH 7.5, 10 mM NaCl, 2.5 mM MgCl2) with protease inhibitors and phosphatase inhibitors, then HLB+2N buffer (HLB+0.4% NP-40, 1N is 0.2% NP-40) was added and carefully mixed. Samples were incubated on ice for 5 minutes and then underlayed with 200 μl HLB+NS buffer (HLB+0.2% NP-40+10% sucrose). Samples were centrifuged at 500 g for 5 minutes and the upper half of the supernatant was collected as the cytoplasmic fraction. The remaining liquid was discarded and the nuclear

pellet was washed once more with HLB buffer and lysed with NP-40 lysis buffer. All procedures were performed on ice.

2.14 Proteomics mass spectrometry

LPS-stimulated mouse B cells were treated with 10 μM GC7 on day 2 for 24 hours. Cells were collected and fractionated for label-free quantitative mass spectrometry (MS) analysis. For SILAC MS, B cells stained with CellTrace Violet (C34557, Thermo Fisher) were cultured in two types of medium: light and heavy. In light medium, SILAC RPMI-1640 medium (89984, Thermo Fisher) supplemented with 1.15 mM L-Arg (Sigma) and 0.22 mM L-Lys (Sigma), 10% dialysed FBS (Sigma), and P/S, L-Glutamine, 50 μM 2-Mercaptoethanol, 20 mM HEPES were used. In heavy medium, $^{13}C_6{}^{15}N_4$-L-Arg (Arg-10, Silantes) and $^{13}C_6{}^{15}N_2$-L-Lys (Lys-8, Silantes) were used instead of the light arginine and lysine respectively. 10 μM GC7 was added to either light or heavy medium in two repeats. After GC7 treatment, dead cells were firstly removed using the Dead Cell Removal Kit (Miltenyi). An identical number of cells duplicated 4 times or more in light or heavy medium were collected by FACS, and mixed for cell fractionation and protein MS analysis.

Peptide samples were prepared using the Filter Aided Sample Preparation (FASP), as previously described (219). Briefly, Vivacon 500 filters (Sartorius, VN01H02 10 kDa/VNCT01) were pre-washed with 200 μl 0.1% trifluoroacetic acid in 50% acetone. Lysate samples were loaded to the filter and denatured with 200 μl 8 M urea in 100 mM triethylammonium bicarbonate buffer (TEAB)

for 30 minutes at room temperature. Denatured proteins were reduced by 10 mM tris (2-carboxyethyl) phosphine (TCEP) for 30 minutes at room temperature and alkylated with 50 mM chloroacetamide for 30 minutes at room temperature in the dark. Subsequently, 1 μg LysC (Wako) in 150 μl 50 mM TEAB containing 6M urea was added and incubated at 37 °C for 4 hours. Then the buffer was diluted to 2 M urea by 50 mM TEAB, followed by adding 0.5 μg trypsin (Promega) overnight at 37 °C. Trypsinised samples were centrifuged and the flow-through containing peptides was dried and re-suspended in 70 μl 10% formic acid (or 5% formic acid and 5% DMSO for SILAC experiment).

Peptides (2 μg) were separated on an Ultimate 3000 UHPLC system (Thermo Fisher) and electrosprayed directly into a QExactive mass spectrometer (Thermo Fisher) through an EASY-Spray nano-electrospray ion source (Thermo Fisher). The peptides were trapped on a C18 PepMap100 pre-column (300 μm i.d. x 5 mm, 100 Å, Thermo Fisher) using solvent A (0.1% formic acid in water) at a pressure of 500 bar, then separated on an in-house packed analytical column (75 μm i.d. packed with ReproSil-Pur 120 C18-AQ, 1.9 μm, 120 Å, Dr. Maisch GmbH) using a linear gradient (length: 120 minutes, 15% to 35% solvent B (0.1% formic acid in acetonitrile), flow rate: 200 nl/min). Data were acquired in a data-dependent mode (DDA). Full scan MS spectra were acquired in the Orbitrap (scan range 350-1500 m/z, resolution 70000, AGC target 3e6, maximum injection time 50 ms). The 10 most intense peaks were selected for HCD fragmentation at 30% of

normalised collision energy at resolution 17500, AGC target 5e4, maximum injection time 120 ms with first fixed mass at 180 *m/z*. Charge exclusion was selected for unassigned and 1+ ions. The dynamic exclusion was set to 20 seconds.

Raw MS data were processed by MaxQuant (version 1.5.0.35i) for peak detection and quantification (220, 221). MS spectra were searched against the *Mus musculus* UniProt Reference proteome (retrieved 12/01/17) alongside a list of common contaminants, using the Andromeda search engine with the following search parameters: full tryptic specificity, allowing two missed cleavage sites, fixed modification was set to carbamidomethyl (C) and the variable modification to acetylation (protein N-terminus) and oxidation (M). The search results were filtered to a false discovery rate (FDR) of 0.01 for proteins, peptides and peptide-spectrum matches (PSM). Protein intensity distributions were log2 transformed and median-centred using Perseus (version 1.5.5.3). For the SILAC analysis, missing values were replaced by an estimated background noise value. Proteins without greater-than-background values in both replicates for at least one condition were removed. MA plots were generated using R (version 3.4.2). Reviewed autophagy proteins were searched against the *Mus musculus* UniProt database. Data from the independently analyzed cytoplasmic and nuclear proteins were shown as overlaid MA-plots wherein the log2 average (GC7 + Vehicle) intensity (A) is plotted on *x* versus the log2 (GC7:Vehicle) fold change (M) plotted on *y*.

2.15 Spermidine measurement by gas chromatography mass spectrometry (GC-MS)

Cells were washed with PBS and the pellet was re-suspended in lysis buffer (80% methanol + 5% Trifluoroacetic acid) spiked with 2.5 μM 1,7-diaminoheptane (Sigma). The cell suspension, together with acid-washed glass beads (G8772, Sigma), was transferred to a bead beater tube and homogenized in a bead beater (Precellys 24, Bertin Technologies) for four cycles (6500 Hz, 45 s) with 1 minute of ice incubation between each cycle. The homogenized samples were centrifuged at 13,000 g for 20 minutes at 4 °C. The supernatant was collected and dried over night. For chemical derivatization, 200 μl trifluoroacetic anhydride was added to the dried pellet and incubated at 60 °C for 1 hour shaking at 1200 rpm. The derivatization product was dried, re-suspended in 30 μl isopropanol and transferred to glass loading-vials. The samples were analyzed using a GCxGC-MS system as described in Yu et al., 2017 (222). The following parameters were used for quantification of the 1D-GC-qMS data: Slope: 1000/min, width: 0.04 s, drift 0/min and T. DBL: 1000 min without any smoothing methods used.

2.16 Ribosome profiling

The sequencing library was prepared according to the reference (223, 224) with the following changes. The LPS-activated B cells were MACS-purified with the Dead Cell Removal Kit (Miltenyi) to remove dead cells prior to cell lysis. 100 μg/ml cycloheximide was used in the lysis buffer. The B cell lysate was spiked with the *S. cerevisiae* lysate at the ratio of 13 million B cells: 270

million yeast cells (which equals to 20:4 μg miRNA). Clarified B cell and yeast lysates were RNase I-digested, ribosome purified and miRNA extracted to determine the miRNA yield for spiking. Size exclusion chromatography (27-5140-01, GE Healthcare) was used to recover ribosomes. The miRNeasy Micro Kit (Qiagen) was used to purify miRNAs. The Ribo-Zero Gold rRNA Removal Kits (illumina, MRZG126, MRZY1306) were used to deplete ribosomal RNAs, in which the Ribo-Zero Removal Solutions from the mouse and yeast kits were mixed at the ratio of 8 μl : 4 μl to remove both mouse and yeast rRNAs. The following barcoding primers were used for next generation sequencing. 1. 5′-AATGATACGGCGACCACCGAGATCTACACGATCGGAAGAGCACACGTCTGAACTCCAGTCACATGCCAATCCGACGATCATTGATGG. 2. 5′-AATGATACGGCGACCACCGAGATCTACACGATCGGAAGAGCACACGTCTGAACTCCAGTCACTGCATCTCCGACGATCATTGATGG. The libraries were sequenced at the Biopolymers Facility, Harvard Medical School.

For the purposes of alignment, the reference genome assemblies for Mus musculus (GRCM38) and Saccharomyces cerevisiae (SacCer3) were concatenated to create a combined genome fasta file. A combined rRNA transcript file was also created using the sequences listed in Table S1. Prior to alignment, Adaptor sequence (ATCTCGTATGCCGTCTTCTGCTTG) was removed from demultiplexed reads and low quality reads (Phred score < 20) were discarded. To remove contaminating rDNA reads, reads were aligned to the combined rDNA genome using bowtie2 and all unaligned reads were kept

for alignment to the combined genome. Non-rDNA reads were aligned to the combined genome using bowtie2 and the following parameters: -t -N 1 and uniquely aligning reads were extracted using samtools view -bq 10.
All post-alignment analysis was performed using custom scripts written in R. P-site offsets for each read-length from 26 to 35 nts in the rpf libraries were determined by generating metagenes relative to the START codon and applied to aligned reads (Table S2). For all metagenes, transcripts with no reads within the window of interest were excluded from analysis before applying any other filters. Additionally, for each position in the windows of the 5' and 3' metagenes, the highest and lowest 0.1% of signals were removed from analysis.

The 100 most stalled PPP motifs were identified using the "stall-ratio" defined as the ratio of coverage over position +3 relative to the first proline against the mean coverage of the entire 80 bp window. The following filters were also applied to exclude windows with only a few sporadic spikes which may not reflect real translation. To be considered, a window must contain > 10 reads outside of the +3 position and the window must have reads in at least 5 positions. After applying these filters, the 100 genes with the highest stall-ratios were selected for metagenes.

2.17 Human samples

Peripheral blood mononuclear cells (PBMCs) were isolated by density gradient centrifugation from blood samples of healthy donors using Ficoll-

Paque. The mean age of old donors was 77.6±6.6 years and all subjects were gave written informed consent. The study was approved by the Ethics Committee of Oxford University.

2.18 Statistical analyses

The GraphPad Prism software was used for statistical analyses. Data are represented as mean ± SEM. Paired or unpaired two-tailed Student's t-test was used for comparisons between two normally distributed data sets with equal variances. One-tailed Student's t-test was used when the null hypothesis has a clear direction according to the knowledge (*e.g.* spermidine is an autophagy inducer rather than an inhibitor in multiple systems; Bafilomycin A1 treatment leads to the accumulation rather than the reduction of LC3-II). Welch's unequal variances t-test was used when the two normally distributed data sets have unequal variances. It is noteworthy that mostly in Chapter 3, t-test was used in comparisons between young and old mice with the null hypothesis "ageing makes no difference between young and old mice", and between old mice and old mice administered with spermidine with the null hypothesis "spermidine does change the parameter/function in old mice". Since the two null hypotheses are independent with each other, and each of them leads to an independent conclusion, statistical analyses were processed separately without pooling analyses together into one family. Therefore two independent t-tests were used without P value adjustment. Data are shown in one graph for visual convenience without changing statistics.

Paired or unpaired one-way ANOVA was used for multiple comparisons of normally distributed datasets with one variable. Paired or unpaired two-way ANOVA was used for multiple comparisons of normally distributed datasets with two variables. Mann-Whitney U test was used for comparisons between non-parametric datasets. Linear regression with 95% confidence interval was used to assess the relationships between age and the expression of target proteins or spermidine levels, in which R^2 was used to assess the goodness of fit and the P value calculated from F test was used to assess if the slope was significantly non-zero. P value was used to quantify the statistical significance of the null hypothesis (*i.e.* the averages were the same) testing. *P≤0.05, **P≤0.01, ***P≤0.001, ****P≤0.0001, ns, not significant.

Chapter 3. The Autophagy Inducer Spermidine Rejuvenates Humoral Immunity in Aged Mice

3.1 Introduction

3.1.1 Murine B cell development

Two types of B cells have been identified in mice, B1 B cells and B2 B cells respectively. B2 B cells are conventional B cells functioning in adaptive immunity, whereas B1 B cells participate in innate immunity secreting poly-specific autoantibodies against self and bacterial antigens such as phosphatidylcholine. I will focus on B2 B cells in this thesis and hereafter B2 B cells are referred to as B cells.

In adult mice, B cells are derived from HSCs in the bone marrow. HSCs generate common lymphoid progenitors (CLPs), which then pass through progenitor B cells (pro-B cells), precursor B cells (pre-B cells), and eventually mature naïve B cells (Fig 3.1).

B cell development is associated with the maturation of B cell receptor (BCR). In contrast to HSCs and CLPs, which have germline genes for BCR and no surface BCR expression, pro-B cells initiate a series of somatic recombination events to form mature diverse BCRs to cope with various antigen epitopes. BCR is a membrane-bound immunoglobulin, which typically comprises two heavy chain subunits and two light chain subunits. Both the heavy (H) chain and the light (L) chain contain one variable domain (V_H or V_L) and several constant domains. The possibly random and error prone DNA recombination of V, D, and J gene segments within the variable domain results in the generation of a highly diverse BCR repertoire. The V-D-J recombination, with the constant domains added later, results in the production of a μH chain.

Then the μH chain is paired with a surrogate light (SL) chain to form a pre-BCR and expressed on cell surface (Fig 3.1) (225). Developing B cells with deficient pre-BCR by either μH mutation (226) or SL chain mutation (227) are arrested at the pre-B cells stage, indicating that the expression of pre-BCR serves as a critical checkpoint for pre-B cell development. Pre-BCR signaling induces the proliferation of pre-B cells (228) and the down regulation of the SL chain. Then the V-J recombination of the light chain gene happens and the mature light chain substitutes SL chain to form mature BCR (Fig 3.1) (surface IgM). Low auto-reactive B cells with self-tolerant BCRs are selected and migrate out of the bone marrow to enter peripheral lymphoid organs and become mature naïve B cells (229).

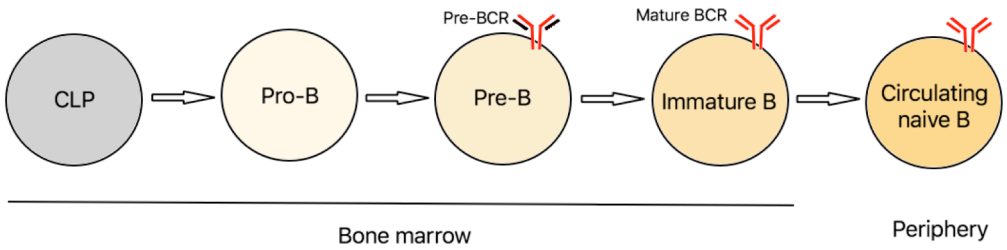


Fig 3.1 Schematic overview of B cell development. CLPs in bone marrow differentiate into Pro-B cells, Pre-B cells, immature B cells and eventually mature naïve B cells which then migrate into the periphery. Differentiation of B cells is accompanied with the maturation of BCR.

Defects of B cell development and selection may lead to malignancy and autoimmune diseases. Self-reactive B cells that have failed to undergo anergy or apoptosis will secrete auto-antibodies, and also function as antigen-

presenting cells to assist T cell-mediated autoimmune reactions. Both auto-reactive antibodies and T cells will lead to tissue damage and autoimmune diseases such as systemic lupus erythematosus and type 1 diabetes (230).

3.1.2 B cell activation

Mature naïve B cells can be activated in different ways to proliferate and differentiate into plasmablasts and then plasma cells. Several bacterial or virus components can directly activate B cells in a T cell-independent manner. There are two types of T independent antigens. Type I includes molecular patterns of bacterial or viral infections such as lipopolysaccharide (LPS) and pathogen DNA/RNA containing CpG motifs or polyinosinic-polycytidylic acid (poly IC), which activate Toll-like receptors of B cells and induce their proliferation and differentiation. The B cell activation induced by type I Toll-like receptor is BCR-independent and thus not antigen-specific. Type II mainly contains repetitive epitopes such as polysaccharides on pathogens. These repetitive epitopes are recognized by multiple cognate BCRs and cause their cross-linking and activation. It has been reported that type II T-independent activation of B cells can generate IgM^+ memory B cells which are like naïve B cells in terms of their lifespan and the sensitivity to antigens (231).

Most antigens activate B cells in a T cell-dependent manner (Fig 3.2). The majority of naïve B cells reside in a special zone called follicles in secondary lymphoid organs, and these B cells are called follicular B cells. When naïve follicular B cells encounter their cognate antigens, they first function as

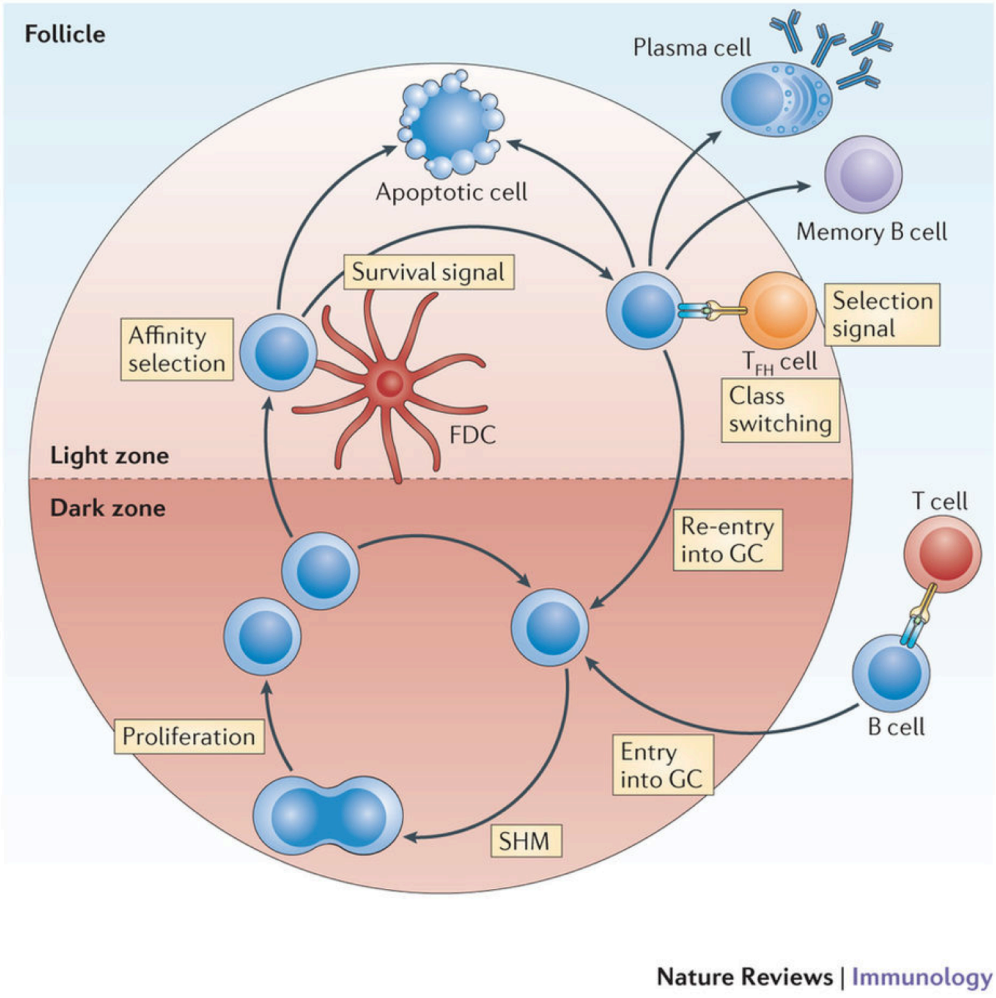


Fig 3.2 Schematic overview of T-dependent B cell activation, focusing on germinal centre reactions. B cells receive co-stimulatory signals from cognate T cells and migrate into the dark zone of the GC, where they undergo several rounds of proliferation and SHM before entering the light zone. In the light zone, the mutated BCRs are exposed to antigens on FDCs and B cells with low-affinity BCRs will undergo apoptosis. Surviving B cells in the light zone will undergo class-switching with the help of T_{FH} cells and then either re-enter into dark zone, or differentiate into memory B cells or plasma cells. Modified from (1).

antigen-presenting cells and present these antigens to their cognate $CD4^+$ T cells together with dendritic cells (232). Activated $CD4^+$ T cells migrate to follicles to become follicular helper T cells (T_{FH} cells), which will then secret cytokines such as IL-4 and up regulate CD40L to assist B cell activation.

Some proliferating B cells will differentiate into short-lived plasma cells which mostly secrete low-affinity IgM as a quick humoral response. Alternatively, proliferating B cells can also enter a distinct region in follicles called germinal centre (GC) for germinal centre reactions (Fig 3.2). A key enzyme for germinal centre reactions is AID, a single-stranded DNA-specific cytidine deaminse induced in activated B cells (233). It functions to deaminate a cytosine base into a uracil base to cause DNA mutations, which is required for class switching and somatic hypermutation (234). Consistent with the phenotype in AID-deficient mice, AID mutations in human also cause the hyper-IgM syndrome including the absence of class switching and somatic hypermutations of immunoglobulin (235). Germinal centre B cells undergo several rounds of proliferation, class switching, somatic hypermutation (SHM), and affinity selection with the help of T_{FH} cells and follicular dendritic cells (FDCs) (Fig 3.2) (1).

The products of germinal centre reactions are class-switched high-affinity plasma cells and memory B cells. Eventually some high-affinity plasma cells home to bone marrow (236) and become long-lived plasma cells. Long-lived plasma cells and memory B cells constitute long-term humoral immunity (236).

Class-switched memory B cells generated from germinal centre reactions can quickly respond to secondary infections and then proliferate and differentiate into plasma cells (and also new memory B cells) to give rise to a robust secondary humoral response (236). Another type of memory B cells, the IgM^+ memory B cells, has also been reported (236). They are more abundant and even longer-lived than class-switched memory B cells, but with less somatic hypermutation (236). They are generated early in primary responses in a germinal centre-independent manner (237). These IgM^+ memory B cells retain the ability to enter germinal centre reactions and may sustain the humoral memory in the long run (236).

Chapter 3. The Autophagy Inducer Spermidine Rejuvenates Humoral Immunity in Aged Mice

3.2 Results

3.2.1 Phenotypic changes of the haematopoiesis in old mice

To assess the overall phenotypic changes of the haematopoietic system in old mice (22 to 24 months) as compared to young mice (12 weeks), flow cytometry was used to identify various haematopoietic lineages, from haematopoietic stem cells in bone marrow to mature lymphoid and myeloid lineages in peripheral blood and spleen. A group of old mice were administered with the autophagy inducer spermidine in the drinking water for 6 weeks to assess the effect of spermidine on their haematopoietic system.

Both the ratio and the absolute number of HSCs ($CD150^+CD48^-LSK$), multipotent progenitor cells (MPPs, $CD150^-CD48^-LSK$), and LSKs ($Lineage^-Sca1^+cKit^+$, a population containing HSCs and MPPs) in bone marrow were significantly increased in old mice (Fig 3.3). In contrast, lymphoid-biased multipotent progenitor cells (LMPPs) remained unchanged in old mice (Fig 3.3). Neither the ratio nor the number of these populations were altered by spermidine administration (Fig 3.3), indicating that spermidine does neither suppress nor promote the self-renewal or proliferation of haematopoietic stem and progenitor cells, at least not after 6 weeks of continuous administration.

A biased differentiation towards myeloid lineages is a well-defined feature of the aged haematopoietic stem cells in mice. Accordingly, it was observed that multiple myeloid progenitors were expanded in old mice, including megakaryocyte progenitors (MkPs), granulocyte-macrophage progenitors (GMPs), pre-granulocyte/macrophages (Pre-GMs), pre-

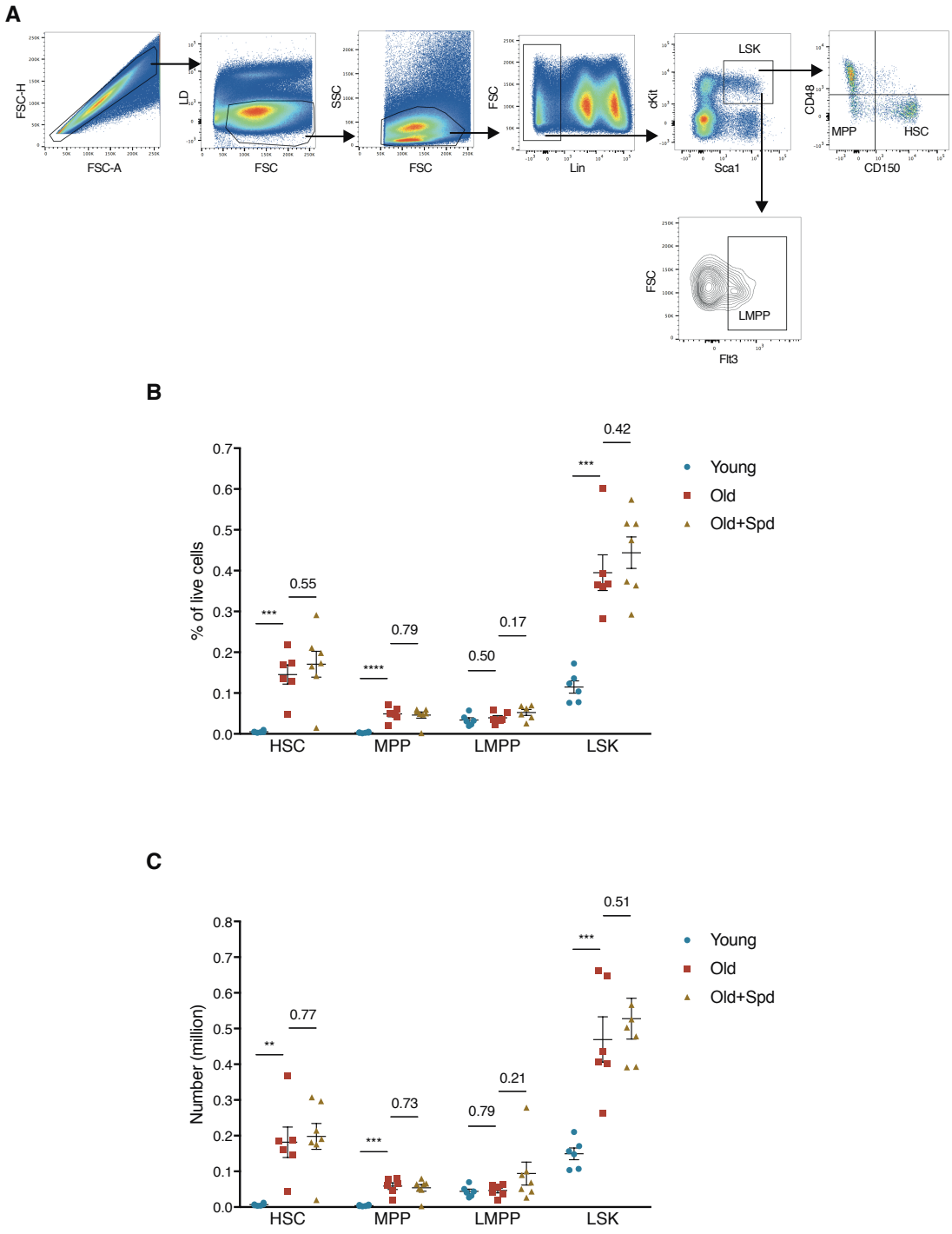


Fig 3.3 Expanded HSCs in bone marrow from old mice. Bone marrow HSCs and MPPs from young (12 weeks), old (22-24 months), and old mice continuously administered with spermidine in drinking water for 6 weeks were assessed by flow cytometry. **A.** Gating strategy for LSK (Lin^- $Sca1^+cKit^+$), HSC ($LSK^+CD48^-CD150^+$), MPP ($LSK^+CD48^-CD150^-$), and LMPP (LSK^+Flt3^+). Relative ratio and absolute number in bone marrow are shown in **B** and **C** respectively. Lin mix: CD4, CD5, CD8a, CD11b, B220, Ter119, Gr1. Data represented as mean ± SEM. n = 6 to 7 mice per group as indicated by dots. Student's t-test with P values labeled out as, **P≤0.01, ***P≤0.001, ****P≤0.0001.

megakaryocytes/erythrocytes (pre-MegEs), and pro-erythroblast cells (Pro-Erys) (Fig 3.4) (238).

The development of B cells was assessed by flow cytometry staining of Hardy fractions (239). The $CD43^+B220^+$ population mainly refers to pro-B cells, with fractions A, B and C correlated with germline pro-B cells (pre-pro-B cells), early pro-B cells, and late pro-B cells. Fractions D, E and F within the CD43-$B220^+$ population are correlated with pre-B cells, newly formed immature B cells, and mature B cells (Fig 3.6A/B). A mild but significant increase of pro-B cells ($CD43^+B220^+$, fraction A/B/C) was observed in old mice, whereas the ratio and number of pre-B cells (fraction D) or newly formed B cells (fraction E) were not changed (Fig 3.6). The observation of accumulated pro-B cells but unaltered pre-B cells and newly formed B cells in old mice is consistent with literatures proposing that there might be a differentiation block from pro-B cells to pre-B cells in old mice (191). Meanwhile the exit of newly formed B cells out of bone marrow is reduced in old mice, leading to a slow turn over of bone marrow B cells with the overall number unchanged (191).

No significant changes of the ratio or number of myeloid progenitors and B cell progenitors caused by spermidine administration was observed (Fig 3.4/5). Therefore, the 6-week administration of spermidine did neither affect the early developmental stages of the haematopoietic system, including the self-renewal and differentiation of HSCs, nor the early developmental stages of myeloid and B cell progenitors in old mice. However, spermidine could still

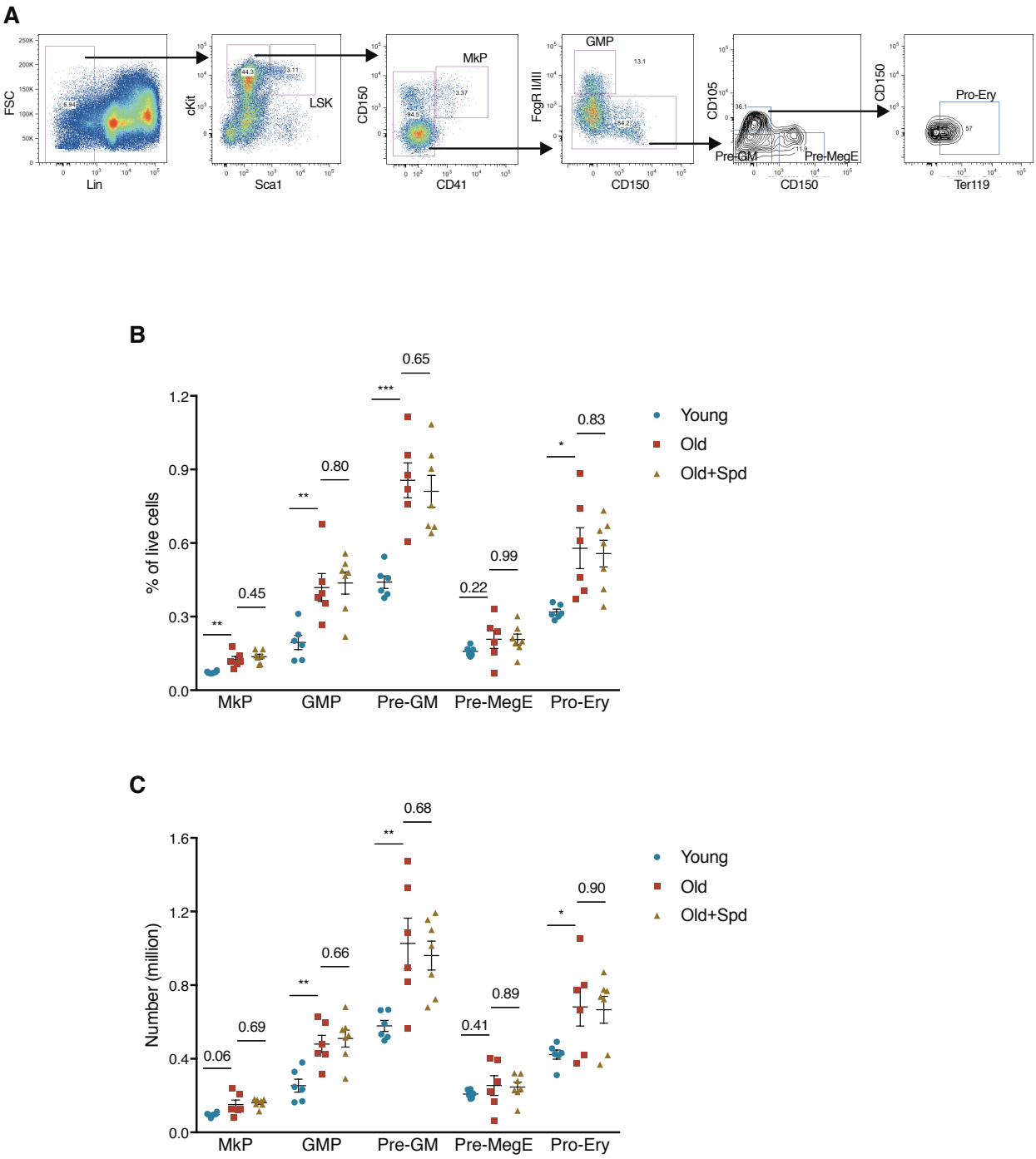


Fig 3.4 Expanded myeloid progenitors in bone marrow from old mice. **A.** Gating strategy for MkP ($Lin^-Sca1^-cKit^+CD41^+CD150^+$), GMP ($Lin^-Sca1^-cKit^+CD41^-CD150^-FcR\ II/III^+$), Pre-GM ($Lin^-Sca1^-cKit^+CD41^-FcR\ II/III^-CD150^-CD105^-$), Pre-MegE ($Lin^-Sca1^-cKit^+CD41^-FcR\ II/III^-CD150^+CD105^-$), and Pro-Ery ($Lin^-Sca1^-cKit^+CD41^-FcR\ II/III^-CD150^-CD105^+Ter119^+$). Relative ratio and absolute number in bone marrow are shown in **B** and **C** respectively. Lin mix: CD4, CD5, CD8a, CD11b, B220, Ter119, Gr1. Data represented as mean ± SEM. n = 6 to 7 mice per group as indicated by dots. Student's t-test with P values labeled out as, *P≤0.05, **P≤0.01, ***P≤0.001.

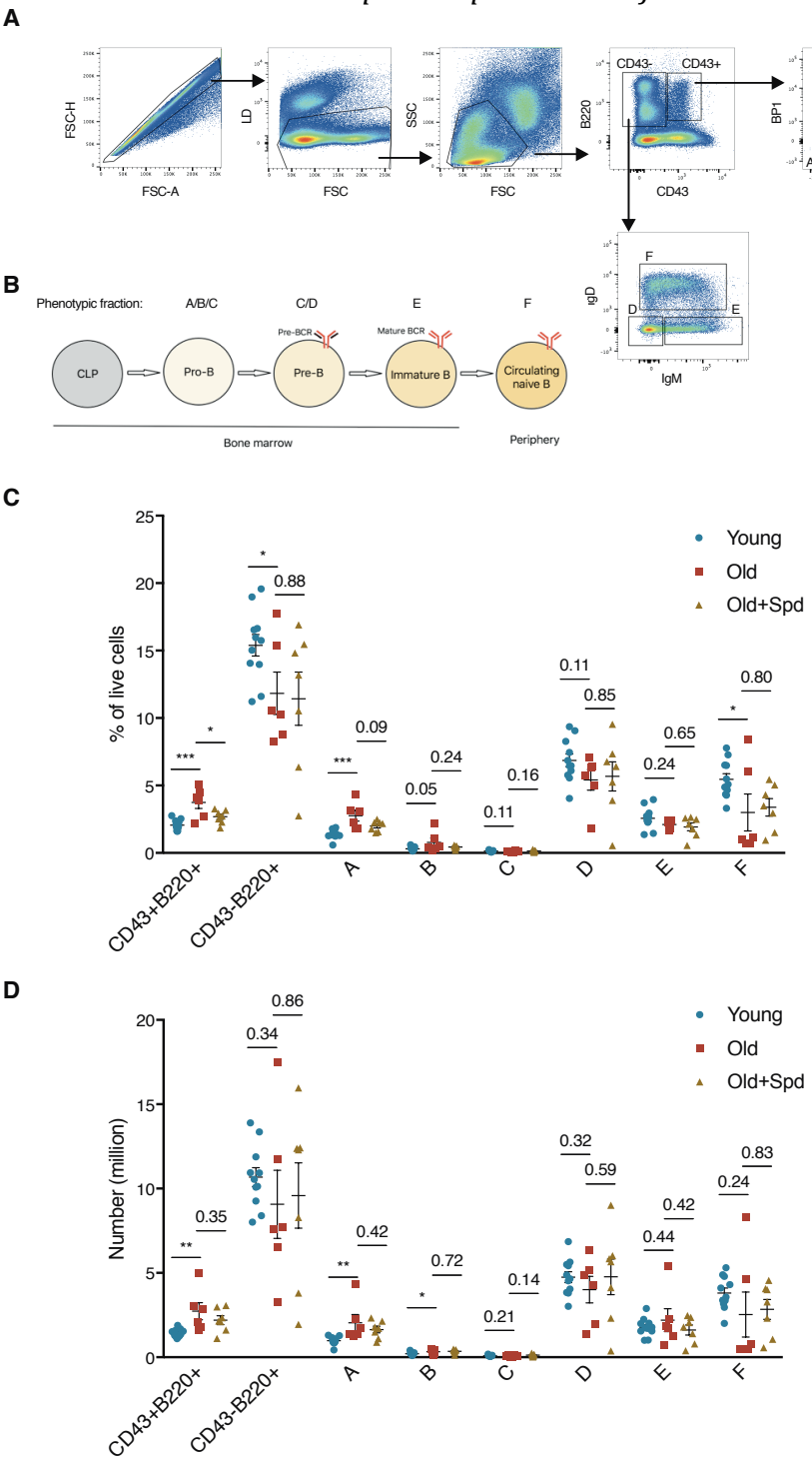


Fig 3.5 Accumulated B cell progenitors in bone marrow from old mice. **A.** Gating strategy for Hardy fractions A ($B220^+CD43^+CD24^-BP1^-$), B($B220^+CD43^+CD24^+BP1^-$), C($B220^+CD43^+CD24^+BP1^+$), D($B220^+CD43^-IgM^-IgD^-$), E($B220^+CD43^-IgM^+IgD^-$), and F($B220^+CD43^-IgD^+$). **B.** Correlation between phenotypic fractions and developmental stages. Relative ratio and absolute number in bone marrow are shown in **C** and **D** respectively. Data represented as mean ± SEM. n = 7 to 11 mice per group as indicated by dots, pooled from 2 independent experiments. Student's t-test with P values labeled out as, *P≤0.05, **P≤0.01, ***P≤0.001.

have an impact on later developmental stages, *i.e.* from precursors to mature lineages. These stages can be distinguished by changes of mature lineages in the periphery.

In both spleen and peripheral blood, an obvious myeloid-biased phenotype was also observed in old mice. Myeloid cells ($CD11b^+Gr1^+$) were significantly increased, whereas lymphoid cells, including B cells, $CD4^+$ T cells, and $CD8^+$ T cells, were all significantly reduced (Fig 3.6/7). The majority of T cells in old mice were $CD44^{hi}$ (Fig 3.8), which is a marker of clonally expanded T cells, indicating the expansion of existing mature T cells and a lack of naïve T cells input. Neither the lymphopenia nor the expansion of myeloid cells in peripheral was rescued by spermidine administration (Fig 3.6/7), except for a significant increase of $CD8^+$ T cells in peripheral blood (Fig 3.7). The input of naïve T cells (non-$CD44^{hi}$) was not changed by spermidine either (Fig 3.8). Therefore spermidine administration failed to exert an effect on the overall haematopoiesis from HSCs to mature lineages in old mice.

Additionally, a mild increase in the spleen cellularity in old mice was observed (Fig 3.9), which is consistent with the splenomegaly phenotype as reported (240). Interestingly, spermidine administration significantly reduced the spleen cellularity. Increased inflammatory cytokines such as IL6, IL23, and TNF can be the cause of splenomegaly in mice (241-244). Spermidine has been shown to reduce the TNF-α levels in old mice, which can be an explanation of this effect.

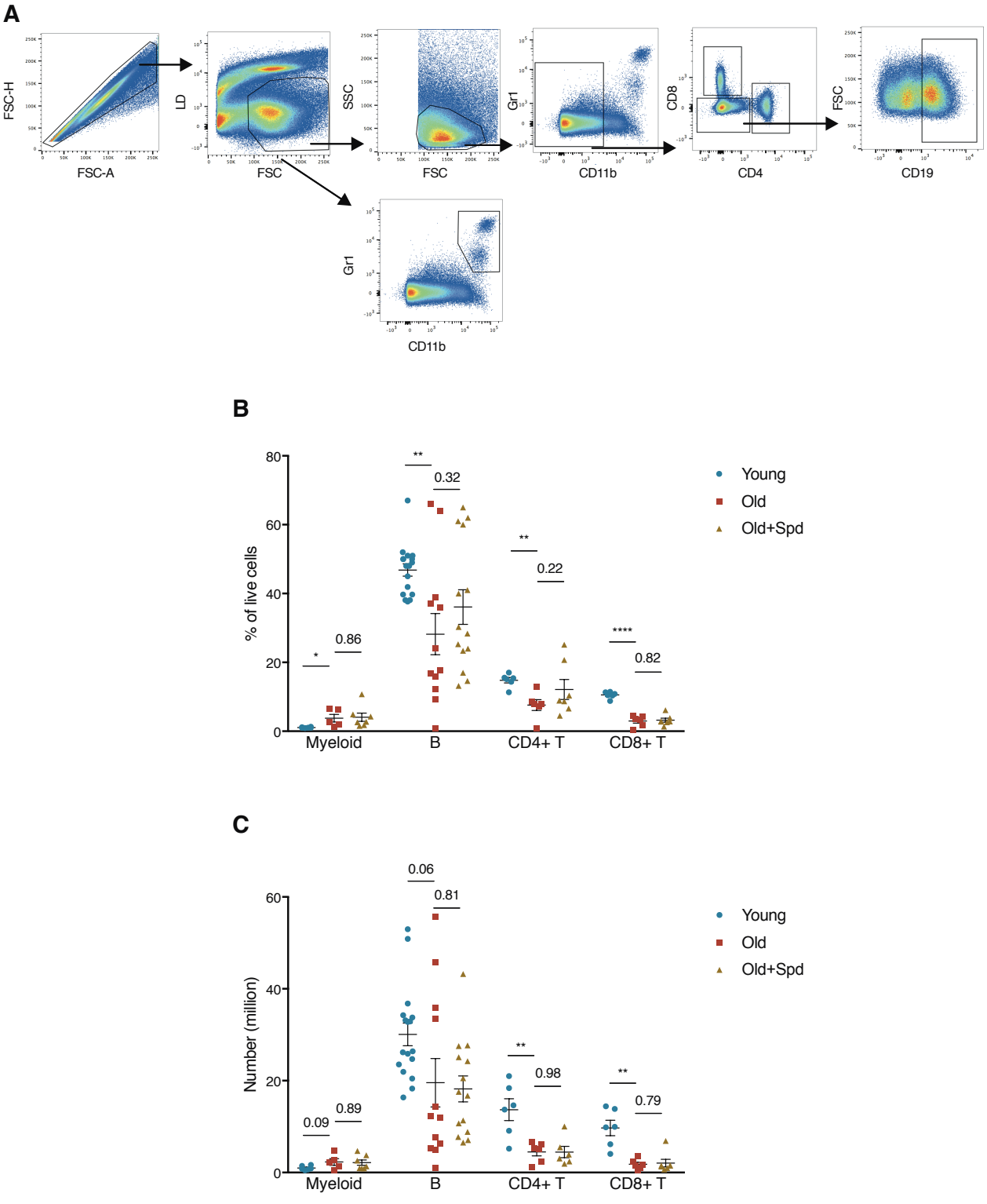


Fig 3.6 Spleen lineages are myeloid-biased in old mice. **A.** Gating strategy for myeloid cells ($CD11b^{+}Gr1^{+}$), $CD8^{+}$ T cells ($CD11b^{-}CD8^{+}$), $CD4^{+}$ T cells ($CD11b^{-}CD4^{+}$), and B cells ($CD11b^{-}CD4^{-}CD8^{-}CD19^{+}$). Relative ratio and absolute number in spleen are shown in **B** and **C** respectively. Data represented as mean ± SEM. n = 6 to 17 mice per group as indicated by dots, pooled from 2 independent experiments. Student's t-test with P values labeled out as, *P≤0.05, **P≤0.01, ****P≤0.0001.

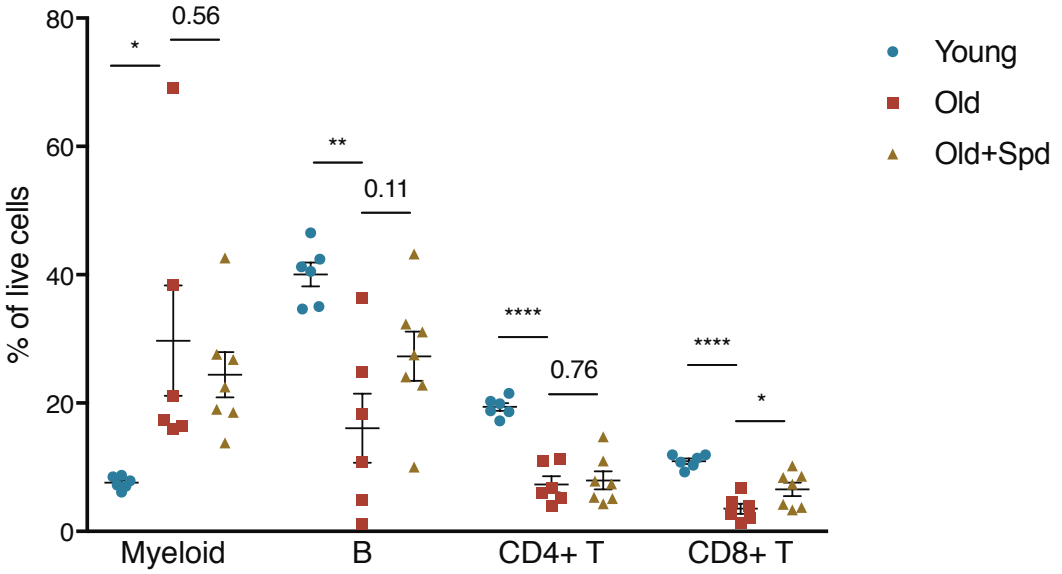


Fig 3.7 Peripheral blood lineages are myeloid-biased in old mice. Data represented as mean ± SEM. n = 6 to 7 mice per group as indicated by dots. Student's t-test with P values labeled out as, *P≤0.05, **P≤0.01, ****P≤0.0001.

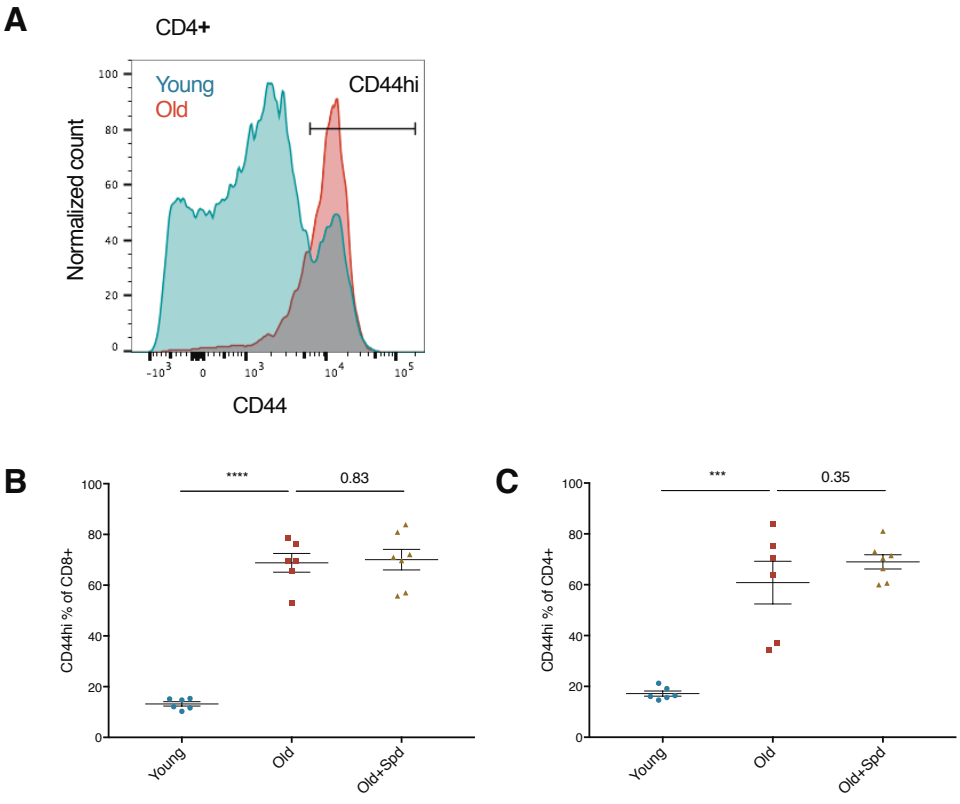


Fig 3.8 CD44^{hi} memory-like T cells are accumulated in old mice. **A.** Representative CD44 staining of CD4^{+} T cells. **B/C.** Quantification of CD44^{hi} in CD8^{+} T cells (**B**) and CD4^{+} T cells (**C**). Data represented as mean ± SEM. n = 6 to 7 mice per group as indicated by dots. Student's t-test with P values labeled out as, ***P≤0.001, ****P≤0.0001.

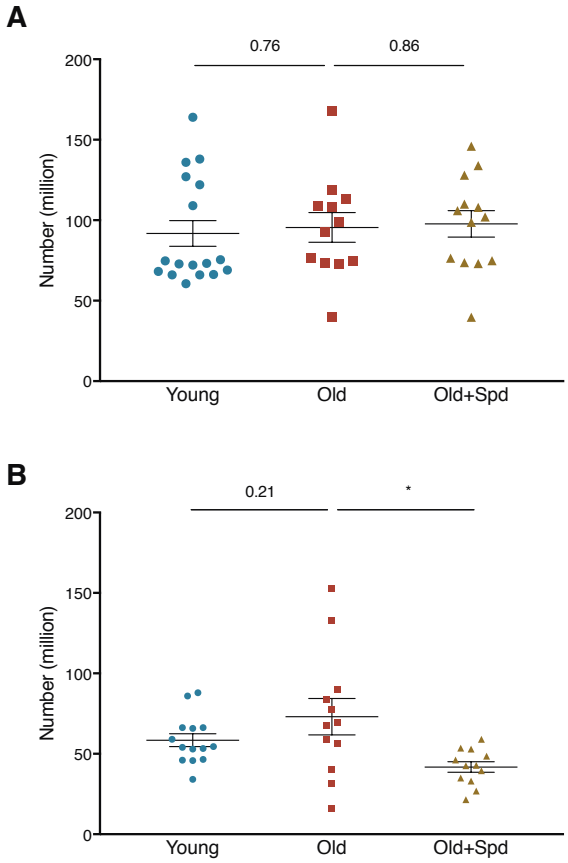


Fig 3.9 Bone marrow and spleen cellularity in young, old, and old mice administered with spermidine. Bone marrow cells from both sides of femur and tibia (A) and spleen cells (B) were collected from young, old, and old mice administered with spermidine for 6 weeks and counted with flow cytometry-counting beads. Data represented as mean ± SEM. n = 12 to 14 mice per group as indicated by dots, pooled from 2 independent experiments. Student's t-test with P values labeled out as, *P≤0.05.

3.2.2 Bone marrow cells from old mice reconstitute well into recipients

I did not observe a reverse of the myeloid bias in heamatopoietic progenitors and peripheral mature immune cells by spermidine administration *in situ*. However it remains possible that the improvement of HSC function was diluted by the already heavily expanded progenitors. To directly assess the functions of HSCs, bone marrow chimera mice were made by transferring a defined number of bone marrow cells from young, old, or old mice administered with spermidine (all of CD45.2 allotype) to lethally irradiated young recipients (CD45.1 allotype) (Fig 3.10). After 16 weeks of long-term reconstitution, the haematopoietic system of recipient mice was assessed.

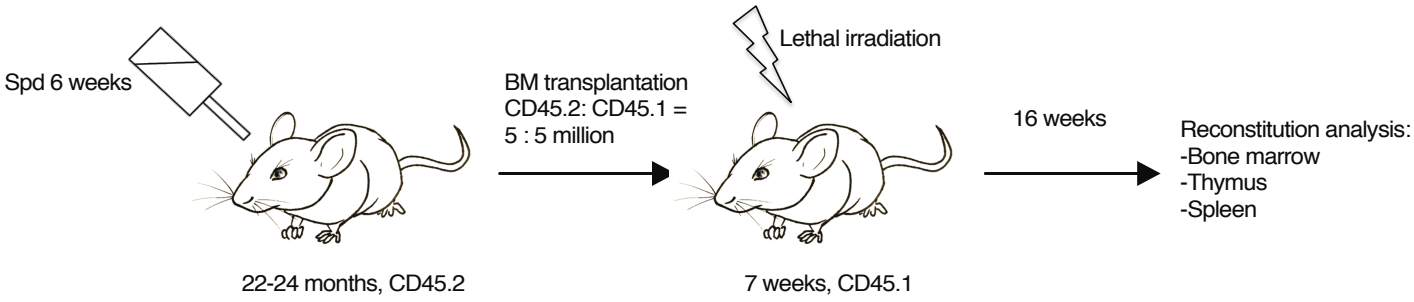


Fig 3.10 Use competitive bone marrow chimera to assess HSCs reconstitution ability. Bone marrow cells taken from mice treated as in Fig 3.3 ($CD45.2^+$) were mixed with the competitor bone marrow cells taken from 7 weeks old $CD45.1^+$ mice at the ratio of 5 : 5 million, and injected i.v. into lethally irradiated $CD45.1^+$ recipient mice. After 16 weeks, the long-term reconstitution of bone marrow haematopoietic stem and progenitor cells, thymus T progenitors, and spleen mature lineages were assessed in recipient mice by staining for CD45.1 (competitor/control) or CD45.2 (test).

It was found that bone marrow from old mice had a higher reconstitution capacity for HSCs and LSKs compared to bone marrow from young mice (Fig 3.11A-C) as reported (245). This is consistent with the increased number of HSCs as observed in old mice (Fig 3.3). The reconstitution of LMPPs is, however, comparable between young and old donors (Fig 3.11D), indicating the attenuated LMPP reconstitution ability of HSCs from old mice at the single-cell level. Spermidine mildly augmented the reconstitution of HSCs

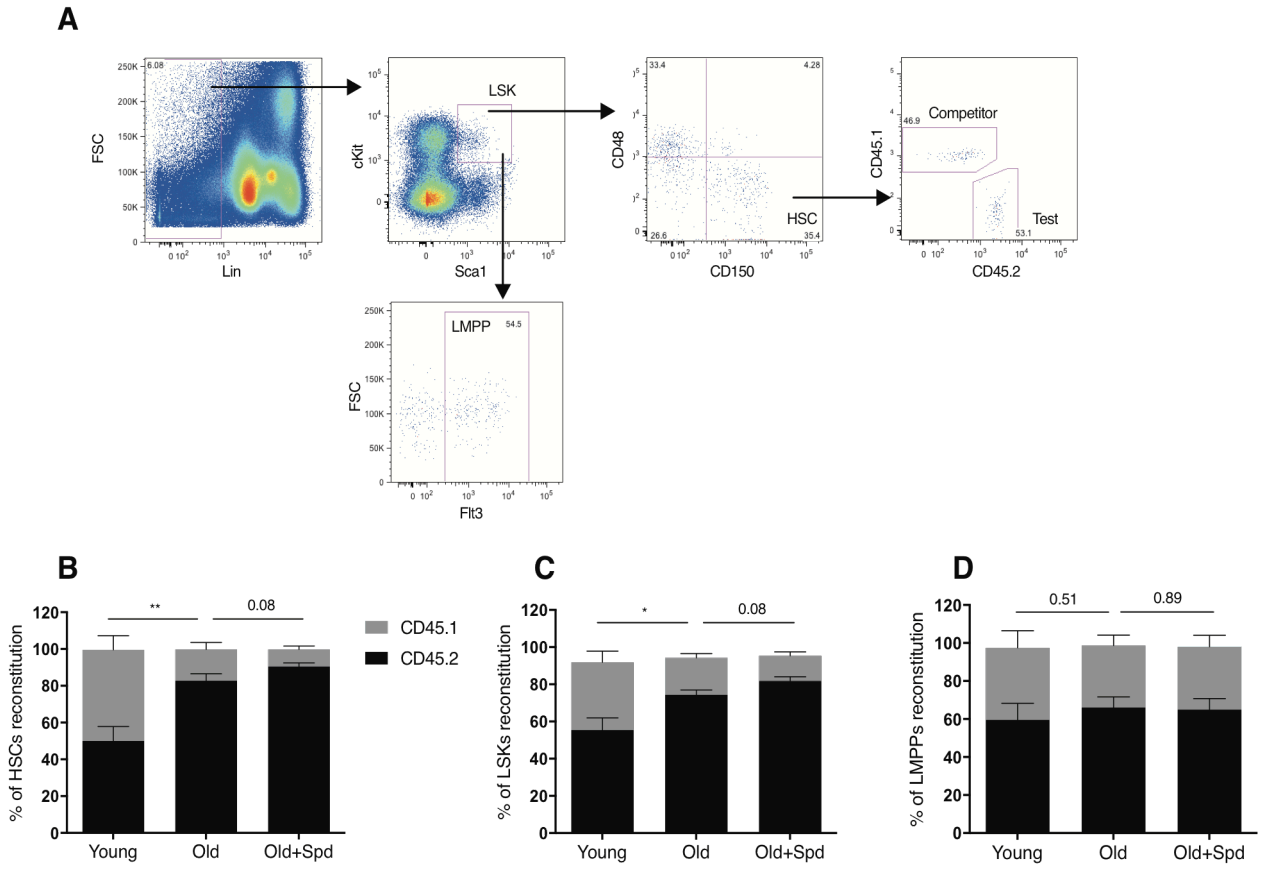


Fig 3.11 Old bone marrow cells have a higher reconstitution ability of HSCs. **A.** Gating strategy showing the CD45.1/CD45.2 staining of HSCs. Quantification results are shown in **B** (HSCs), **C** (LSKs), and **D** (LMPPs). Data represented as mean ± SEM. n = 6 to 10 mice per group. Student's t-test of $CD45.2^+$ fractions with P values labeled out, *P≤0.05, **P≤0.01.

from old bone marrow (not statistically significant, Fig 3.11). Therefore bone marrow from old mice is not only competent, but even more capable in reconstituting HSCs than young mice due to the elevated numbers of HSCs that possibly compensate for functional loss.

Despite of the significantly increased reconstitution of HSCs, the reconstitution of myeloid progenitors, including MkPs, GMPs, Pro Erys, Pre GMs, and Pre MegEs, was only mildly but not significantly increased from old bone marrow (Fig 3.12A-F). The reconstitution of mature myeloid lineages in spleen from old bone marrow was found significantly increased compared to young bone marrow (Fig 3.12A/G), consistent with the phenotype in old mice (Fig 3.4). Therefore the increased production of myeloid progenitors and mature myeloid lineages in old mice is partly due to intrinsic changes of HSCs. The reason why old mice accumulate many more myeloid progenitors compared to chimera mice receiving old bone marrow can either be attributed to a longer period of time required for this accumulation, but more likely is an age-related change extrinsic to HSCs. Spermidine administration did not affect the reconstitution of myeloid progenitors and mature myeloid lineages (Fig 3.12).

T lymphopenia is a distinct phenotype of the aged haematopoietic system. However, it was found that bone marrow from old mice gives rise to comparable thymic T cell progenitors compared to young bone marrow (Fig 3.13A-F), and eventually comparable mature T cells in spleen (Fig 3.13A/G).

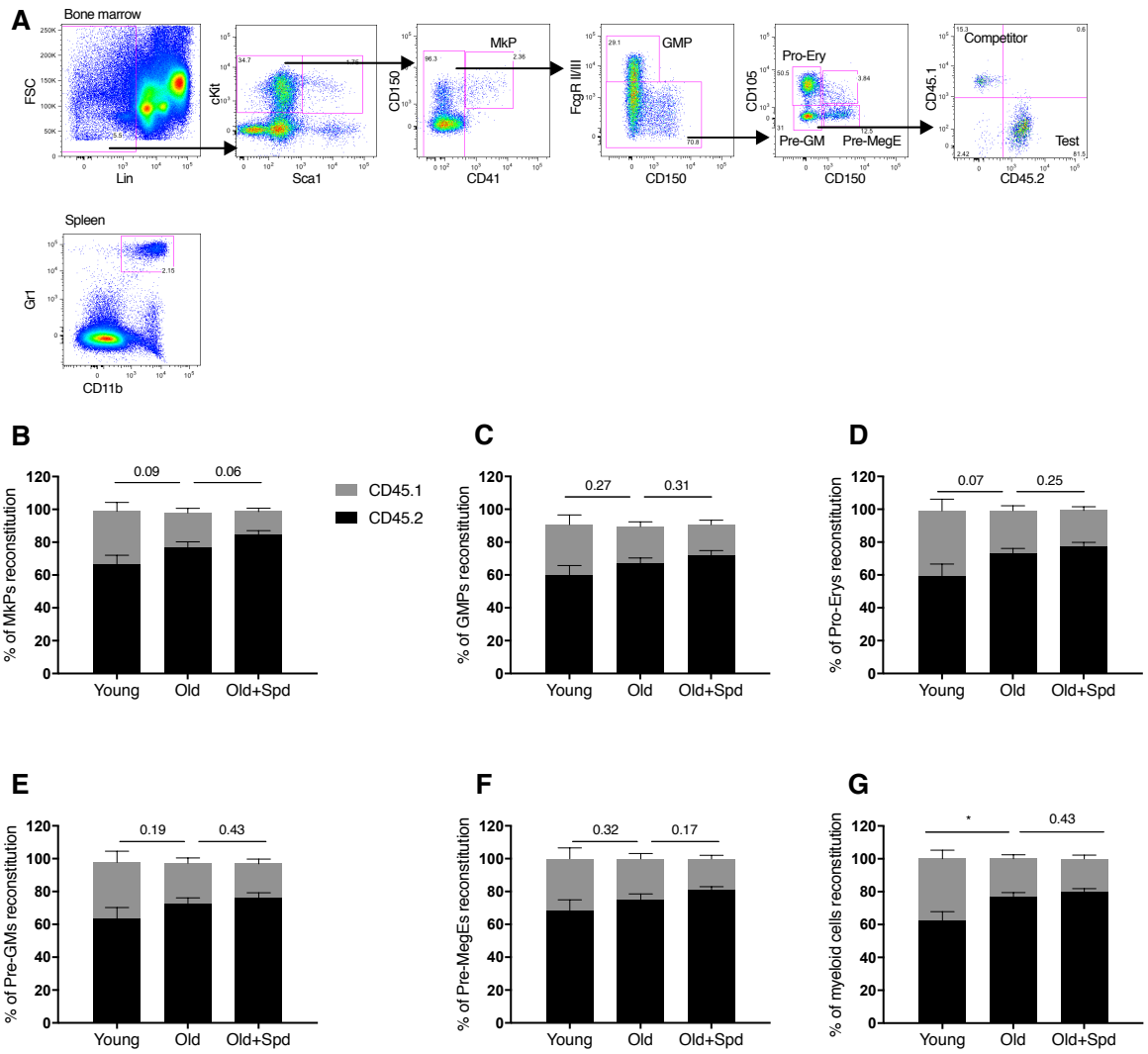


Fig 3.12 Comparable reconstitution ability of myeloid progenitors between young and old bone marrow. **A.** Gating strategy showing the CD45.1/CD45.2 staining of the Pre-GM population. Quantification results are shown in **B** (MkPs), **C** (GMPs), **D** (Pro-Erys), **E** (Pre-GMs), **F** (Pre-MegEs), and **G** (spleen myeloid cells). Data represented as mean ± SEM. n = 6 to 10 mice per group. Student's t-test of $CD45.2^+$ fractions with P values labeled out, *P≤0.05.

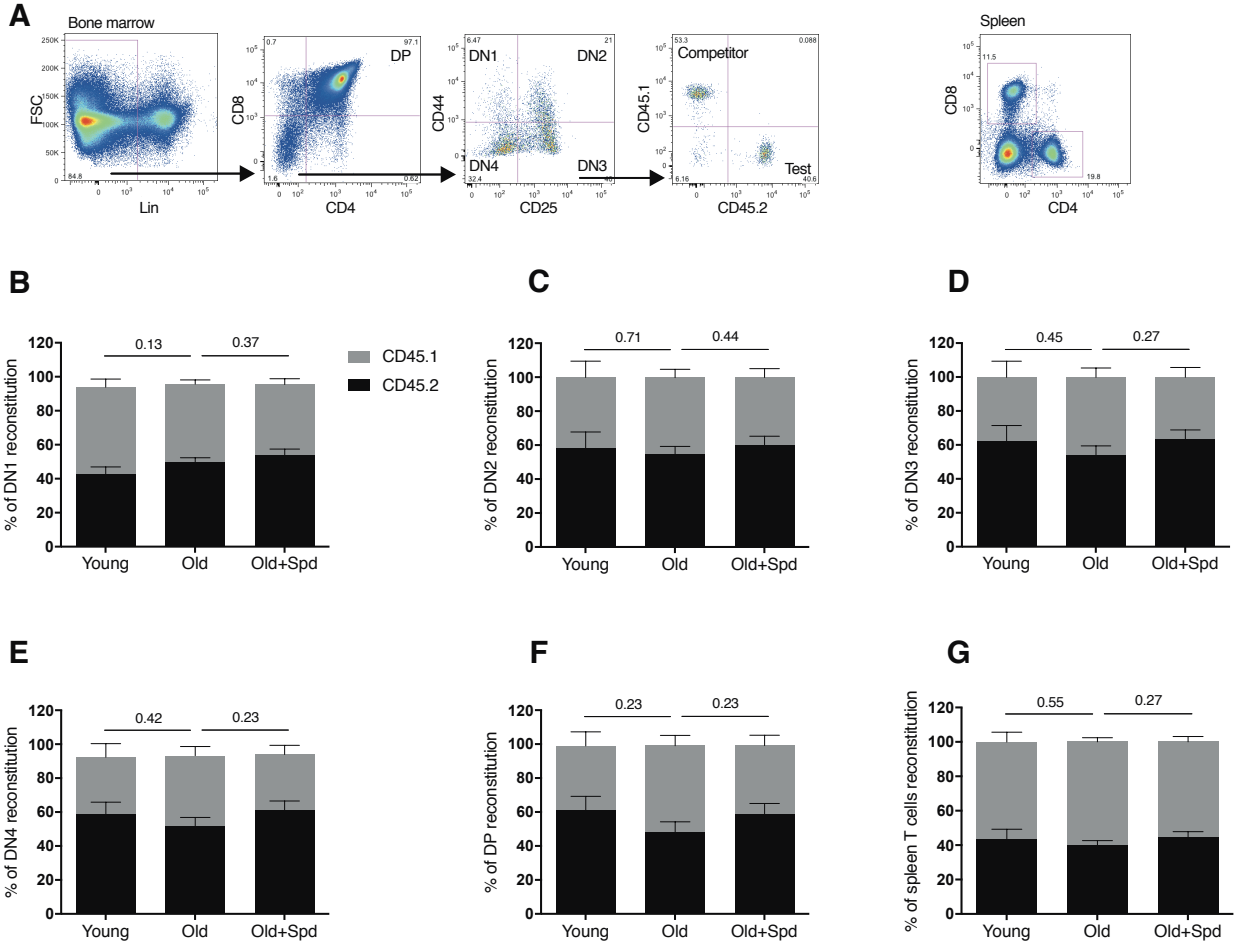


Fig 3.13 Comparable reconstitution ability of T cell progenitors between young and old bone marrow. **A.** Gating strategy showing the CD45.1/CD45.2 staining of the DN3 population. Quantification results are shown in **B** (DN1, early thymic progenitors), **C** (DN2), **D** (DN3), **E** (DN4), **F** (DP), and **G** (the sum of spleen $CD4^+$ and $CD8^+$ T cells). Lin mix: CD3e, TCRg, TCRb, NK1.1, B220, Ter119, Gr1, CD11b, CD11c. Data represented as mean ± SEM. n = 6 to 10 mice per group. Student's t-test of $CD45.2^+$ fractions with P values labeled out.

Therefore T lymphopenia in old mice is largely attributed to changes independent of HSCs, such as thymic involution. Accordingly, old and young bone marrow contributed equally to T-cell development and spermidine administration did not affect the reconstitution of T cell progenitors and mature T lineages in recipients (Fig 3.13).

Similarly, B cell development is not remarkably affected in old mice. Accordingly, bone marrow from old mice was competent to produce new B cell progenitors and mature B cells in recipient mice (Fig 3.14). Spermidine administration did not affect B cell reconstitution either (Fig 3.14).

Therefore marked changes in haematopoiesis in old mice were observed as expected, but spermidine administration exhibited little effect on the overall developmental process.

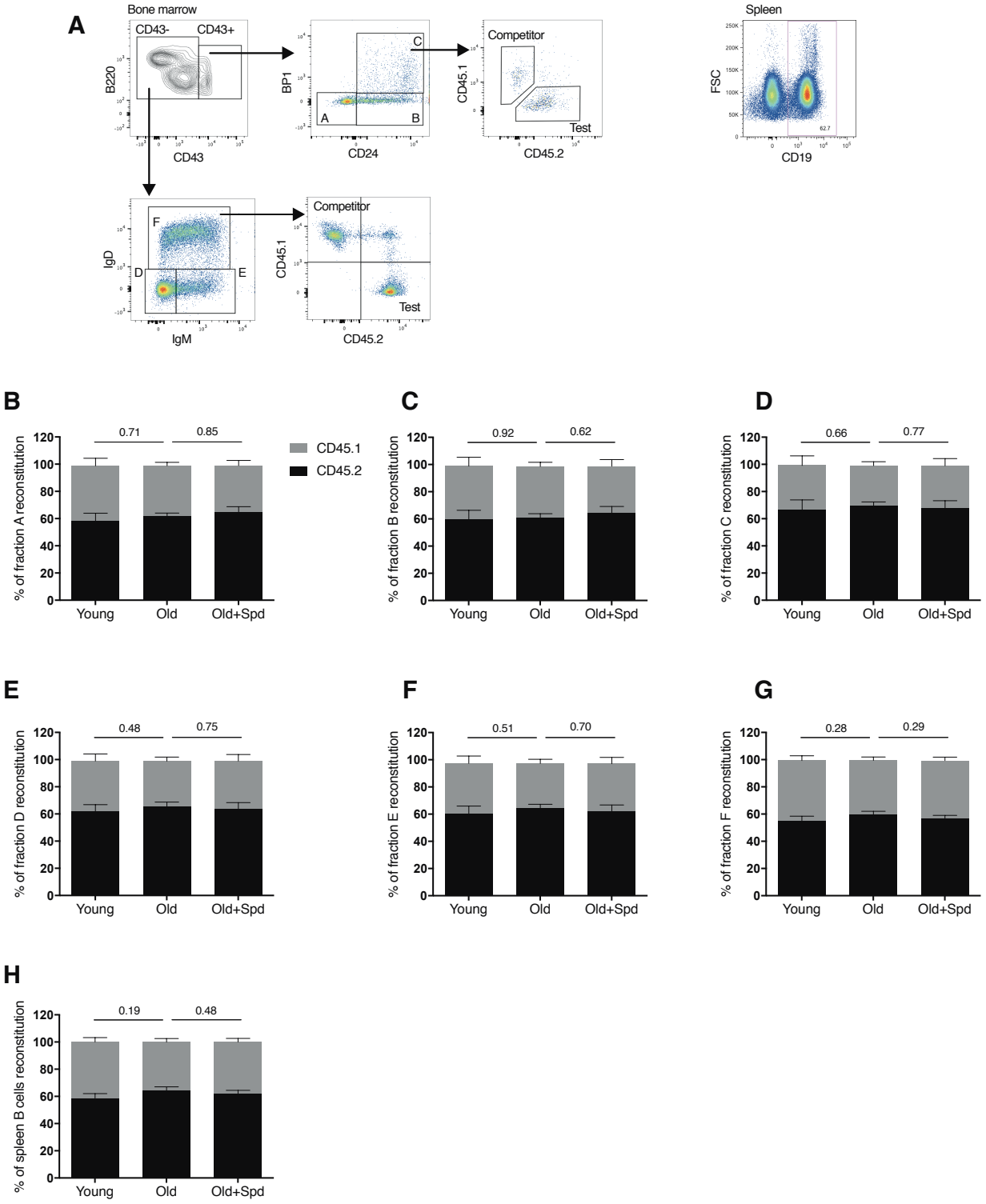


Fig 3.14 Comparable reconstitution ability of B cell progenitors between young and old bone marrow. **A.** Gating strategy showing the CD45.1/CD45.2 staining of fraction C and F. Quantification results are shown in **B** (fraction A), **C** (fraction B), **D** (fraction C), **E** (fraction D), **F** (fraction E), **G** (fraction F), and **H** (spleen B cells). Data represented as mean ± SEM. n = 6 to 10 mice per group. Student's t-test of $CD45.2^+$ fractions with P values labeled out.

3.2.3 Autophagy is impaired in lymphocytes from old mice

Autophagy has been reported to be impaired during ageing in multiple tissues and cell types including mouse/human neuron (246, 247), mouse skeletal muscle (57), and mouse/human T cells (59, 170). Using a newly developed autophagy detection kit based on LC3-II flow cytometry staining, uniquely able to identify the different haematopoietic lineages, while evaluating the autophagic flux (Fig 3.15). Addition of Bafilomycin A1 (BafA1), a lysosomal V-ATPase inhibitor which prevents the acidification of lysosomes, results in blocked autophagosome-lysosome fusion and lysosomal degradation. BafA1 treatment causes the accumulation of both the autophagic cargo and the autophagosome marker LC3-II, the latter being therefore an indicator of the dynamic autophagic flux. I found a general reduction of autophagic flux during differentiation in both young (12 weeks) and old (22-24 months) mice, with HSCs possessing the highest autophagic flux and spleen myeloid cells the lowest (Fig 3.15B). Moreover, autophagy is not evenly affected in different cell types. Autophagic flux is most significantly reduced in mature lymphocytes, including spleen B cells and T cells, whereas HSCs, MPPs, LMPPs, and myeloid cells did not show a significant reduction of autophagic flux (Fig 3.15B). Spermidine administration in the drinking water to old mice for 6 weeks increased the autophagic flux in nearly all cell types (Fig 3.15).

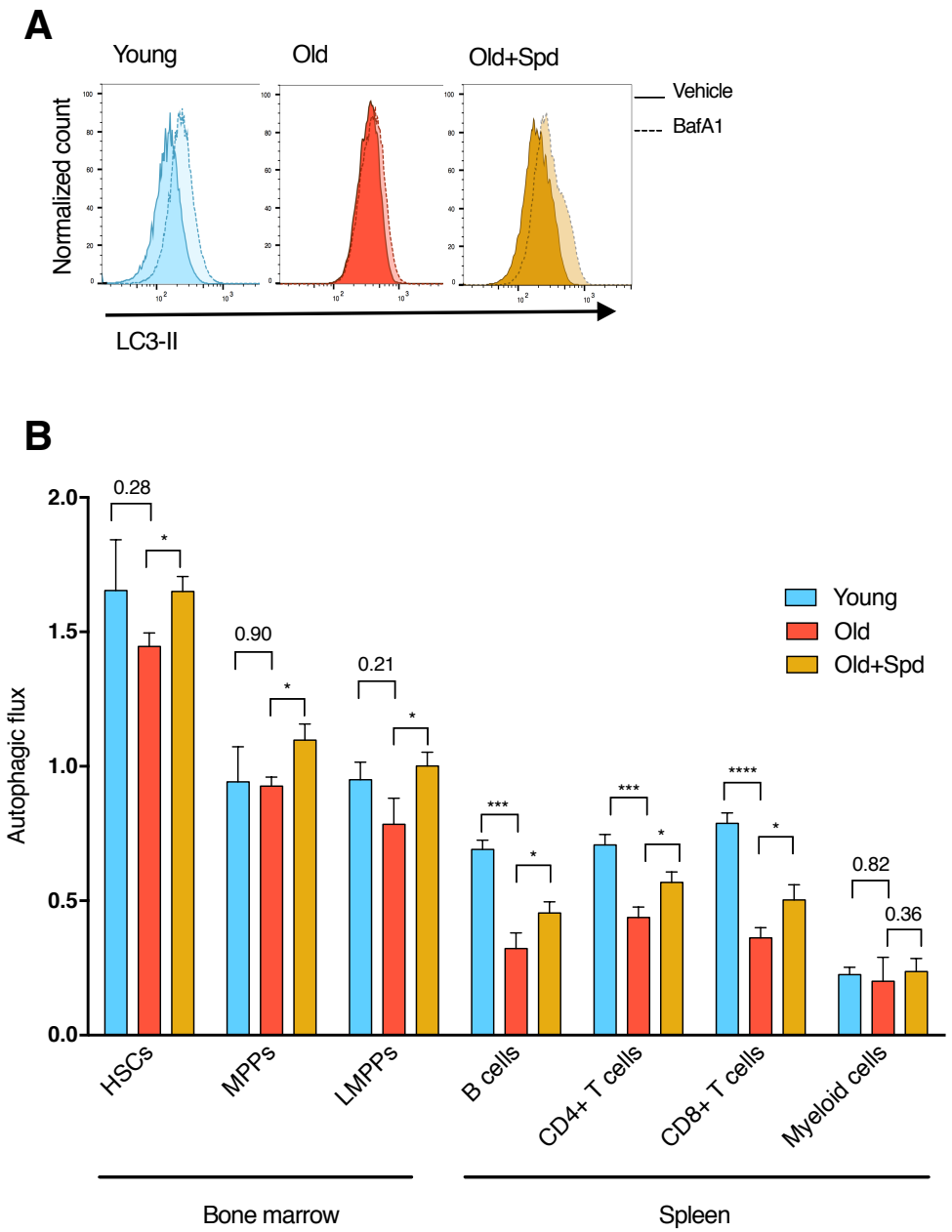


Fig 3.15 Autophagic flux is significantly reduced in lymphocytes from old mice, and spermidine increases autophagic flux *in vivo*. Bone marrow and spleen cells taken from mice treated as in Fig 3.3 were measured by LC3-II staining using flow cytometry after 2h treatment with bafilomycin A1 (BafA1) or vehicle. **A.** Representative plot of LC3-II staining of B cells. **B.** Autophagic flux was calculated as LC3-II mean fluorescence intensity (BafA1-Vehicle)/Vehicle. Data represented as mean ± SEM. n = 5 to 6 mice per group. Student's t-test (two-tailed for Young-Old comparison, one-tailed for Old-Old+Spd comparison) with P values labeled out, *P≤0.05, ***P≤0.001, ****P≤0.0001.

3.2.4 Autophagic flux is blocked in B cells from old mice

Next I focused on B cells and confirmed the reduction of autophagic flux in B cells from old mice. The flow cytometry plot shows that the LC3-II shift from Vehicle to BafA1 is reduced in old B cells compared to young B cells, which is elevated by spermidine administration (Fig 3.15A). The reduced shift in old B cells is actually caused by increased fluorescence of LC3-II of Vehicle rather than reduced effect of BafA1 (Fig 3.15A). Consistently and more directly, western blot and confocal microscopy imaging results show that BafA1 caused a significant accumulation of LC3-II or GFP-LC3 dots in B cells sorted from young mice (Fig 3.16/17), suggesting an active autophagic flux. In contrast, higher LC3-II protein levels (Fig 3.17A/B) and increased number of GFP-LC3 dots (Fig 3.17C/D) were found in old B cells compared to young B cells under basal (Vehicle) conditions, which were not further increased by BafA1 treatment (Fig 3.17), indicating that the increased LC3-II in old B cells was caused by blocked lysosomal degradation rather than increased LC3-II formation. Spermidine administration reduced the basal LC3-II levels and improved the autophagic flux of old B cells (Fig 3.17). Therefore autophagy is impaired in old B cells due to reduced lysosomal degradation, and spermidine increases autophagic flux *in vivo*.

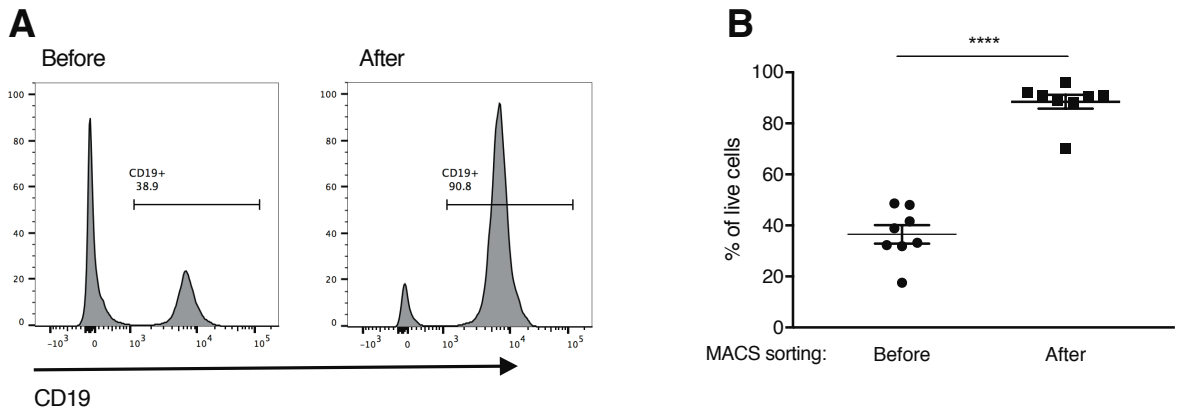


Fig 3.16 Purity check of magnetic-activated cell sorting (MACS) of murine B cells. Splenocytes before or after MACS purification of B cells were assessed by flow cytometry (**A**). The quantification is shown in **B**. Data represented as mean ± SEM. n = 8 mice per group as indicated by dots. Paired Student's t-test, ****P≤0.0001.

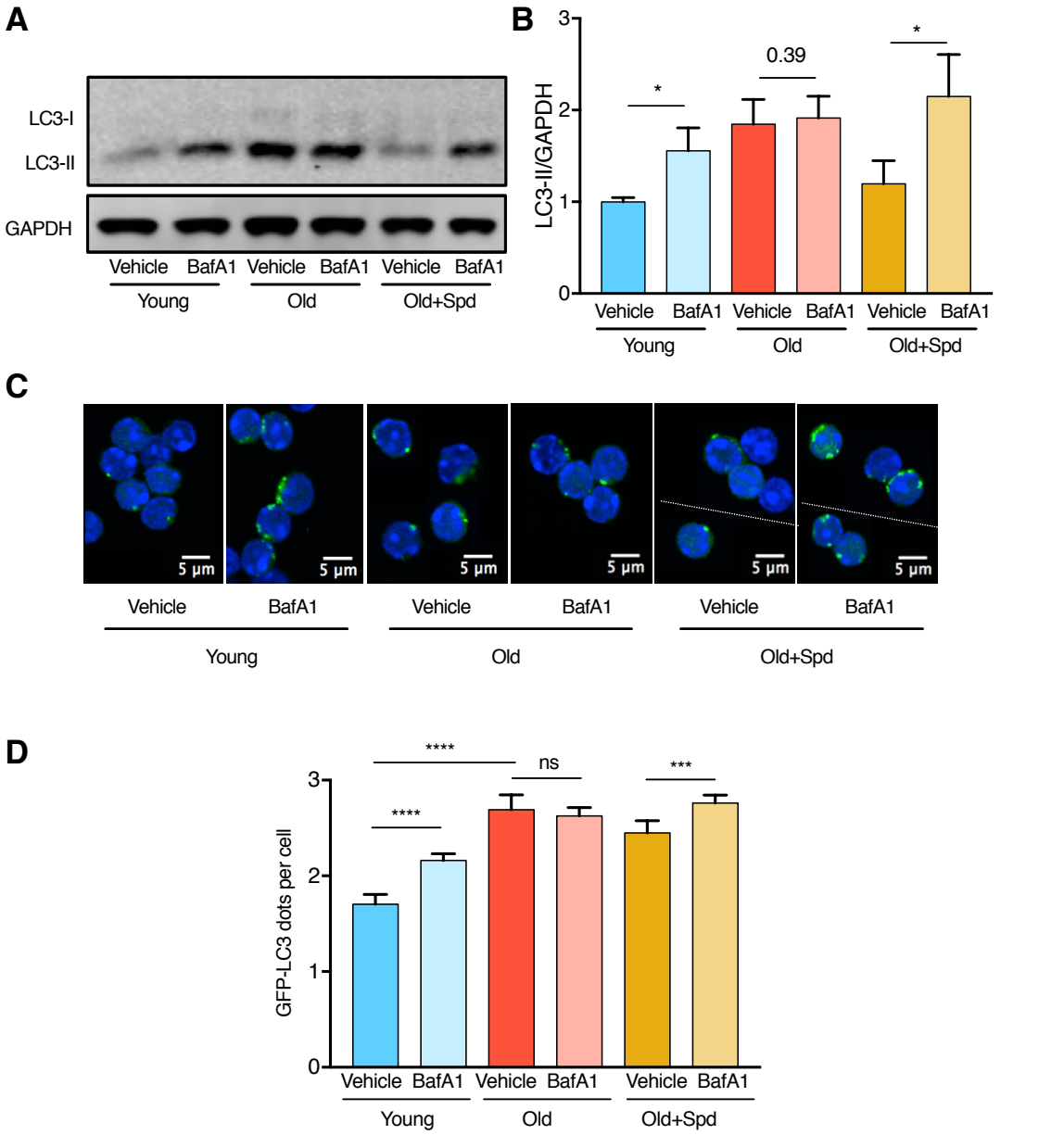


Fig 3.17 Autophagy is impaired at the lysosomal degradation level in B cells from old mice, which is ameliorated by spermidine administration. **A/B.** Representative LC3-II immunoblot of sorted B cells from young, old, or old mice administered with spermidine (**A**) with the quantification shown in **B**. The LC3-II band intensity was normalized to GAPDH first, and then to the Young Vehicle sample. Data represented as mean ± SEM. n = 6 to 7 mice per group. Paired one-tailed Student's t-test with P values labeled out, *P≤0.05. **C/D.** Confocal microscopy images were acquired of sorted B cells from young, old, or old GFP-LC3 transgenic mice treated with spermidine (**C**). The quantification results of GFP-LC3 dots per cell are shown in **C.** Data represented as mean ± SEM. N = 210 to 616 cells pooled from 4 to 6 mice per group. Mann-Whitney test with P values labeled out, ***P≤0.001, ****P≤0.0001, ns, not significant.

3.2.5 Spermidine improves the humoral responses in old mice

I next assessed the function of B cells by measuring immunoglobulin titers (humoral responses) in old mice using the model antigen NP-CGG. Upon first immunization, a fast and robust IgM primary response was induced in young mice (Fig 3.18A, day 0 to day 42) and a gradually increasing long-term IgG1 response (Fig 3.18B, day 0 to day 42). In contrast, the IgM primary response in old mice was delayed and significantly compromised in titer (Fig 3.18A), and the overall IgG1 response was also severely compromised (Fig 3.18B).

A secondary immunization (boost) was performed to assess the memory humoral responses. Young mice had an acute response and their NP-specific IgM and IgG1 productions reached their peak in 7 days post boost (Fig 3.18, after day 42). Old mice also showed a quick but compromised IgM memory response but a very weak IgG1 memory response (Fig 3.18).

Spermidine was continuously given in the drinking water to old mice throughout the whole experiment to test if it improves the humoral responses *in vivo*. It was found that IgG1 primary and more remarkably, memory responses in old mice were significantly improved by spermidine (Fig 3.18B). A significant improvement of memory IgM responses was also observed on day 49 and 56 (Fig 3.18A).

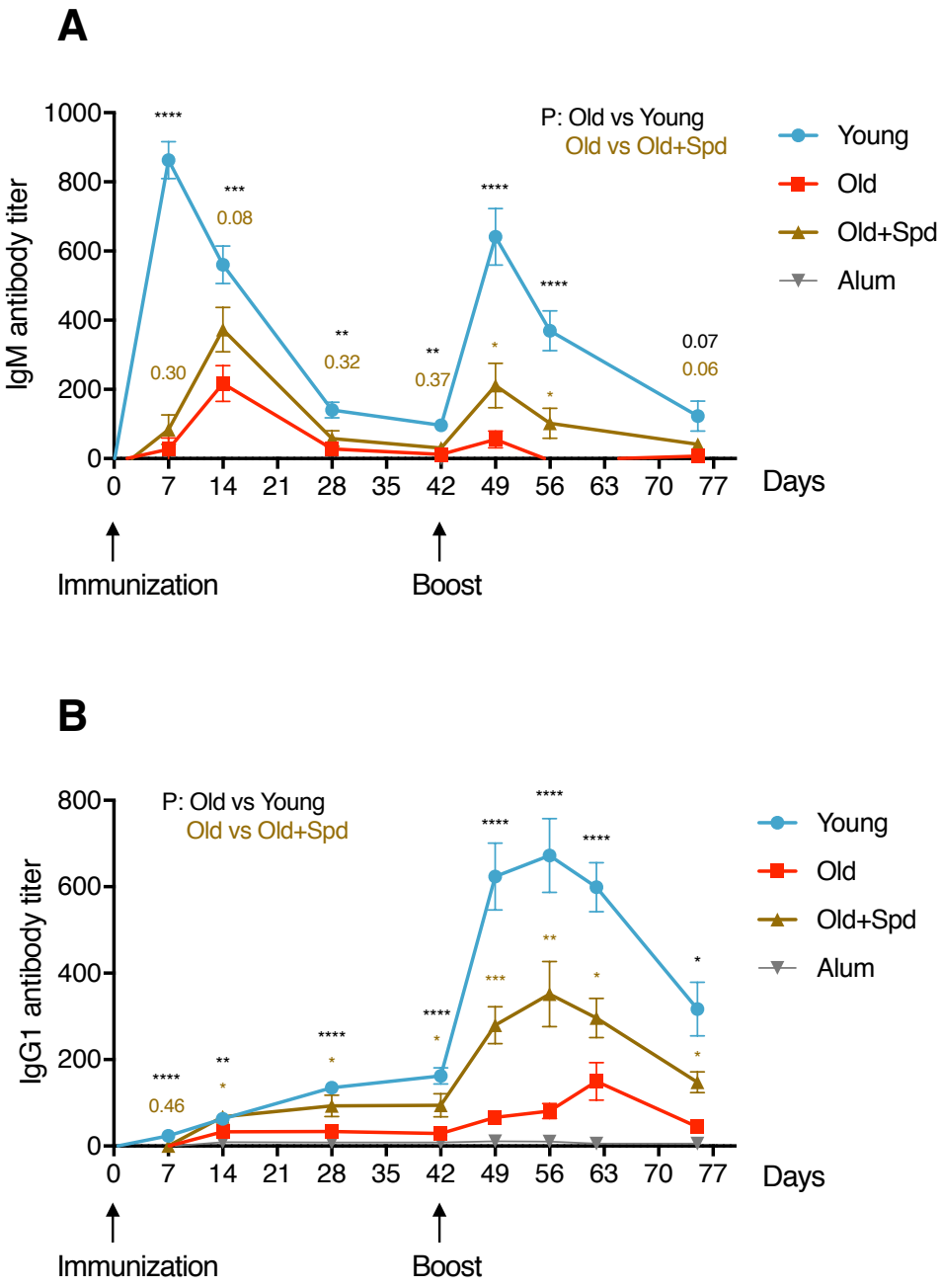


Fig 3.18 Spermidine improves humoral responses in old mice. Young or old mice were immunized with NP-CGG precipitated in the adjuvant alum (immunization) and boosted with NP-CGG in PBS. Spermidine was given 2 days before the first immunization and then continuously in drinking water. Serum was collected on indicated days and NP-specific IgM (**A**) or IgG1 (**B**) measured by ELISA. Data represented as mean ± SEM. n = 10 to 14 mice per group, pooled from 2 independent experiments. Welch's t-test, *P≤0.05, **P≤0.01, ***P≤0.001, ****P≤0.0001.

I also measured the number of NP-specific IgG1-secreting plasma cells in bone marrow at the time of sacrifice (day 39 post boost) (Fig 3.19A), which are supposed to be long-lived plasma cells (248, 249). Consistent with the antibody titer, both the ratio (Fig 3.19B) and the absolute number (Fig 3.19C) of NP-specific IgG1-secreting plasma cells were markedly reduced, which were restored by spermidine administration (Fig 3.19). The measurement of NP-specific IgM-secreting plasma cells failed possibly due to the low binding specificity of IgM in the ELISpot assay where alum samples showed an equivalent number of dots as the young samples (data not shown).

In conclusion, both IgM and more strongly IgG1 primary and secondary responses are severely compromised in old mice, which are improved by spermidine administration.

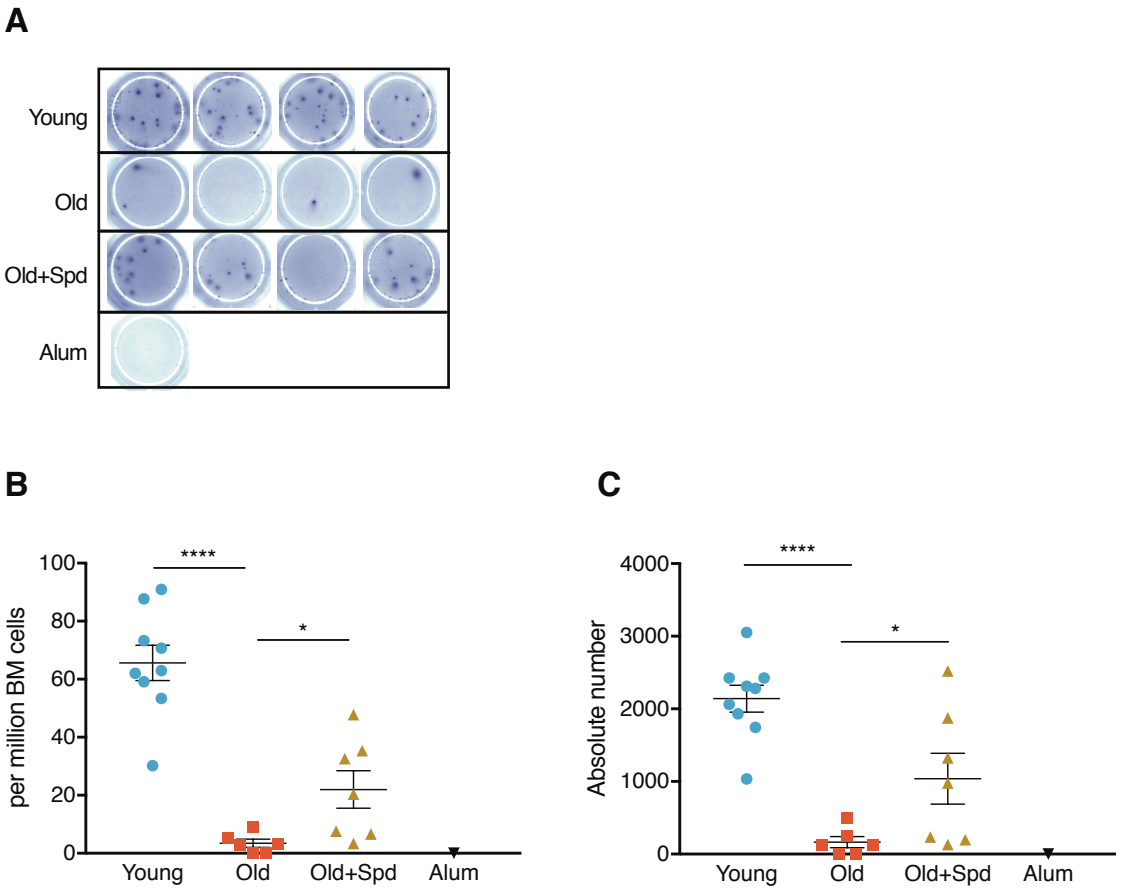


Fig 3.19 Spermidine increases the number of long-term NP-IgG1-secreting cells in old mice. Mice treated as in Fig 3.18 were culled on day 75 and plasma cells secreting NP-specific IgG1 from bone marrow were measured by ELISpot (**A**). The quantification of relative and absolute number is shown in **B** and **C** respectively. Data represented as mean ± SEM. n = 6 to 9 mice per group as indicated by dots. Welch's t-test, *P≤0.05, ****P≤0.0001.

3.2.6 Spermidine improves the humoral responses in an autophagy-dependent manner

It has been shown that spermidine induces autophagy and improves humoral immune responses in old mice. However, whether autophagy is required for spermidine's immune-boosting effects remains elusive. To address this question, we used B cell-specific *Atg7*-knockout (*B-Atg7*$^{-/-}$) mice, in which the essential autophagy gene *Atg7* is deleted by *Mb1-Cre* at the early pro-B cell stage (250).

The complete loss of ATG7 was firstly confirmed in B cells sorted from *B-Atg7*$^{-/-}$ mice (Fig 3.20A/B). ATG7 is essential for the formation of autophagosomes (251, 252). Accordingly, *Atg7*-knockout (-/-) B cells showed an accumulation of LC3-I proteins with less LC3-II under basal conditions (Vehicle), and failed to accumulate LC3-II upon BafA1 treatment (Fig 3.20C/D), both indicate that the autophagic flux was efficiently blocked.

The NP-CGG-induced humoral responses were then assessed in *B-Atg7*$^{-/-}$ mice administered with or without spermidine. Both the primary and the secondary IgG1 responses were severely compromised in *B-Atg7*$^{-/-}$ mice (Fig 3.21A), mimicking the phenotype of old mice (Fig 3.18B). Spermidine administration, however, failed to improve the IgG1 responses in *B-Atg7*$^{-/-}$ mice (Fig 3.21A), consistent with the hypothesis that spermidine improves compromised humoral responses in an *Atg7*- or autophagy-dependent manner.

In contrast to impaired IgG1 responses, IgM responses were not significantly altered in *B-Atg7*$^{-/-}$ mice (Fig 3.21B), and spermidine did not affect IgM responses either (Fig 3.21B). This is consistent with the observation that spermidine did not significantly improve primary IgM responses in old mice (Fig 3.18A). Moreover, the compromised IgM responses in old mice (Fig 3.18A) are likely not caused by autophagy deficiency in B cells either, and the improved IgM memory responses by spermidine may be attributable to B-cell autophagy-independent mechanisms.

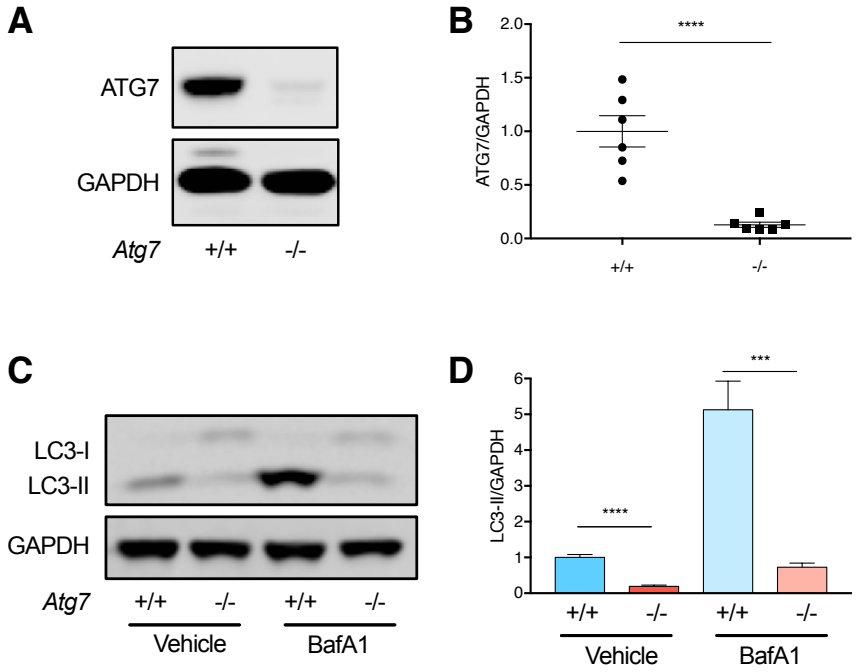


Fig 3.20 Reduced autophagy in Atg7-/- B cells. **A/B.** B cells were purified from *Mb1-Cre-, Atg7*$^{flox/flox}$ (+/+) and *Mb1-Cre+, Atg7*$^{flox/flox}$ (-/-) mice and the expression of ATG7 assessed by Western blot. The quantification is shown in B. The ATG7 band intensity was normalized to GAPDH first and then to +/+. n = 6 mice per group as indicated by dots. One-tailed unpaired Student's t-test. **C/D.** Purified B cells were cultured with or without BafA1 for 2h to assess LC3-II expression by Western blot. The quantification is shown in **D**. The LC3-II band intensity was normalized to GAPDH first and then to +/+ Vehicle. n = 4 mice per group. One-tailed paired Student's t-test. ***P≤0.001, ****P≤0.0001. Data represented as mean ± SEM.

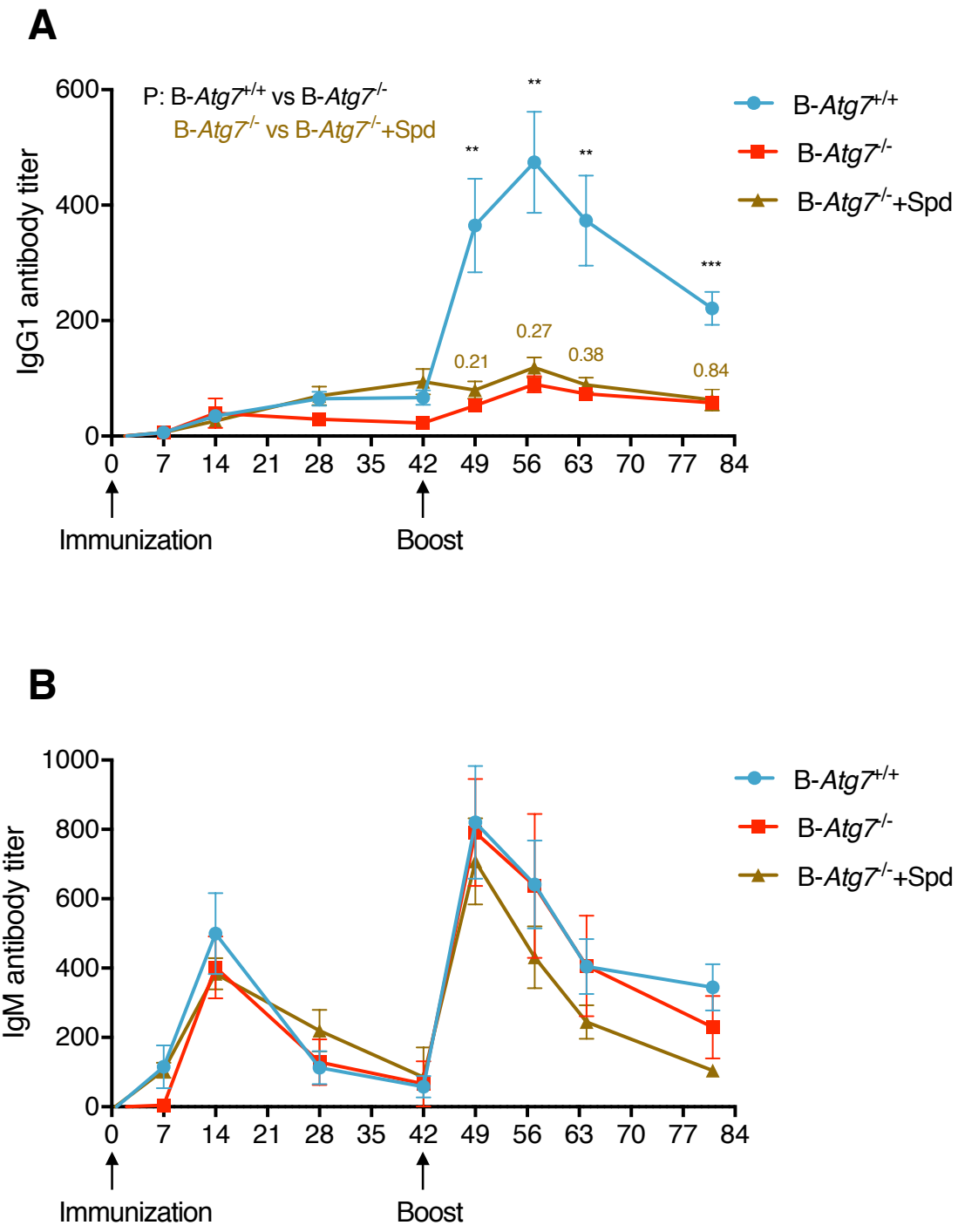


Fig 3.21 Spermidine fails to improve the humoral responses in B cell-specific autophagy-deficient mice. B cell-specific *Atg7* knockout (B-*Atg7*$^{-/-}$) mice were immunized with NP-CGG and treated with spermidine as in Fig 3.18. Serum NP-specific IgG1 (**A**) and IgM (**B**) were measured by ELISA. Data represented as mean ± SEM. n = 3 to 7 mice per group. Welch's t-test, **P≤0.01, ***P≤0.001.

3.2.7 Spermidine does not improve humoral responses in young mice

Spermidine improves NP-specific IgG1 responses in old mice, which are already immune-compromised. We next questioned if spermidine might also improve humoral responses in healthy young adult mice. It was found that constant administration of spermidine during the whole immunization experiment did not significantly affect their IgG1 humoral responses (Fig 3.22). This might be due to that spermidine and autophagy in B cells from healthy young mice are sufficient for robust responses, which cannot be further improved by more spermidine.

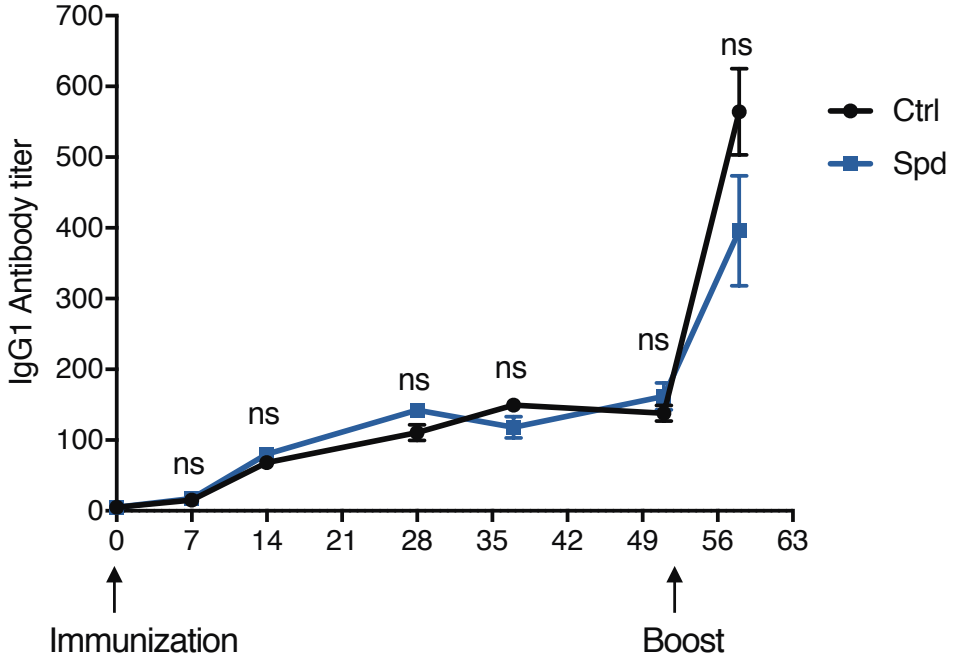


Fig 3.22 Spermidine does not improve humoral responses in young mice. Young adult mice (6-8 weeks) were immunized with NP-CGG precipitated in alum and boosted with NP-CGG in PBS on day 51. Spermidine administration and serum NP-specific IgG1 measurement were processed as in Fig 3.18. Data represented as mean ± SEM. n = 6 to19 mice per group, pooled from 3 independent experiments. Student's t-test, ns, not significant.

Chapter 3. The Autophagy Inducer Spermidine Rejuvenates Humoral Immunity in Aged Mice

3.3 Discussion

3.3.1 Can we target HSCs to improve haematopoiesis/immunity in old individuals?

Reduced adaptive immune responses are key features of haematopoietic ageing, causing increased morbidity and mortality due to infections. Moreover, ageing of the haematopoietic system is associated with a higher incidence of anemia (253) and myeloproliferative diseases (254, 255). HSCs give rise to the entire haematopoietic system. Therefore the working hypothesis in this chapter is to improve the deficient functions of aged HSCs to control the homeostasis of the entire haematopoietic system.

The phenotypes of aged HSCs have been well studied. Phenotypic HSCs in human ($CD34^+CD38^+CD90^+$) increase in number with age (256), which is similar to what I have observed in old C57BL/6 mice (Fig 3.3) (245). Meanwhile the reconstitution capacity of HSCs at the single cell level declines with age (70, 257). Accordingly bone marrow HSCs from older human donors (> 45 years) also have reduced transplantation success comparing to the same number of HSCs from younger donors (258). Moreover the skewed differentiation towards myeloid lineages is another age-associated phenotype of HSCs (Fig 3.4/6), consistent with the increase in myeloproliferative diseases.

However, when a similar number of whole bone marrow cells (with more HSCs in old bone marrow) were used for reconstitution, old bone marrow-derived progenitors and mature lineages are comparable to young bone

marrow (Fig 3.11-14). Therefore the increase in phenotypic HSCs numbers might be an adaptive response to compensate the reduced functions at the single cell level. Such compensatory mechanism seems to be very successful as they, although with a larger number, reconstitute and differentiate as well as young HSCs in adoptive transfer experiments. This suggests that intrinsic changes in old HSCs are not a major cause of the haematopoietic ageing. Interventions targeting HSCs themselves may not be an efficient way to rejuvenate the old haematopoietic system.

The myeloid-bias phenotype observed in the aged haematopoietic system (Fig 3.4/5/6/7) is much stronger than that when old HSCs have been adoptively transferred (Fig 3.12/13/14), indicating that the aged niche environment has a remarkable contribution to the imbalanced differentiation of HSCs or impaired development of progenitors. Consistent with our results, a lower engraftment efficiency, increased myeloid differentiation, and severely reduced T cell development were observed when transferring young (2 months) bone marrow cells into old (18 months) recipient mice (259). Mechanically, multiple age-related niche factors, such as the inflammatory cytokine CCL5 (259) and the HSC-chemoattractant chemokine CXCL12 (260, 261), may all contribute to reduced HSCs reconstitution and unbalanced differentiation in old niche. Therefore, instead of targeting old but still 'healthy' HSCs to improve haematopoiesis, niche factors may be more effective targets.

3.3.2 How does autophagy modulation contribute to the aged haematopoietic system?

As the only bulk-degradation mechanism in cells, autophagy plays a key role in re-shaping the cells during differentiation and maintaining the homeostasis of long-lived cells. Knockout of the essential autophagy gene *Atg7* in HSCs causes a severe impairment of self-renewal and differentiation, and the almost complete loss of their reconstitution ability (214). Inducible knockout of *Atg12* in HSCs of adult mice also leads to an ageing-like phenotype, *i.e.* increased generation of myeloid cells and reduced reconstitution efficiency (262). Autophagy-deficiency in neutrophil, T cell, or B cell progenitors shows defective differentiation (170, 201, 215). Autophagy is also required for phagocytosis (216, 263, 264), antigen presentation (265-268), and lysosomal degranulation (269) during innate immune responses, and the long-term memory of adaptive immune responses (170, 183, 202, 204). Since the phenotypes of ageing highly correspond to the autophagy deficiency (2), it is reasonable to hypothesize that autophagy deficiency might be a general cause of ageing in these cell types.

Here we show that autophagy is significantly impaired in B cells and T cells (Fig 3.15 and Fig 3.17). Considering the fact that autophagy is required for memory responses of B cells and T cells (170, 183, 202, 204), and autophagy inducers including spermidine and rapamycin are able to improve B cell (204) and T cell (170) responses, we can draw the conclusion that autophagy deficiency contributes to the senescence of B cells and T cells. Therefore

autophagy is also a practical target to improve adaptive immune responses in the elderly.

On the other hand, I have found that autophagy is not or only mildly attenuated in HSCs, MPPs and mature myeloid cells from old mice, indicating that autophagy is not a direct driving force of their ageing, although knockout of essential autophagic genes leads to an ageing-like phenotype. However, it remains possible that autophagy inducers may still improve the behavior of these cells in old individuals. For example, knockout of the essential autophagy gene *Atg5* in mouse bone marrow Leptin-receptor-expressing stromal cells causes a significant reduction of both myeloid and lymphoid cells (270), indicating that autophagy is also required for HSC niche maintenance. This enhances the possibility to modulate haematopoiesis via inducing autophagy in niche cells. However I did not observe a significant improvement of haematopoiesis by spermidine treatment in old mice although spermidine shall also get access to niche cells. This can be due to too short treatment and the turnover of the established haematopoietic system is too slow. Bone marrow chimera mice using lethally irradiated old mice (old niche) as recipient treated with or without autophagy inducers will help better address that.

Moreover, spermidine down regulates the pro-inflammatory cytokine TNF-α in plasma of old mice (212). TNF-α affects haematopoiesis in multiple ways, including suppressing the colony formation and reconstitution of human haematopoietic stem cells ($CD34^+CD38^-$) (271), and suppressing the

erythropoiesis in fanconi anemia patients (272). Additionally, since autophagy is required for optimal innate immune responses, it will be intriguing to see if autophagy induction may further boost their responses.

Therefore, autophagy deficiency directly contributes to adaptive immune senescence. Autophagy induction may directly or indirectly improve the haematopoiesis and immune responses in the elderly.

3.3.3 Does spermidine improve humoral responses in old mice via autophagy?

Spermidine has been reported to prolong the lifespan of yeast, worms, flies, and mice in an autophagy-dependent manner (210, 212, 273). Spermidine also improves the heart and $CD8^+$ T cell functions in old mice in an autophagy-dependent manner, similar to our observations in B cells (Fig 3.18/19 and Fig 3.21) (170, 212). Based on the observations that deletion of essential autophagy genes counteracts spermidine's anti-ageing effects, the word 'autophagy-dependent' is carefully used to suggest that the *in vivo* mechanism is autophagy induction. However, 'autophagy-dependent' (necessity) does not necessarily mean 'via autophagy' (sufficiency). Actually, it is very hard to design a simple experiment directly showing that autophagy induction is sufficient for the drug effect, and this is what we are faced with here in the case of B cells.

Autophagy-deficient memory B cells have a higher level of apoptosis and fail to attain long-term survival (203), indicating autophagy is essential for memory B cell maintenance. Spermidine fails to improve autophagy-deficient memory B cell responses (Fig 3.21), indicating the necessity of autophagy for spermidine's effect. Meanwhile, other results indirectly suggest the sufficiency. Autophagic flux in B cells from old mice is reduced, which, according to the phenotype of *Atg7*$^{-/-}$ B cells, should contribute to the impaired memory responses (although may not be necessarily an initiating factor of B cell senescence). Therefore autophagy induction in autophagy-deficient B cells should be able to improve their memory responses, just as re-introducing ATG7 into *Atg7*$^{-/-}$ B cells would rescue their phenotype. Accordingly, spermidine increases autophagic flux in old B cells, which are deficient in autophagy, and improves their memory responses. Therefore, autophagy induction in B cells shall be at least one mechanism for spermidine's immune-boosting effect, although alternative mechanisms, such as via $CD4^+$ follicular helper T cells, might also help to explain impaired IgM responses in old mice and their improvement by spermidine (Fig 3.18 and Fig 3.21). It is evident that experiments such as genetically inducing autophagy (via over-expression of Atg5 (274) for example) in B cells from old mice would be more convincing to demonstrate that autophagy induction in B cells is sufficient to improve their responses.

To sum up, we conclude, albeit not definitely, that autophagy is essential for spermidine's immune-boosting effect (in both young and old mice), and

spermidine improves humoral responses in old mice at least partially via inducing autophagy in B cells.

3.3.4 Potential side effects of spermidine

Although we have not observed any detrimental effects of spermidine after up to 11 weeks of administration in drinking water, the potential side effects should be carefully considered for clinical applications. The best described function of spermidine at the cellular level is to promote cell proliferation. Spermidine-depleted cells fail to proliferate (208). Consistently, a higher spermidine level was found in the urine of patients with solid tumours or leukaemias (275), suggesting that cancer cells produce a significant amount of spermidine. The spermidine-depleting drug difluoromethylornithine (DFMO/ Eflornithine) is also used to control cancer progression in clinical trials (276, 277) and has been approved for the treatment of human African trypanosomiasis in which protozoa parasites require spermidine for proliferation (278, 279). Therefore higher levels of spermidine may potentially accelerate the disease progression of cancer and parasitic infections, and spermidine may be incompatible with treatments involving DFMO.

On the other hand, spermidine prevents liver fibrosis and hepatocellular carcinoma via inducing autophagy in livers (213), and suppresses 1,2-dimethylhydrazine (DMH)-induced tumorigenesis in large intestine of mice (280), indicating that spermidine is able to prevent the pathogenesis of cancer via maintaining cellular homeostasis under stresses. Moreover, spermidine

also promotes adaptive immune responses, which are crucial for immune surveillance and treatment of cancer (281, 282). Additionally, fast B-cell proliferation occurs during IgM primary responses, which was indeed not improved by spermidine (Fig 3.18/21), indicating that spermidine does not necessarily induce cell proliferation. Therefore the relationship between spermidine and cancer may be more complex than previously assumed.

3.3.5 Conclusions

In this chapter, the ageing of the murine haematpoietic system was assessed and the autophagy inducer spermidine was used to rejuvenate the aged haematopoietic system. Consistent with previous studies, the aged haematopoietic system is myeloid-biased, with increased number of myeloid lineages and reduced lymphoid lineages. The adoptive transfer experiment showed that HSCs from old bone marrow are capable of reconstitution and giving rise to comparable lymphoid progenitors and mature lymphocytes comparing to young bone marrow, indicating that the lymphopenia in old mice is not due to intrinsic deficiencies of HSCs. HSCs also have a high basal autophagic flux, which are not much impaired during ageing. Spermidine treatment further increases autophagic flux in old HSCs, but does not alter their reconstitution or differentiation.

In contrast to HSCs, autophagy in lymphocytes from old mice is significantly impaired at the lysosomal degradation level. B cell responses in old mice are also severely impaired. Spermidine increases autophagic flux in old B cells

and significantly improves long-term humoral responses in old mice. *Atg7*$^{-/-}$ B cells display the blocked autophagic flux and compromised memory IgG1 responses, mimicking the phenotype of ageing. Spermidine administration fails to improve memory responses of *Atg7*$^{-/-}$ B cells, in agreement with the hypothesis that spermidine's immune-boosting effect is autophagy-dependent.

Chapter 4. Spermidine Regulates Autophagy via eIF5A Hypusination

4.1 Introduction

4.1.1 Molecular functions of spermidine

Spermidine has been reported to interact with a variety of molecules. For example, as a positively charged polyamine, spermidine is able to bind to negatively charged molecules such as DNA and RNA via electrostatic forces to stabilize their structures (207, 283, 284). Spermidine can also undergo conformational changes to form a complex with ATP (207, 285, 286), thus has a potential to interfere with ATP-related functions. Moreover, enzyme kinetic studies also show that high concentration of spermidine (2 M) is able to compete with Na^+ and K^+ for the cation binding sites on Na^+, K^+-ATPase and blocks the enzyme activity (208, 287). Another specific function of spermidine is to post-translationally modify the eukaryotic translation initiation factor 5A (eIF5A), which will be discussed in detail in 4.1.2.

Regarding the mechanism of autophagy induction by spermidine, it was proposed by Eisenberg *et al.*, that spermidine may inhibit the activity of histone acetyltransferases (HATs), which then leads to an altered transcriptome and the increased expression of autophagy genes such as *ATG7, ATG11, and ATG15* at the transcriptional level (210). As the authors have also pointed out, a drawback of this hypothesis is that the direct effect of reduced HAT activities shall be gene silencing rather than activation, contradicting with their observation that the transcription of autophagy genes was “selectively” turned on.

4.1.2 Hypusination of eIF5A and its molecular functions

Being the unique substrate of hypusination reaction is the best defined function of spermidine. During hypusination, spermidine transfers its aminobutyl moiety to a specific lysine on eIF5A (K50 for human and mouse eIF5A1) to transform it into hypusine (Fig 4.1). Hypusine is an unusual amino acid and so far has only been identified as part of eIF5A. Park *et al.* first reported in 1981 that heavy-isotope (^{3}H)-labeled spermidine was predominantly incorporated into a single protein in cultured human peripheral lymphocytes (288, 289), which was identified later to be eIF5A (eIF4D) (290). The majority of spermidine (54%) is used for hypusination reaction when intracellular spermidine is limiting in yeast, indicating that the major function of spermidine is to hypusinate eIF5A (291). Structure studies showed that both eIF5A and its bacterial homolog elongation factor P (EF-P) bind to the

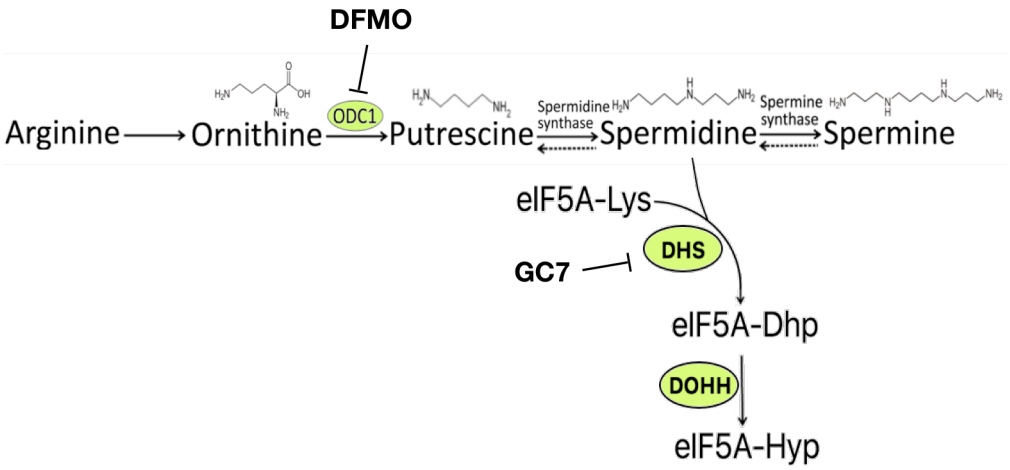


Fig 4.1 Schematic overview of the polyamine synthesis and the eIF5A hypusination pathway. DFMO is an irreversible inhibitor of ODC and used to block cellular polyamine synthesis. GC7 is a reversible competitive inhibitor of DHS and used to block hypusination.

ribosome adjacent to the peptidyl (P) site (292-294), with hypusine at the peptidyltransferase center (293, 294), suggesting that eIF5A may interfere with the peptide bond formation with its hypusine arm.

eIF5A and the two hypusination enzymes deoxyhypusine synthase (DHS) and deoxyhypusine hydroxylase (DOHH) (Fig 4.1) are highly conserved in eukaryotes (295). Interestingly, although bacterial EF-P does not have hypusine, a similar modification (lysinylation) is found on its lysine in a homologous region (K34) (296). The evolutionary conservation indicates that hypusine is a key structure for eIF5A and its basic cellular process.

eIF5A was originally named as a translation initiation factor due to its function to promote the methionine-puromycin conjugation *in vitro*, which mimics the translation initiation reaction (297, 298). Follow-on studies show that eIF5A and EF-P also promote translation elongation (299). In the absence of EF-P or eIF5A, the translation rate is reduced especially for peptides containing three or more consecutive prolines (polyprolines) (300-302). Unlike other amino acids, proline contains a pyrrolidine ring, which constrains its conformation and makes it a poor peptide bond donor and acceptor (Fig 4.2)

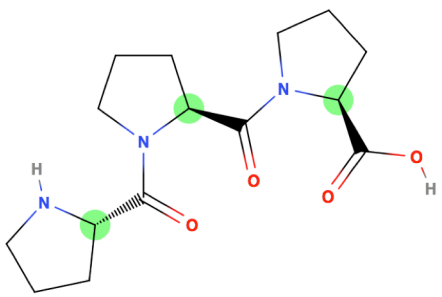


Fig 4.2 Schematic overview of the tri-proline structure. α-carbons of the amino acid residues are highlighted in green.

(300, 303).

The reaction between puromycin and proline is 10 to 1000 times slower than reactions between puromycin and other amino acids in bacterial cell-free system without EF-P, and EF-P accelerates the puromycin-proline reaction by about 90 folds (300). EF-P is also required for polyproline synthesis *in vivo*, but dispensable for single- or double-proline synthesis possibly due to a more sophisticated translation machinery in cells (302). Similarly in yeast, eIF5A accelerates the synthesis of polyproline peptides (MPPPK) by over 20-fold in a cell-free system (301). Ribosomal profiling, a technique revealing translation at the single-nucleotide resolution by directly sequencing mRNA fragments bound to ribosomes, shows that eIF5A also promotes the translation of several other non-polyproline motifs such as GPP, DDP, and RDK in yeast (304). Moreover, deletion of eIF5A in yeast causes accumulation of ribosomes at the stop codon, indicating that eIF5A also assists translation termination (304). In contrast to a broad function of eIF5A in assisting the overall translation, the hypusination of eIF5A seems to be more specifically required for polyproline synthesis in yeast (301, 304). Relevant molecular functional studies of eIF5A are still lacking in mammalian cells.

4.1.3 Cellular functions of polyamines and eIF5A

Phytohaemagglutinin (PHA)- or anti-CD3-stimulated human lymphocytes increase hypusinated eIF5A by over 30 folds compared to resting cells on a per cell basis, while the total protein content only increases by about 3-fold,

indicating that eIF5A and its hypusination modification are coordinatively up-regulated during lymphocyte activation and proliferation (289, 305). Accordingly, both genetic deletion of *Eif5a* and chemically induced inhibition of hypusination suppress cell proliferation at G1 phase in yeast and cell lines (306-309). Consistently, DFMO-induced depletion of polyamines (Fig 4.1) also arrests mammalian cell proliferation at G1 phase (310). Therefore promoting cell proliferation is the best defined function for both spermidine and eIF5A when this project was initiated.

4.1.4 Physiological functions of polyamines and eIF5A

Possibly owing to their indispensable role in basic cellular process such as proliferation, polyamine depletion or eIF5A hypusination inhibition causes a severe phenotype in mice. Knockout of the key polyamine synthesis gene *Odc* (Fig 4.1) in mice leads to embryonic lethality. $Odc^{-/-}$ embryos are capable of uterine implantation on E3.5 but then degenerate quickly before E5.5 (311). Cultured $Odc^{-/-}$ blastocysts show compromised proliferation and then apoptosis (311), indicating that ODC and spermidine are required for cellular proliferation *in vivo*, which is required for early embryonic development. $Odc^{+/-}$ mice are viable and have comparable polyamine levels under basal conditions to those in $Odc^{+/+}$ mice (312). In contrast, overexpression of *Odc* in mice does not directly lead to obvious phenotypical changes (313-315), but predisposes mice to increased sensitivity to carcinogens (316, 317), consistent with the pro-proliferation function of spermidine.

Similar to *Odc*$^{-/-}$ mice, *Eif5a*$^{-/-}$ and *Dhs*$^{-/-}$ mice are also embryonic lethal. Their blastocysts develop normally in morphology upto E3.5 but quickly degenerate by E6.5 (318, 319). *In vitro* culture shows that *Eif5a*$^{-/-}$ and *Dhs*$^{-/-}$ blastocysts fail to proliferate (318). Moreover, inducible knockout of *Dhs* or *Dohh* in adult mice also leads to a wasting syndrome within 2 weeks of induction and eventually death. Haemotoxylin and eosin (H&E) staining reveals loss of integrity of multiple organs in *Dhs*$^{-/-}$ mice, including reduced cellularity in bone marrow and spleen and damaged intestine epithelial structure (319).

Therefore, consistent with *in vitro* data, maintaining proliferation is a key function of polyamines and eIF5A *in vivo*, and is required for early embryonic development. In the absence of mouse models with tissue-specific inducible knockout of *Odc*, *Eif5a*, or *Dhs* to avoid lethality, we are still devoid of knowledge about tissue-specific functions of spermidine and eIF5A.

Chapter 4. Spermidine Regulates Autophagy via eIF5A Hypusination

4.2. Results

4.2.1 Spermidine is required for autophagy

To investigate the mechanism of autophagy regulation by spermidine *in vitro*, I first used Jurkat cells, a $CD4^+$ T lymphocyte cell line. Spermidine (100 μM and above) increases LC3-II levels while reducing LC3-I in Jurkat cells as shown by Western blot (Fig 4.3A), indicating that LC3-I is converted to LC3-II and autophagy is induced by spermidine treatment as reported in other cell lines (210, 320, 321). CytoID (CYTO-ID®) is a cationic amphiphilic probe specifically labeling autophagosomes and autolysosomes in a pH-dependent manner. CytoID staining also confirmed that autophagy is induced upon spermidine treatment in Jurkat cells (Fig 4.3B). Neither 100 μM nor 500 μM spermidine caused significant cell death within 6 hours of treatment, but a prolonged treatment of 24 hours reduced cell viability in a dose-dependent manner (Fig 4.3C), indicating that long-term treatment with spermidine causes cellular stress.

mTOR is a key autophagy regulator and inhibition of mTOR by drugs such as rapamycin induces autophagy via activating ULK complex and other pathways (12). However, due to the pleotropic functions of mTOR in controlling cell growth and metabolism, mTOR-dependent autophagy inducers have a variety of potential side effects. It was found that spermidine did not reduce the phosphorylation of S6 (Fig 4.4A), a downstream target of mTOR, indicating that spermidine induces autophagy in an mTOR-independent manner.

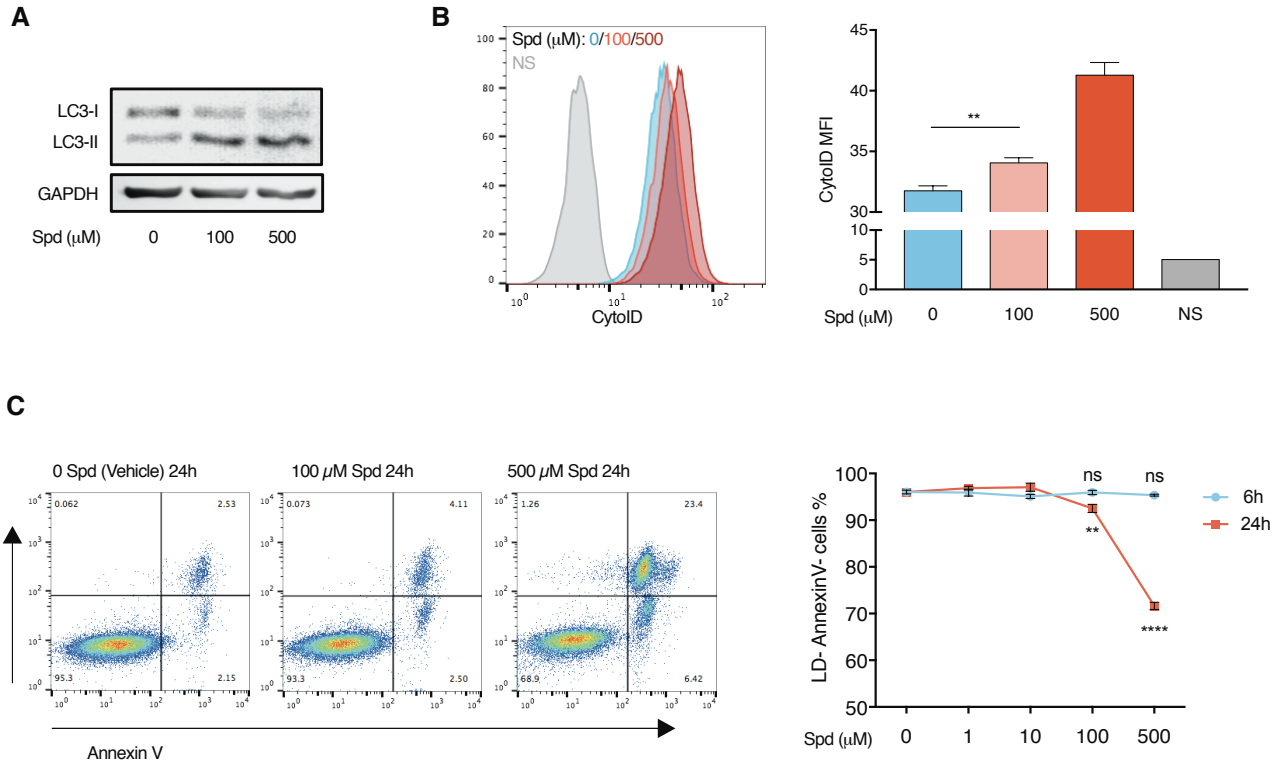


Fig 4.3 Spermidine induces autophagy. **A/B.** Jurkat cells were treated with spermidine (Spd) of indicated concentrations for 6 hours. Autophagy was assessed by LC3-II Western blot (**A**) (Representative of 5 independent repeats), or CytoID staining measured by flow cytometry (**B**) (n = 4, unpaired Student's t-test, **P≤0.01, NS: non-staining). **C.** Jurkat cells were treated with spermidine of indicated concentrations for 6 or 24 hours. Cell viabilities were assessed by Live-Dead (LD) and Annexin V stainings (n = 3. Unpaired two-way ANOVA compared to 0 μM, **P≤0.01, ****P≤0.0001, ns, not significant). Data represented as mean ± SEM.

Since spermidine can interact with ATP (207, 285, 286), it is possible that spermidine may interfere with the cellular energy status and thus stimulate the energy sensor AMPK and autophagy. However, it was found that spermidine did not increase the phosphorylation of AMPKα (Fig 4.4B), the catalytic domain of AMPK, indicating that spermidine treatment does not activate AMPK. Therefore, spermidine induces autophagy in an mTOR- and AMPK-independent manner.

Spermidine is a polyamine metabolite being synthesized from ornithine in cells (Fig 4.1). DFMO inhibits the activity of the key polyamine-synthesizing enzyme ODC (Fig 4.1) and caused the depletion of spermidine in Jurkat cells (Fig 4.5A). Spermidine treatment rescued the depletion induced by DFMO, which demonstrates the function of DFMO (Fig 4.5A). Consistently, autophagic flux was reduced upon DFMO-induced depletion of spermidine, which was rescued by a low dose (10 μM) of spermidine supplementation (Fig 4.5B). Therefore spermidine is a novel intracellular metabolite maintaining basal autophagy. Unraveling its mechanism may reveal a novel autophagy signaling pathway.

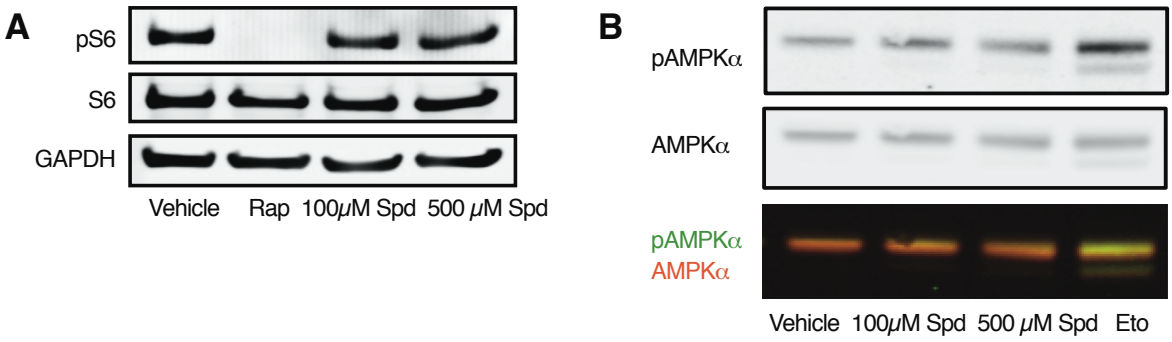


Fig 4.4 Spermidine does not affect mTOR and AMPK activity. Jurkat cells were treated with spermidine of indicated concentrations for 6 hours. mTOR activity was assessed by S6 phosphorylation (**A**), and AMPK by AMPKα phosphorylation. Cells were treated with 50 nM rapamycin or 10 μM etoposide for 6 hours as the positive control. Representative of 3 independent repeats.

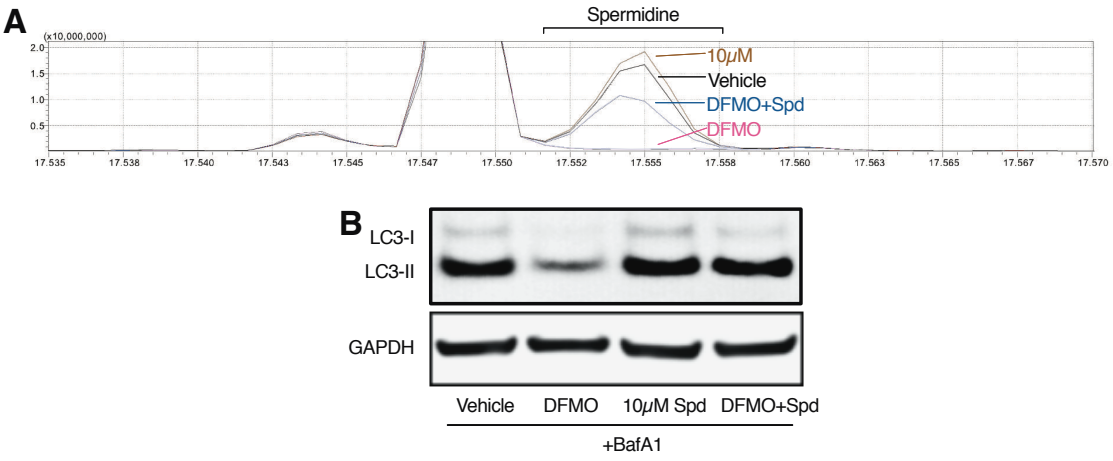


Fig 4.5 Spermidine is required for autophagy. Jurkat cells were treated with 1 mM DFMO, 10 μM spermidine, or both together for 48 hours. Cellular spermidine levels were measured by GC-MS (**A**). Cells were treated with 10 nM bafilomycin A1 (BafA1) for the final 2 hours of treatment for autophagic flux measurement using LC3-II Western blot (**B**). Representative of 3 independent repeats. The raw data of GC-MS were obtained by Zhanru Yu at the Target Discovery Institute, University of Oxford.

4.2.2 Spermidine does not inhibit HAT activity in Jurkat cells

Eisenberg *et al.* showed that spermidine inhibits HAT activity in yeast nuclear extracts and induces the expression of autophagy genes such as *ATG7* in yeast (210). I started by testing this proposed mechanism in mammalian cells. It was found that different from yeast, spermidine treatment did not increase the expression of *ATG5*, *ATG7*, *BECLIN1*, or *ATG10* in Jurkat cells (Fig 4.6). Intriguingly, a significant time-dependent up regulation of *GABARAPL1* and *SQSTM1* was observed (Fig 4.6). Different from ATG5, ATG7 and other autophagy enzymes which catalyze the autophagic reactions and can be recycled, GABARAPL1 and SQSTM1 are autophagy adaptors being degraded during autophagic degradation. Therefore it is possible that the late up regulation of these 'consumable'-like autophagy genes are due to feedback responses to autophagy induced by other mechanisms.

Besides the function of acetylating histones to regulate gene transcription, HATs also directly acetylate cytoplasmic proteins to modify their activities. De-acetylation of certain autophagy proteins such as ATG7 induces autophagy (39, 322, 323). Therefore I measured the acetylation of ATG7 with or without Spd treatment using immunoprecipitation (IP). Neither IP with the acetylated-Lysine antibody (Fig 4.7A) nor with the ATG7 antibody (Fig 4.7B) showed the acetylation changes of ATG7. Indeed there was a minor increase in acetylation of histone H3 instead of reduction (Fig 4.7A). Therefore the acetylation of neither histone nor ATG7 is reduced by spermidine treatment.

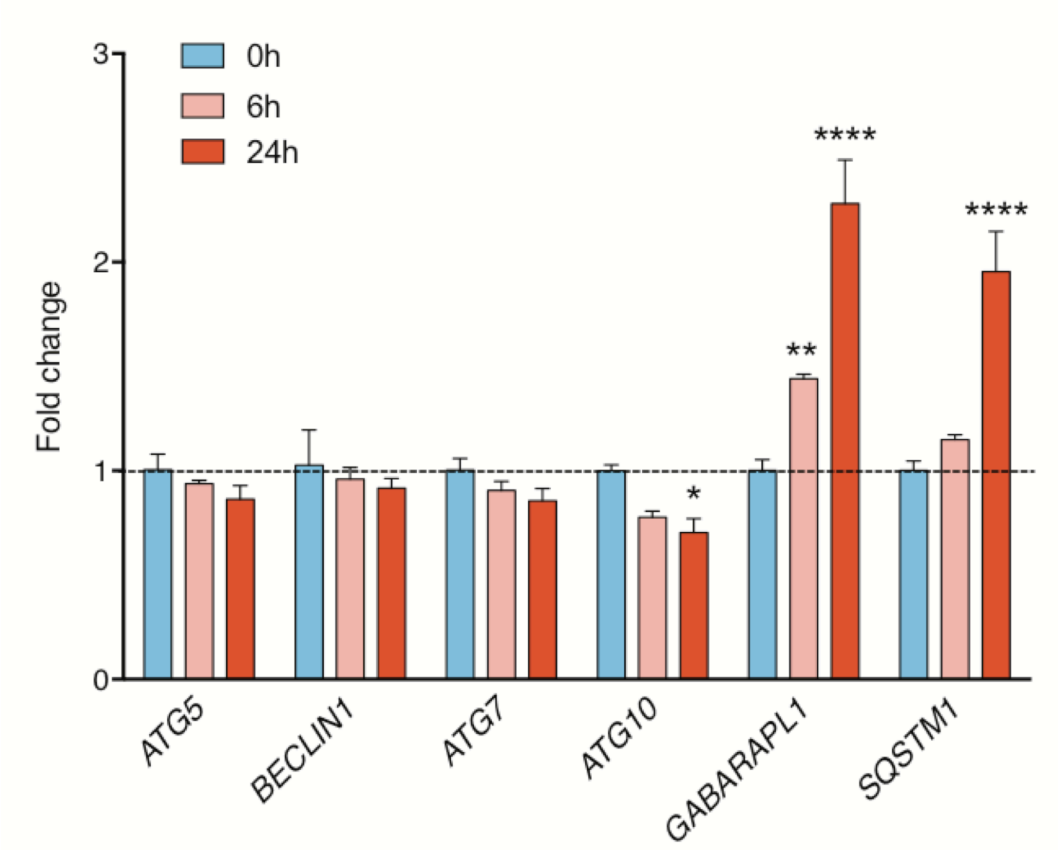


Fig 4.6 Selected autophagy gene expression changes caused by spermidine treatment. Jurkat cells were treated with 100 μM spermidine for 6 or 24 hours. mRNA levels of indicated genes were assessed by quantitative PCR (qPCR) with *GAPDH* used as the reference gene. Data represented as mean ± SEM. n = 3. Unpaired two-way ANOVA compared to 0 hours treatment, *P≤0.05, **P≤0.01, ****P≤0.0001.

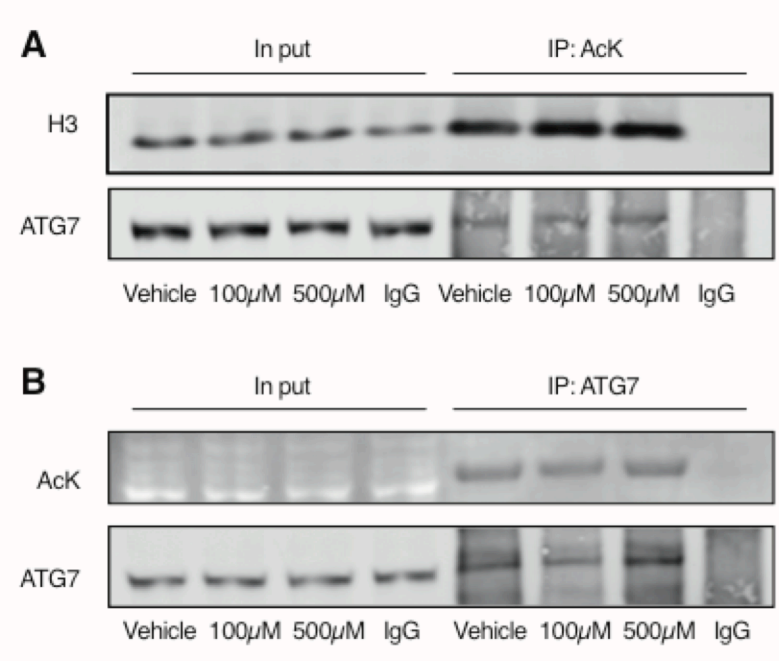


Fig 4.7 Spermidine does not reduce the acetylation of H3 or ATG7. Jurkat cells were treated with spermidine for 6 hours and lysed with NP-40 lysis buffer. Proteins with acetylated lysine residues were pulled down (IP: AcK) from the lysate, and assessed for H3 and ATG7 acetylation (**A**). To assess ATG7 acetylation in another way, ATG7 was pulled down (IP: ATG7) and acetylation measured by the antibody against AcK (**B**).

To directly assess HAT activities, I performed the HAT activity assay in two different ways. Firstly using a cell-free system as reported by Eisenberg *et al.* (210), Jurkat nuclei extract was directly incubated with spermidine for HAT activity measurement. Different from the published result showing an inhibition of HAT activities by 100 nM of spermidine in yeast, no significant changes were observed in our system (Fig 4.8A). Next I used spermidine-treated cells under autophagy-inducing conditions as established previously (100 μM or 500 μM for 6 hours, Fig 4.3) to perform the HAT activity assay. Interestingly, it was found that HAT activities were significantly increased upon spermidine treatment in a dose-dependent manner (Fig 4.8B). This is consistent with our acetylation IP result showing increased H3 acetylation (Fig 4.7A) and a similar result is also reported in human dermal fibroblasts (324). Therefore spermidine does not directly inhibit HAT activities at the concentrations I used, and the treatment with spermidine indirectly up-regulates cellular HAT activities.

It is still unknown whether the reported inhibitory effect of spermidine on HAT activities of nuclear extracts is yeast-specific (210), but it is reproducible that spermidine treatment increases cellular HAT activities and meanwhile autophagy as shown by us and others (324), indicating that inhibition of HAT activities shall not be the mechanism of spermidine-mediated autophagy induction at least in mammalian cells. Moreover, the reduced H3 acetylation and the up regulation of autophagy genes mRNA were observed after 10 to 20 days of spermidine treatment in yeast, which can also be secondary

effects of long-term spermidine treatment or persistent autophagy induction (210).

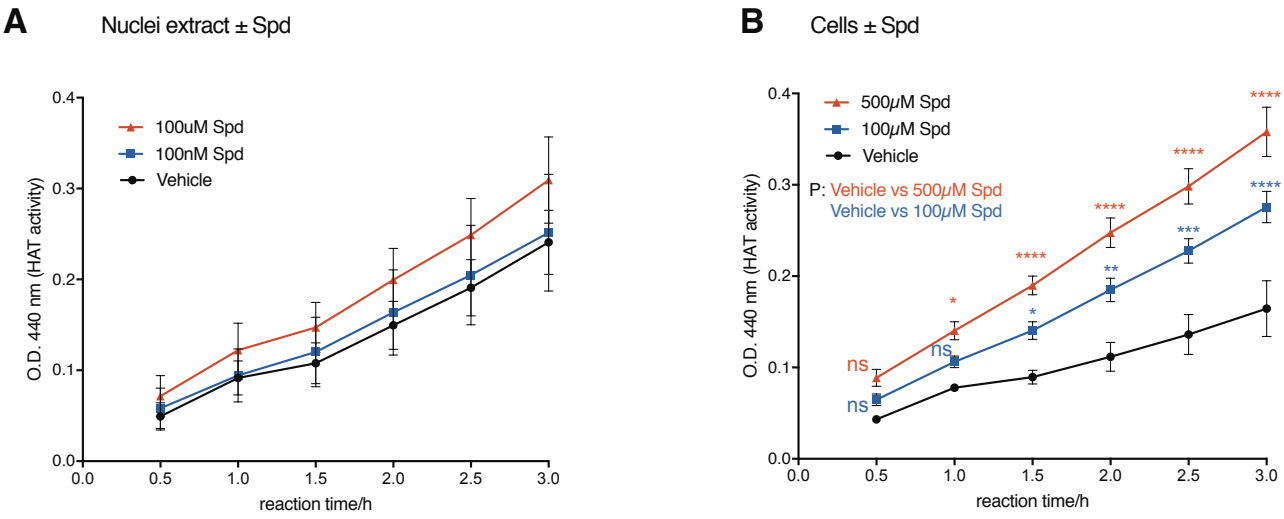


Fig 4.8 Spermidine does not inhibit HAT activity. **A.** Jurkat nuclei extract was incubated with spermidine of indicated concentrations (starting from 0h) and the relative HAT activity was measured using the HAT Activity Colorimetric Assay KIT (Biovision). **B.** Jurkat cells were treated with spermidine at the indicated concentrations for 6 hours, and then nuclei were extracted for HAT activity analysis. Data represented as mean ± SEM. n = 3. Unpaired two-way ANOVA compared to Vehicle of the corresponding time point, *P≤0.05, **P≤0.01, ***P≤0.001, ****P≤0.0001, ns, not significant.

4.2.3 High dose spermidine induces ER stress in Jurkat cells

A variety of insults could cause the accumulation of unfolded proteins in ER and triggers ER stress signaling pathways. One of the ER-stress signaling pathways is via the activation of the ER transmembrane kinase PERK and the following signals as shown in Fig 4.9A. We found that the expression of ATF4 was induced with increasing concentrations of spermidine (Fig 4.9B), being consistent with the conditions of autophagy induction. Moreover, the activation of eIF2α (assessed by phosphorylation) (Fig 4.9C) and the expression of *CHOP* (Fig 4.9D) were also induced by spermidine treatment. Therefore spermidine induces ER stress at high concentrations of over 100 μM, which might be a mechanism of autophagy induction.

Interestingly, spermidine depletion by DFMO treatment also increased the expression of *CHOP* (Fig 4.9D), indicating that spermidine is not required for ER stress responses. Therefore, the induced ER stress responses, possibly together with other stress-responses and the induced autophagy might be non-specifically triggered by high dose drug toxicity. However, considering that depletion of spermidine reduces autophagic flux (Fig 4.5), there should be an alternative mechanism of spermidine's maintenance of basal autophagy under physiological conditions.

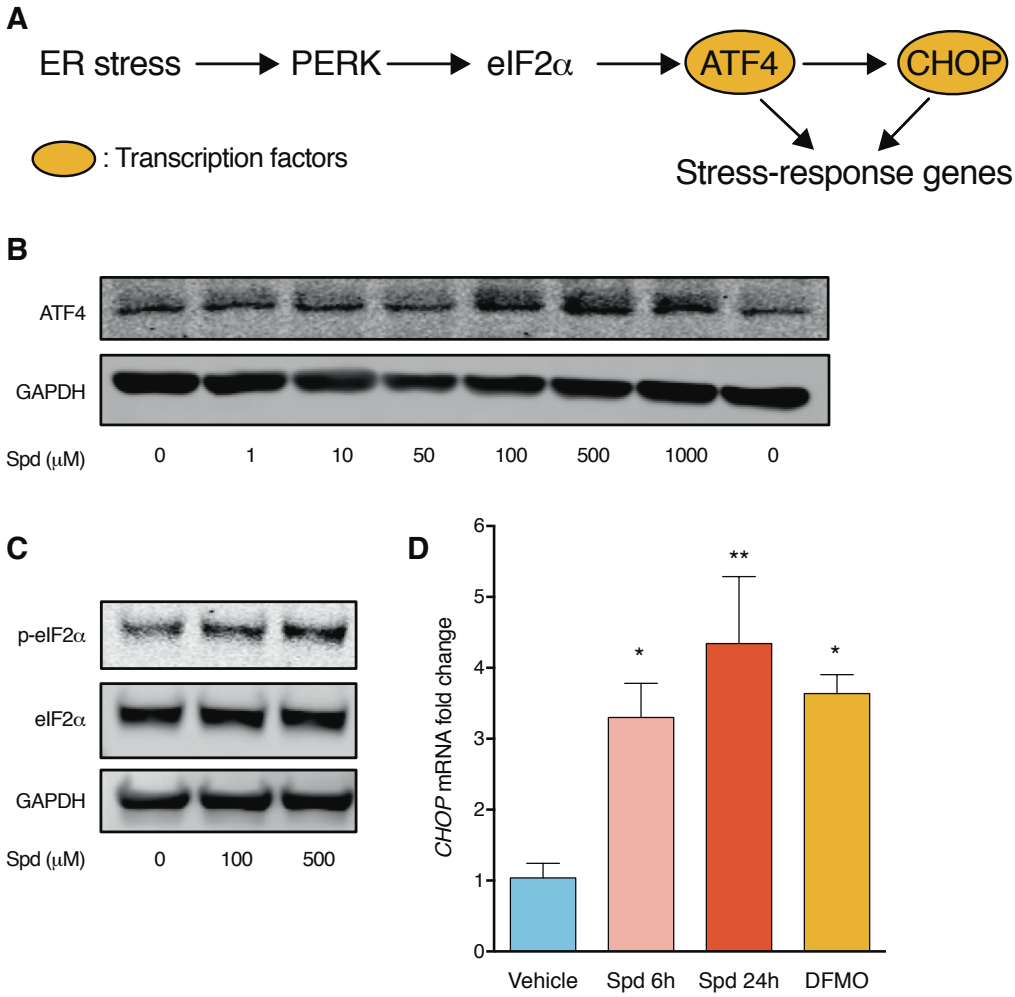


Fig 4.9 High-dose spermidine induces ER stress. **A.** Schematic overview of the ER stress PERK- eIF2α-ATF4-CHOP pathway. ER stress activates the protein kinase R-like endoplasmic reticulum kinase (PERK), which phosphorylates eIF2α. Phosphorylated eIF2α facilitates the translation of the transcription factor ATF4, which then induces the expression of CHOP. ATF4 and CHOP induces the expression of multiple stress-response genes including chaperones, apoptosis, and autophagy. **B/C.** Jurkat cells were treated with spermidine of indicated concentrations for 6 hours. The expression of ER stress markers ATF4 (**B**) and phosphorylation of eIF2α (**C**) were assessed by Western blot. Representative of 3 independent repeats. **D.** Jurkat cells were treated with 100 μM spermidine for 6 or 24 hours, or with 1 mM DFMO for 48 hours. The expression of the ER stress marker *CHOP* was assessed by qPCR. *GAPDH* was used as the reference gene. Data represented as mean ± SEM. n = 3. Unpaired one-way ANOVA compared to Vehicle, *P≤0.05, **P≤0.01.

4.2.4 Hypusinated eIF5A is required for autophagy

Spermidine functions as the unique substrate for eIF5A hypusination. I confirmed that DFMO treatment reduced the hypusination of eIF5A, which was rescued by adding together with spermidine (Fig 4.10), indicating that spermidine is required for eIF5A hypusination in Jurkat cells.

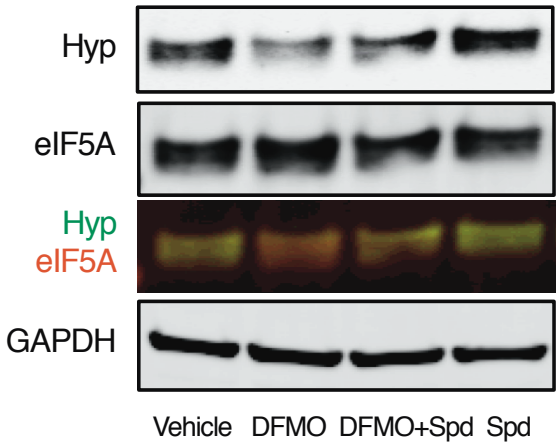


Fig 4.10 Spermidine is required for the hypusination of eIF5A. Jurkat cells were treated with 1 mM DFMO, 10 μM spermidine, or both together for 48 hours. The expression of the overall eIF5A (eIF5A) and the hypusinated eIF5A (Hyp) was assessed by Western blot. Representative of 3 independent repeats.

To test if eIF5A is required for autophagy, we inducibly knocked down *Eif5a* in mouse NIH 3T3 cells. It was found that removal of eIF5A caused a reduction of LC3-II with BafA1 treatment (Fig 4.11), indicating that eIF5A is required for autophagic flux.

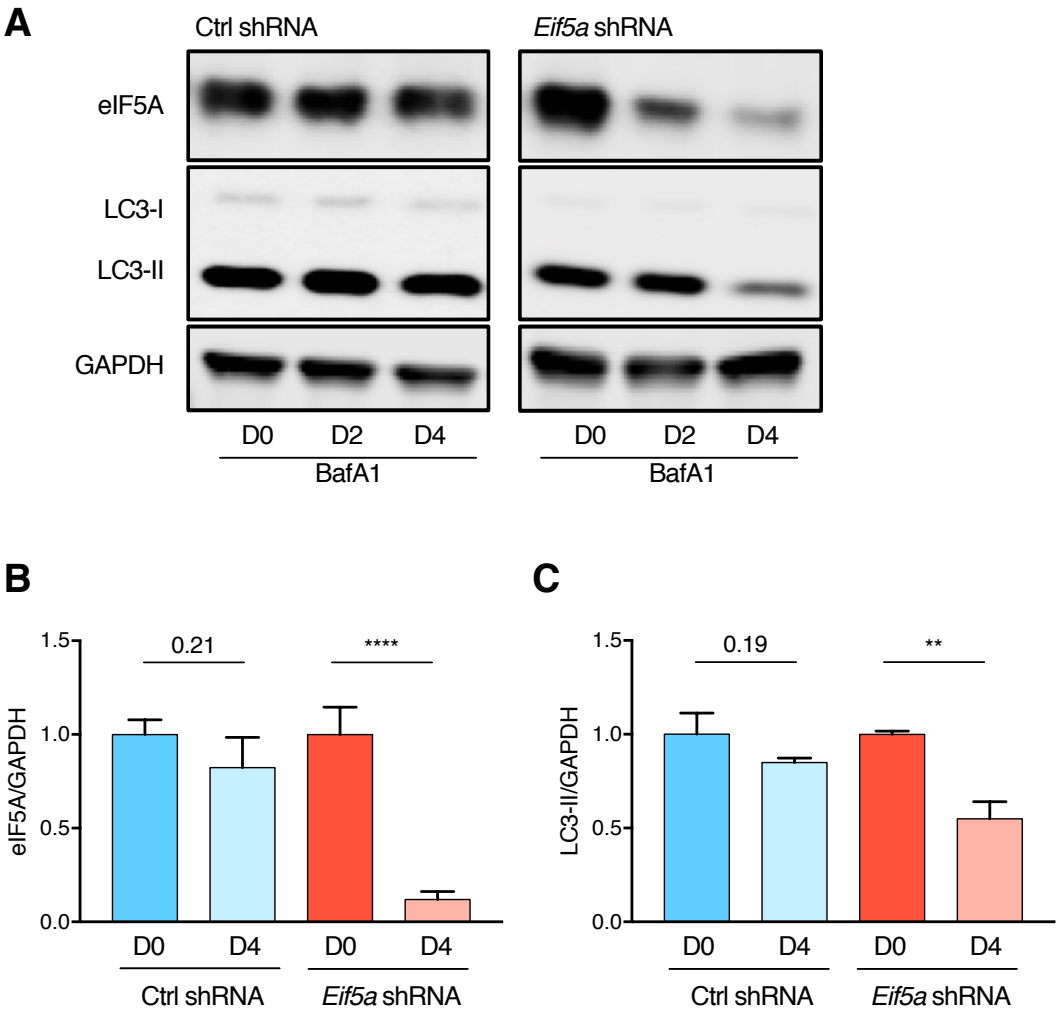


Fig 4.11 eIF5A is required for autophagy. **A.** The knockdown of *Eif5a* was induced by IPTG in NIH3T3 cells expressing inducible *Eif5a* shRNA. The expression of eIF5A and LC3-II on indicated days after IPTG induction was measured by Western blot. All cells were treated with BafA1 for 2 hours. The quantification results are shown in **B** and **C**. The eIF5A or LC3-II band intensity was normalized to GAPDH first and then to D0. n = 3 to 6 independent repeats per group. One-tailed (B) and two-tailed (C) unpaired Student's t-test with P values labelled out, **P≤0.01, ****P≤0.0001. Data represented as mean ± SEM.

To test if the hypusination plays a role in eIF5A's control of autophagy, we inducibly knocked out the essential hypusination gene *Dohh* (Fig 4.1) in 3T3 cells. Deletion of *Dohh* resulted in a reduction of eIF5A hypusination without affecting the overall eIF5A protein abundance, and the autophagic flux was also reduced (Fig 4.12A-C). Moreover, I also used GC7, a specific inhibitor of the hypusination enzyme DHS (Fig 4.1) to block hypusination in Jurkat cells. Similar to *Dohh* knockout, GC7 treatment led to a reduction of the eIF5A hypusination (Fig 4.12D) and the autophagic flux (Fig 4.12E). Therefore, hypusinated eIF5A is required for autophagic flux under basal conditions.

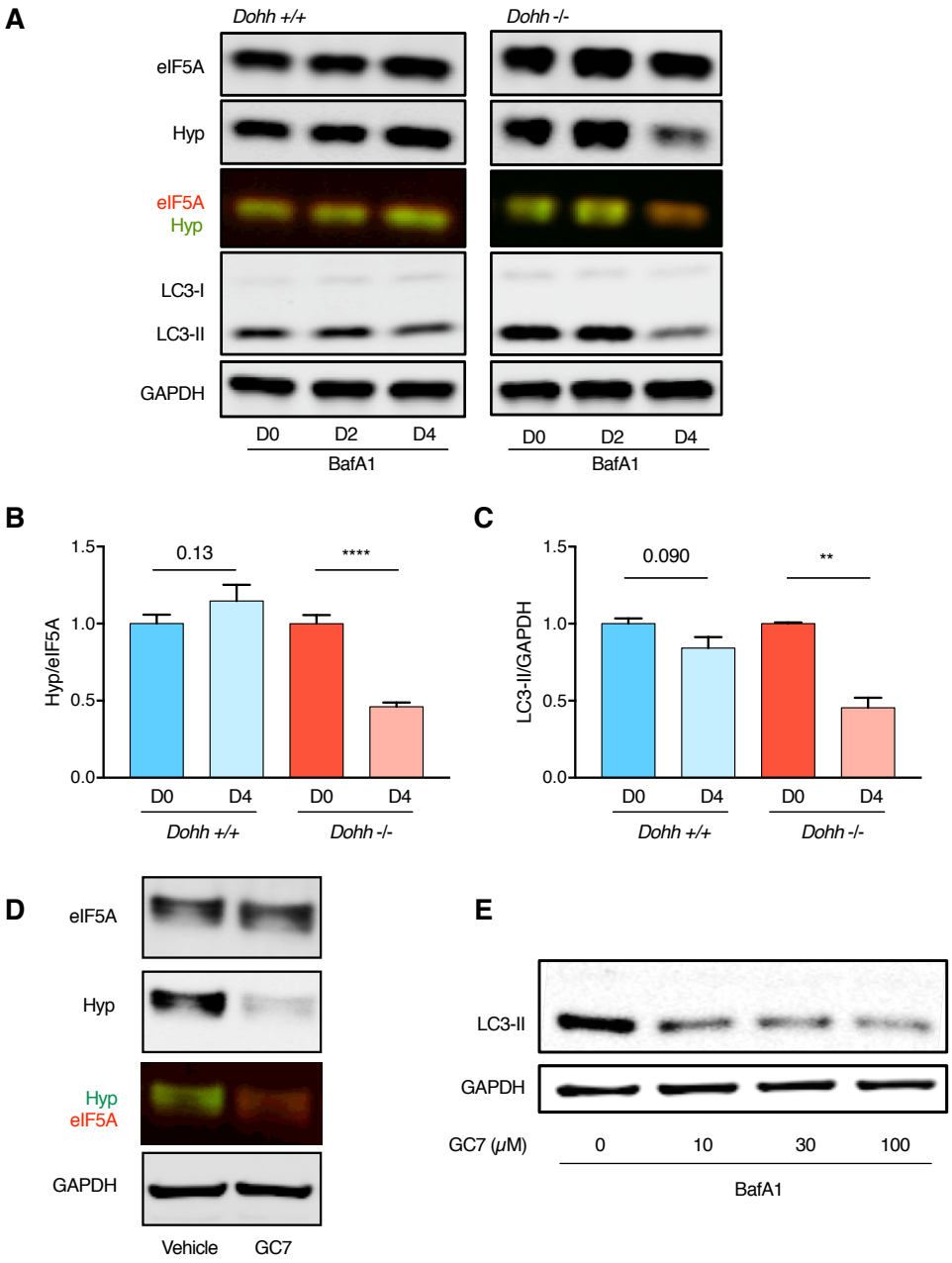


Fig 4.12 Hypusination of eIF5A is required for autophagy. **A-C.** The deletion of *Dohh* was induced by 4-OHT in 3T3 cells derived from transgenic mouse embryonic fibroblasts. The hypusination of eIF5A and LC3-II were measured by Western blot on indicated days after 4-OHT induction. All cells were treated with BafA1. The quantification results are shown in B and C. Hypusine was normalized to eIF5A first and then to D0. LC3-II was normalized to GAPDH first and then to D0. n = 3 to 6 independent repeats. One-tailed (B) and two-tailed (C) unpaired Student's t-test with P values labelled out, **P≤0.01, ****P≤0.0001. Data represented as mean ± SEM. **D.** Jurkat cells were treated with 100 μM GC7 for 24 hours, and the hypusination of eIF5A was assessed by Western blot. **E.** Jurkat cells were treated with GC7 at indicated concentrations for 24 hours, and the LC3-II expression was assessed by Western blot. All cells were treated with BafA1. Representative of 3 independent repeats.

4.2.5 Autophagy and the expression of eIF5A are induced during primary B cell activation

To confirm that eIF5A is also required for autophagy in primary cells, the mouse spleen B cells were chosen as our model. It was found that LPS-stimulated murine B cells significantly up regulated their LC3-II expression as shown by flow cytometry staining (Fig 4.13A/B) and western blot (Fig 4.13C), indicating that autophagy is induced during B cell activation. The expression of eIF5A and its hypusination were also increased during B cell activation (Fig 4.13C-E). Interestingly, the quantification results showed that the protein levels of overall eIF5A reached the peak on day 1 post stimulation, whereas the hypusinated eIF5A proteins reach the peak on day 2 (Fig 4.13D/E). Such delay of eIF5A hypusination indicates that the hypusination system (DHS and DOHH) is coordinately stimulated post the increase of eIF5A.

4.2.6 Hypusinated eIF5A is required for autophagy in primary B cells

To assess if hypusinated eIF5A is also required for autophagy in primary B cells, the DHS inhibitor GC7 was used. GC7 treatment reduced the hypusination of eIF5A without affecting the overall eIF5A expression in primary B cells (Fig 4.14A-C), and the autophagic flux was also reduced (Fig 4.14A/D). GC7 treatment did not increase the phosphorylation of S6 (Fig 4.15), indicating that the reduced autophagic flux is not due to activation of mTOR. Therefore, hypusinated eIF5A maintains autophagic flux in activated primary B cells in an mTOR-independent manner.

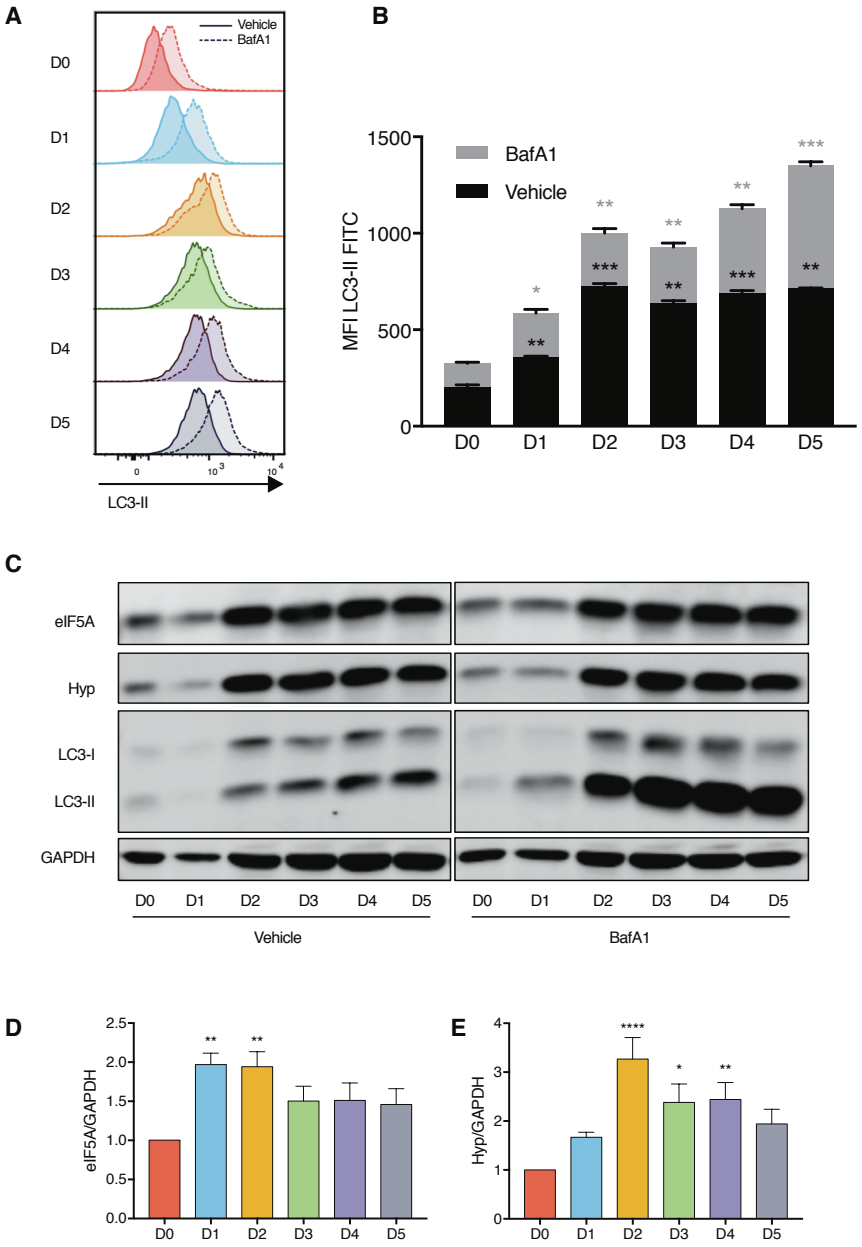


Fig 4.13 Autophagy and the expression of hypusinated eIF5A are induced during primary B cell activation. B cells were sorted from spleens of young mice (6-12 weeks), cultured with LPS for indicated number of days, with or without BafA1 for the final 2 hours of culture. **A/B.** LC3-II was measured by flow cytometry (**A**) with the quantification shown in **B**. The grey bars refer to BafA1 minus Vehicle. n = 3 independent repeats. One-way ANOVA was used to compare the LC3-II staining of either vehicle or BafA1 treatment on indicated days to D0. **C-E.** The expression of LC3-II, overall eIF5A and hypusinated eIF5A were assessed by Western blot (**C**), and the quantification results are shown in **D** and **E**. Target protein band intensity was normalized to GAPDH first, and then to D0. One-way ANOVA compared to D0. n = 7. Data represented as mean ± SEM. *P≤0.05, **P≤0.01, ***P≤0.001, ****P≤0.0001.

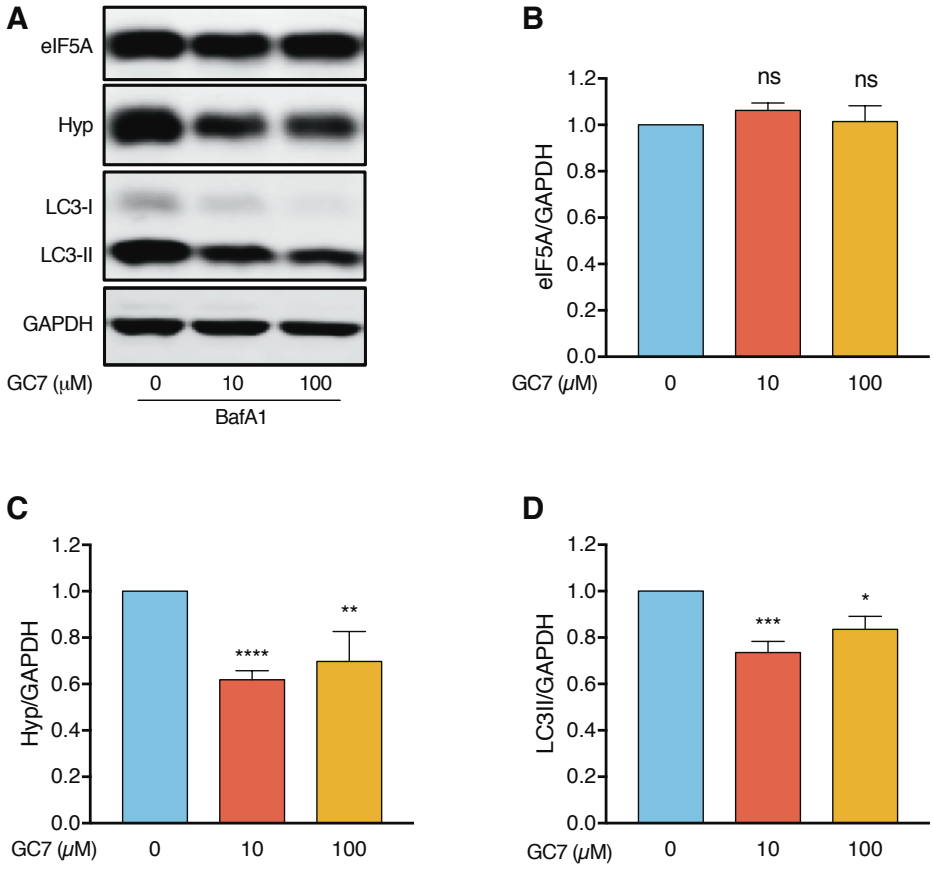


Fig 4.14 eIF5A hypusination is required for autophagy in B cells. B cells were activated with LPS as in Fig 4.13, and treated on day 2 of activation with GC7 of indicated concentrations for 24 hours. LC3-II and eIF5A hypusination were assessed by Western blot (**A**). The protein bands intensity of overall eIF5A (**B**), hypusinated eIF5A (**C**), and LC3-II (**D**) was quantified and normalized to GAPDH first and then to the vehicle control (0 μM GC7). Data represented as mean ± SEM. n = 6 to 10. One-way ANOVA compared to 0 μM GC7. *P≤0.05, **P≤0.01, ***P≤0.001, ****P≤0.0001.

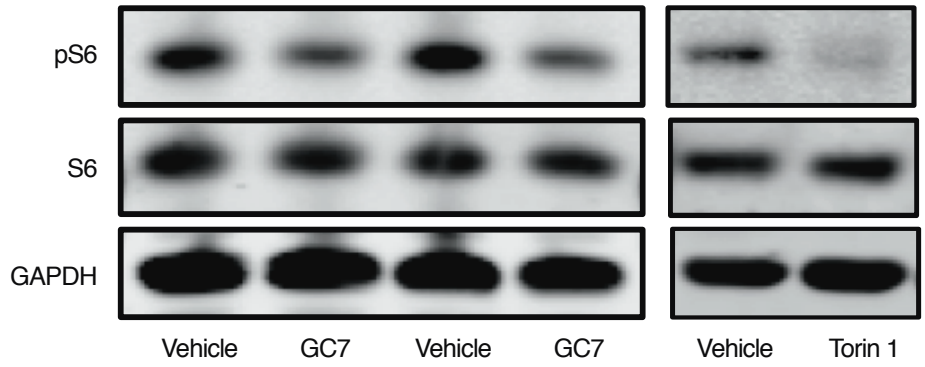


Fig 4.15 Hypusinated eIF5A regulates autophagy in an mTOR-independent manner. LPS-activated mouse B cells were treated with 10 μM GC7 for 24 hours as in Fig 4.2.7.1 (left), or with the mTOR inhibitor Torin 1 for 2 hours (right). The phosphorylation of S6 was assessed by Western blot. Representative of 5 independent repeats.

4.2.7 Hypusinated eIF5A is required for optimal protein synthesis

Since eIF5A is a translation factor, I firstly tested if eIF5A controls overall protein synthesis using O-propargyl-puromycin (OPP)-Click assay (Fig 4.16A). The protein synthesis rate is measured by the amount of incorporation of OPP into newly synthesized peptides within half hour of incubation time. It was found that the protein synthesis rate was reduced with GC7 treatment in Jurkat cells, but not to the same extent as using the potent translation elongation inhibitor cycloheximide (Fig 4.16B/C), indicating that the hypusinated eIF5A is required for optimal protein translation but may not be essential for all translational events. Moreover, spermidine depletion by DFMO treatment also led to a significant reduction of protein synthesis, which was rescued by adding spermidine together (Fig 4.16D). Therefore, spermidine and hypusinated eIF5A positively regulate protein translation.

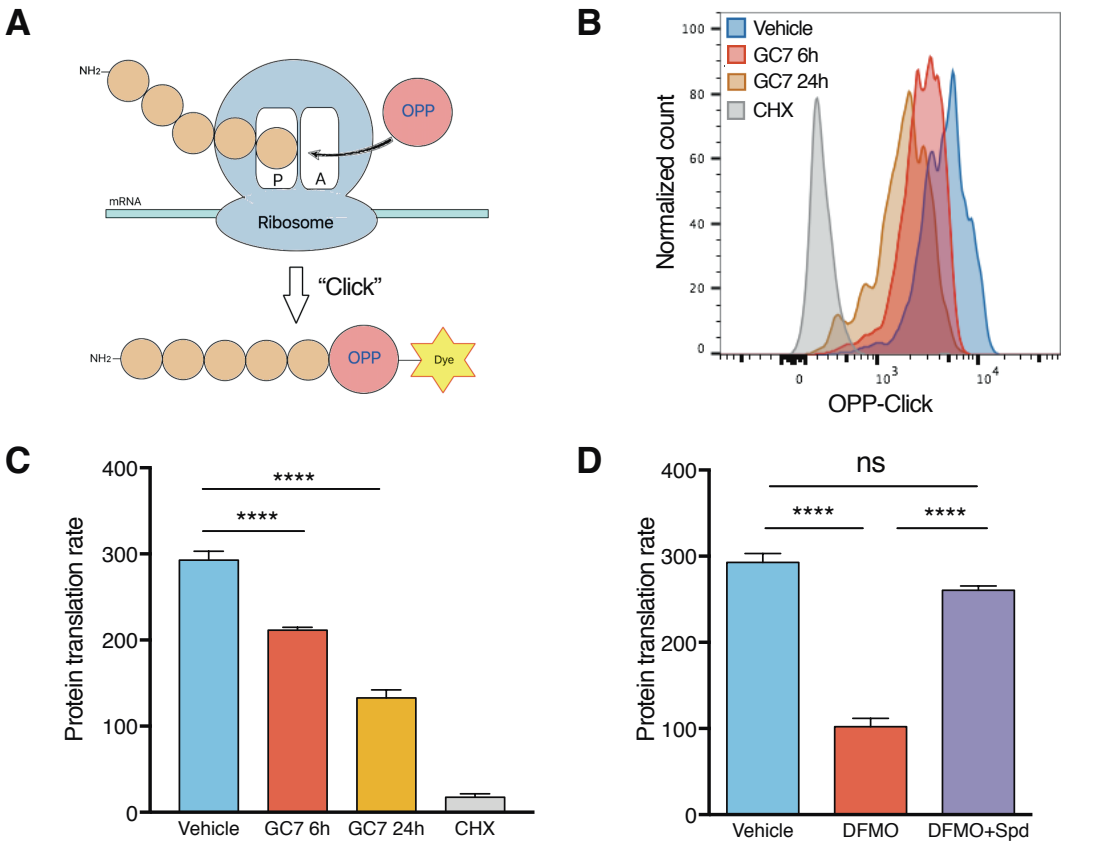


Fig 4.16 Hypusinated eIF5A is required for optimal protein synthesis. **A.** Schematic overview of the OPP-Click assay measuring protein synthesis rate. O-propargyl-puromycin (OPP) is incorporated into newly synthesized peptides. A fluorophore is then conjugated to OPP via Click reaction for detection. **B/C.** Jurkat cells were treated with 100 μM GC7 for 6 or 24 hours, and the protein translation rate was measured by OPP-Click assay. Cells were treated with the protein translation inhibitor cycloheximide (CHX) for 2 hours as the positive control. **D.** Jurkat cells were treated with 1 mM DFMO or 1 mM DFMO+10 μM spermidine for 48 hours followed with OPP-Click assay. n = 3 to 4. Unpaired one-way ANOVA, ****P≤0.0001, ns, not significant. Data represented as mean ± SEM.

4.2.8 Hypusinated eIF5A is required for translation initiation and termination in primary B cells

To further investigate the functions of eIF5A in primary B cells, we performed ribosome profiling which measures the ribosome occupancy on mRNAs at single nucleotide resolution. This is the first ribosome profiling study in mammalian cells to reveal the functions of hypusinated eIF5A (304, 325). We found that GC7 treatment resulted in higher ribosome occupancy at the start codon and before the stop codon (Fig 4.17), indicating that the translation initiation and termination is paused upon removal of eIF5A hypusination. This is consistent with the OPP-Click result (Fig 4.16), both indicating that hypusinated eIF5A is required for the overall translation probably in a non-gene-specific manner in mammalian cells.

4.2.9 Polyproline causes translation stalls in primary B cells

Both bacteria and yeast studies showed that polyproline motifs cause translational stalling, which requires EF-P or hypusinated eIF5A to resolve (300, 302, 304, 325, 326). We observed that there was a genome-wide stalling of ribosomes at the tri-proline (PPP) motif in the vehicle sample (Fig 4.18A). Unexpectedly, a milder stalling was found in the GC7 sample (Fig 4.18A). The expected increased stalling at PPP with GC7 treatment was only seen when we focused on 100 genes with highest stalling ratio at PPP (Fig 4.18B). Therefore different genes containing PPP motifs may respond differently to GC7 treatment at least in primary B cells. The potential cause of the reduced stalling by GC7 treatment will be discussed later.

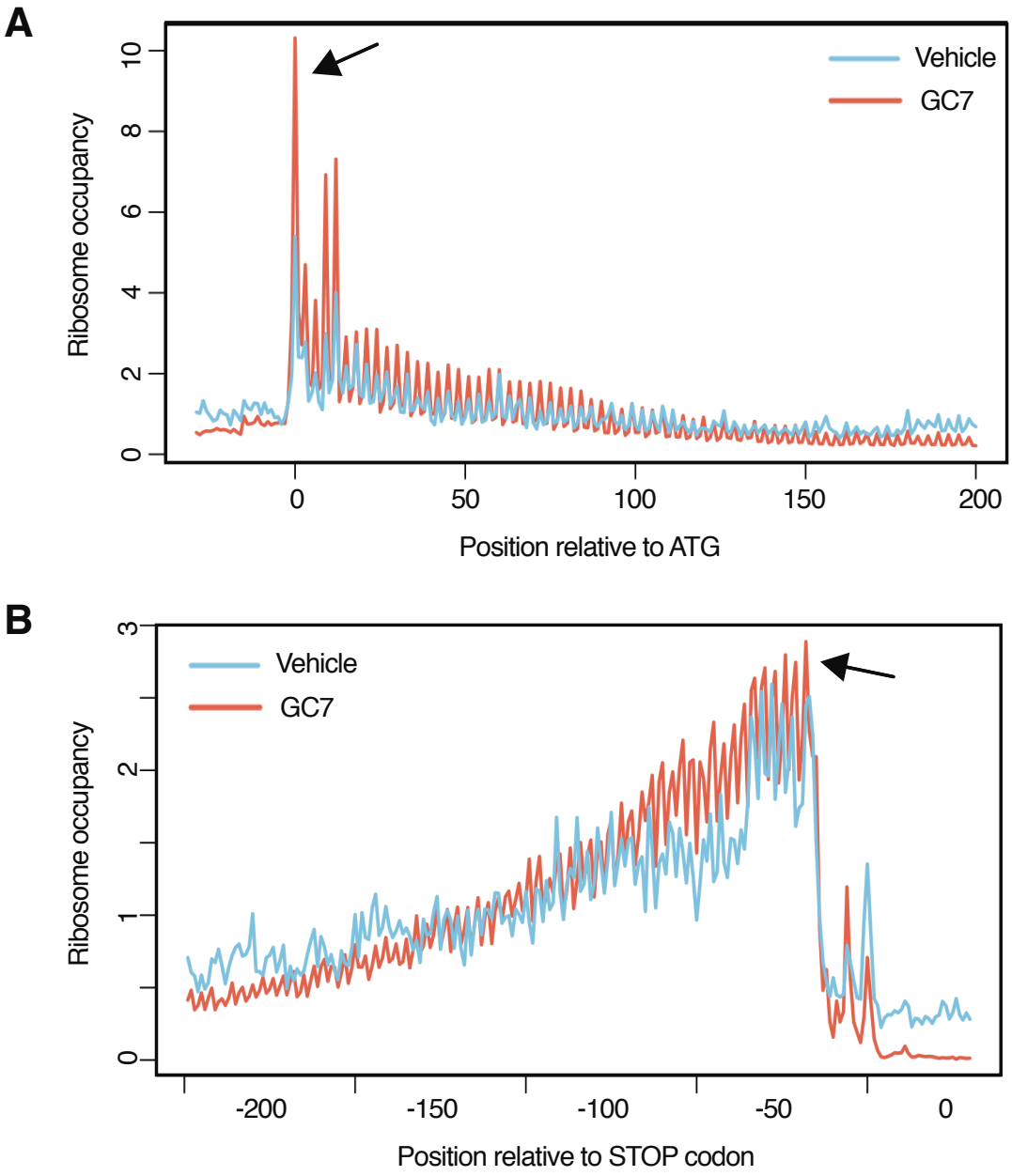


Fig 4.17 Hypusinated eIF5A controls translation initiation and termination. Mouse B cells were treated with 10 μM GC7 as in Fig 4.14 and processed for ribosome profiling. Ribosome occupancy of all genes is aligned at the start codon (**A**) or stop codon (**B**) and normalized to a mean value of 1 for each gene. Arrows indicate the stalling of initiation (A) and termination (B). The ribosome profiling was carried out in collaboration with Jack Feltham in Jane Mellor's group, Department of Biochemistry, University of Oxford. The sequencing library was prepared and the sequencing data were analyzed with Jack.

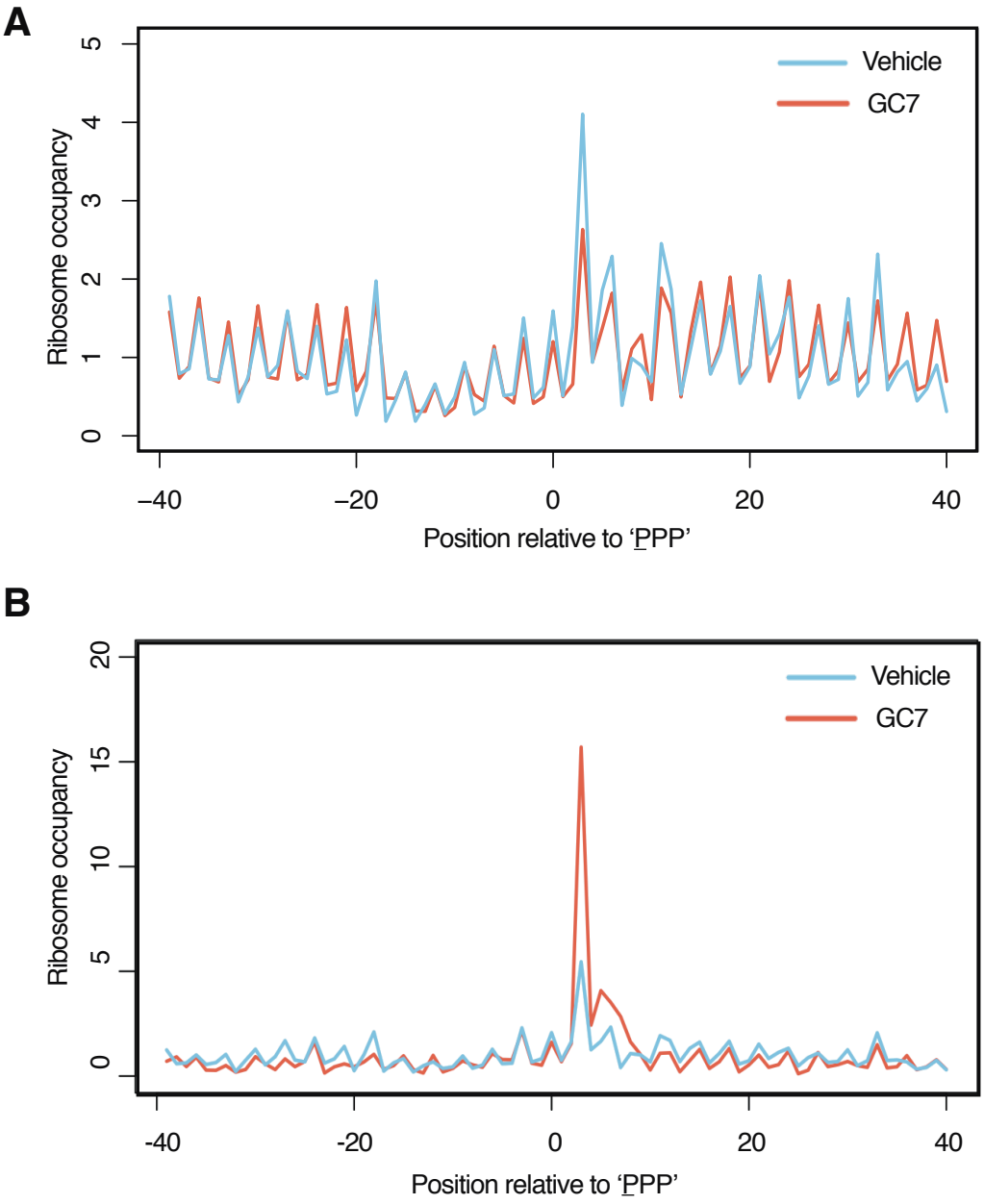


Fig 4.18 Polyproline stalls translation. Mouse B cells treated with GC7 were processed for ribosome profiling as in Fig 4.17. **A.** Ribosome occupancy of all genes with PPP is aligned to the underlined Pro on the P site of the ribosome and normalized to a mean value of 1 for each gene. **B.** 100 genes with highest stalling ratio at PPP without or with GC7 are aligned to the underlined Pro on the P site of the ribosome. Data were obtained and analyzed with Jack Feltham as in Fig 4.17.

Chapter 4. Spermidine Regulates Autophagy via eIF5A Hypusination

4.3 Discussion

4.3.1 Can we induce eIF5A hypusination?

In this chapter, we show that spermidine regulates eIF5A hypusination, which is key for eIF5A's functions including maintaining autophagic flux. Therefore drugs inducing eIF5A hypusination may mimic spermidine's effect to induce autophagy and delay ageing. This post-translational modification involves a series of enzymatic reactions, serving as potential drug targets. The three forms of eIF5A (Fig 4.1, eIF5A-Lys, eIF5A-Dhp, and eIF5A-Hyp) can be distinguished according to their different pI values using 2-dementional western blot, which shows that about 30% of eIF5A is present in a non-hypusinated form in cultured NT2 cells (327).

To increase hypusination efficiency, either the substrate concentration or the enzyme activity (DHS and DOHH) or both need to be improved. It is generally easier to inhibit rather than to increase the activity of an enzyme using drugs. Therefore in theory DHS and DOHH are not ideal targets for drug screening to improve their activities. Another way is to increase the cellular concentration of spermidine. Instead of directly giving more spermidine to cells, the catabolic enzymes of spermidine such as the spermidine/spermine-N1-acetyltransferase (208) would be an ideal target to inhibit.

Indeed, aaptamine, a natural compound isolated from the marine sponge, was found to be able to reduce the non-hypusinated eIF5A in NT2 cells (327). The target or the mechanism of aaptamine leading to reduced non-hypusinated eIF5A is still unknown, but it would be worthwhile administering this

compound to cultured cells or old mice to see if hypusination of eIF5A and more importantly immune senescence can be improved.

4.3.2 Why is PPP stalling reduced upon GC7 treatment in primary B cells?

According to the reported functions of EF-P or hypusinated eIF5A to improve translation of PPP motifs in bacteria and yeast (300, 302, 304, 325), the chance is very low that ribosomes without hypusinated eIF5A would translate PPP motifs better in primary B cells. Instead, it is likely to be the complexity of the system we are using (stimulated primary cells with drug treatment) that causes the difference between our ribosome profiling results and the results obtained in model organisms yeast and bacteria.

Is the discrepancy caused by the way we blocked hypusination, *i.e.* GC7 treatment versus genetic knockout? The inhibitor GC7 fails to fully block eIF5A hypusination as shown in Fig 4.14. It might be sufficient for cells to use half-hypusinated eIF5A to assist their translation, and therefore no further stalling occurs. However, this hypothesis cannot explain why there is a reduction (Fig 4.18A) of the stalling rather than no difference, and actually the stalling does happen to a group of genes (Fig 4.18B) but for unknown reasons is hidden in the genome-wide analysis. Compared to a complete removal of hypusination using a genetic knockout, the advantage of half-removal is that it more closely mimics the physiological conditions, where usually a reduction of protein expression happens rather than full deletion. The functions of a protein may vary in a dose-dependent manner, but unfortunately the majority of

current biomedical research describing phenotypes largely relies on full genetic knockout, which cannot quantitatively control protein expression in complex biological systems. Highly specific small compounds may help with this, exerting their effects in a dose-dependent manner.

An alternative hypothesis to explain the reduced ribosome occupancy or loss of reads at PPP motifs by GC7 treatment is mRNA decay. Actually it has been reported that stalls in translation elongation could target the mRNA for endonucleolytic cleavage, named 'no-go decay' (328). In contrast to bacteria and yeast, activated B cells differentiate into cells with a heavy protein synthesis burden, *i.e.* professional antibody-secreting plasmablasts and plasma cells (329, 330). Considering that there is already a marked stalling at PPP motifs in activated B cells (Fig 4.18A), it is possible that removal of hypusinated eIF5A may cause more severe stallings, some of which are accumulated and detected in Fig 4.18B, whereas others are degraded resulting in reduced reads and the neutralization of the overall stalling in Fig 4.18A. To test this hypothesis of mRNA decay, the half-life of mRNAs could be measured.

4.3.3 Conclusions

In this chapter, we focused on the molecular mechanism of autophagy regulation by spermidine. Spermidine was proposed to be an inhibitor of HAT to induce autophagy but the supporting data were weak (210). We repeated relevant experiments and found that spermidine did not directly inhibit HAT

activities in Jurkat cells. Instead, high-dose spermidine non-specifically induces cellular stress and autophagy. It is possible that the cellular spermidine is saturated to maintain autophagy, therefore it is more reasonable to deplete spermidine rather than adding more to find out the target of spermidine under physiological conditions.

To find out how spermidine maintains basal autophagic flux, we depleted cellular polyamines and found that the hypusination of eIF5A was reduced, confirming that spermidine is essential for eIF5A hypusination in mammalian cells. Genetic or drug-inhibition of eIF5A hypusination reduced autophagic flux in cell lines and primary B cells, indicating that hypusinated eIF5A regulates autophagy. Following analysis of protein translation using ribosome profiling showed that hypusinated eIF5A controls overall translation initiation and termination. Similar to bacteria and yeast, polyproline motifs cause translational stalling in activated B cells. Removal of hypusinated eIF5A leads to more severe stalling of certain mRNAs at polyproline motifs.

Chapter 5. eIF5A Controls TFEB Expression

5.1 Introduction

5.1.1 MiT transcription factors

Transcription factor EB (TFEB) is a member of the microphthalmia transcription factor (MiT) family belonging to the basic helix-loop-helix leucine zipper transcription factors (bHLH-Zip) superfamily. The MiT family has four members in mammals: TFEB, MITF, TFE3 and TFEC. They share an identical basic domain that is used for DNA binding and similar HLH and Zip domains to form homo- or hetero-dimers (331, 332). TFEB, MITF, and TFE3 are activators of gene expression, whereas TFEC is more evolutionarily and functionally divergent being a mild inhibitor or activator of transcription in different organisms (333-335).

Only one MiT ortholog has been identified in invertebrates, called HLH-30 in *Caenorhabditis elegans* (336), and Mitf in *Drosophila melanogaster* (337). Two orthologs of MiT family have been described in fish and *Xenopus laevis* (338, 339). This suggests that two duplication events happened between invertebrates and mammalian cells. Whether MiT families acquire novel functions with the increasing developmental and functional complexity is still unclear.

5.1.2 TFEB is a key autophagy/lysosome transcription factor

TFEB activates the transcription of multiple autophagy and lysosomal genes through binding to the Coordinated Lysosomal Expression and Regulation (CLEAR) motif in mammalian cells (30, 340). Accordingly, *TFEB* overexpression leads to increased numbers of autophagosomes, expanded

lysosomal compartments, increased lysosomal enzyme activity, and enhanced autophagic flux (30, 340). Conversely, knockdown of *TFEB* results in reduced autophagic flux (30). Similarly, HLH-30, the TFEB ortholog in worms, induces the transcription of autophagy and lysosomal genes (341), suggesting the conserved functions between HLH-30 and TFEB. Overexpression of the other three MiT transcription factors, MITF, TFE3, or TFEC does not induce the expression of lysosomal genes, indicating that the pro-autophagy/lysosomal function is TFEB-specific (340). Interestingly, TFEB also promotes the transcription of its own gene by direct binding to CLEAR elements on its promoter, suggesting an autoregulatory feedback loop of TFEB expression and autophagy (342).

In addition to autophagy/lysosome-related functions, TFEB has been reported to control other biological process. For example, murine TFEB directly binds to the CLEAR motif on promoter of *Glut1* and *Glut4* to induce the expression of these glucose transporters and promote glucose uptake (343). Moreover, TFEB is involved in innate immune responses and may control the expression of cytokine genes. Upon infection or LPS-stimulation, TFEB and TFE3 are activated and translocated into the nucleus of murine macrophages (344-346). Knockout of either TFEB or TFE3 results in a modest but significant reduction of cytokine expression such as IL-1β, IL-6 and TNF-α (344, 347). Mechanistically, chromatin immunoprecipitation- (ChIP-) seq shows that TFE3 directly binds to the promoter of several cytokine genes. CLEAR motifs are

also found on their promoters, suggesting that they may directly recruit TFEB (344).

5.1.3 Molecular mechanisms of TFEB activation

The activity of TFEB is mainly controlled by phosphorylation. At the steady state, TFEB is phosphorylated at Ser142 and Ser211 (Fig 5.1) (28, 30, 348, 349). Point mutation of either Ser142 or Ser211 into Ala leads to TFEB nuclear translocation and activation (28, 30, 348, 349), indicating that these two phosphorylation sites are required for its cytosolic retention. TFEB with Ser211 phosphorylation interacts with 14-3-3 chaperone proteins, which possibly masks the nuclear localization signal (NLS) of TFEB and thus prevents its nuclear translocation (348, 349).

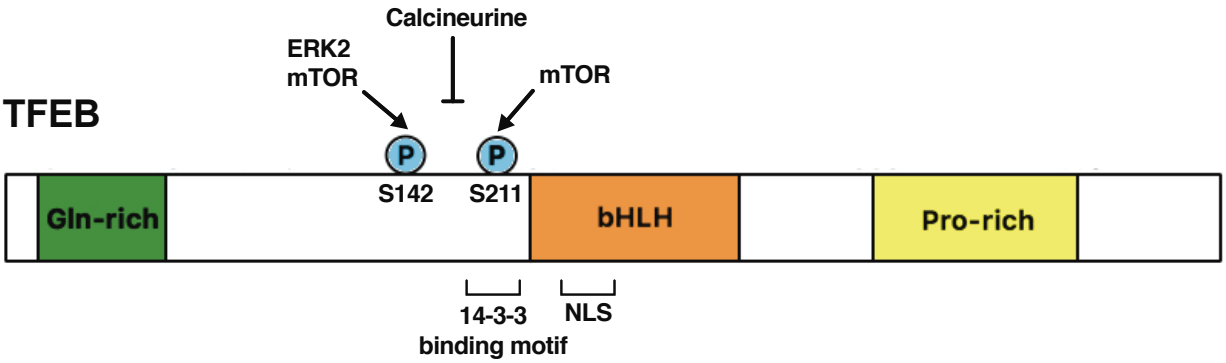


Fig 5.1 Human TFEB protein structure. The phosphorylation of S142 and S211 are regulated by the kinase ERK2 and mTORC1, and the phosphatase calcineurin. Phosphorylation of S211 promotes the binding to 14-3-3, which may mask the NLS domain for nuclear translocation.

The phosphorylation status of TFEB is a finely regulated by multiple kinases and phosphatases. In the presence of nutrients, S142 and Ser211 residues of TFEB are phosphorylated by mTORC1 present on lysosomal surfaces (349-351). Another cell growth regulator ERK2 phosphorylates TFEB at Ser142, although the related retention mechanism is still unclear (30). On the other hand, both Ser142 and Ser211 of TFEB are dephosphorylated by calcineurin (352), which is a Ca^{2+}-dependent protein phosphatase. Starvation induces dephosphorylation of TFEB in two ways: mTORC1 dissociates from lysosomal surface (350) and gets inactivated (353), while Ca^{2+} is released from lysosomes and activates calcineurin (352).

5.1.4 TFEB functions *in vivo*

5.1.4.1 TFEB knockout is embryonic lethal

Whole-body knockout of *Tfeb* in mice leads to embryonic lethality on E9.5-10.5 due to primarily placental vascularization defects (354), indicating that the MiT family members are not functionally redundant and TFEB has distinct functions from the other three MiT family members. Cultured embryonic bodies with *Tfeb* mutations also show impaired endodermal specification possibly due to lysosomal defects (355). Because of the survival problem of full *Tfeb* knockout, conditional knockout mouse models have been used to uncover more specialized functions of TFEB in various healthy tissues, with a few examples listed below.

5.1.4.2 TFEB in liver

TFEB controls lipid metabolism in liver (342). Mice with liver-specific TFEB knockout acquire obesity, whereas TFEB overexpression reduces body fat and rescues obesity (342). Starvation induces TFEB expression in hepatocytes, which drives degradation of lipid droplets in an autophagy-dependent manner. Interestingly, TFEB also directly regulates the expression of *Pgc-1α*, a transcription co-activator controlling mitochondria biogenesis and thus energy metabolism (356). Therefore TFEB coordinates lipid autophagy (lipophagy) with subsequent mitochondrial degradation of free fatty acids.

5.1.4.3 TFEB in muscle

The glucose metabolism is controlled by TFEB in skeletal muscle (343). Acute exhausting contraction activates TFEB in myofibers, which then triggers mitochondrial biogenesis and enhances mitochondrial respiration (343). Surprisingly, TFEB activation does not activate autophagy, and knockout of TFEB does not impair autophagic flux in skeletal muscles (343), indicating that TFEB controls mitochondria metabolism independent of autophagy in this tissue. Indeed TFEB can be directly recruited to the promoters of mitochondrial biogenesis genes such as *Nrf1* and *Nrf2*, and glucose transporter genes such as *Glut1* and *Glut4* (343). Therefore TFEB directly regulates mitochondrial biogenesis and energy metabolism in cells, which is a novel function of TFEB besides regulating autophagy and lysosomal biogenesis.

5.1.4.4 TFEB in immune cells

The expression of TFEB is induced in LPS-stimulated murine dendritic cells (357). TFEB promotes the phagosomal acidification and protein degradation, and enhances the antigen presentation via MHC class II (357). Interestingly, the MHC class I-mediated exogenous antigen presentation was suppressed by TFEB overexpression (357), suggesting that TFEB is involved in differential regulation of antigen presentation of dendritic cells. TFEB and TFE3 are also activated in LPS-stimulated macrophages and directly regulate the production of cytokines as introduced in 5.1.2.

Of the members of the MiT family only TFEB and TFE3 are expressed in murine T cells. Expression of a dominant negative form of TFE3 in T cells disrupts the functions of TFEB and TFE3 and causes impaired activation of $CD4^+$ T cells and the subsequent T cell-dependent humoral responses (358). Chromatin immunoprecipitation shows that TFE3 and TFEB directly bind to the promoter of *Cd40lg*, which is a costimulatory molecule for T cell activation (358). Whether TFEB regulates T cell responses also via autophagy or lysosomal degradation is unknown.

5.1.4.5 TFEB in ageing

Autophagy/lysosomal degradation is a major catabolic pathway that is crucial for cellular homeostasis and is thought to prevent ageing (106). As a master regulator of autophagy, TFEB is likely to regulate the ageing process. *C. elegans* is a short-lived animal model widely used in the ageing research.

HLH-30, the TFEB homolog in *C. elegans*, has been shown to regulate autophagy and lysosomal degradation similar to TFEB in mammalian cells (341, 342). Moreover, HLH-30 is required for the long lifespan of multiple long-lived mutants, and overexpression of *hlh-30* further extends the lifespan of *C. elegans* (341). Inhibition of autophagy reduces the lifespan of the *hlh-30*-overexpressing worms, suggesting that HLH-30 prolongs lifespan at least partially via autophagy induction (341). So far there are very few reports assessing the role of TFEB in mammalian ageing. However, considering the broad functions of TFEB in controlling autophagy and metabolism, it is very likely that TFEB also prevents mammalian ageing as HLH-30 does in worms. Mice models with conditional knockout or overexpression of TFEB will help to address that.

Chapter 5. eIF5A Controls TFEB Expression

5.2 Results

5.2.1 Identify the targets of eIF5A using protein mass spectrometry

Since eIF5A is a translation factor, we hypothesized that the synthesis of certain autophagy proteins might require eIF5A but could not identify these using a hypothesis-driven approach. Two autophagy proteins containing polyproline motifs were randomly chosen (ATG3 and PIK3C3) and found unchanged in the presence of GC7 in Jurkat cells (Fig 5.2), indicating that blocking hypusination of eIF5A does not necessarily reduce the expression of all polyproline-containing proteins.

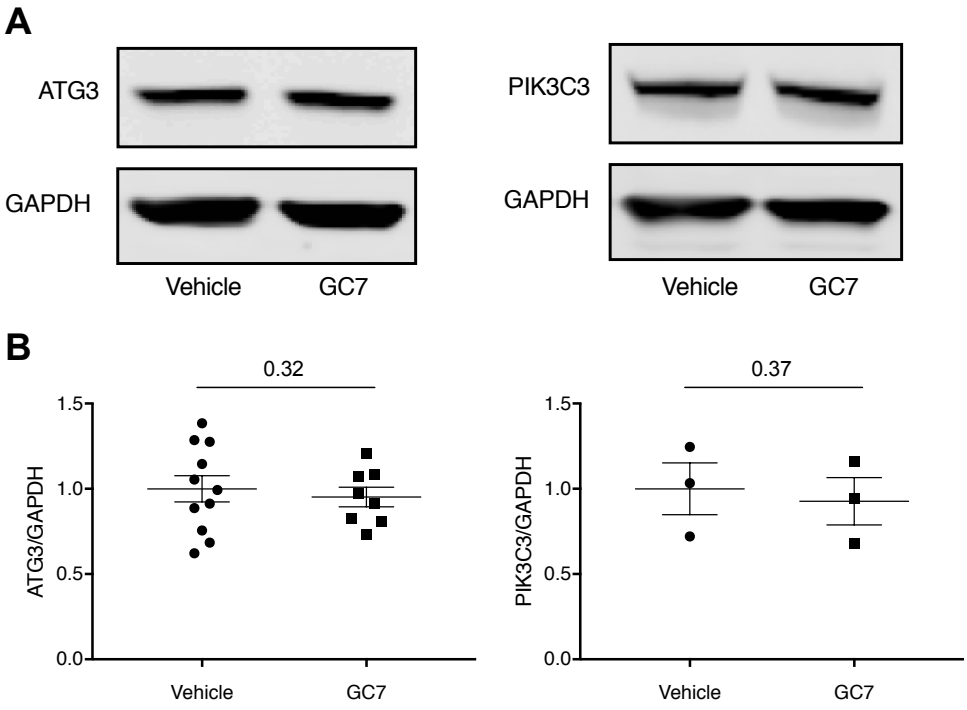


Fig 5.2 GC7 does not affect the expression of the chosen polyproline-containing autophagy proteins. **A.** Jurkat cells were treated with 100 μM GC7 for 24 hours and the expression of ATG3 and PIK3C3 were assessed by Western blot. The quantification results are shown in **B**. The ATG3 or PIK3C3 band intensity was normalized to GAPDH first and then to Vehicle. n = 3 to 11 independent repeats per group as indicated by dots. One-tailed unpaired Student's t-test with P values labelled out. Data represented as mean ± SEM.

We therefore used a hypothesis-free approach to identify changes in autophagy components at the protein level upon inhibition of eIF5A hypusination. Label-free quantitative protein mass spectrometry (MS) was performed using LPS-stimulated primary B cells with GC7 treatment. According to our lab's previous experience, autophagy proteins are generally of low abundance, and very few autophagy proteins could be identified in the whole cell lysate by MS. Lymphocytes have a relatively large nucleus. Therefore to enrich autophagy proteins in the lysate, cell fractionation of cytosol and nuclei was performed (Fig 5.3A). When focusing on autophagy proteins a total of 17 autophagy-related proteins were identified by MS, among which IRGM1, SNAP29, TBC1D17 in cytoplasm and TFEB in nucleus were the most down-regulated proteins in the GC7 sample (Fig 5.3B). In contrast, cytoplasmic SQSTM1, an autophagy adaptor and substrate, was accumulated in the GC7 sample (Fig 5.3B), being consistent with the reduced autophagic flux by GC7 treatment. GAPDH remained unchanged by GC7 treatment, validating the use of GAPDH as a loading control in Western blots.

To confirm the results of the label-free protein MS, a more quantitative MS was performed using stable isotope labeling with amino acids in cell culture (SILAC). Sufficient incorporation (≥95%) of heavy amino acids into cellular proteins is a prerequisite for SILAC MS, which for cell lines is usually achieved by 1 to 2 weeks culture with heavy isotope-labeled amino acids. However, LPS-stimulated B cells die quickly after 4 days of culture, while displaying a large variation in duplication rates at the single cell level. To obtain the best

incorporation of heavy isotope-labeled amino acids, we sorted B cells that had replicated 4 times or more and confirmed that the overall incorporation rate was 97.67% (Gating strategy shown in Fig 5.4A). Then the proteomes of heavy (vehicle) and light (GC7) isotope labeled B cells (duplicated four times or more) were compared, followed by a repeat where the labeling was swapped. GAPDH expression was again found very little changed by GC7 treatment (Fig 5.4B). A total of 7 autophagy proteins were identified by both repeats (Fig 5.4B). Only 2 proteins were repeatedly identified in the label-free MS and the SILAC MS: one being SQSTM1, found increased in cytoplasm, and another one being TEFB, found reduced in the nucleus. The accumulation of SQSTM1 is likely to be the result of the reduced autophagic flux, whereas the reduction of the master autophagy transcription factor TFEB may be a cause of the reduced autophagic flux by blocking eIF5A hypusination.

5.2.2 eIF5A controls the expression of TFEB

The reduction of TFEB expression by GC7 treatment was firstly confirmed in primary B cells by Western blot (Fig 5.5A). Genetic knockdown of *Eif5a* in NIH 3T3 cells also led to reduced TFEB protein levels (Fig 5.5B). Because activated TFEB is largely confined to the nucleus, it was further confirmed that nuclear TFEB was also reduced by GC7 treatment (Fig 5.6), which is consistent with the protein MS results. Therefore eIF5A and its hypusination are required for the overall expression of TFEB and its nuclear localization.

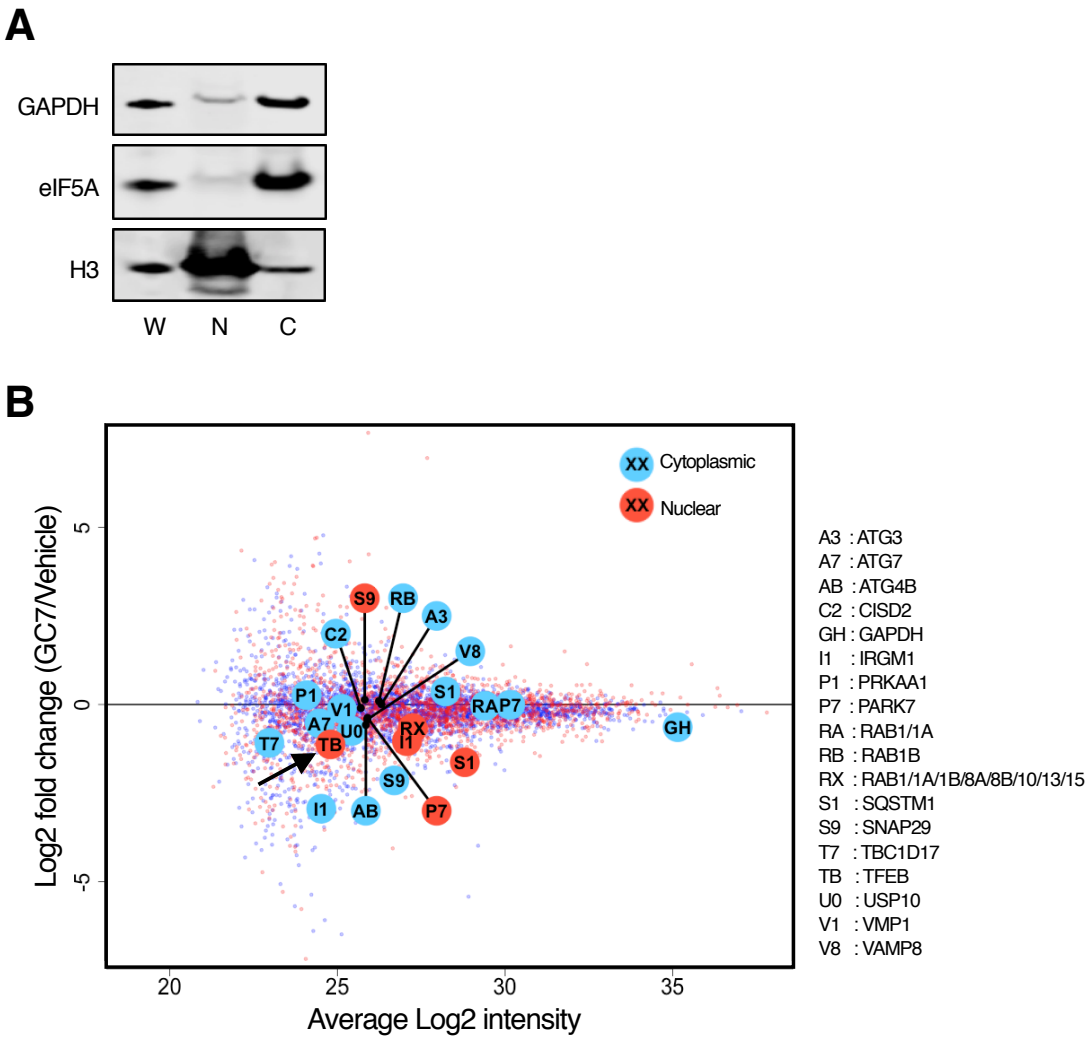


Fig 5.3 Label-free quantitative protein MS to identify autophagy proteins regulated by eIF5A. B cells were sorted from young mice (6-12 weeks) and cultured with LPS for 3 days. **A.** Cell fractionation efficiency was tested by Western blot. W: whole cell lysate; N: nuclear fraction; C: cytoplasmic fraction. **B.** B cells treated with vehicle or 10 μM GC7 for 24 hours were fractionated for label-free quantitative protein MS analysis. Data from the independently analysed cytoplasmic (blue) and nuclear (red) experiments are shown as overlaid MA-plots wherein the log2 average (GC7 + Vehicle) intensity (A) is plotted on x versus the log2 (GC7:Vehicle) fold change (M) plotted on y. Identified autophagy proteins are highlighted by enlarged, annotated circles and TFEB is further indicated by a black arrow. The protein samples were analyzed by MS in collaboration with Shabaz Mohammed's group at the Department of Biochemistry, University of Oxford.

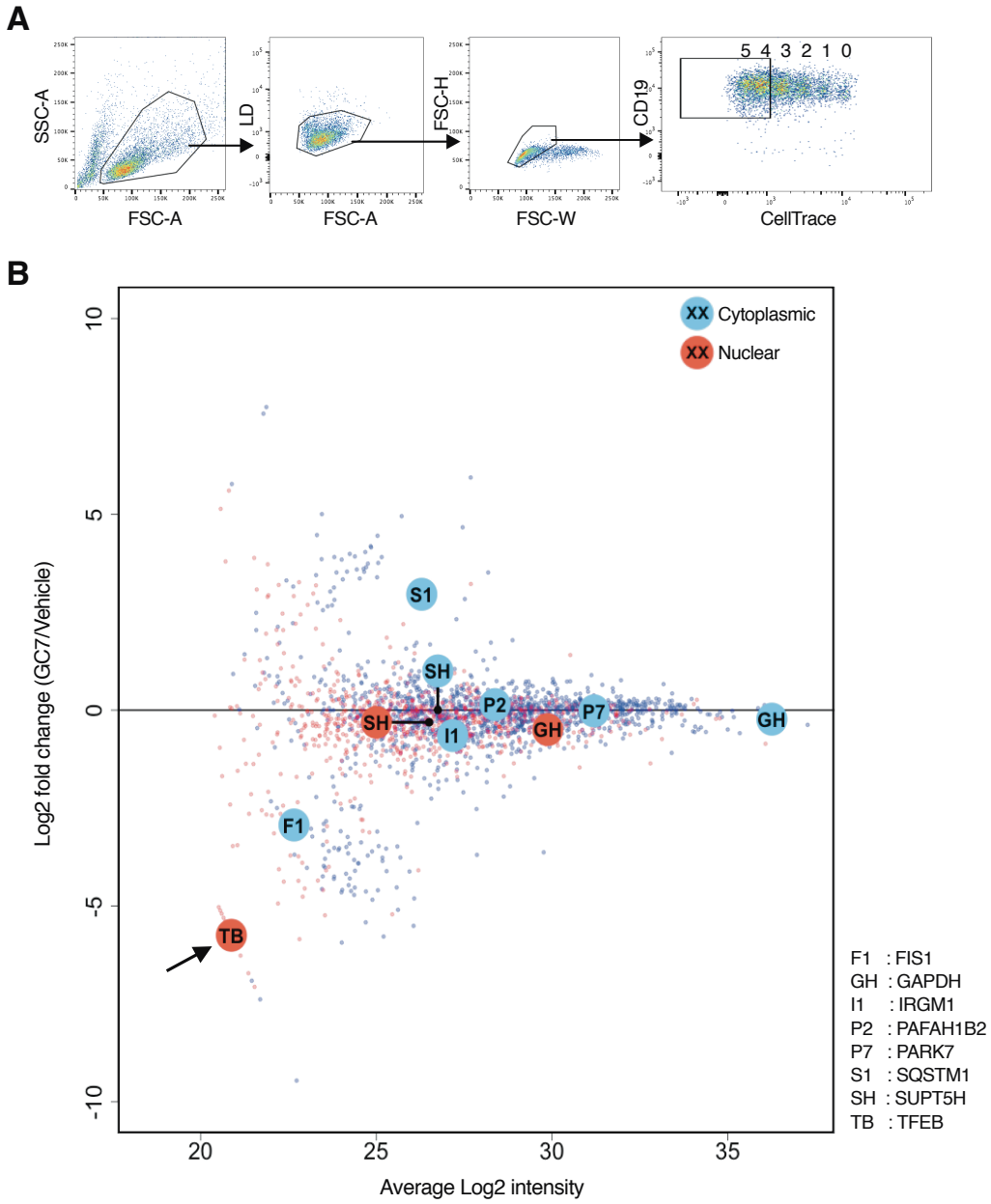


Fig 5.4 SILAC protein MS to identify autophagy proteins regulated by eIF5A. LPS-activated mouse B cells were cultured in medium containing amino acids with heavy isotope labeling (vehicle) or light isotopes (GC7-treated). Cells replicated four times or more were sorted by flow cytometry (**A**) and mixed at 1:1 ratio (heavy: light isotope labelling), followed by cell fractionation and protein MS analysis (**B**). For the repeat the labeling was swapped. The cytoplasmic (blue) and nuclear (red) fractions were analysed in a set of consecutive MS runs. The data are shown as an overlaid MA plot with autophagy proteins highlighted as in Fig 5.3. The protein samples were analyzed by MS in collaboration with Shabaz Mohammed's group as in Fig 5.3.

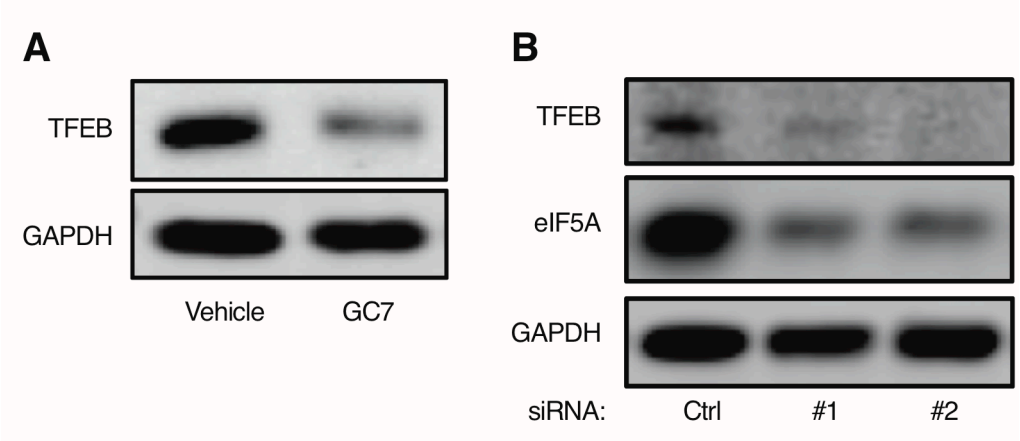


Fig 5.5 eIF5A controls the expression of TFEB. **A.** LPS-stimulated mouse B cells were treated with 10 μM GC7 for 24 hours as in Fig 5.3. The overall TFEB expression was measured by Western blot. Representative of 6 independent repeats. **B.** NIH 3T3 cells were transfected with control or *Eif5a* siRNA and protein expression assessed by Western blot. Representative of 3 independent repeats.

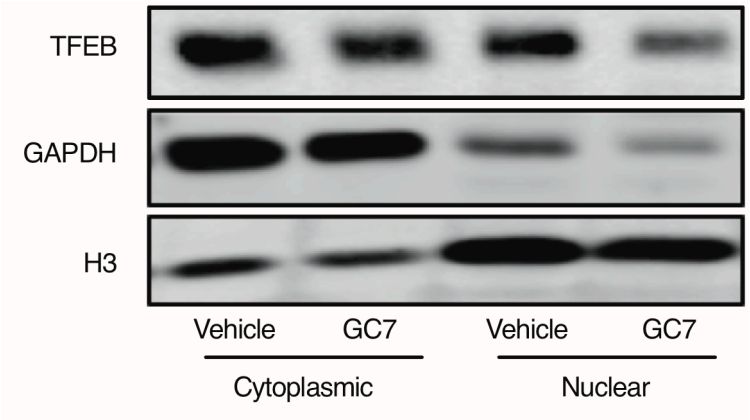


Fig 5.6 Nuclear TFEB is reduced by GC7 treatment. B cells were treated with GC7 as in Fig 5.5 and fractionated for cytoplasmic and nuclear TFEB measurement by Western blot. Representative of 3 independent repeats.

TFEB is a master transcription factor promoting the transcription of key autophagy and lysosomal genes (30, 340). According to target gene identification experiments in Hela cells and mouse liver, 6 representative genes were chosen which have been repeatedly reported being direct targets of TFEB (30, 340, 342, 359). GC7 treatment led to a significant reduction of their mRNAs (Fig 5.7), indicating that the function of TFEB was reduced.

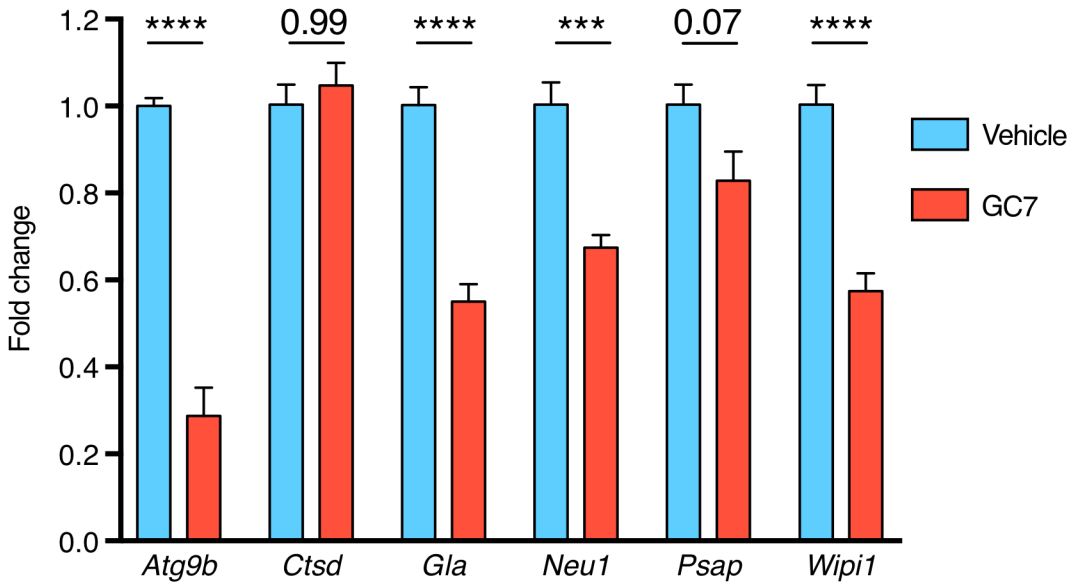


Fig 5.7 The expression of TFEB target genes is reduced by GC7 treatment. B cells were treated with GC7 as in Fig 5.5. mRNA was extracted for qPCR analysis of indicated genes, normalized to *B2m* and to vehicle. Data represented as mean ± SEM. n = 4 mice. Two-way ANOVA, ***P≤0.001, ****P≤0.0001.

5.2.3 GC7 promotes the decay of *Tfeb* mRNA

It has been reported that TFEB protein has a very short half life of less than 4 hours in both N2a neural cell line and LPS-stimulated macrophages (344, 360), indicating that the turn over of TFEB is very fast and efficient protein translation is required for cellular TFEB homeostasis. We have found that triproline motifs stall protein translation in primary B cells (Fig 4.18). Mouse TFEB contains one triproline motif and human TFEB contains two (Fig 5.8A). Moreover, it has been reported that SPP and PPV motifs also cause translation stalling in yeast (304), which interestingly are the two motifs around the triproline motif of TFEB (Fig 5.8A/B). Therefore it is possible that hypusinated eIF5A promotes TFEB translation via alleviating the stalling around the triproline motif. Interestingly, the triproline motif of TFEB is only conserved in higher vertebrates but not in fish and invertebrates (Fig 5.8B). The appearance of the triproline motif may bring some functional or regulatory changes of TFEB during evolution, which will be discussed later.

Next we re-analyzed the previously obtained ribosome profiling data to see if the ribosome occupancy on the triproline motif of *Tfeb* was affected by GC7 treatment. An accumulation of reads was found at the start codon and also the triproline region of *Tfeb* in the vehicle sample, consistent with the whole genome-wide analysis showing an overall paused translation at triproline motifs. Interestingly, a lack of reads, instead of an accumulation of reads, was found at the triproline motif of *Tfeb* (Fig 5.9). It should be noted that although the reproducibility of reads at the gene level is very high in ribosome profiling

(similar to RNA-seq), the reproducibility at the single nucleotide resolution of single genes is low and only 30% of the peaks are reproducible (361). Therefore the absence of peak at the TFEB triproline motif in GC7-treated cells could be due to a random loss. However, as discussed in 4.3.2, an alternative explanation for the reduced reads upon GC7 treatment is mRNA decay due to extremely severe translational stalling. This motivated us to measure the half life of *Tfeb* mRNA.

To measure mRNA half life, I used actinomycin D to inhibit *de novo* protein transcription. Upon actinomycin D treatment, the amount of *Tfeb* mRNA is reduced at a fast rate in LPS-stimulated B cells with a half life of less than 2 hours (Fig 5.10), which is much shorter compared with the median half life of all genes (about 5 hours in activated human T cells) (362). Therefore *Tfeb* mRNA is rapidly decayed in activated B cells.

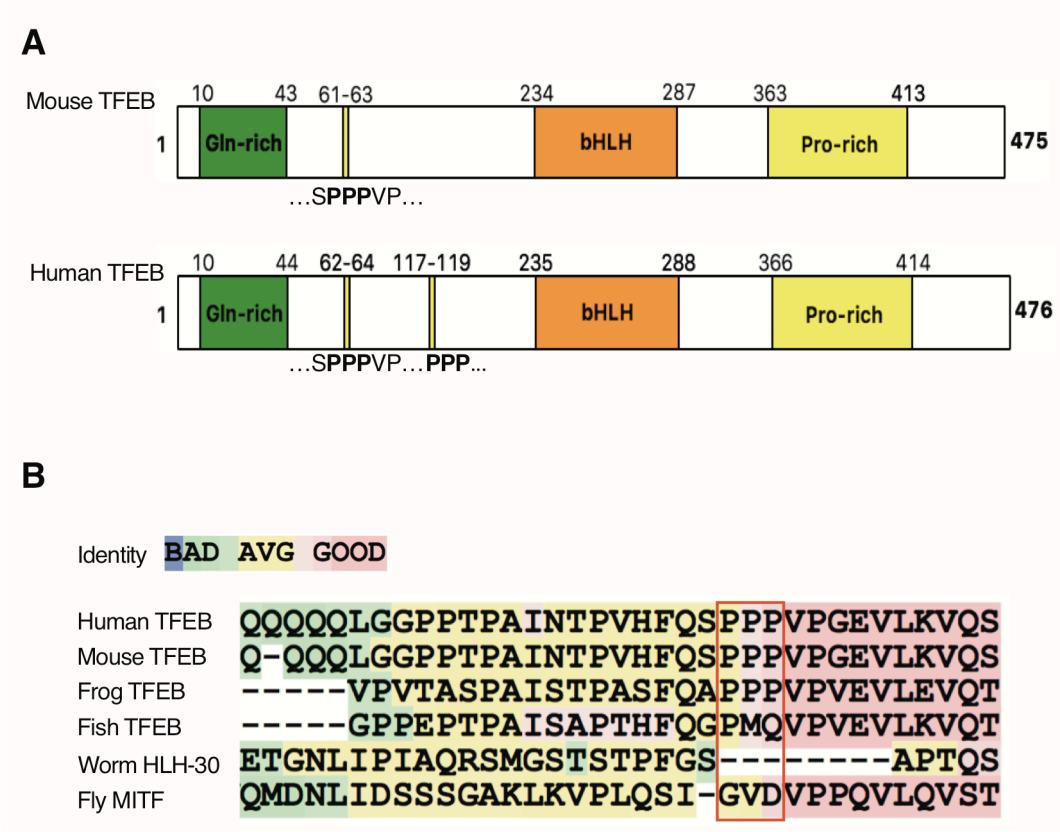


Fig 5.8 TFEB protein sequence alignment across species. **A.** Mouse and human TFEB structures with triproline motifs labeled out. **B.** Protein sequence alignment of TFEB homologs in human (*Homo sapiens*), mouse (*Mus musculus*), frog (*Xenopus tropicalis*), fish (*Danio rerio*), worm (*Caenorhabditis elegans*), and fly (*Drosophila melanogaster*). Regions around the triproline motif are shown here. Colors from blue to red refer to the sequence identity between homologs from low (BAD) to high (GOOD).

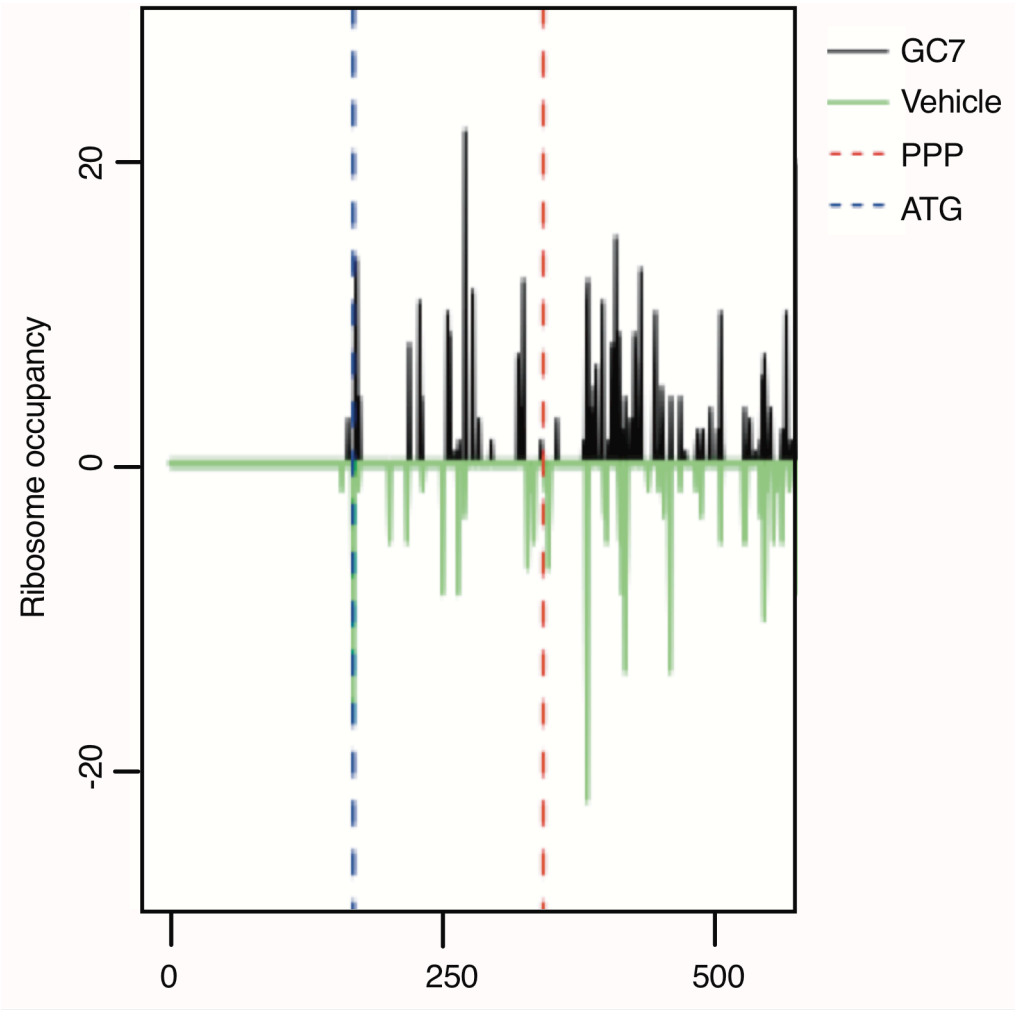


Fig 5.9 Ribosome occupancy of *Tfeb* mRNA. Ribosome profiling was performed as in Fig 4.17. The ribosome occupancy of *Tfeb* mRNA is compared between vehicle- and GC7-treated primary B cells. Positions of the start codon (ATG) and the triproline (PPP) motif are labeled out. Data were obtained and analyzed with Jack Feltham as in Fig 4.17.

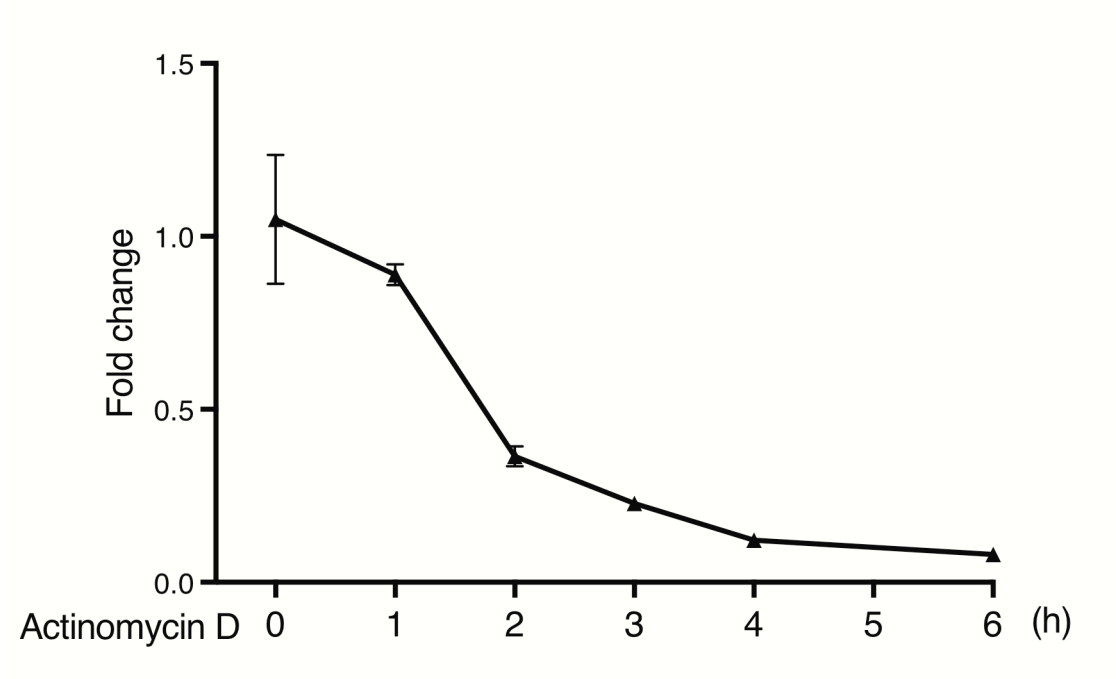


Fig 5.10 *Tfeb* mRNA has a short half life of less than 2 hours. B cells were cultured with LPS for 3 days and treated with the transcription inhibitor actinomycin D. Cells were collected at the indicated hours of treatment and mRNA was extracted for qPCR analysis of *Tfeb*, normalized to *B2m* and to 0 hour. Data represented as mean ± SEM. n = 4 mice.

GC7 treatment for 24 hours resulted in a significant reduction of *Tfeb* mRNA (Fig 5.11B). Interestingly, although the overall *Tfeb* mRNA levels were comparable between vehicle- and GC7-treated cells (Fig 5.11B), the half life of *Tfeb* mRNA had already started to decrease after 12 hours of GC7 treatment (Fig 5.11C). Therefore the reduced *Tfeb* mRNA at 24 hours in GC7-treated cells might be due to accelerated decay starting at 12 hours. Because *Tfeb* is self-regulated (342), it is possible that a positive feedback loop may occur between reduced TFEB protein synthesis due to accelerated mRNA decay and further reduced *Tfeb* mRNA transcription.

In summary, TFEB contains a special triproline-containing motif (SPPPVP), which causes ribosomal stalling. Hypusinated eIF5A facilitates the translation of these hard-to-read motifs. My data suggest that inhibition of hypusinated eIF5A leads to ribosomal stalling followed by mRNA decay. Accordingly, GC7 causes accelerated decay of *Tfeb* mRNA in activated B cells and eventually a reduction of the overall *Tfeb* mRNA and protein. However it is still unclear whether the TFEB polyproline motif is sufficient to cause accelerated mRNA decay and reduced protein synthesis upon removal of hypusinated eIF5A. To answer this question, a fusion protein that links this motif to a reporter protein will be generated.

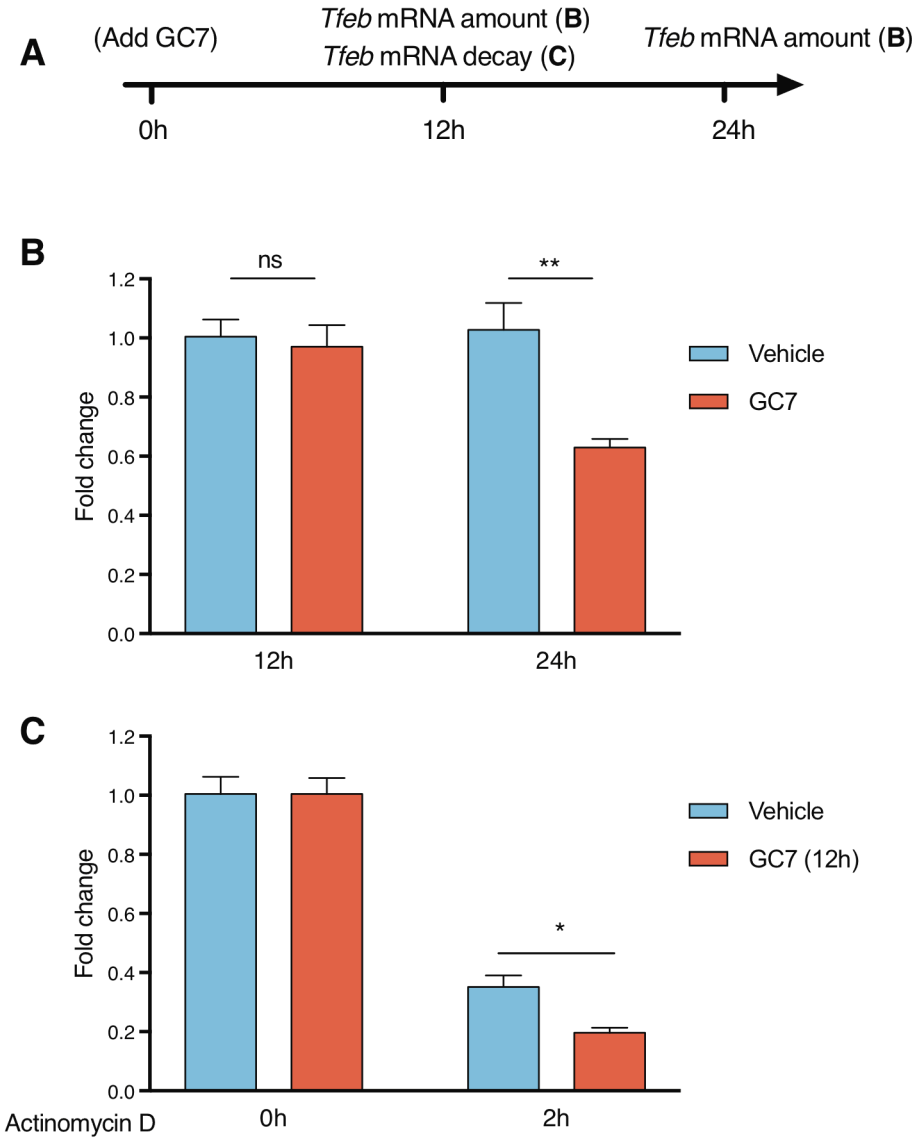


Fig 5.11 GC7 induces the decay of *Tfeb* mRNA. **A.** An overview of the experimental design. LPS-stimulated B cells were treated with vehicle or 10 μM GC7 for 12 or 24 hours, and the amount and the decay rate of *Tfeb* mRNA were assessed and quantified in **B** and **C**. **B.** After 12 or 24 hours of treatment by GC7, the cellular *Tfeb* mRNA was measured by qPCR, normalized to *B2m* and to Vehicle. n=4-8. Paired two-way ANOVA, **P≤0.01, ns, not significant. **C.** B cells were treated with GC7 for 12 hours, followed with actinomycin D block of *de novo* transcription. Cells were collected at 0 or 2 hours post actinomycin D treatment for qPCR analysis of *Tfeb* mRNA, normalized to *B2m* and to 0 hour of actinomycin D treatment. Data represented as mean ± SEM. n = 4 mice. Paired Student's t-test, *P≤0.05.

5.2.4 Reduced expression of TFEB in mice during ageing

To find out whether TFEB is a contributor to the observed reduced autophagic flux in B cells from old mice (Fig 3.15/17), I measured TFEB protein levels in sorted B cells from young (12 weeks) and old mice (22-24 months). Interestingly, TFEB was highly consistently reduced in old B cells (Fig 5.12). The reduction of TFEB explains the reduced autophagic flux we observed in B cells from old mice (Fig 3.16-18). However it is still unknown if this is a major cause of B cell senescence, which can only be answered by conditional knockout of *Tfeb* in B cells.

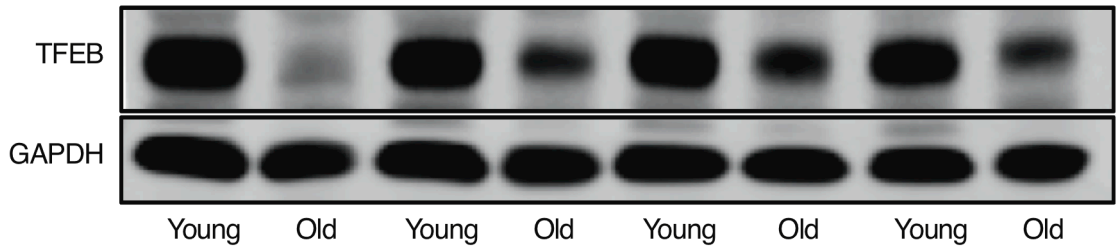


Fig 5.12 Reduced TFEB expression in B cells from old mice. TFEB expression of B cells sorted from young (12 weeks) or old mice (22-24 months) was assessed by Western blot.

5.2.5 The spermidine-eIF5A-TFEB pathway is affected in old people

To assess if the findings of the reduced TFEB in old mice is translatable to humans, we used human peripheral blood mononuclear cells (PBMCs). Similar to mice, a very significant reduction of TFEB protein abundance was observed in PBMCs from old donors (≥ 65 years), and more severely TFEB expression was below detection levels in about half of these donors (Fig

5.13A/B). Therefore, we would suggest that TFEB can be used as a blood biomarker for human ageing. It would be also interesting to investigate whether TFEB is reduced in other organs during ageing and if this is a key contributor to human ageing as well as age-related diseases by re-introducing TFEB to old cells.

Similarly, the expression of overall eIF5A and the hypusinated eIF5A was reduced in PBMCs from old donors (Fig 5.13A/C/D), correlating with reduced TFEB expression. We also confirmed that spermidine levels were reduced with age in human PBMCs as reported before (Fig 5.14) (363). However the relationship between depleted spermidine and reduced eIF5A protein during ageing is complex because not only the hypusinated form, but also the overall levels of eIF5A protein were reduced. It is possible that alternative mechanisms may cause the reduced eIF5A expression, or there could be some feedback controls between spermidine and overall eIF5A expression.

Taken together, the entire pathway spermidine-eIF5A-TFEB is reduced during ageing in human. The components in this pathway, especially TFEB, can be used as novel biomarkers of ageing in human. Interventions targeting this pathway may be helpful in 'treating' ageing or age-related diseases.

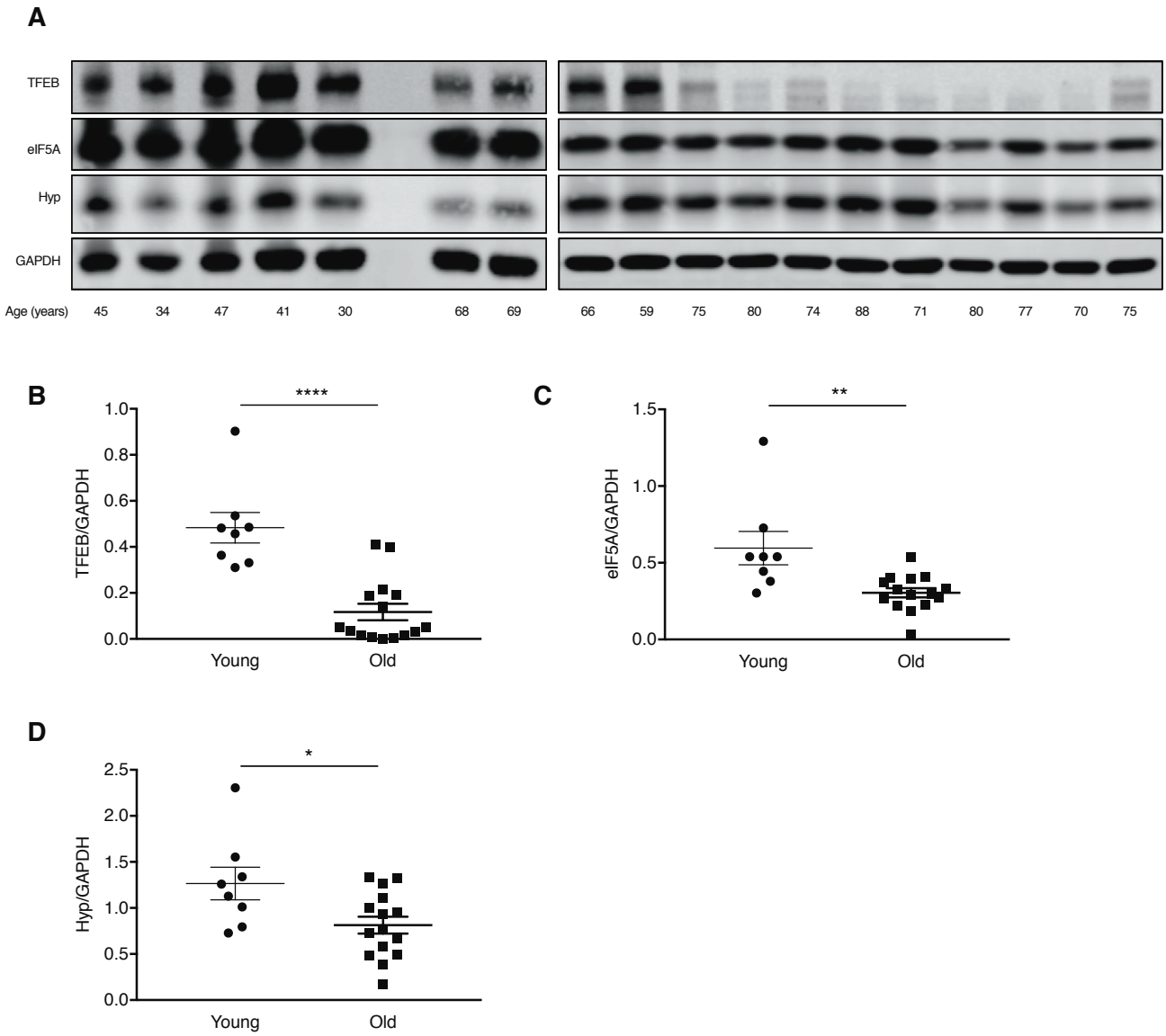


Fig 5.13 Reduced expression of TFEB and eIF5A in PBMCs from old people. **A.** The expression of TFEB, overall eIF5A, and hypusinated eIF5A of PBMCs from healthy human donors of different ages was assessed by Western blot, and quantified by normalizing target band intensity to GAPDH (**B-D**). Young<65 years, Old≥65 years, each dot represents a donor. n = 8 to 15 donors per group as indicated by dots. Unpaired Student's t-test, *P≤0.05, **P≤0.01, ****P≤0.0001. Data represented as mean ± SEM. The PBMC isolation was performed and data analyzed with Ghada Alsaleh in our group.

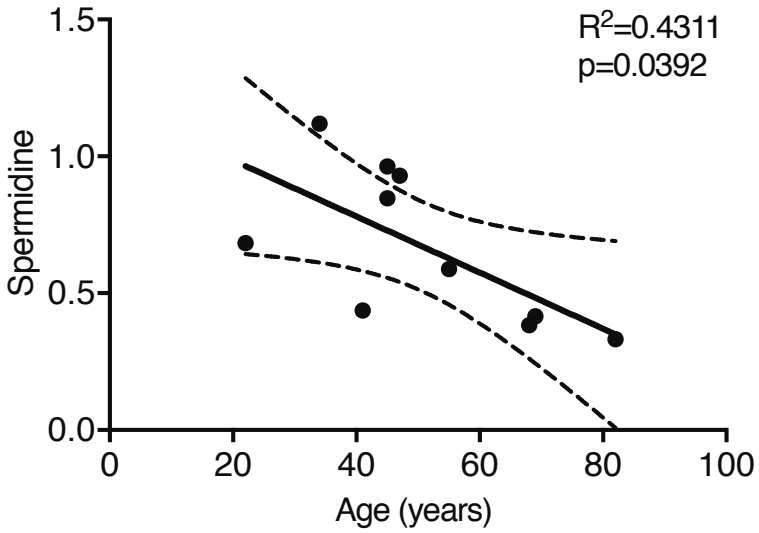


Fig 5.14 Spermidine levels in human PBMCs are reduced with age. Spermidine of PBMCs collected from healthy donors was measured by GC-MS. Each dot represents a donor. n =10 donors as indicated by dots. Linear regression with 95% confidence intervals. The goodness of fit is assessed by R^2. The P value of the slope is calculated by F test. The PBMC isolation was performed by Ghada Alsaleh in our group. The raw data of GC-MS were obtained by Zhanru Yu at the Target Discovery Institute, and analyzed with Ghada Alsaleh.

Chapter 5. eIF5A Controls TFEB Expression

5.3 Discussion

5.3.1 Why does mammalian TFEB require polyproline motifs?

The multiple sequence alignment of TFEB homologs in different species shows that the polyproline motif in mice TFEB only appears in higher vertebrates (Fig 5.8B). Polyproline motifs cause translational stalling and reduce the translation efficiency of the protein, which seems to be an evolutionary disadvantage. Therefore TFEB may gain some special regulatory mechanisms or functions with the polyproline motif during evolution, which compensates for the reduction of the translation efficiency.

Repeated proline residues form a polyproline helix, which is a frequent structure pattern in addition to α-helix and β-structures (364). In aqueous solvents, polyproline helixes exist in left-handed trans isomer called polyproline II (PPII) helix, which is more stable than the right-handed cis isomer polyproline I (PPI) helix adopted in organic solvents (365). PPII helix mostly serves as an interdomain linker in protein structures (364). Determined by the geometry of exposed backbone carbonyl and amide groups, PPII preferably occurs on surface of folded proteins (366), which gives its potential to interact with other cellular components. Actually PPII helix can interact with proteins containing proline-recognition domains (PRDs) such as SH3 and WW domains (364, 367-369). PPII helix also mediates protein-nucleic acid interactions (370). Although the polyproline motif (61-63) is far away from the bHLH domain (234-287) which is the main DNA-binding domain of TFEB (Fig 5.8) (371), it is possible that the C-terminal polyproline motif also has a regulatory role in DNA- or RNA-binding. Therefore the polyproline motif-

containing mammalian TFEB may have a more complex interacting profile than its homologs in lower organisms, making it more competent to regulate the complex developmental and functional programs in the mammalian context.

On the other hand, polyproline-induced translation elongation stalling might also be of evolutionary advantage. Protein synthesis rate is determined by the rate-limiting stalling. In bacteria, polyproline-induced stalls only reduce protein levels when they limit the translation more significantly than the stalling induced by translation initiation (372). Stalling during translation elongation may actually help with the co-translational folding of proteins (373). Indeed we have observed that there is a genome-wide ribosome stalling at the translation initiation site (Fig 4.17A), and the translation initiation of *Tfeb* mRNA is also stalled (Fig 5.9). Therefore it is possible that the polyproline-induced stalling in the absence of GC7 does not necessarily lead to reduced TFEB protein synthesis in primary B cells. Instead, it ensures correct folding and function of TFEB.

To sum up, due to multiple functions of the polyproline motif, it is interesting to further investigate if TFEB gains novel regulatory roles or structural advantages with the motif during evolution. Mammalian cell lines and mice with point mutations of this motif would help to address this question.

5.3.2 How can we improve TFEB functions during ageing?

A marked reduction of TFEB is observed in lymphocytes from both old mice and old people (Fig 5.12/13). As a key regulator of autophagy/lysosomal degradation, metabolism, and innate immune responses (as discussed in 5.1.2), TFEB controls the homeostasis and the functions of multiple organs (as discussed in 5.1.4). Therefore the reduction of TFEB might be an important contributor to age-related deteriorations, which can be delayed or reversed by improving TFEB functions.

Finding the cause of the reduced TFEB expression will help to provide effective targets against ageing. We show in this chapter that TFEB is translationally regulated by eIF5A, and that the expression of eIF5A is also reduced during ageing (Fig 5.13). Therefore reduced overall protein synthesis could be a cause of reduced TFEB protein synthesis, and interventions improving translation efficiency and protein folding might help increase the translation of TFEB.

On the other hand, TFEB activity is regulated via phosphorylation by mTORC1, ERK2, and calcineurin as introduced in 5.1.3. Actually the TFEB suppressor mTORC1 is found over activated in HSCs and skeletal muscles from aged mice (69, 70). Similarly, the activity of the TFEB activator calcineurin is significantly reduced in brains from old rats and Alzheimer's disease patients (374, 375). Therefore TFEB function could be suppressed first by the activated mTORC1 and the deactivated calcineurin, which results

in reduced TFEB transcription (via the self-regulatory loop) and eventually depletion of the overall protein. In that case inhibition of mTORC1 or activation of calcineurin could help rescue TFEB synthesis.

A third way way of increasing TFEB proteins could be achieved independently of targeting its upstream signaling pathways. Instead, we could directly deliver TFEB proteins into old cells. Human immunodeficiency virus (HIV) TAT protein contains an arginine-rich cationic protein transduction domain (PTD) that can drive the protein delivery into cells through macropinocytosis in a receptor-independent fashion (376, 377). Fusion of the PTD with target proteins of up to 120-kilodalton could deliver the target proteins in their biologically active form into multiple tissues of mice (378). Actually the autophagy-inducing domain of beclin1 has been fused with the TAT PTD to achieve high cell-permeability with potent autophagy-inducing effects *in vivo* (379). Similarly the whole protein or a truncated form of TFEB could be fused with PTD and delivered into cells to rescue their functions.

5.3.3 Conclusions

In this chapter, we continued to investigate the mechanism of autophagy regulation by spermidine, focusing on the targets of eIF5A. The master autophagy transcription factor TFEB was repeatedly found down regulated by GC7 treatment in primary B cells in label-free protein MS and SILAC protein MS. More specifically both overall and nuclear TFEB proteins were confirmed to be down regulated by GC7 treatment by Western blot. Moreover, siRNA

knockdown of *Eif5a* in NIH 3T3 cells also leads to a reduction of TFEB, indicating that the regulation of TFEB by eIF5A is possibly a general mechanism in mammalian cells.

The loss of reads is found at the triproline region of *Tfeb* mRNA by GC7 treatment in ribosome profiling, suggesting accelerated mRNA decay. *Tfeb* mRNA is quickly decayed in activated primary B cells with a half life of less than 2 hours. GC7 treatment accelerates the decay of *Tfeb* mRNA, which eventually leads to reduced *Tfeb* mRNA. It is proposed that eIF5A solves the translational stalling on *Tfeb* mRNA at regions such as triproline to help maintain the *Tfeb* mRNA stability and thus regulates TFEB protein synthesis. Therefore, a novel mechanism regulating TFEB expression at the translational level by eIF5A is identified on top of the transcriptional control of TFEB expression and the phosphorylation control of TFEB activation.

A marked reduction of TFEB is found in B cells from old mice and PBMCs from old people, therefore can be considered as a biomarker of ageing in human. Spermidine and eIF5A are also reduced with age in human PBMCs, which may be a contributor of the reduced TFEB expression. The discovery of this age-related pathway provides novel targets to ‘treat’ ageing.

Chapter 6. General Discussion

6.1 Changes of protein translation during ageing

Both *in vitro* analyses using cell-free system and *in vivo* analyses show that the protein synthesis rate is generally reduced with age in livers of rodents (from 20% to 75%) (380). Genetic removal of specific ribosomal proteins in yeast and worms reduces translation rate and extends the lifespan (381-383). Therefore translation inhibition might be an adaptive response to age-related stresses. Indeed extracts from old but still proliferating fibroblasts have an increased misincorporation rate of amino acids during *in vitro* translation compared to extracts from young fibroblasts, indicating that protein translation is more error-prone in old cells, and possibly even higher in senescent cells (384). Misincorporation of amino acids may cause failure of protein folding and increase the tendency of protein aggregation. Therefore reduced protein synthesis may help reduce the formation of toxic protein aggregates and meanwhile reduce the load for proteolytic and chaperone systems to maintain proteostasis. Accordingly, improved proteostasis through up regulation of chaperones in worms extends their lifespan (385, 386).

Indeed, reduced overall protein translation rate does not necessarily lead to reduced expression of all protein proteins. Instead, ribosomal units can be modified to switch the translation profile to promote the translation of specific mRNAs. For example, the α subunit of the translation initiation factor eIF2 is phosphorylated under stress conditions, which inhibits general translation and meanwhile alleviates the suppression of the correct translation of ATF4 by upstream open reading frames (uORFs) (387). Subsequently ATF4 induces

the transcription of multiple stress-related genes (388). Accordingly, the expression of ATF4 is increased in mice with life-span extending interventions such as calorie restriction (389, 390). Similarly, depletion of 60S ribosomal subunits also prolongs the life span of yeast via inducing Gcn4 (the yeast homolog of ATF4) (381). Interestingly, both eIF2α phosphorylation and ATF4 expression are reduced with age (391), suggesting that age-related translation suppression is not via inducing eIF2α phosphorylation. The eIF2α-ATF4 stress response pathway could therefore be a novel target for anti-ageing interventions. Moreover, it remains an interesting question how ribosomal subunits change with age and how these changes affect the translation of specific genes.

Here we show that the expression of eIF5A is reduced with age in human PBMCs. As shown in our results and by others, eIF5A is a protein translation factor controlling initiation, elongation and termination (301, 304). Accordingly, lack of eIF5A may cause the reduction of overall translation. Since the hypusinated eIF5A is especially required for solving translational pauses at polyproline regions, our data would suggest that proteins with these specific hard-to-read motifs are more severely affected due to reduced eIF5A expression. More specifically, the master autophagy transcription factor TFEB contains one polyproline motif. Therefore reduced eIF5A expression may lead to impaired TFEB expression and then compromised autophagy and the accumulation of cellular damage. It is possible that although general inhibition of translation shows an anti-ageing effect (381-383), preserving the function of

specific translation factors such as eIF5A is also important for cellular homeostasis through maintaining autophagy and other repair mechanisms.

6.2 The potential regulatory role of proline in protein translation

As introduced in 4.1, spermidine is the unique substrate of eIF5A hypusination, which promotes protein translation and is essential for cell proliferation. The rigid structure of proline makes it hard to form peptide bonds, and therefore the polyproline motifs cause translational stalling that requires hypusinated eIF5A to solve. Ornithine is the direct precursor of polyamines including spermidine (Fig 1.5). Three amino acids can be metabolized into ornithine: arginine, glutamine/glutamate, and proline (392). However, a usage bias exists among these three sources for ornithine synthesis. For example, porcine placenta mainly uses proline rather than arginine for ornithine and spermidine synthesis to support its fast growth (393, 394). Polyamines in the intestine of suckling pigs are also synthesized from proline with no detectable synthesis from arginine or glutamine (395). Therefore proline is the main source of ornithine and polyamines at least in some tissues.

Then an interestingly loop appears when putting our findings together with the known pathways (Fig 6.1). Prolines are transformed into polyamines to assist eIF5A hypusination. Hypusinated eIF5A promotes the translation of polyproline-containing proteins including the master autophagy transcription factor TFEB. Autophagy recycles cellular components to maintain the cellular

proline pool.

More intriguingly, there might be a sophisticated regulatory mechanism (or just a coincidence) that prolines are used to form polyamines to assist their own translation (polyprolines) and maintains their own availability via autophagy. Indeed, mathematical simulation of yeast protein translation based on a fixed number of tRNA, mRNA and ribosome molecules shows that proline is among the most rate-limiting amino acids for protein synthesis (396). 10-fold starvation of specific amino acids such as proline, alanine and leucine reduces total protein production by over 10 folds, whereas 10-fold starvation of arginine only leads to a 2-fold reduction of overall protein production (396). The rate-limiting effect of proline during protein translation might be more marked if eIF5A hypusination was also taken into consideration. Due to its multiple regulatory roles in protein translation, the proline concentration might be used as a nutrient signal for cells to control protein translation and cellular growth (Fig 6.1). To test this hypothesis, cellular prolines could be depleted to assess whether autophagy, eIF5A hypusination, protein translation, and cellular growth are more severely compromised than when depleting other amino acids.

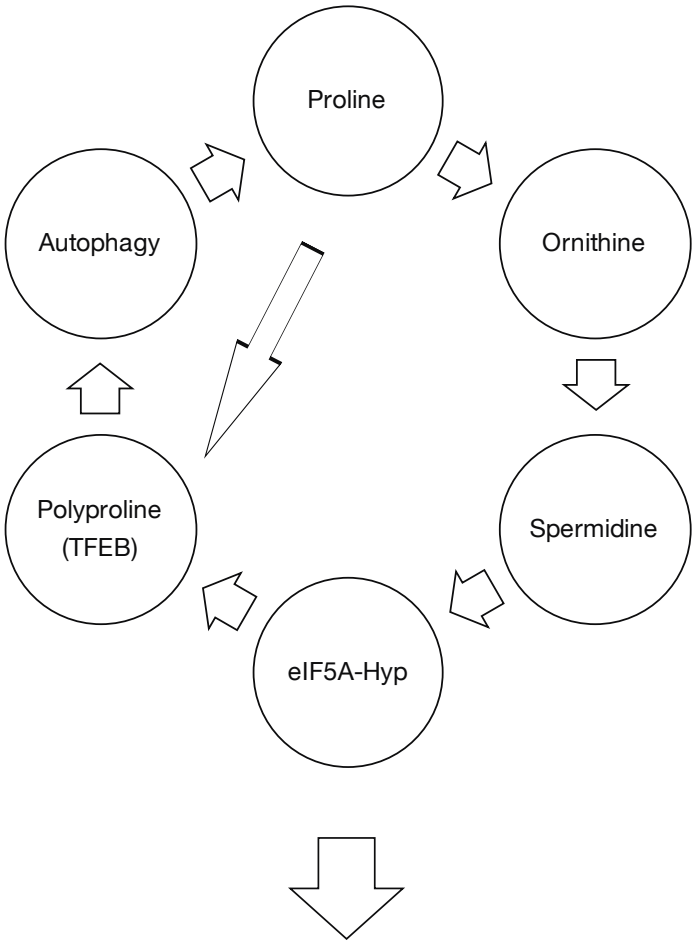


Fig 6.1 Proposed model for the potential regulatory role of proline in protein synthesis and cell growth. Proline is the substrate for synthesis of ornithine and spermidine. Spermidine is used for eIF5A hypusination, which promotes the translation of polyproline-containing proteins, including the master autophagy transcription factor TFEB. Autophagy recycles unwanted cellular components to maintain the proline pool. Proline promotes protein translation via being a rate-limiting amino acid itself during

6.3 Protein translation and autophagy are coordinated with each other

Only a limited number of mechanisms have been described so far that link protein translation and autophagy, of which mTOR is a well studied one. As a key regulator promoting cellular anabolism, mTOR induces translation and inhibits autophagy (397). However, protein translation and autophagy are not always mutually exclusive processes occurring in the cell. Instead, a fine balance may exist to adapt cells to different metabolic requirements. One example is B-cell activation as we have observed in Fig 4.13. Naïve B cells are in a metabolic quiescent state and have a very low translational rate (using eIF5A as an indicator) and autophagic flux. LPS stimulation quickly up regulates both protein translation and autophagy and drives cells into proliferation. Moreover, both translation (Fig 4.16/17) and autophagy (4.5/11/12/14) are regulated by spermidine and eIF5A. Therefore the spermidine-eIF5A pathway may have an important regulatory role in coordinating protein translation and autophagy. Once cells are stimulated, translation is turned on to generate the needed new proteins, while autophagy provides sufficient nutrient and energy supply to support fast cellular growth.

The coordinated induction of protein translation and autophagy is based on a regulatory loop: autophagy provides amino acids and energy for translation, while translation maintains the synthesis of autophagic proteins. For example, starvation inhibits mTOR and induces autophagy, but prolonged starvation reactivates mTOR (and thus anabolism) through autophagy-assisted nutrient generation (398). On the other hand, our results show that reduced translation

efficiency by blocking eIF5A hypusination selectively affects the expression of certain proteins including the master autophagy transcription factor TFEB (Fig 5.3-5).

6.4 Therapeutic prospects

Focusing on the immune-boosting effect of spermidine in ageing and its mechanism regulating autophagy, this project has a great potential for the translational use of spermidine as an anti-ageing compound. The pathways upstream and downstream of spermidine further open the choices of anti-ageing targets.

Firstly, spermidine administration via drinking water significantly improves humoral immune responses (Fig 3.18/19) and also $CD8^+$ T cell responses (170) in old mice. Oral administration is the simplest mode of drug administration. Old people could keep taking spermidine as a food supplement to improve their immune efficacy against daily infections and reduce overall inflammation. Vaccines administration could be accompanied with a single high dose of spermidine to improve vaccination efficacy. In that case, it remains to be tested whether spermidine can be injected together with the vaccine or whether a single administration of spermidine works efficiently to improve humoral immune responses. Moreover, spermidine has also been found to protect heart functions and prolong the lifespan of old mice without

obvious side effects (212, 213). All of these anti-ageing effects suggest that spermidine can be a potent anti-ageing compound for human.

Secondly, spermidine could be taken as a drug for treating age-related diseases, especially those involving autophagy deficiency. For example, autophagy is reduced in degenerated neurons in mice (58), which contributes to the accumulation of amyloid protein aggregates and disease progression (399). Autophagy inducers such as rapamycin and its analogs have been found to protect against neurodegeneration in animal models (400-402). It would be interesting to see if spermidine can pass the blood-brain barrier and induce autophagy in neuron cells to relieve neuronal degeneration. Another more controversial idea is to use spermidine to treat cancer. Compromised immune responses lead to loss of immune surveillance and thus promote tumorigenesis and progression (403). Considering that spermidine is required for cell proliferation, spermidine administration to cancer patients may aggravate the proliferation of cancer cells. Instead, spermidine could be used *in vitro* to improve the activation/expansion of tumour-specific immune cells, which can then be transferred back to patients, without spermidine to minimize its potential side effects.

Thirdly, we found that downstream of spermidine, hypusinated eIF5A also regulates autophagy. Therefore interventions improving eIF5A hypusination may have similar effects as spermidine to rejuvenate ageing. As discussed in 4.3.1, aaptamine, a naturally occurring alkaloid from marine sponges, has

been reported to induce the hypusination in cell lines (327). It is worth testing whether aaptamine may induce autophagy and improve adaptive immune responses or any other physiological functions in old mice. Moreover, drug screening using eIF5A hypusination as a read out may also help identify more anti-ageing compounds.

Fourthly, spermidine levels decline with age in human and other organisms as we have shown in Fig 5.14 and as reported before (211, 363, 404), which might be a cause of ageing or age-related functional declines. In addition to direct supplement with large amounts of spermidine, one could also target pathways regulating spermidine levels to increase spermidine. For example, gut microbiota is thought to be an important source of polyamines in human (405), and reduced spermidine levels could be due to disturbed gut microbiota composition with age. Therefore reintroducing polyamine-producing bacterial species or stimulating polyamine production of gut bacteria may help increase spermidine levels in the elderly. On the other hand, human cells can also synthesize, degrade or export spermidine themselves (406, 407). The spermidine metabolizing enzymes could thus be targeted to modulate cellular spermidine levels.

Finally, we showed that hypusinated eIF5A regulates TFEB expression (Fig 5.3-5), and the protein abundance of TFEB markedly reduces with age in both mice and human (Fig 5.12/13). Being a master regulator of autophagy/lysosome and metabolism, the reduction of TFEB may play an

important role in mammalian ageing. As discussed in 5.2.5 and 5.3.2, TFEB can be considered as a novel biomarker of ageing, and interventions increasing cellular TFEB levels may help improve cellular autophagy and metabolism and protect cells from ageing.

It should be noted that clinical trials targeting ageing is still a big challenge for the translation of findings of ageing research. Although it leads to the decline of multiple tissues and age-related diseases, ageing itself is still not taken as a 'disease' or approved by FDA as an indication. The huge consumption of 'anti-ageing' dietary supplements such as antioxidants suggests that people are willing to take special compounds to delay ageing and prevent age-related diseases, therefore they may also be willing to participate in more standardized anti-ageing clinical trials. Markers or symptoms of ageing are also very complex, making it hard to perform rigorous clinical trials. The golden standard of ageing is functional tissue decline, therefore a comprehensive assessment of physiological functions need to be considered including neurologic, immune, musculoskeletal, cardiovascular, and endocrine systems (408). Moreover, ageing may start from changes at the molecular level before obvious functional body decline. Therefore a panel of reliable molecular biomarkers will be key to help with early diagnosis of ageing.

6.5 Thesis summary

The adaptive immune system undergoes a series of age-related developmental and functional declines with age, termed adaptive immune

senescence, which contributes to multiple age-related diseases such as increased infections and cancer. As the main bulk degradation mechanism in cells, autophagy maintains cellular homeostasis and prevents cellular senescence in different aspects. In this DPhil project, I started with rejuvenating humoral immune responses in old mice using the autophagy inducer spermidine, followed by the molecular mechanism studies of spermidine. The findings are summarized in Fig 6.2.

Autophagic flux is significantly reduced in lymphocytes from old mice, which can be induced by spermidine *in vivo*. Spermidine administration improves the humoral responses without affecting the reconstitution ability of HSCs or the development of B cells in old mice. Autophagy-deficient B cells show severely compromised IgG1 memory responses, mimicking the functional decline of ageing. Spermidine fails to improve the IgG1 responses of autophagy-deficient B cells, indicating that the immune-boosting effect of spermidine is autophagy-dependent.

One of the best defined functions of spermidine is being the substrate for eIF5A hypusination. Depletion of cellular spermidine leads to a reduction of both eIF5A hypusination and the autophagic flux in mammalian cells. Blocking of eIF5A hypusination reduces autophagyic flux, indicating that hypusinated eIF5A regulates autophagy. Being a translation factor, hypusinated eIF5A is required for optimal protein synthesis, suggesting that eIF5A may control autophagy via promoting the translation of certain autophagy proteins.

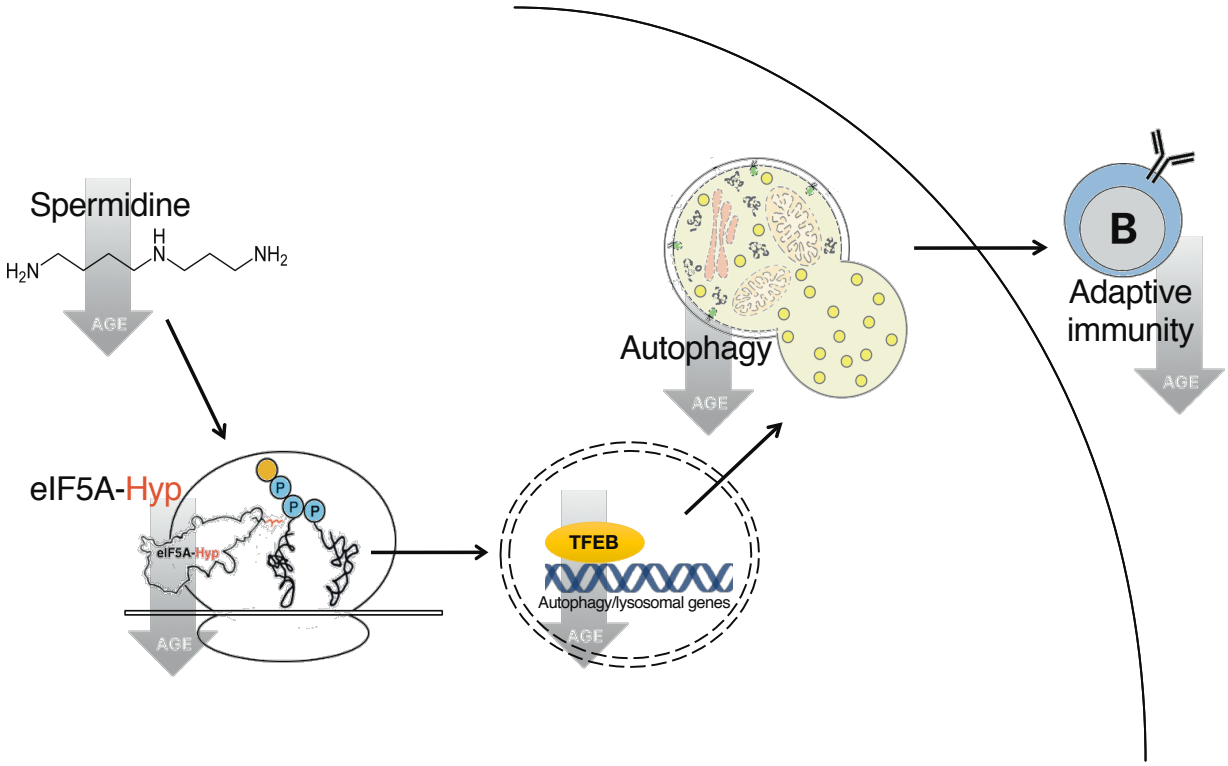


Fig 6.2 Proposed working model of a novel autophagy signaling pathway and its involvement in ageing. Spermidine is a unique substrate for the hypusination of eIF5A. Hypusinated eIF5A regulates TFEB at the translational level. TFEB is a master transcription factor of autophagy, which is required for long-term adaptive immune responses. Spermidine levels, hypusinated eIF5A, TFEB, autophagy, and adaptive immunity are reduced with age and spermidine administration rejuvenates B cell responses in an autophagy-dependent manner.

Two proteomic experiments were performed to identify the target proteins of eIF5A. Interestingly, only one autophagy protein was repeatedly found down regulated by GC7-mediated blocking of hypusination in primary B cells, which is the master autophagy transcription factor TFEB. It was further confirmed that both the overall and the activated nuclear TFEB proteins are reduced by GC7 treatment. The transcription of TFEB target genes is also reduced, suggesting the functional decline of TFEB. Mechanistic studies revealed that *Tfeb* mRNA has a short half life of less than 2 hours in LPS-stimulated B cells, and blocking of eIF5A hypusination accelerates the decay of *Tfeb* mRNA which eventually leads to reduced *Tfeb* mRNA in cells. It is proposed that eIF5A stabilizes *Tfeb* mRNA via solving the translational stalling at the polyproline region of *Tfeb* mRNA to prevent the stalling-induced no-go decay.

Therefore I have identified a novel autophagy signaling pathway regulating TFEB at the translational level. Interestingly, the whole pathway, spermidine-eIF5A-TFEB-autophagy is down regulated in PBMCs in the elderly, indicating that this pathway may also control the ageing process and can be targeted to delay or rejuvenate ageing.

Bibliography

1. Heesters BA, Myers RC, Carroll MC. 2014. Follicular dendritic cells: dynamic antigen libraries. *Nat Rev Immunol* 14: 495-504
2. Zhang H, Puleston DJ, Simon AK. 2016. Autophagy and Immune Senescence. *Trends Mol Med* 22: 671-86
3. Sahu R, Kaushik S, Clement CC, Cannizzo ES, Scharf B, Follenzi A, Potolicchio I, Nieves E, Cuervo AM, Santambrogio L. 2011. Microautophagy of cytosolic proteins by late endosomes. *Dev Cell* 20: 131-9
4. Mijaljica D, Prescott M, Devenish RJ. 2011. Microautophagy in mammalian cells: revisiting a 40-year-old conundrum. *Autophagy* 7: 673-82
5. Marzella L, Ahlberg J, Glaumann H. 1980. In vitro uptake of particles by lysosomes. *Exp Cell Res* 129: 460-6
6. Bandyopadhyay U, Kaushik S, Varticovski L, Cuervo AM. 2008. The chaperone-mediated autophagy receptor organizes in dynamic protein complexes at the lysosomal membrane. *Mol Cell Biol* 28: 5747-63
7. Cuervo AM, Wong E. 2014. Chaperone-mediated autophagy: roles in disease and aging. *Cell Res* 24: 92-104
8. Dice JF. 1990. Peptide sequences that target cytosolic proteins for lysosomal proteolysis. *Trends Biochem Sci* 15: 305-9
9. Noda NN, Inagaki F. 2015. Mechanisms of Autophagy. *Annu Rev Biophys* 44: 101-22
10. Karanasios E, Stapleton E, Manifava M, Kaizuka T, Mizushima N, Walker SA, Ktistakis NT. 2013. Dynamic association of the ULK1 complex with omegasomes during autophagy induction. *J Cell Sci* 126: 5224-38
11. Hamasaki M, Furuta N, Matsuda A, Nezu A, Yamamoto A, Fujita N, Oomori H, Noda T, Haraguchi T, Hiraoka Y, Amano A, Yoshimori T. 2013. Autophagosomes form at ER-mitochondria contact sites. *Nature* 495: 389-93
12. Hurley JH, Young LN. 2017. Mechanisms of Autophagy Initiation. *Annu Rev Biochem* 86: 225-44
13. Axe EL, Walker SA, Manifava M, Chandra P, Roderick HL, Habermann A, Griffiths G, Ktistakis NT. 2008. Autophagosome formation from membrane compartments enriched in phosphatidylinositol 3-phosphate and dynamically connected to the endoplasmic reticulum. *J Cell Biol* 182: 685-701

14. Roberts R, Ktistakis NT. 2013. Omegasomes: PI3P platforms that manufacture autophagosomes. *Essays Biochem* 55: 17-27
15. Dooley HC, Razi M, Polson HE, Girardin SE, Wilson MI, Tooze SA. 2014. WIPI2 links LC3 conjugation with PI3P, autophagosome formation, and pathogen clearance by recruiting Atg12-5-16L1. *Mol Cell* 55: 238-52
16. Graef M, Friedman JR, Graham C, Babu M, Nunnari J. 2013. ER exit sites are physical and functional core autophagosome biogenesis components. *Mol Biol Cell* 24: 2918-31
17. Ichimura Y, Kirisako T, Takao T, Satomi Y, Shimonishi Y, Ishihara N, Mizushima N, Tanida I, Kominami E, Ohsumi M, Noda T, Ohsumi Y. 2000. A ubiquitin-like system mediates protein lipidation. *Nature* 408: 488-92
18. Kirisako T, Ichimura Y, Okada H, Kabeya Y, Mizushima N, Yoshimori T, Ohsumi M, Takao T, Noda T, Ohsumi Y. 2000. The reversible modification regulates the membrane-binding state of Apg8/Aut7 essential for autophagy and the cytoplasm to vacuole targeting pathway. *J Cell Biol* 151: 263-76
19. Padman BS, Nguyen TN, Lazarou M. 2017. Autophagosome formation and cargo sequestration in the absence of LC3/GABARAPs. *Autophagy* 13: 772-4
20. Mancias JD, Wang X, Gygi SP, Harper JW, Kimmelman AC. 2014. Quantitative proteomics identifies NCOA4 as the cargo receptor mediating ferritinophagy. *Nature* 509: 105-9
21. Lazarou M, Sliter DA, Kane LA, Sarraf SA, Wang C, Burman JL, Sideris DP, Fogel AI, Youle RJ. 2015. The ubiquitin kinase PINK1 recruits autophagy receptors to induce mitophagy. *Nature* 524: 309-14
22. Bjorkoy G, Lamark T, Brech A, Outzen H, Perander M, Overvatn A, Stenmark H, Johansen T. 2005. p62/SQSTM1 forms protein aggregates degraded by autophagy and has a protective effect on huntingtin-induced cell death. *J Cell Biol* 171: 603-14
23. Kirkin V, Lamark T, Sou YS, Bjorkoy G, Nunn JL, Bruun JA, Shvets E, McEwan DG, Clausen TH, Wild P, Bilusic I, Theurillat JP, Overvatn A, Ishii T, Elazar Z, Komatsu M, Dikic I, Johansen T. 2009. A role for NBR1 in autophagosomal degradation of ubiquitinated substrates. *Mol Cell* 33: 505-16
24. Mancias JD, Pontano Vaites L, Nissim S, Biancur DE, Kim AJ, Wang X, Liu Y, Goessling W, Kimmelman AC, Harper JW. 2015. Ferritinophagy via NCOA4 is required for erythropoiesis and is regulated by iron dependent HERC2-mediated proteolysis. *Elife* 4

25. Milan G, Romanello V, Pescatore F, Armani A, Paik JH, Frasson L, Seydel A, Zhao J, Abraham R, Goldberg AL, Blaauw B, DePinho RA, Sandri M. 2015. Regulation of autophagy and the ubiquitin-proteasome system by the FoxO transcriptional network during muscle atrophy. *Nat Commun* 6: 6670
26. Zoncu R, Bar-Peled L, Efeyan A, Wang S, Sancak Y, Sabatini DM. 2011. mTORC1 senses lysosomal amino acids through an inside-out mechanism that requires the vacuolar H(+)-ATPase. *Science* 334: 678-83
27. Rebsamen M, Pochini L, Stasyk T, de Araujo ME, Galluccio M, Kandasamy RK, Snijder B, Fauster A, Rudashevskaya EL, Bruckner M, Scorzoni S, Filipek PA, Huber KV, Bigenzahn JW, Heinz LX, Kraft C, Bennett KL, Indiveri C, Huber LA, Superti-Furga G. 2015. SLC38A9 is a component of the lysosomal amino acid sensing machinery that controls mTORC1. *Nature* 519: 477-81
28. Settembre C, Zoncu R, Medina DL, Vetrini F, Erdin S, Erdin S, Huynh T, Ferron M, Karsenty G, Vellard MC, Facchinetti V, Sabatini DM, Ballabio A. 2012. A lysosome-to-nucleus signalling mechanism senses and regulates the lysosome via mTOR and TFEB. *EMBO J* 31: 1095-108
29. Song W, Wang F, Savini M, Ake A, di Ronza A, Sardiello M, Segatori L. 2013. TFEB regulates lysosomal proteostasis. *Hum Mol Genet* 22: 1994-2009
30. Settembre C, Di Malta C, Polito VA, Garcia Arencibia M, Vetrini F, Erdin S, Erdin SU, Huynh T, Medina D, Colella P, Sardiello M, Rubinsztein DC, Ballabio A. 2011. TFEB links autophagy to lysosomal biogenesis. *Science* 332: 1429-33
31. van der Horst A, Burgering BM. 2007. Stressing the role of FoxO proteins in lifespan and disease. *Nat Rev Mol Cell Biol* 8: 440-50
32. Zhao J, Brault JJ, Schild A, Goldberg AL. 2008. Coordinate activation of autophagy and the proteasome pathway by FoxO transcription factor. *Autophagy* 4: 378-80
33. Carling D, Mayer FV, Sanders MJ, Gamblin SJ. 2011. AMP-activated protein kinase: nature's energy sensor. *Nat Chem Biol* 7: 512-8
34. Egan DF, Shackelford DB, Mihaylova MM, Gelino S, Kohnz RA, Mair W, Vasquez DS, Joshi A, Gwinn DM, Taylor R, Asara JM, Fitzpatrick J, Dillin A, Viollet B, Kundu M, Hansen M, Shaw RJ. 2011. Phosphorylation of ULK1 (hATG1) by AMP-activated protein kinase connects energy sensing to mitophagy. *Science* 331: 456-61

35. Kim J, Kim YC, Fang C, Russell RC, Kim JH, Fan W, Liu R, Zhong Q, Guan KL. 2013. Differential regulation of distinct Vps34 complexes by AMPK in nutrient stress and autophagy. *Cell* 152: 290-303
36. Inoki K, Zhu T, Guan KL. 2003. TSC2 mediates cellular energy response to control cell growth and survival. *Cell* 115: 577-90
37. Revollo JR, Li X. 2013. The ways and means that fine tune Sirt1 activity. *Trends Biochem Sci* 38: 160-7
38. Qiu G, Li X, Che X, Wei C, He S, Lu J, Jia Z, Pang K, Fan L. 2015. SIRT1 is a regulator of autophagy: Implications in gastric cancer progression and treatment. *FEBS Lett* 589: 2034-42
39. Lee IH, Cao L, Mostoslavsky R, Lombard DB, Liu J, Bruns NE, Tsokos M, Alt FW, Finkel T. 2008. A role for the NAD-dependent deacetylase Sirt1 in the regulation of autophagy. *Proc Natl Acad Sci U S A* 105: 3374-9
40. Kume S, Uzu T, Horiike K, Chin-Kanasaki M, Isshiki K, Araki S, Sugimoto T, Haneda M, Kashiwagi A, Koya D. 2010. Calorie restriction enhances cell adaptation to hypoxia through Sirt1-dependent mitochondrial autophagy in mouse aged kidney. *J Clin Invest* 120: 1043-55
41. Hou X, Xu S, Maitland-Toolan KA, Sato K, Jiang B, Ido Y, Lan F, Walsh K, Wierzbicki M, Verbeuren TJ, Cohen RA, Zang M. 2008. SIRT1 regulates hepatocyte lipid metabolism through activating AMP-activated protein kinase. *J Biol Chem* 283: 20015-26
42. Price NL, Gomes AP, Ling AJ, Duarte FV, Martin-Montalvo A, North BJ, Agarwal B, Ye L, Ramadori G, Teodoro JS, Hubbard BP, Varela AT, Davis JG, Varamini B, Hafner A, Moaddel R, Rolo AP, Coppari R, Palmeira CM, de Cabo R, Baur JA, Sinclair DA. 2012. SIRT1 is required for AMPK activation and the beneficial effects of resveratrol on mitochondrial function. *Cell Metab* 15: 675-90
43. Canto C, Gerhart-Hines Z, Feige JN, Lagouge M, Noriega L, Milne JC, Elliott PJ, Puigserver P, Auwerx J. 2009. AMPK regulates energy expenditure by modulating NAD+ metabolism and SIRT1 activity. *Nature* 458: 1056-60
44. Ruderman NB, Xu XJ, Nelson L, Cacicedo JM, Saha AK, Lan F, Ido Y. 2010. AMPK and SIRT1: a long-standing partnership? *Am J Physiol Endocrinol Metab* 298: E751-60
45. Kroemer G, Marino G, Levine B. 2010. Autophagy and the integrated stress response. *Mol Cell* 40: 280-93

46. Levine B, Mizushima N, Virgin HW. 2011. Autophagy in immunity and inflammation. *Nature* 469: 323-35
47. Rahman MM, McFadden G. 2011. Modulation of NF-kappaB signalling by microbial pathogens. *Nat Rev Microbiol* 9: 291-306
48. Lawrence T. 2009. The nuclear factor NF-kappaB pathway in inflammation. *Cold Spring Harb Perspect Biol* 1: a001651
49. Zhong Z, Umemura A, Sanchez-Lopez E, Liang S, Shalapour S, Wong J, He F, Boassa D, Perkins G, Ali SR, McGeough MD, Ellisman MH, Seki E, Gustafsson AB, Hoffman HM, Diaz-Meco MT, Moscat J, Karin M. 2016. NF-kappaB Restricts Inflammasome Activation via Elimination of Damaged Mitochondria. *Cell* 164: 896-910
50. Copetti T, Bertoli C, Dalla E, Demarchi F, Schneider C. 2009. p65/RelA modulates BECN1 transcription and autophagy. *Mol Cell Biol* 29: 2594-608
51. Nivon M, Richet E, Codogno P, Arrigo AP, Kretz-Remy C. 2009. Autophagy activation by NFkappaB is essential for cell survival after heat shock. *Autophagy* 5: 766-83
52. Criollo A, Senovilla L, Authier H, Maiuri MC, Morselli E, Vitale I, Kepp O, Tasdemir E, Galluzzi L, Shen S, Tailler M, Delahaye N, Tesniere A, De Stefano D, Younes AB, Harper F, Pierron G, Lavandero S, Zitvogel L, Israel A, Baud V, Kroemer G. 2010. The IKK complex contributes to the induction of autophagy. *EMBO J* 29: 619-31
53. Comb WC, Cogswell P, Sitcheran R, Baldwin AS. 2011. IKK-dependent, NF-kappaB-independent control of autophagic gene expression. *Oncogene* 30: 1727-32
54. Shi CS, Kehrl JH. 2010. TRAF6 and A20 regulate lysine 63-linked ubiquitination of Beclin-1 to control TLR4-induced autophagy. *Sci Signal* 3: ra42
55. Travassos LH, Carneiro LA, Ramjeet M, Hussey S, Kim YG, Magalhaes JG, Yuan L, Soares F, Chea E, Le Bourhis L, Boneca IG, Allaoui A, Jones NL, Nunez G, Girardin SE, Philpott DJ. 2010. Nod1 and Nod2 direct autophagy by recruiting ATG16L1 to the plasma membrane at the site of bacterial entry. *Nat Immunol* 11: 55-62
56. Sosulski ML, Gongora R, Danchuk S, Dong C, Luo F, Sanchez CG. 2015. Deregulation of selective autophagy during aging and pulmonary fibrosis: the role of TGFbeta1. *Aging Cell* 14: 774-83

57. Sebastian D, Sorianello E, Segales J, Irazoki A, Ruiz-Bonilla V, Sala D, Planet E, Berenguer-Llergo A, Munoz JP, Sanchez-Feutrie M, Plana N, Hernandez-Alvarez MI, Serrano AL, Palacin M, Zorzano A. 2016. Mfn2 deficiency links age-related sarcopenia and impaired autophagy to activation of an adaptive mitophagy pathway. *EMBO J* 35: 1677-93
58. Giaime E, Tong Y, Wagner LK, Yuan Y, Huang G, Shen J. 2017. Age-Dependent Dopaminergic Neurodegeneration and Impairment of the Autophagy-Lysosomal Pathway in LRRK-Deficient Mice. *Neuron*
59. Phadwal K, Alegre-Abarrategui J, Watson AS, Pike L, Anbalagan S, Hammond EM, Wade-Martins R, McMichael A, Klenerman P, Simon AK. 2012. A novel method for autophagy detection in primary cells: impaired levels of macroautophagy in immunosenescent T cells. *Autophagy* 8: 677-89
60. Lin K, Dorman JB, Rodan A, Kenyon C. 1997. daf-16: An HNF-3/forkhead family member that can function to double the life-span of Caenorhabditis elegans. *Science* 278: 1319-22
61. Koubova J, Guarente L. 2003. How does calorie restriction work? *Genes Dev* 17: 313-21
62. Colman RJ, Anderson RM, Johnson SC, Kastman EK, Kosmatka KJ, Beasley TM, Allison DB, Cruzen C, Simmons HA, Kemnitz JW, Weindruch R. 2009. Caloric restriction delays disease onset and mortality in rhesus monkeys. *Science* 325: 201-4
63. Lin SJ, Defossez PA, Guarente L. 2000. Requirement of NAD and SIR2 for life-span extension by calorie restriction in Saccharomyces cerevisiae. *Science* 289: 2126-8
64. Schumacher B, van der Pluijm I, Moorhouse MJ, Kosteas T, Robinson AR, Suh Y, Breit TM, van Steeg H, Niedernhofer LJ, van Ijcken W, Bartke A, Spindler SR, Hoeijmakers JH, van der Horst GT, Garinis GA. 2008. Delayed and accelerated aging share common longevity assurance mechanisms. *PLoS Genet* 4: e1000161
65. Bartke A, Chandrashekar V, Bailey B, Zaczek D, Turyn D. 2002. Consequences of growth hormone (GH) overexpression and GH resistance. *Neuropeptides* 36: 201-8
66. Iranmanesh A, Lizarralde G, Veldhuis JD. 1991. Age and relative adiposity are specific negative determinants of the frequency and amplitude of growth

hormone (GH) secretory bursts and the half-life of endogenous GH in healthy men. *J Clin Endocrinol Metab* 73: 1081-8

67. Yeap BB, Chubb SA, Ho KK, Setoh JW, McCaul KA, Norman PE, Jamrozik K, Flicker L. 2010. IGF1 and its binding proteins 3 and 1 are differentially associated with metabolic syndrome in older men. *Eur J Endocrinol* 162: 249-57
68. Bartke A. 2016. Healthspan and longevity can be extended by suppression of growth hormone signaling. *Mamm Genome*
69. Sandri M, Barberi L, Bijlsma AY, Blaauw B, Dyar KA, Milan G, Mammucari C, Meskers CG, Pallafacchina G, Paoli A, Pion D, Roceri M, Romanello V, Serrano AL, Toniolo L, Larsson L, Maier AB, Munoz-Canoves P, Musaro A, Pende M, Reggiani C, Rizzuto R, Schiaffino S. 2013. Signalling pathways regulating muscle mass in ageing skeletal muscle: the role of the IGF1-Akt-mTOR-FoxO pathway. *Biogerontology* 14: 303-23
70. Chen C, Liu Y, Liu Y, Zheng P. 2009. mTOR regulation and therapeutic rejuvenation of aging hematopoietic stem cells. *Sci Signal* 2: ra75
71. Kaeberlein M, Powers RW, 3rd, Steffen KK, Westman EA, Hu D, Dang N, Kerr EO, Kirkland KT, Fields S, Kennedy BK. 2005. Regulation of yeast replicative life span by TOR and Sch9 in response to nutrients. *Science* 310: 1193-6
72. Kapahi P, Zid BM, Harper T, Koslover D, Sapin V, Benzer S. 2004. Regulation of lifespan in Drosophila by modulation of genes in the TOR signaling pathway. *Curr Biol* 14: 885-90
73. Lamming DW, Ye L, Sabatini DM, Baur JA. 2013. Rapalogs and mTOR inhibitors as anti-aging therapeutics. *J Clin Invest* 123: 980-9
74. Reznick RM, Zong H, Li J, Morino K, Moore IK, Yu HJ, Liu ZX, Dong J, Mustard KJ, Hawley SA, Befroy D, Pypaert M, Hardie DG, Young LH, Shulman GI. 2007. Aging-associated reductions in AMP-activated protein kinase activity and mitochondrial biogenesis. *Cell Metab* 5: 151-6
75. Slamova K, Papousek F, Janovska P, Kopecky J, Kolar F. 2015. Adverse effects of AMP-activated protein kinase alpha2-subunit deletion and high-fat diet on heart function and ischemic tolerance in aged female mice. *Physiol Res*
76. Bujak AL, Crane JD, Lally JS, Ford RJ, Kang SJ, Rebalka IA, Green AE, Kemp BE, Hawke TJ, Schertzer JD, Steinberg GR. 2015. AMPK activation of

muscle autophagy prevents fasting-induced hypoglycemia and myopathy during aging. *Cell Metab* 21: 883-90

77. Salminen A, Kaarniranta K. 2012. AMP-activated protein kinase (AMPK) controls the aging process via an integrated signaling network. *Ageing Res Rev* 11: 230-41
78. Anisimov VN. 2010. Metformin for aging and cancer prevention. *Aging (Albany NY)* 2: 760-74
79. Ulgherait M, Rana A, Rera M, Graniel J, Walker DW. 2014. AMPK modulates tissue and organismal aging in a non-cell-autonomous manner. *Cell Rep* 8: 1767-80
80. Martins R, Lithgow GJ, Link W. 2015. Long live FOXO: unraveling the role of FOXO proteins in aging and longevity. *Aging Cell*
81. Greer EL, Dowlatshahi D, Banko MR, Villen J, Hoang K, Blanchard D, Gygi SP, Brunet A. 2007. An AMPK-FOXO pathway mediates longevity induced by a novel method of dietary restriction in C. elegans. *Curr Biol* 17: 1646-56
82. Willcox BJ, Donlon TA, He Q, Chen R, Grove JS, Yano K, Masaki KH, Willcox DC, Rodriguez B, Curb JD. 2008. FOXO3A genotype is strongly associated with human longevity. *Proc Natl Acad Sci U S A* 105: 13987-92
83. Satoh A, Brace CS, Rensing N, Cliften P, Wozniak DF, Herzog ED, Yamada KA, Imai S. 2013. Sirt1 extends life span and delays aging in mice through the regulation of Nk2 homeobox 1 in the DMH and LH. *Cell Metab* 18: 416-30
84. Morselli E, Maiuri MC, Markaki M, Megalou E, Pasparaki A, Palikaras K, Criollo A, Galluzzi L, Malik SA, Vitale I, Michaud M, Madeo F, Tavernarakis N, Kroemer G. 2010. Caloric restriction and resveratrol promote longevity through the Sirtuin-1-dependent induction of autophagy. *Cell Death Dis* 1: e10
85. Morselli E, Maiuri MC, Markaki M, Megalou E, Pasparaki A, Palikaras K, Criollo A, Galluzzi L, Malik SA, Vitale I, Michaud M, Madeo F, Tavernarakis N, Kroemer G. 2010. The life span-prolonging effect of sirtuin-1 is mediated by autophagy. *Autophagy* 6: 186-8
86. Howitz KT, Bitterman KJ, Cohen HY, Lamming DW, Lavu S, Wood JG, Zipkin RE, Chung P, Kisielewski A, Zhang LL, Scherer B, Sinclair DA. 2003. Small molecule activators of sirtuins extend Saccharomyces cerevisiae lifespan. *Nature* 425: 191-6

87. Wood JG, Rogina B, Lavu S, Howitz K, Helfand SL, Tatar M, Sinclair D. 2004. Sirtuin activators mimic caloric restriction and delay ageing in metazoans. *Nature* 430: 686-9

88. Viswanathan M, Kim SK, Berdichevsky A, Guarente L. 2005. A role for SIR-2.1 regulation of ER stress response genes in determining C. elegans life span. *Dev Cell* 9: 605-15

89. Lagouge M, Argmann C, Gerhart-Hines Z, Meziane H, Lerin C, Daussin F, Messadeq N, Milne J, Lambert P, Elliott P, Geny B, Laakso M, Puigserver P, Auwerx J. 2006. Resveratrol improves mitochondrial function and protects against metabolic disease by activating SIRT1 and PGC-1alpha. *Cell* 127: 1109-22

90. Timmers S, Konings E, Bilet L, Houtkooper RH, van de Weijer T, Goossens GH, Hoeks J, van der Krieken S, Ryu D, Kersten S, Moonen-Kornips E, Hesselink MKC, Kunz I, Schrauwen-Hinderling VB, Blaak E, Auwerx J, Schrauwen P. 2011. Calorie restriction-like effects of 30 days of resveratrol supplementation on energy metabolism and metabolic profile in obese humans. *Cell Metab* 14: 612-22

91. Park SJ, Ahmad F, Philp A, Baar K, Williams T, Luo H, Ke H, Rehmann H, Taussig R, Brown AL, Kim MK, Beaven MA, Burgin AB, Manganiello V, Chung JH. 2012. Resveratrol ameliorates aging-related metabolic phenotypes by inhibiting cAMP phosphodiesterases. *Cell* 148: 421-33

92. Minciullo PL, Catalano A, Mandraffino G, Casciaro M, Crucitti A, Maltese G, Morabito N, Lasco A, Gangemi S, Basile G. 2015. Inflammaging and Anti-Inflammaging: The Role of Cytokines in Extreme Longevity. *Arch Immunol Ther Exp (Warsz)*

93. Coppe JP, Desprez PY, Krtolica A, Campisi J. 2010. The senescence-associated secretory phenotype: the dark side of tumor suppression. *Annu Rev Pathol* 5: 99-118

94. Smith ED, Prieto GA, Tong L, Sears-Kraxberger I, Rice JD, Steward O, Cotman CW. 2014. Rapamycin and interleukin-1beta impair brain-derived neurotrophic factor-dependent neuron survival by modulating autophagy. *J Biol Chem* 289: 20615-29

95. Fu MY, He YJ, Lv X, Liu ZH, Shen Y, Ye GR, Deng YM, Shu JC. 2014. Transforming growth factorbeta1 reduces apoptosis via autophagy activation in hepatic stellate cells. *Mol Med Rep* 10: 1282-8

96. Korah J, Canaff L, Lebrun JJ. 2016. The Retinoblastoma Tumor Suppressor Protein (pRb)/E2 Promoter Binding Factor 1 (E2F1) Pathway as a Novel Mediator of TGFbeta-induced Autophagy. *J Biol Chem* 291: 2043-54
97. Sharma G, Dutta RK, Khan MA, Ishaq M, Sharma K, Malhotra H, Majumdar S. 2014. IL-27 inhibits IFN-gamma induced autophagy by concomitant induction of JAK/PI3 K/Akt/mTOR cascade and up-regulation of Mcl-1 in Mycobacterium tuberculosis H37Rv infected macrophages. *Int J Biochem Cell Biol* 55: 335-47
98. Qin B, Zhou Z, He J, Yan C, Ding S. 2015. IL-6 Inhibits Starvation-induced Autophagy via the STAT3/Bcl-2 Signaling Pathway. *Sci Rep* 5: 15701
99. Wang MX, Cheng XY, Jin M, Cao YL, Yang YP, Wang JD, Li Q, Wang F, Hu LF, Liu CF. 2015. TNF compromises lysosome acidification and reduces alpha-synuclein degradation via autophagy in dopaminergic cells. *Exp Neurol* 271: 112-21
100. Schmeisser H, Fey SB, Horowitz J, Fischer ER, Balinsky CA, Miyake K, Bekisz J, Snow AL, Zoon KC. 2013. Type I interferons induce autophagy in certain human cancer cell lines. *Autophagy* 9: 683-96
101. Xu D, Zhang T, Xiao J, Zhu K, Wei R, Wu Z, Meng H, Li Y, Yuan J. 2015. Modification of BECN1 by ISG15 plays a crucial role in autophagy regulation by type I IFN/interferon. *Autophagy* 11: 617-28
102. Kurz DJ, Decary S, Hong Y, Erusalimsky JD. 2000. Senescence-associated (beta)-galactosidase reflects an increase in lysosomal mass during replicative ageing of human endothelial cells. *J Cell Sci* 113 (Pt 20): 3613-22
103. Harman D. 1956. Aging: a theory based on free radical and radiation chemistry. *J Gerontol* 11: 298-300
104. Zhang C, Cuervo AM. 2008. Restoration of chaperone-mediated autophagy in aging liver improves cellular maintenance and hepatic function. *Nat Med* 14: 959-65
105. Cuervo AM, Dice JF. 2000. Age-related decline in chaperone-mediated autophagy. *J Biol Chem* 275: 31505-13
106. Carmona-Gutierrez D, Hughes AL, Madeo F, Ruckenstuhl C. 2016. The crucial impact of lysosomes in aging and longevity. *Ageing Res Rev* 32: 2-12
107. McBride HM, Neuspiel M, Wasiak S. 2006. Mitochondria: more than just a powerhouse. *Curr Biol* 16: R551-60

108. Yamano K, Matsuda N, Tanaka K. 2016. The ubiquitin signal and autophagy: an orchestrated dance leading to mitochondrial degradation. *EMBO Rep* 17: 300-16
109. Heo JM, Ordureau A, Paulo JA, Rinehart J, Harper JW. 2015. The PINK1-PARKIN Mitochondrial Ubiquitylation Pathway Drives a Program of OPTN/NDP52 Recruitment and TBK1 Activation to Promote Mitophagy. *Mol Cell* 60: 7-20
110. Lemasters JJ. 2005. Selective mitochondrial autophagy, or mitophagy, as a targeted defense against oxidative stress, mitochondrial dysfunction, and aging. *Rejuvenation Res* 8: 3-5
111. Kissova I, Deffieu M, Manon S, Camougrand N. 2004. Uth1p is involved in the autophagic degradation of mitochondria. *J Biol Chem* 279: 39068-74
112. Mortensen M, Ferguson DJ, Edelmann M, Kessler B, Morten KJ, Komatsu M, Simon AK. 2010. Loss of autophagy in erythroid cells leads to defective removal of mitochondria and severe anemia in vivo. *Proc Natl Acad Sci U S A* 107: 832-7
113. Bin-Umer MA, McLaughlin JE, Butterly MS, McCormick S, Tumer NE. 2014. Elimination of damaged mitochondria through mitophagy reduces mitochondrial oxidative stress and increases tolerance to trichothecenes. *Proc Natl Acad Sci U S A* 111: 11798-803
114. Harman D. 1972. The biologic clock: the mitochondria? *J Am Geriatr Soc* 20: 145-7
115. Tanase M, Urbanska AM, Zolla V, Clement CC, Huang L, Morozova K, Follo C, Goldberg M, Roda B, Reschiglian P, Santambrogio L. 2016. Role of Carbonyl Modifications on Aging-Associated Protein Aggregation. *Sci Rep* 6: 19311
116. Petersen KF, Befroy D, Dufour S, Dziura J, Ariyan C, Rothman DL, DiPietro L, Cline GW, Shulman GI. 2003. Mitochondrial dysfunction in the elderly: possible role in insulin resistance. *Science* 300: 1140-2
117. Sohal RS, Sohal BH. 1991. Hydrogen peroxide release by mitochondria increases during aging. *Mech Ageing Dev* 57: 187-202
118. Grimm S, Hoehn A, Davies KJ, Grune T. 2011. Protein oxidative modifications in the ageing brain: consequence for the onset of neurodegenerative disease. *Free Radic Res* 45: 73-88

119. Nie B, Gan W, Shi F, Hu GX, Chen LG, Hayakawa H, Sekiguchi M, Cai JP. 2013. Age-dependent accumulation of 8-oxoguanine in the DNA and RNA in various rat tissues. *Oxid Med Cell Longev* 2013: 303181
120. Pickrell AM, Youle RJ. 2015. The roles of PINK1, parkin, and mitochondrial fidelity in Parkinson's disease. *Neuron* 85: 257-73
121. Cai Q, Tammineni P. 2016. Alterations in Mitochondrial Quality Control in Alzheimer's Disease. *Front Cell Neurosci* 10: 24
122. Qiu X, Brown K, Hirschey MD, Verdin E, Chen D. 2010. Calorie restriction reduces oxidative stress by SIRT3-mediated SOD2 activation. *Cell Metab* 12: 662-7
123. Hekimi S, Lapointe J, Wen Y. 2011. Taking a "good" look at free radicals in the aging process. *Trends Cell Biol* 21: 569-76
124. Mesquita A, Weinberger M, Silva A, Sampaio-Marques B, Almeida B, Leao C, Costa V, Rodrigues F, Burhans WC, Ludovico P. 2010. Caloric restriction or catalase inactivation extends yeast chronological lifespan by inducing H2O2 and superoxide dismutase activity. *Proc Natl Acad Sci U S A* 107: 15123-8
125. Van Raamsdonk JM, Hekimi S. 2009. Deletion of the mitochondrial superoxide dismutase sod-2 extends lifespan in Caenorhabditis elegans. *PLoS Genet* 5: e1000361
126. Yang W, Hekimi S. 2010. A mitochondrial superoxide signal triggers increased longevity in Caenorhabditis elegans. *PLoS Biol* 8: e1000556
127. Scherz-Shouval R, Elazar Z. 2011. Regulation of autophagy by ROS: physiology and pathology. *Trends Biochem Sci* 36: 30-8
128. Szilard L. 1959. On the Nature of the Aging Process. *Proc Natl Acad Sci U S A* 45: 30-45
129. Wang Y. 2008. Bulky DNA lesions induced by reactive oxygen species. *Chem Res Toxicol* 21: 276-81
130. Ponte F, Sousa R, Fernandes AP, Goncalves C, Barbot J, Carvalho F, Porto B. 2012. Improvement of genetic stability in lymphocytes from Fanconi anemia patients through the combined effect of alpha-lipoic acid and N-acetylcysteine. *Orphanet J Rare Dis* 7: 28
131. Hewitt G, Jurk D, Marques FD, Correia-Melo C, Hardy T, Gackowska A, Anderson R, Taschuk M, Mann J, Passos JF. 2012. Telomeres are favoured targets of a persistent DNA damage response in ageing and stress-induced senescence. *Nat Commun* 3: 708

132. Fumagalli M, Rossiello F, Clerici M, Barozzi S, Cittaro D, Kaplunov JM, Bucci G, Dobreva M, Matti V, Beausejour CM, Herbig U, Longhese MP, d'Adda di Fagagna F. 2012. Telomeric DNA damage is irreparable and causes persistent DNA-damage-response activation. *Nat Cell Biol* 14: 355-65
133. Koga H, Kaushik S, Cuervo AM. 2011. Protein homeostasis and aging: The importance of exquisite quality control. *Ageing Res Rev* 10: 205-15
134. Lim KL, Lim GG. 2011. K63-linked ubiquitination and neurodegeneration. *Neurobiol Dis* 43: 9-16
135. McKeon JE, Sha D, Li L, Chin LS. 2015. Parkin-mediated K63-polyubiquitination targets ubiquitin C-terminal hydrolase L1 for degradation by the autophagy-lysosome system. *Cell Mol Life Sci* 72: 1811-24
136. Olzmann JA, Li L, Chudaev MV, Chen J, Perez FA, Palmiter RD, Chin LS. 2007. Parkin-mediated K63-linked polyubiquitination targets misfolded DJ-1 to aggresomes via binding to HDAC6. *J Cell Biol* 178: 1025-38
137. Komatsu M, Waguri S, Koike M, Sou YS, Ueno T, Hara T, Mizushima N, Iwata J, Ezaki J, Murata S, Hamazaki J, Nishito Y, Iemura S, Natsume T, Yanagawa T, Uwayama J, Warabi E, Yoshida H, Ishii T, Kobayashi A, Yamamoto M, Yue Z, Uchiyama Y, Kominami E, Tanaka K. 2007. Homeostatic levels of p62 control cytoplasmic inclusion body formation in autophagy-deficient mice. *Cell* 131: 1149-63
138. Nicot AS, Lo Verso F, Ratti F, Pilot-Storck F, Streichenberger N, Sandri M, Schaeffer L, Goillot E. 2014. Phosphorylation of NBR1 by GSK3 modulates protein aggregation. *Autophagy* 10: 1036-53
139. Kawaguchi Y, Kovacs JJ, McLaurin A, Vance JM, Ito A, Yao TP. 2003. The deacetylase HDAC6 regulates aggresome formation and cell viability in response to misfolded protein stress. *Cell* 115: 727-38
140. Gal J, Chen J, Barnett KR, Yang L, Brumley E, Zhu H. 2013. HDAC6 regulates mutant SOD1 aggregation through two SMIR motifs and tubulin acetylation. *J Biol Chem* 288: 15035-45
141. David DC, Ollikainen N, Trinidad JC, Cary MP, Burlingame AL, Kenyon C. 2010. Widespread protein aggregation as an inherent part of aging in C. elegans. *PLoS Biol* 8: e1000450
142. Labbadia J, Morimoto RI. 2015. The biology of proteostasis in aging and disease. *Annu Rev Biochem* 84: 435-64

143. Latz E, Schoenemeyer A, Visintin A, Fitzgerald KA, Monks BG, Knetter CF, Lien E, Nilsen NJ, Espevik T, Golenbock DT. 2004. TLR9 signals after translocating from the ER to CpG DNA in the lysosome. *Nat Immunol* 5: 190-8

144. Lee HK, Lund JM, Ramanathan B, Mizushima N, Iwasaki A. 2007. Autophagy-dependent viral recognition by plasmacytoid dendritic cells. *Science* 315: 1398-401

145. Weindel CG, Richey LJ, Bolland S, Mehta AJ, Kearney JF, Huber BT. 2015. B cell autophagy mediates TLR7-dependent autoimmunity and inflammation. *Autophagy* 11: 1010-24

146. Henault J, Martinez J, Riggs JM, Tian J, Mehta P, Clarke L, Sasai M, Latz E, Brinkmann MM, Iwasaki A, Coyle AJ, Kolbeck R, Green DR, Sanjuan MA. 2012. Noncanonical autophagy is required for type I interferon secretion in response to DNA-immune complexes. *Immunity* 37: 986-97

147. Dupont N, Jiang S, Pilli M, Ornatowski W, Bhattacharya D, Deretic V. 2011. Autophagy-based unconventional secretory pathway for extracellular delivery of IL-1beta. *EMBO J* 30: 4701-11

148. Castillo EF, Dekonenko A, Arko-Mensah J, Mandell MA, Dupont N, Jiang S, Delgado-Vargas M, Timmins GS, Bhattacharya D, Yang H, Hutt J, Lyons CR, Dobos KM, Deretic V. 2012. Autophagy protects against active tuberculosis by suppressing bacterial burden and inflammation. *Proc Natl Acad Sci U S A* 109: E3168-76

149. Shi H, Zhang Z, Wang X, Li R, Hou W, Bi W, Zhang X. 2015. Inhibition of autophagy induces IL-1beta release from ARPE-19 cells via ROS mediated NLRP3 inflammasome activation under high glucose stress. *Biochem Biophys Res Commun* 463: 1071-6

150. Nakahira K, Haspel JA, Rathinam VA, Lee SJ, Dolinay T, Lam HC, Englert JA, Rabinovitch M, Cernadas M, Kim HP, Fitzgerald KA, Ryter SW, Choi AM. 2011. Autophagy proteins regulate innate immune responses by inhibiting the release of mitochondrial DNA mediated by the NALP3 inflammasome. *Nat Immunol* 12: 222-30

151. Abdel Fattah E, Bhattacharya A, Herron A, Safdar Z, Eissa NT. 2015. Critical role for IL-18 in spontaneous lung inflammation caused by autophagy deficiency. *J Immunol* 194: 5407-16

152. Zhou R, Yazdi AS, Menu P, Tschopp J. 2011. A role for mitochondria in NLRP3 inflammasome activation. *Nature* 469: 221-5
153. Gustot A, Gallea JI, Sarroukh R, Celej MS, Ruysschaert JM, Raussens V. 2015. Amyloid fibrils are the molecular trigger of inflammation in Parkinson's disease. *Biochem J* 471: 323-33
154. Zhu Y, Armstrong JL, Tchkonia T, Kirkland JL. 2014. Cellular senescence and the senescent secretory phenotype in age-related chronic diseases. *Curr Opin Clin Nutr Metab Care* 17: 324-8
155. Boehm T, Swann JB. 2013. Thymus involution and regeneration: two sides of the same coin? *Nat Rev Immunol* 13: 831-8
156. Almanzar G, Schwaiger S, Jenewein B, Keller M, Herndler-Brandstetter D, Wurzner R, Schonitzer D, Grubeck-Loebenstein B. 2005. Long-term cytomegalovirus infection leads to significant changes in the composition of the CD8+ T-cell repertoire, which may be the basis for an imbalance in the cytokine production profile in elderly persons. *J Virol* 79: 3675-83
157. Fagnoni FF, Vescovini R, Passeri G, Bologna G, Pedrazzoni M, Lavagetto G, Casti A, Franceschi C, Passeri M, Sansoni P. 2000. Shortage of circulating naive CD8(+) T cells provides new insights on immunodeficiency in aging. *Blood* 95: 2860-8
158. Jagger A, Shimojima Y, Goronzy JJ, Weyand CM. 2014. Regulatory T cells and the immune aging process: a mini-review. *Gerontology* 60: 130-7
159. Gregg R, Smith CM, Clark FJ, Dunnion D, Khan N, Chakraverty R, Nayak L, Moss PA. 2005. The number of human peripheral blood CD4+ CD25high regulatory T cells increases with age. *Clin Exp Immunol* 140: 540-6
160. Khan N, Shariff N, Cobbold M, Bruton R, Ainsworth JA, Sinclair AJ, Nayak L, Moss PA. 2002. Cytomegalovirus seropositivity drives the CD8 T cell repertoire toward greater clonality in healthy elderly individuals. *J Immunol* 169: 1984-92
161. Messaoudi I, Warner J, Nikolich-Zugich D, Fischer M, Nikolich-Zugich J. 2006. Molecular, cellular, and antigen requirements for development of age-associated T cell clonal expansions in vivo. *J Immunol* 176: 301-8
162. Ahmed M, Lanzer KG, Yager EJ, Adams PS, Johnson LL, Blackman MA. 2009. Clonal expansions and loss of receptor diversity in the naive CD8 T cell repertoire of aged mice. *J Immunol* 182: 784-92

163. Yager EJ, Ahmed M, Lanzer K, Randall TD, Woodland DL, Blackman MA. 2008. Age-associated decline in T cell repertoire diversity leads to holes in the repertoire and impaired immunity to influenza virus. *J Exp Med* 205: 711-23
164. Weiskopf D, Weinberger B, Grubeck-Loebenstein B. 2009. The aging of the immune system. *Transpl Int* 22: 1041-50
165. Brien JD, Uhrlaub JL, Hirsch A, Wiley CA, Nikolich-Zugich J. 2009. Key role of T cell defects in age-related vulnerability to West Nile virus. *J Exp Med* 206: 2735-45
166. Jiang J, Gross D, Elbaum P, Murasko DM. 2007. Aging affects initiation and continuation of T cell proliferation. *Mech Ageing Dev* 128: 332-9
167. Po JL, Gardner EM, Anaraki F, Katsikis PD, Murasko DM. 2002. Age-associated decrease in virus-specific CD8+ T lymphocytes during primary influenza infection. *Mech Ageing Dev* 123: 1167-81
168. Kapasi ZF, Murali-Krishna K, McRae ML, Ahmed R. 2002. Defective generation but normal maintenance of memory T cells in old mice. *Eur J Immunol* 32: 1567-73
169. Smithey MJ, Renkema KR, Rudd BD, Nikolich-Zugich J. 2011. Increased apoptosis, curtailed expansion and incomplete differentiation of CD8+ T cells combine to decrease clearance of L. monocytogenes in old mice. *Eur J Immunol* 41: 1352-64
170. Puleston DJ, Zhang H, Powell TJ, Lipina E, Sims S, Panse I, Watson AS, Cerundolo V, Townsend AR, Klenerman P, Simon AK. 2014. Autophagy is a critical regulator of memory CD8(+) T cell formation. *Elife* 3
171. Haynes L, Eaton SM, Burns EM, Randall TD, Swain SL. 2003. CD4 T cell memory derived from young naive cells functions well into old age, but memory generated from aged naive cells functions poorly. *Proc Natl Acad Sci U S A* 100: 15053-8
172. Williams-Bey Y, Jiang J, Murasko DM. 2011. Expansion of regulatory T cells in aged mice following influenza infection. *Mech Ageing Dev* 132: 163-70
173. Nishioka T, Shimizu J, Iida R, Yamazaki S, Sakaguchi S. 2006. CD4+CD25+Foxp3+ T cells and CD4+CD25-Foxp3+ T cells in aged mice. *J Immunol* 176: 6586-93

174. Lages CS, Suffia I, Velilla PA, Huang B, Warshaw G, Hildeman DA, Belkaid Y, Chougnet C. 2008. Functional regulatory T cells accumulate in aged hosts and promote chronic infectious disease reactivation. *J Immunol* 181: 1835-48

175. Sun L, Hurez VJ, Thibodeaux SR, Kious MJ, Liu A, Lin P, Murthy K, Pandeswara S, Shin T, Curiel TJ. 2012. Aged regulatory T cells protect from autoimmune inflammation despite reduced STAT3 activation and decreased constraint of IL-17 producing T cells. *Aging Cell* 11: 509-19

176. Pua HH, Dzhagalov I, Chuck M, Mizushima N, He YW. 2007. A critical role for the autophagy gene Atg5 in T cell survival and proliferation. *J Exp Med* 204: 25-31

177. Parekh VV, Wu L, Boyd KL, Williams JA, Gaddy JA, Olivares-Villagomez D, Cover TL, Zong WX, Zhang J, Van Kaer L. 2013. Impaired autophagy, defective T cell homeostasis, and a wasting syndrome in mice with a T cell-specific deletion of Vps34. *J Immunol* 190: 5086-101

178. Willinger T, Flavell RA. 2012. Canonical autophagy dependent on the class III phosphoinositide-3 kinase Vps34 is required for naive T-cell homeostasis. *Proc Natl Acad Sci U S A* 109: 8670-5

179. Pua HH, Guo J, Komatsu M, He YW. 2009. Autophagy is essential for mitochondrial clearance in mature T lymphocytes. *J Immunol* 182: 4046-55

180. Jia W, He YW. 2011. Temporal regulation of intracellular organelle homeostasis in T lymphocytes by autophagy. *J Immunol* 186: 5313-22

181. Hubbard VM, Valdor R, Patel B, Singh R, Cuervo AM, Macian F. 2010. Macroautophagy regulates energy metabolism during effector T cell activation. *J Immunol* 185: 7349-57

182. Jia W, He MX, McLeod IX, Guo J, Ji D, He YW. 2015. Autophagy regulates T lymphocyte proliferation through selective degradation of the cell-cycle inhibitor CDKN1B/p27Kip1. *Autophagy* 11: 2335-45

183. Xu X, Araki K, Li S, Han JH, Ye L, Tan WG, Konieczny BT, Bruinsma MW, Martinez J, Pearce EL, Green DR, Jones DP, Virgin HW, Ahmed R. 2014. Autophagy is essential for effector CD8(+) T cell survival and memory formation. *Nat Immunol* 15: 1152-61

184. Schlie K, Westerback A, DeVorkin L, Hughson LR, Brandon JM, MacPherson S, Gadawski I, Townsend KN, Poon VI, Elrick MA, Cote HC, Abraham N, Wherry EJ, Mizushima N, Lum JJ. 2015. Survival of effector CD8+ T cells

during influenza infection is dependent on autophagy. *J Immunol* 194: 4277-86

185. Ron-Harel N, Sharpe AH, Haigis MC. 2015. Mitochondrial metabolism in T cell activation and senescence: a mini-review. *Gerontology* 61: 131-8

186. Araki K, Turner AP, Shaffer VO, Gangappa S, Keller SA, Bachmann MF, Larsen CP, Ahmed R. 2009. mTOR regulates memory CD8 T-cell differentiation. *Nature* 460: 108-12

187. Wei J, Long L, Yang K, Guy C, Shrestha S, Chen Z, Wu C, Vogel P, Neale G, Green DR, Chi H. 2016. Autophagy enforces functional integrity of regulatory T cells by coupling environmental cues and metabolic homeostasis. *Nat Immunol* 17: 277-85

188. Kabat AM, Harrison OJ, Riffelmacher T, Moghaddam AE, Pearson CF, Laing A, Abeler-Dorner L, Forman SP, Grencis RK, Sattentau Q, Simon AK, Pott J, Maloy KJ. 2016. The autophagy gene Atg16l1 differentially regulates Treg and TH2 cells to control intestinal inflammation. *Elife* 5

189. CDC. 2015. Influenza Activity — United States, 2014–15 Season and Composition of the 2015–16 Influenza Vaccine. In *Influenza Activity — United States, 2014–15 Season and Composition of the 2015–16 Influenza Vaccine*. https://www.cdc.gov/mmwr/preview/mmwrhtml/mm6421a5.htm - Fig3: Morbidity and Mortality Weekly Report (MMWR)

190. Sasaki S, Sullivan M, Narvaez CF, Holmes TH, Furman D, Zheng NY, Nishtala M, Wrammert J, Smith K, James JA, Dekker CL, Davis MM, Wilson PC, Greenberg HB, He XS. 2011. Limited efficacy of inactivated influenza vaccine in elderly individuals is associated with decreased production of vaccine-specific antibodies. *J Clin Invest* 121: 3109-19

191. Johnson KM, Owen K, Witte PL. 2002. Aging and developmental transitions in the B cell lineage. *Int Immunol* 14: 1313-23

192. Johnson SA, Rozzo SJ, Cambier JC. 2002. Aging-dependent exclusion of antigen-inexperienced cells from the peripheral B cell repertoire. *J Immunol* 168: 5014-23

193. Tabibian-Keissar H, Hazanov L, Schiby G, Rosenthal N, Rakovsky A, Michaeli M, Shahaf GL, Pickman Y, Rosenblatt K, Melamed D, Dunn-Walters D, Mehr R, Barshack I. 2016. Aging affects B-cell antigen receptor repertoire diversity in primary and secondary lymphoid tissues. *Eur J Immunol* 46: 480-92

194. Wang C, Liu Y, Xu LT, Jackson KJ, Roskin KM, Pham TD, Laserson J, Marshall EL, Seo K, Lee JY, Furman D, Koller D, Dekker CL, Davis MM, Fire AZ, Boyd SD. 2014. Effects of aging, cytomegalovirus infection, and EBV infection on human B cell repertoires. *J Immunol* 192: 603-11

195. Roukens AH, Soonawala D, Joosten SA, de Visser AW, Jiang X, Dirksen K, de Gruijter M, van Dissel JT, Bredenbeek PJ, Visser LG. 2011. Elderly subjects have a delayed antibody response and prolonged viraemia following yellow fever vaccination: a prospective controlled cohort study. *PLoS One* 6: e27753

196. Park S, Nahm MH. 2011. Older adults have a low capacity to opsonize pneumococci due to low IgM antibody response to pneumococcal vaccinations. *Infect Immun* 79: 314-20

197. Frasca D, Landin AM, Lechner SC, Ryan JG, Schwartz R, Riley RL, Blomberg BB. 2008. Aging down-regulates the transcription factor E2A, activation-induced cytidine deaminase, and Ig class switch in human B cells. *J Immunol* 180: 5283-90

198. Frasca D, Blomberg BB. 2011. Aging impairs murine B cell differentiation and function in primary and secondary lymphoid tissues. *Aging Dis* 2: 361-73

199. Frasca D, Diaz A, Romero M, Landin AM, Phillips M, Lechner SC, Ryan JG, Blomberg BB. 2010. Intrinsic defects in B cell response to seasonal influenza vaccination in elderly humans. *Vaccine* 28: 8077-84

200. Arsov I, Adebayo A, Kucerova-Levisohn M, Haye J, MacNeil M, Papavasiliou FN, Yue Z, Ortiz BD. 2011. A role for autophagic protein beclin 1 early in lymphocyte development. *J Immunol* 186: 2201-9

201. Miller BC, Zhao Z, Stephenson LM, Cadwell K, Pua HH, Lee HK, Mizushima NN, Iwasaki A, He YW, Swat W, Virgin HWt. 2008. The autophagy gene ATG5 plays an essential role in B lymphocyte development. *Autophagy* 4: 309-14

202. Pengo N, Scolari M, Oliva L, Milan E, Mainoldi F, Raimondi A, Fagioli C, Merlini A, Mariani E, Pasqualetto E, Orfanelli U, Ponzoni M, Sitia R, Casola S, Cenci S. 2013. Plasma cells require autophagy for sustainable immunoglobulin production. *Nat Immunol* 14: 298-305

203. Chen M, Kodali S, Jang A, Kuai L, Wang J. 2015. Requirement for autophagy in the long-term persistence but not initial formation of memory B cells. *J Immunol* 194: 2607-15

204. Chen M, Hong MJ, Sun H, Wang L, Shi X, Gilbert BE, Corry DB, Kheradmand F, Wang J. 2014. Essential role for autophagy in the maintenance of immunological memory against influenza infection. *Nat Med* 20: 503-10
205. Hardy RR. 2006. B-1 B cells: development, selection, natural autoantibody and leukemia. *Curr Opin Immunol* 18: 547-55
206. Stall AM, Farinas MC, Tarlinton DM, Lalor PA, Herzenberg LA, Strober S, Herzenberg LA. 1988. Ly-1 B-cell clones similar to human chronic lymphocytic leukemias routinely develop in older normal mice and young autoimmune (New Zealand Black-related) animals. *Proc Natl Acad Sci U S A* 85: 7312-6
207. Igarashi K, Kashiwagi K. 2000. Polyamines: mysterious modulators of cellular functions. *Biochem Biophys Res Commun* 271: 559-64
208. Pegg AE. 2016. Functions of Polyamines in Mammals. *J Biol Chem* 291: 14904-12
209. Igarashi K, Kashiwagi K. 2010. Characteristics of cellular polyamine transport in prokaryotes and eukaryotes. *Plant Physiol Biochem* 48: 506-12
210. Eisenberg T, Knauer H, Schauer A, Buttner S, Ruckenstuhl C, Carmona-Gutierrez D, Ring J, Schroeder S, Magnes C, Antonacci L, Fussi H, Deszcz L, Hartl R, Schraml E, Criollo A, Megalou E, Weiskopf D, Laun P, Heeren G, Breitenbach M, Grubeck-Loebenstein B, Herker E, Fahrenkrog B, Frohlich KU, Sinner F, Tavernarakis N, Minois N, Kroemer G, Madeo F. 2009. Induction of autophagy by spermidine promotes longevity. *Nat Cell Biol* 11: 1305-14
211. Gupta VK, Scheunemann L, Eisenberg T, Mertel S, Bhukel A, Koemans TS, Kramer JM, Liu KS, Schroeder S, Stunnenberg HG, Sinner F, Magnes C, Pieber TR, Dipt S, Fiala A, Schenck A, Schwaerzel M, Madeo F, Sigrist SJ. 2013. Restoring polyamines protects from age-induced memory impairment in an autophagy-dependent manner. *Nat Neurosci* 16: 1453-60
212. Eisenberg T, Abdellatif M, Schroeder S, Primessnig U, Stekovic S, Pendl T, Harger A, Schipke J, Zimmermann A, Schmidt A, Tong M, Ruckenstuhl C, Dammbrueck C, Gross AS, Herbst V, Magnes C, Trausinger G, Narath S, Meinitzer A, Hu Z, Kirsch A, Eller K, Carmona-Gutierrez D, Buttner S, Pietrocola F, Knittelfelder O, Schrepfer E, Rockenfeller P, Simonini C, Rahn A, Horsch M, Moreth K, Beckers J, Fuchs H, Gailus-Durner V, Neff F, Janik D, Rathkolb B, Rozman J, de Angelis MH, Moustafa T, Haemmerle G, Mayr

M, Willeit P, von Frieling-Salewsky M, Pieske B, Scorrano L, Pieber T, Pechlaner R, Willeit J, Sigrist SJ, Linke WA, Muhlfeld C, Sadoshima J, Dengjel J, Kiechl S, Kroemer G, Sedej S, Madeo F. 2016. Cardioprotection and lifespan extension by the natural polyamine spermidine. *Nat Med*

213. Yue F, Li W, Zou J, Jiang X, Xu G, Huang H, Liu L. 2017. Spermidine prolongs lifespan and prevents liver fibrosis and hepatocellular carcinoma by activating MAP1S-mediated autophagy. *Cancer Res*
214. Mortensen M, Soilleux EJ, Djordjevic G, Tripp R, Lutteropp M, Sadighi-Akha E, Stranks AJ, Glanville J, Knight S, Jacobsen SE, Kranc KR, Simon AK. 2011. The autophagy protein Atg7 is essential for hematopoietic stem cell maintenance. *J Exp Med* 208: 455-67
215. Riffelmacher T, Clarke A, Richter FC, Stranks A, Pandey S, Danielli S, Hublitz P, Yu Z, Johnson E, Schwerd T, McCullagh J, Uhlig H, Jacobsen SEW, Simon AK. 2017. Autophagy-Dependent Generation of Free Fatty Acids Is Critical for Normal Neutrophil Differentiation. *Immunity* 47: 466-80 e5
216. Stranks AJ, Hansen AL, Panse I, Mortensen M, Ferguson DJ, Puleston DJ, Shenderov K, Watson AS, Veldhoen M, Phadwal K, Cerundolo V, Simon AK. 2015. Autophagy Controls Acquisition of Aging Features in Macrophages. *J Innate Immun* 7: 375-91
217. Preukschas M, Hagel C, Schulte A, Weber K, Lamszus K, Sievert H, Pallmann N, Bokemeyer C, Hauber J, Braig M, Balabanov S. 2012. Expression of eukaryotic initiation factor 5A and hypusine forming enzymes in glioblastoma patient samples: implications for new targeted therapies. *PLoS One* 7: e43468
218. Sievert H, Pallmann N, Miller KK, Hermans-Borgmeyer I, Venz S, Sendoel A, Preukschas M, Schweizer M, Boettcher S, Janiesch PC, Streichert T, Walther R, Hengartner MO, Manz MG, Brummendorf TH, Bokemeyer C, Braig M, Hauber J, Duncan KE, Balabanov S. 2014. A novel mouse model for inhibition of DOHH-mediated hypusine modification reveals a crucial function in embryonic development, proliferation and oncogenic transformation. *Dis Model Mech* 7: 963-76
219. Wisniewski JR, Zougman A, Nagaraj N, Mann M. 2009. Universal sample preparation method for proteome analysis. *Nat Methods* 6: 359-62

220. Cox J, Mann M. 2008. MaxQuant enables high peptide identification rates, individualized p.p.b.-range mass accuracies and proteome-wide protein quantification. *Nat Biotechnol* 26: 1367-72
221. Cox J, Neuhauser N, Michalski A, Scheltema RA, Olsen JV, Mann M. 2011. Andromeda: a peptide search engine integrated into the MaxQuant environment. *J Proteome Res* 10: 1794-805
222. Yu Z, Huang H, Reim A, Charles PD, Northage A, Jackson D, Parry I, Kessler BM. 2017. Optimizing 2D gas chromatography mass spectrometry for robust tissue, serum and urine metabolite profiling. *Talanta* 165: 685-91
223. Ingolia NT, Brar GA, Rouskin S, McGeachy AM, Weissman JS. 2013. Genome-wide annotation and quantitation of translation by ribosome profiling. *Curr Protoc Mol Biol* Chapter 4: Unit 4 18
224. Ingolia NT. 2010. Genome-wide translational profiling by ribosome footprinting. *Methods Enzymol* 470: 119-42
225. Zhang M, Srivastava G, Lu L. 2004. The pre-B cell receptor and its function during B cell development. *Cell Mol Immunol* 1: 89-94
226. Kitamura D, Roes J, Kuhn R, Rajewsky K. 1991. A B cell-deficient mouse by targeted disruption of the membrane exon of the immunoglobulin mu chain gene. *Nature* 350: 423-6
227. Kitamura D, Kudo A, Schaal S, Muller W, Melchers F, Rajewsky K. 1992. A critical role of lambda 5 protein in B cell development. *Cell* 69: 823-31
228. Hess J, Werner A, Wirth T, Melchers F, Jack HM, Winkler TH. 2001. Induction of pre-B cell proliferation after de novo synthesis of the pre-B cell receptor. *Proc Natl Acad Sci U S A* 98: 1745-50
229. Ubelhart R, Jumaa H. 2015. Autoreactivity and the positive selection of B cells. *Eur J Immunol* 45: 2971-7
230. Tobon GJ, Izquierdo JH, Canas CA. 2013. B lymphocytes: development, tolerance, and their role in autoimmunity-focus on systemic lupus erythematosus. *Autoimmune Dis* 2013: 827254
231. Obukhanych TV, Nussenzweig MC. 2006. T-independent type II immune responses generate memory B cells. *J Exp Med* 203: 305-10
232. Kurosaki T, Kometani K, Ise W. 2015. Memory B cells. *Nat Rev Immunol* 15: 149-59
233. Dickerson SK, Market E, Besmer E, Papavasiliou FN. 2003. AID mediates hypermutation by deaminating single stranded DNA. *J Exp Med* 197: 1291-6

234. Muramatsu M, Kinoshita K, Fagarasan S, Yamada S, Shinkai Y, Honjo T. 2000. Class switch recombination and hypermutation require activation-induced cytidine deaminase (AID), a potential RNA editing enzyme. *Cell* 102: 553-63

235. Revy P, Muto T, Levy Y, Geissmann F, Plebani A, Sanal O, Catalan N, Forveille M, Dufourcq-Labelouse R, Gennery A, Tezcan I, Ersoy F, Kayserili H, Ugazio AG, Brousse N, Muramatsu M, Notarangelo LD, Kinoshita K, Honjo T, Fischer A, Durandy A. 2000. Activation-induced cytidine deaminase (AID) deficiency causes the autosomal recessive form of the Hyper-IgM syndrome (HIGM2). *Cell* 102: 565-75

236. Pape KA, Taylor JJ, Maul RW, Gearhart PJ, Jenkins MK. 2011. Different B cell populations mediate early and late memory during an endogenous immune response. *Science* 331: 1203-7

237. Taylor JJ, Pape KA, Jenkins MK. 2012. A germinal center-independent pathway generates unswitched memory B cells early in the primary response. *J Exp Med* 209: 597-606

238. Pronk CJ, Rossi DJ, Mansson R, Attema JL, Norddahl GL, Chan CK, Sigvardsson M, Weissman IL, Bryder D. 2007. Elucidation of the phenotypic, functional, and molecular topography of a myeloerythroid progenitor cell hierarchy. *Cell Stem Cell* 1: 428-42

239. Hardy RR, Carmack CE, Shinton SA, Kemp JD, Hayakawa K. 1991. Resolution and characterization of pro-B and pre-pro-B cell stages in normal mouse bone marrow. *J Exp Med* 173: 1213-25

240. Liu JJ, Segre M, Segre D. 1982. Changes in suppressor, helper, and B-cell functions in aging mice. *Cell Immunol* 66: 372-82

241. Liverani E, Rico MC, Yaratha L, Tsygankov AY, Kilpatrick LE, Kunapuli SP. 2014. LPS-induced systemic inflammation is more severe in P2Y12 null mice. *J Leukoc Biol* 95: 313-23

242. Yen D, Cheung J, Scheerens H, Poulet F, McClanahan T, McKenzie B, Kleinschek MA, Owyang A, Mattson J, Blumenschein W, Murphy E, Sathe M, Cua DJ, Kastelein RA, Rennick D. 2006. IL-23 is essential for T cell-mediated colitis and promotes inflammation via IL-17 and IL-6. *J Clin Invest* 116: 1310-6

243. Suematsu S, Matsuda T, Aozasa K, Akira S, Nakano N, Ohno S, Miyazaki J, Yamamura K, Hirano T, Kishimoto T. 1989. IgG1 plasmacytosis in interleukin 6 transgenic mice. *Proc Natl Acad Sci U S A* 86: 7547-51
244. Cretney E, Street SE, Smyth MJ. 2002. TNF contributes to the immunopathology of perforin/Fas ligand double deficiency. *Immunol Cell Biol* 80: 436-40
245. Sudo K, Ema H, Morita Y, Nakauchi H. 2000. Age-associated characteristics of murine hematopoietic stem cells. *J Exp Med* 192: 1273-80
246. Giaime E, Tong Y, Wagner LK, Yuan Y, Huang G, Shen J. 2017. Age-Dependent Dopaminergic Neurodegeneration and Impairment of the Autophagy-Lysosomal Pathway in LRRK-Deficient Mice. *Neuron* 96: 796-807 e6
247. Frake RA, Ricketts T, Menzies FM, Rubinsztein DC. 2015. Autophagy and neurodegeneration. *J Clin Invest* 125: 65-74
248. Slifka MK, Matloubian M, Ahmed R. 1995. Bone marrow is a major site of long-term antibody production after acute viral infection. *J Virol* 69: 1895-902
249. Chu VT, Berek C. 2013. The establishment of the plasma cell survival niche in the bone marrow. *Immunol Rev* 251: 177-88
250. Hobeika E, Thiemann S, Storch B, Jumaa H, Nielsen PJ, Pelanda R, Reth M. 2006. Testing gene function early in the B cell lineage in mb1-cre mice. *Proc Natl Acad Sci U S A* 103: 13789-94
251. Kaur J, Debnath J. 2015. Autophagy at the crossroads of catabolism and anabolism. *Nat Rev Mol Cell Biol* 16: 461-72
252. Komatsu M, Waguri S, Ueno T, Iwata J, Murata S, Tanida I, Ezaki J, Mizushima N, Ohsumi Y, Uchiyama Y, Kominami E, Tanaka K, Chiba T. 2005. Impairment of starvation-induced and constitutive autophagy in Atg7-deficient mice. *J Cell Biol* 169: 425-34
253. Guralnik JM, Eisenstaedt RS, Ferrucci L, Klein HG, Woodman RC. 2004. Prevalence of anemia in persons 65 years and older in the United States: evidence for a high rate of unexplained anemia. *Blood* 104: 2263-8
254. Lichtman MA, Rowe JM. 2004. The relationship of patient age to the pathobiology of the clonal myeloid diseases. *Semin Oncol* 31: 185-97
255. Balderman SR, Li AJ, Hoffman CM, Frisch BJ, Goodman AN, LaMere MW, Georger MA, Evans AG, Liesveld JL, Becker MW, Calvi LM. 2016. Targeting

of the bone marrow microenvironment improves outcome in a murine model of myelodysplastic syndrome. *Blood* 127: 616-25

256. Pang WW, Price EA, Sahoo D, Beerman I, Maloney WJ, Rossi DJ, Schrier SL, Weissman IL. 2011. Human bone marrow hematopoietic stem cells are increased in frequency and myeloid-biased with age. *Proc Natl Acad Sci U S A* 108: 20012-7

257. Janzen V, Forkert R, Fleming HE, Saito Y, Waring MT, Dombkowski DM, Cheng T, DePinho RA, Sharpless NE, Scadden DT. 2006. Stem-cell ageing modified by the cyclin-dependent kinase inhibitor p16INK4a. *Nature* 443: 421-6

258. Kollman C, Howe CW, Anasetti C, Antin JH, Davies SM, Filipovich AH, Hegland J, Kamani N, Kernan NA, King R, Ratanatharathorn V, Weisdorf D, Confer DL. 2001. Donor characteristics as risk factors in recipients after transplantation of bone marrow from unrelated donors: the effect of donor age. *Blood* 98: 2043-51

259. Ergen AV, Boles NC, Goodell MA. 2012. Rantes/Ccl5 influences hematopoietic stem cell subtypes and causes myeloid skewing. *Blood* 119: 2500-9

260. Tuljapurkar SR, McGuire TR, Brusnahan SK, Jackson JD, Garvin KL, Kessinger MA, Lane JT, BJ OK, Sharp JG. 2011. Changes in human bone marrow fat content associated with changes in hematopoietic stem cell numbers and cytokine levels with aging. *J Anat* 219: 574-81

261. Ding L, Morrison SJ. 2013. Haematopoietic stem cells and early lymphoid progenitors occupy distinct bone marrow niches. *Nature* 495: 231-5

262. Ho TT, Warr MR, Adelman ER, Lansinger OM, Flach J, Verovskaya EV, Figueroa ME, Passegue E. 2017. Autophagy maintains the metabolism and function of young and old stem cells. *Nature*

263. Jacquel A, Obba S, Boyer L, Dufies M, Robert G, Gounon P, Lemichez E, Luciano F, Solary E, Auberger P. 2012. Autophagy is required for CSF-1-induced macrophagic differentiation and acquisition of phagocytic functions. *Blood* 119: 4527-31

264. Kambas K, Mitroulis I, Apostolidou E, Girod A, Chrysanthopoulou A, Pneumatikos I, Skendros P, Kourtzelis I, Koffa M, Kotsianidis I, Ritis K. 2012. Autophagy mediates the delivery of thrombogenic tissue factor to neutrophil extracellular traps in human sepsis. *PLoS One* 7: e45427

265. Romao S, Gasser N, Becker AC, Guhl B, Bajagic M, Vanoaica D, Ziegler U, Roesler J, Dengjel J, Reichenbach J, Munz C. 2013. Autophagy proteins stabilize pathogen-containing phagosomes for prolonged MHC II antigen processing. *J Cell Biol* 203: 757-66

266. Mintern JD, Macri C, Chin WJ, Panozza SE, Segura E, Patterson NL, Zeller P, Bourges D, Bedoui S, McMillan PJ, Idris A, Nowell CJ, Brown A, Radford KJ, Johnston AP, Villadangos JA. 2015. Differential use of autophagy by primary dendritic cells specialized in cross-presentation. *Autophagy* 11: 906-17

267. Lee HK, Mattei LM, Steinberg BE, Alberts P, Lee YH, Chervonsky A, Mizushima N, Grinstein S, Iwasaki A. 2010. In vivo requirement for Atg5 in antigen presentation by dendritic cells. *Immunity* 32: 227-39

268. Reed M, Morris SH, Jang S, Mukherjee S, Yue Z, Lukacs NW. 2013. Autophagy-inducing protein beclin-1 in dendritic cells regulates CD4 T cell responses and disease severity during respiratory syncytial virus infection. *J Immunol* 191: 2526-37

269. Bhattacharya A, Wei Q, Shin JN, Abdel Fattah E, Bonilla DL, Xiang Q, Eissa NT. 2015. Autophagy Is Required for Neutrophil-Mediated Inflammation. *Cell Rep* 12: 1731-9

270. Arsiwala S, Ding W, Wang H. 2015. Selective Deletion of ATG5 in Bone Marrow Leptin-Receptor-Expressing Perivascular Stromal Cells Causes Leukopenia. *Blood* 126

271. Schuettpelz LG, Link DC. 2013. Regulation of hematopoietic stem cell activity by inflammation. *Front Immunol* 4: 204

272. Dufour C, Corcione A, Svahn J, Haupt R, Poggi V, Beka'ssy AN, Scime R, Pistorio A, Pistoia V. 2003. TNF-alpha and IFN-gamma are overexpressed in the bone marrow of Fanconi anemia patients and TNF-alpha suppresses erythropoiesis in vitro. *Blood* 102: 2053-9

273. Morselli E, Galluzzi L, Kepp O, Criollo A, Maiuri MC, Tavernarakis N, Madeo F, Kroemer G. 2009. Autophagy mediates pharmacological lifespan extension by spermidine and resveratrol. *Aging (Albany NY)* 1: 961-70

274. Pyo JO, Yoo SM, Ahn HH, Nah J, Hong SH, Kam TI, Jung S, Jung YK. 2013. Overexpression of Atg5 in mice activates autophagy and extends lifespan. *Nat Commun* 4: 2300

275. Russell DH. 1971. Increased polyamine concentrations in the urine of human cancer patients. *Nat New Biol* 233: 144-5
276. Bassiri H, Benavides A, Haber M, Gilmour SK, Norris MD, Hogarty MD. 2015. Translational development of difluoromethylornithine (DFMO) for the treatment of neuroblastoma. *Transl Pediatr* 4: 226-38
277. Meyskens FL, Jr., Gerner EW. 1999. Development of difluoromethylornithine (DFMO) as a chemoprevention agent. *Clin Cancer Res* 5: 945-51
278. Chappuis F, Udayraj N, Stietenroth K, Meussen A, Bovier PA. 2005. Eflornithine is safer than melarsoprol for the treatment of second-stage Trypanosoma brucei gambiense human African trypanosomiasis. *Clin Infect Dis* 41: 748-51
279. Kennedy PG. 2004. Human African trypanosomiasis of the CNS: current issues and challenges. *J Clin Invest* 113: 496-504
280. Soda K, Kano Y, Chiba F, Koizumi K, Miyaki Y. 2013. Increased polyamine intake inhibits age-associated alteration in global DNA methylation and 1,2-dimethylhydrazine-induced tumorigenesis. *PLoS One* 8: e64357
281. Dranoff G. 2004. Cytokines in cancer pathogenesis and cancer therapy. *Nat Rev Cancer* 4: 11-22
282. Tsou P, Katayama H, Ostrin EJ, Hanash SM. 2016. The Emerging Role of B Cells in Tumor Immunity. *Cancer Res* 76: 5597-601
283. Igarashi K, Kakegawa T, Hirose S. 1982. Stabilization of 30 S ribosomal subunits of Bacillus subtilis W168 by spermidine and magnesium ions. *Biochim Biophys Acta* 697: 185-92
284. Ouyang K, Li J, Huang H, Que Q, Li P, Chen X. 2014. A simple method for RNA isolation from various tissues of the tree Neolamarckia cadamba. *Biotechnol Biotechnol Equip* 28: 1008-13
285. Maruyoshi K, Nonaka K, Sagane T, Demura T, Yamaguchi T, Matsumori N, Oishi T, Murata M. 2009. Conformational change of spermidine upon interaction with adenosine triphosphate in aqueous solution. *Chemistry* 15: 1618-26
286. Song Z, Parker KJ, Enoh I, Zhao H, Olubajo O. 2010. Elucidation of spermidine interaction with nucleotide ATP by multiple NMR techniques. *Magn Reson Chem* 48: 123-8
287. Garcon DP, Lucena MN, Franca JL, McNamara JC, Fontes CF, Leone FA. 2011. Na(+),K(+)-ATPase activity in the posterior gills of the blue crab,

Callinectes ornatus (Decapoda, Brachyura): modulation of ATP hydrolysis by the biogenic amines spermidine and spermine. *J Membr Biol* 244: 9-20

288. Park MH, Cooper HL, Folk JE. 1981. Identification of hypusine, an unusual amino acid, in a protein from human lymphocytes and of spermidine as its biosynthetic precursor. *Proc Natl Acad Sci U S A* 78: 2869-73
289. Cooper HL, Park MH, Folk JE. 1982. Posttranslational formation of hypusine in a single major protein occurs generally in growing cells and is associated with activation of lymphocyte growth. *Cell* 29: 791-7
290. Cooper HL, Park MH, Folk JE, Safer B, Braverman R. 1983. Identification of the hypusine-containing protein hy+ as translation initiation factor eIF-4D. *Proc Natl Acad Sci U S A* 80: 1854-7
291. Chattopadhyay MK, Park MH, Tabor H. 2008. Hypusine modification for growth is the major function of spermidine in Saccharomyces cerevisiae polyamine auxotrophs grown in limiting spermidine. *Proc Natl Acad Sci U S A* 105: 6554-9
292. Blaha G, Stanley RE, Steitz TA. 2009. Formation of the first peptide bond: the structure of EF-P bound to the 70S ribosome. *Science* 325: 966-70
293. Melnikov S, Mailliot J, Shin BS, Rigger L, Yusupova G, Micura R, Dever TE, Yusupov M. 2016. Crystal Structure of Hypusine-Containing Translation Factor eIF5A Bound to a Rotated Eukaryotic Ribosome. *J Mol Biol* 428: 3570-6
294. Schmidt C, Becker T, Heuer A, Braunger K, Shanmuganathan V, Pech M, Berninghausen O, Wilson DN, Beckmann R. 2016. Structure of the hypusinylated eukaryotic translation factor eIF-5A bound to the ribosome. *Nucleic Acids Res* 44: 1944-51
295. Dever TE, Gutierrez E, Shin BS. 2014. The hypusine-containing translation factor eIF5A. *Crit Rev Biochem Mol Biol*: 1-13
296. Rossi D, Kuroshu R, Zanelli CF, Valentini SR. 2014. eIF5A and EF-P: two unique translation factors are now traveling the same road. *Wiley Interdiscip Rev RNA* 5: 209-22
297. Schreier MH, Erni B, Staehelin T. 1977. Initiation of mammalian protein synthesis. I. Purification and characterization of seven initiation factors. *J Mol Biol* 116: 727-53
298. Benne R, Hershey JW. 1978. The mechanism of action of protein synthesis initiation factors from rabbit reticulocytes. *J Biol Chem* 253: 3078-87

299. Saini P, Eyler DE, Green R, Dever TE. 2009. Hypusine-containing protein eIF5A promotes translation elongation. *Nature* 459: 118-21
300. Doerfel LK, Wohlgemuth I, Kothe C, Peske F, Urlaub H, Rodnina MV. 2013. EF-P is essential for rapid synthesis of proteins containing consecutive proline residues. *Science* 339: 85-8
301. Gutierrez E, Shin BS, Woolstenhulme CJ, Kim JR, Saini P, Buskirk AR, Dever TE. 2013. eIF5A promotes translation of polyproline motifs. *Mol Cell* 51: 35-45
302. Ude S, Lassak J, Starosta AL, Kraxenberger T, Wilson DN, Jung K. 2013. Translation elongation factor EF-P alleviates ribosome stalling at polyproline stretches. *Science* 339: 82-5
303. Tollerson R, 2nd, Witzky A, Ibba M. 2017. Elongation Factor P Interactions with the Ribosome Are Independent of Pausing. *MBio* 8
304. Schuller AP, Wu CC, Dever TE, Buskirk AR, Green R. 2017. eIF5A Functions Globally in Translation Elongation and Termination. *Mol Cell* 66: 194-205 e5
305. Bevec D, Klier H, Holter W, Tschachler E, Valent P, Lottspeich F, Baumruker T, Hauber J. 1994. Induced gene expression of the hypusine-containing protein eukaryotic initiation factor 5A in activated human T lymphocytes. *Proc Natl Acad Sci U S A* 91: 10829-33
306. Hanauske-Abel HM, Park MH, Hanauske AR, Popowicz AM, Lalande M, Folk JE. 1994. Inhibition of the G1-S transition of the cell cycle by inhibitors of deoxyhypusine hydroxylation. *Biochim Biophys Acta* 1221: 115-24
307. Kang HA, Hershey JW. 1994. Effect of initiation factor eIF-5A depletion on protein synthesis and proliferation of Saccharomyces cerevisiae. *J Biol Chem* 269: 3934-40
308. Lee Y, Kim HK, Park HE, Park MH, Joe YA. 2002. Effect of N1-guanyl-1,7-diaminoheptane, an inhibitor of deoxyhypusine synthase, on endothelial cell growth, differentiation and apoptosis. *Mol Cell Biochem* 237: 69-76
309. Park MH, Wolff EC, Lee YB, Folk JE. 1994. Antiproliferative effects of inhibitors of deoxyhypusine synthase. Inhibition of growth of Chinese hamster ovary cells by guanyl diamines. *J Biol Chem* 269: 27827-32
310. Seidenfeld J, Gray JW, Marton LJ. 1981. Depletion of 9L rat brain tumor cell polyamine content by treatment with D,L-alpha-difluoromethylornithine inhibits proliferation and the G1 to S transition. *Exp Cell Res* 131: 209-16

311. Pendeville H, Carpino N, Marine JC, Takahashi Y, Muller M, Martial JA, Cleveland JL. 2001. The ornithine decarboxylase gene is essential for cell survival during early murine development. *Mol Cell Biol* 21: 6549-58
312. Guo Y, Cleveland JL, O'Brien TG. 2005. Haploinsufficiency for odc modifies mouse skin tumor susceptibility. *Cancer Res* 65: 1146-9
313. Lukkarainen J, Kauppinen RA, Koistinaho J, Halmekyto, Alhonen LM, Janne J. 1995. Cerebral energy metabolism and immediate early gene induction following severe incomplete ischaemia in transgenic mice overexpressing the human ornithine decarboxylase gene: evidence that putrescine is not neurotoxic in vivo. *Eur J Neurosci* 7: 1840-9
314. Alhonen L, Heikkinen S, Sinervirta R, Halmekyto M, Alakuijala P, Janne J. 1996. Transgenic mice expressing the human ornithine decarboxylase gene under the control of mouse metallothionein I promoter. *Biochem J* 314 (Pt 2): 405-8
315. Shantz LM, Feith DJ, Pegg AE. 2001. Targeted overexpression of ornithine decarboxylase enhances beta-adrenergic agonist-induced cardiac hypertrophy. *Biochem J* 358: 25-32
316. Halmekyto M, Hyttinen JM, Sinervirta R, Utriainen M, Myohanen S, Voipio HM, Wahlfors J, Syrjanen S, Syrjanen K, Alhonen L, et al. 1991. Transgenic mice aberrantly expressing human ornithine decarboxylase gene. *J Biol Chem* 266: 19746-51
317. Halmekyto M, Syrjanen K, Janne J, Alhonen L. 1992. Enhanced papilloma formation in response to skin tumor promotion in transgenic mice overexpressing the human ornithine decarboxylase gene. *Biochem Biophys Res Commun* 187: 493-7
318. Nishimura K, Lee SB, Park JH, Park MH. 2012. Essential role of eIF5A-1 and deoxyhypusine synthase in mouse embryonic development. *Amino Acids* 42: 703-10
319. Pallmann N, Braig M, Sievert H, Preukschas M, Hermans-Borgmeyer I, Schweizer M, Nagel CH, Neumann M, Wild P, Haralambieva E, Hagel C, Bokemeyer C, Hauber J, Balabanov S. 2015. Biological Relevance and Therapeutic Potential of the Hypusine Modification System. *J Biol Chem*
320. Morselli E, Marino G, Bennetzen MV, Eisenberg T, Megalou E, Schroeder S, Cabrera S, Benit P, Rustin P, Criollo A, Kepp O, Galluzzi L, Shen S, Malik SA, Maiuri MC, Horio Y, Lopez-Otin C, Andersen JS, Tavernarakis N, Madeo F,

Kroemer G. 2011. Spermidine and resveratrol induce autophagy by distinct pathways converging on the acetylproteome. *J Cell Biol* 192: 615-29

321. Pietrocola F, Lachkar S, Enot DP, Niso-Santano M, Bravo-San Pedro JM, Sica V, Izzo V, Maiuri MC, Madeo F, Marino G, Kroemer G. 2015. Spermidine induces autophagy by inhibiting the acetyltransferase EP300. *Cell Death Differ* 22: 509-16
322. Lee IH, Finkel T. 2009. Regulation of autophagy by the p300 acetyltransferase. *J Biol Chem* 284: 6322-8
323. Su H, Yang F, Wang Q, Shen Q, Huang J, Peng C, Zhang Y, Wan W, Wong CCL, Sun Q, Wang F, Zhou T, Liu W. 2017. VPS34 Acetylation Controls Its Lipid Kinase Activity and the Initiation of Canonical and Non-canonical Autophagy. *Mol Cell* 67: 907-21 e7
324. Park IH, Kim MM. 2012. Spermidine inhibits MMP-2 via modulation of histone acetyltransferase and histone deacetylase in HDFs. *Int J Biol Macromol* 51: 1003-7
325. Woolstenhulme CJ, Guydosh NR, Green R, Buskirk AR. 2015. High-precision analysis of translational pausing by ribosome profiling in bacteria lacking EFP. *Cell Rep* 11: 13-21
326. Wruck F, Katranidis A, Nierhaus KH, Buldt G, Hegner M. 2017. Translation and folding of single proteins in real time. *Proc Natl Acad Sci U S A* 114: E4399-E407
327. Dyshlovoy SA, Naeth I, Venz S, Preukschas M, Sievert H, Jacobsen C, Shubina LK, Gesell Salazar M, Scharf C, Walther R, Krepstakies M, Priyadarshini P, Hauber J, Fedorov SN, Bokemeyer C, Stonik VA, Balabanov S, Honecker F. 2012. Proteomic profiling of germ cell cancer cells treated with aaptamine, a marine alkaloid with antiproliferative activity. *J Proteome Res* 11: 2316-30
328. Doma MK, Parker R. 2006. Endonucleolytic cleavage of eukaryotic mRNAs with stalls in translation elongation. *Nature* 440: 561-4
329. Wu J, Kaufman RJ. 2006. From acute ER stress to physiological roles of the Unfolded Protein Response. *Cell Death Differ* 13: 374-84
330. Shaffer AL, Shapiro-Shelef M, Iwakoshi NN, Lee AH, Qian SB, Zhao H, Yu X, Yang L, Tan BK, Rosenwald A, Hurt EM, Petroulakis E, Sonenberg N, Yewdell JW, Calame K, Glimcher LH, Staudt LM. 2004. XBP1, downstream of

Blimp-1, expands the secretory apparatus and other organelles, and increases protein synthesis in plasma cell differentiation. *Immunity* 21: 81-93

331. Hemesath TJ, Steingrimsson E, McGill G, Hansen MJ, Vaught J, Hodgkinson CA, Arnheiter H, Copeland NG, Jenkins NA, Fisher DE. 1994. microphthalmia, a critical factor in melanocyte development, defines a discrete transcription factor family. *Genes Dev* 8: 2770-80
332. Pogenberg V, Ogmundsdottir MH, Bergsteinsdottir K, Schepsky A, Phung B, Deineko V, Milewski M, Steingrimsson E, Wilmanns M. 2012. Restricted leucine zipper dimerization and specificity of DNA recognition of the melanocyte master regulator MITF. *Genes Dev* 26: 2647-58
333. Steingrimsson E, Copeland NG, Jenkins NA. 2004. Melanocytes and the microphthalmia transcription factor network. *Annu Rev Genet* 38: 365-411
334. Zhao GQ, Zhao Q, Zhou X, Mattei MG, de Crombrugghe B. 1993. TFEC, a basic helix-loop-helix protein, forms heterodimers with TFE3 and inhibits TFE3-dependent transcription activation. *Mol Cell Biol* 13: 4505-12
335. Napolitano G, Ballabio A. 2016. TFEB at a glance. *J Cell Sci* 129: 2475-81
336. Rehli M, Den Elzen N, Cassady AI, Ostrowski MC, Hume DA. 1999. Cloning and characterization of the murine genes for bHLH-ZIP transcription factors TFEC and TFEB reveal a common gene organization for all MiT subfamily members. *Genomics* 56: 111-20
337. Hallsson JH, Haflidadottir BS, Stivers C, Odenwald W, Arnheiter H, Pignoni F, Steingrimsson E. 2004. The basic helix-loop-helix leucine zipper transcription factor Mitf is conserved in Drosophila and functions in eye development. *Genetics* 167: 233-41
338. Lister JA, Close J, Raible DW. 2001. Duplicate mitf genes in zebrafish: complementary expression and conservation of melanogenic potential. *Dev Biol* 237: 333-44
339. Kumasaka M, Sato H, Sato S, Yajima I, Yamamoto H. 2004. Isolation and developmental expression of Mitf in Xenopus laevis. *Dev Dyn* 230: 107-13
340. Sardiello M, Palmieri M, di Ronza A, Medina DL, Valenza M, Gennarino VA, Di Malta C, Donaudy F, Embrione V, Polishchuk RS, Banfi S, Parenti G, Cattaneo E, Ballabio A. 2009. A gene network regulating lysosomal biogenesis and function. *Science* 325: 473-7
341. Lapierre LR, De Magalhaes Filho CD, McQuary PR, Chu CC, Visvikis O, Chang JT, Gelino S, Ong B, Davis AE, Irazoqui JE, Dillin A, Hansen M. 2013.

The TFEB orthologue HLH-30 regulates autophagy and modulates longevity in Caenorhabditis elegans. *Nat Commun* 4: 2267

342. Settembre C, De Cegli R, Mansueto G, Saha PK, Vetrini F, Visvikis O, Huynh T, Carissimo A, Palmer D, Klisch TJ, Wollenberg AC, Di Bernardo D, Chan L, Irazoqui JE, Ballabio A. 2013. TFEB controls cellular lipid metabolism through a starvation-induced autoregulatory loop. *Nat Cell Biol* 15: 647-58
343. Mansueto G, Armani A, Viscomi C, D'Orsi L, De Cegli R, Polishchuk EV, Lamperti C, Di Meo I, Romanello V, Marchet S, Saha PK, Zong H, Blaauw B, Solagna F, Tezze C, Grumati P, Bonaldo P, Pessin JE, Zeviani M, Sandri M, Ballabio A. 2017. Transcription Factor EB Controls Metabolic Flexibility during Exercise. *Cell Metab* 25: 182-96
344. Pastore N, Brady OA, Diab HI, Martina JA, Sun L, Huynh T, Lim JA, Zare H, Raben N, Ballabio A, Puertollano R. 2016. TFEB and TFE3 cooperate in the regulation of the innate immune response in activated macrophages. *Autophagy* 12: 1240-58
345. Vural A, Al-Khodor S, Cheung GY, Shi CS, Srinivasan L, McQuiston TJ, Hwang IY, Yeh AJ, Blumer JB, Briken V, Williamson PR, Otto M, Fraser ID, Kehrl JH. 2016. Activator of G-Protein Signaling 3-Induced Lysosomal Biogenesis Limits Macrophage Intracellular Bacterial Infection. *J Immunol* 196: 846-56
346. Visvikis O, Ihuegbu N, Labed SA, Luhachack LG, Alves AF, Wollenberg AC, Stuart LM, Stormo GD, Irazoqui JE. 2014. Innate host defense requires TFEB-mediated transcription of cytoprotective and antimicrobial genes. *Immunity* 40: 896-909
347. Visvikis O, Ihuegbu N, Labed SA, Luhachack LG, Alves AM, Wollenberg AC, Stuart LM, Stormo GD, Irazoqui JE. 2014. Innate host defense requires TFEB-mediated transcription of cytoprotective and antimicrobial genes. *Immunity* 40: 896-909
348. Martina JA, Chen Y, Gucek M, Puertollano R. 2012. MTORC1 functions as a transcriptional regulator of autophagy by preventing nuclear transport of TFEB. *Autophagy* 8: 903-14
349. Roczniak-Ferguson A, Petit CS, Froehlich F, Qian S, Ky J, Angarola B, Walther TC, Ferguson SM. 2012. The transcription factor TFEB links mTORC1 signaling to transcriptional control of lysosome homeostasis. *Sci Signal* 5: ra42

350. Sancak Y, Bar-Peled L, Zoncu R, Markhard AL, Nada S, Sabatini DM. 2010. Ragulator-Rag complex targets mTORC1 to the lysosomal surface and is necessary for its activation by amino acids. *Cell* 141: 290-303
351. Martina JA, Puertollano R. 2013. Rag GTPases mediate amino acid-dependent recruitment of TFEB and MITF to lysosomes. *J Cell Biol* 200: 475-91
352. Medina DL, Di Paola S, Peluso I, Armani A, De Stefani D, Venditti R, Montefusco S, Scotto-Rosato A, Prezioso C, Forrester A, Settembre C, Wang W, Gao Q, Xu H, Sandri M, Rizzuto R, De Matteis MA, Ballabio A. 2015. Lysosomal calcium signalling regulates autophagy through calcineurin and TFEB. *Nat Cell Biol* 17: 288-99
353. Gonzalez A, Hall MN. 2017. Nutrient sensing and TOR signaling in yeast and mammals. *EMBO J* 36: 397-408
354. Steingrimsson E, Tessarollo L, Reid SW, Jenkins NA, Copeland NG. 1998. The bHLH-Zip transcription factor Tfeb is essential for placental vascularization. *Development* 125: 4607-16
355. Young NP, Kamireddy A, Van Nostrand JL, Eichner LJ, Shokhirev MN, Dayn Y, Shaw RJ. 2016. AMPK governs lineage specification through Tfeb-dependent regulation of lysosomes. *Genes Dev* 30: 535-52
356. Wenz T. 2013. Regulation of mitochondrial biogenesis and PGC-1alpha under cellular stress. *Mitochondrion* 13: 134-42
357. Samie M, Cresswell P. 2015. The transcription factor TFEB acts as a molecular switch that regulates exogenous antigen-presentation pathways. *Nat Immunol* 16: 729-36
358. Huan C, Kelly ML, Steele R, Shapira I, Gottesman SR, Roman CA. 2006. Transcription factors TFE3 and TFEB are critical for CD40 ligand expression and thymus-dependent humoral immunity. *Nat Immunol* 7: 1082-91
359. Palmieri M, Impey S, Kang H, di Ronza A, Pelz C, Sardiello M, Ballabio A. 2011. Characterization of the CLEAR network reveals an integrated control of cellular clearance pathways. *Hum Mol Genet* 20: 3852-66
360. Xiao Q, Yan P, Ma X, Liu H, Perez R, Zhu A, Gonzales E, Tripoli DL, Czerniewski L, Ballabio A, Cirrito JR, Diwan A, Lee JM. 2015. Neuronal-Targeted TFEB Accelerates Lysosomal Degradation of APP, Reducing Abeta Generation and Amyloid Plaque Pathogenesis. *J Neurosci* 35: 12137-51

361. Diament A, Tuller T. 2016. Estimation of ribosome profiling performance and reproducibility at various levels of resolution. *Biol Direct* 11: 24
362. Raghavan A, Ogilvie RL, Reilly C, Abelson ML, Raghavan S, Vasdewani J, Krathwohl M, Bohjanen PR. 2002. Genome-wide analysis of mRNA decay in resting and activated primary human T lymphocytes. *Nucleic Acids Res* 30: 5529-38
363. Pucciarelli S, Moreschini B, Micozzi D, De Fronzo GS, Carpi FM, Polzonetti V, Vincenzetti S, Mignini F, Napolioni V. 2012. Spermidine and spermine are enriched in whole blood of nona/centenarians. *Rejuvenation Res* 15: 590-5
364. Adzhubei AA, Sternberg MJ, Makarov AA. 2013. Polyproline-II helix in proteins: structure and function. *J Mol Biol* 425: 2100-32
365. Crespo L, Sanclimens G, Montaner B, Perez-Tomas R, Royo M, Pons M, Albericio F, Giralt E. 2002. Peptide dendrimers based on polyproline helices. *J Am Chem Soc* 124: 8876-83
366. Cubellis MV, Caillez F, Blundell TL, Lovell SC. 2005. Properties of polyproline II, a secondary structure element implicated in protein-protein interactions. *Proteins* 58: 880-92
367. Jia CY, Nie J, Wu C, Li C, Li SS. 2005. Novel Src homology 3 domain-binding motifs identified from proteomic screen of a Pro-rich region. *Mol Cell Proteomics* 4: 1155-66
368. Lim WA, Richards FM, Fox RO. 1994. Structural determinants of peptide-binding orientation and of sequence specificity in SH3 domains. *Nature* 372: 375-9
369. Nguyen JT, Turck CW, Cohen FE, Zuckermann RN, Lim WA. 1998. Exploiting the basis of proline recognition by SH3 and WW domains: design of N-substituted inhibitors. *Science* 282: 2088-92
370. Hicks JM, Hsu VL. 2004. The extended left-handed helix: a simple nucleic acid-binding motif. *Proteins* 55: 330-8
371. Halazonetis TD, Kandil AN. 1991. Determination of the c-MYC DNA-binding site. *Proc Natl Acad Sci U S A* 88: 6162-6
372. Hersch SJ, Elgamal S, Katz A, Ibba M, Navarre WW. 2014. Translation initiation rate determines the impact of ribosome stalling on bacterial protein synthesis. *J Biol Chem* 289: 28160-71

373. Zhang G, Hubalewska M, Ignatova Z. 2009. Transient ribosomal attenuation coordinates protein synthesis and co-translational folding. *Nat Struct Mol Biol* 16: 274-80

374. Agbas A, Zaidi A, Michaelis EK. 2005. Decreased activity and increased aggregation of brain calcineurin during aging. *Brain Res* 1059: 59-71

375. Lian Q, Ladner CJ, Magnuson D, Lee JM. 2001. Selective changes of calcineurin (protein phosphatase 2B) activity in Alzheimer's disease cerebral cortex. *Exp Neurol* 167: 158-65

376. Green M, Loewenstein PM. 1988. Autonomous functional domains of chemically synthesized human immunodeficiency virus tat trans-activator protein. *Cell* 55: 1179-88

377. Kaplan IM, Wadia JS, Dowdy SF. 2005. Cationic TAT peptide transduction domain enters cells by macropinocytosis. *J Control Release* 102: 247-53

378. Schwarze SR, Ho A, Vocero-Akbani A, Dowdy SF. 1999. In vivo protein transduction: delivery of a biologically active protein into the mouse. *Science* 285: 1569-72

379. Shoji-Kawata S, Sumpter R, Leveno M, Campbell GR, Zou Z, Kinch L, Wilkins AD, Sun Q, Pallauf K, MacDuff D, Huerta C, Virgin HW, Helms JB, Eerland R, Tooze SA, Xavier R, Lenschow DJ, Yamamoto A, King D, Lichtarge O, Grishin NV, Spector SA, Kaloyanova DV, Levine B. 2013. Identification of a candidate therapeutic autophagy-inducing peptide. *Nature* 494: 201-6

380. Ward W, Richardson A. 1991. Effect of age on liver protein synthesis and degradation. *Hepatology* 14: 935-48

381. Steffen KK, MacKay VL, Kerr EO, Tsuchiya M, Hu D, Fox LA, Dang N, Johnston ED, Oakes JA, Tchao BN, Pak DN, Fields S, Kennedy BK, Kaeberlein M. 2008. Yeast life span extension by depletion of 60s ribosomal subunits is mediated by Gcn4. *Cell* 133: 292-302

382. Hansen M, Taubert S, Crawford D, Libina N, Lee SJ, Kenyon C. 2007. Lifespan extension by conditions that inhibit translation in Caenorhabditis elegans. *Aging Cell* 6: 95-110

383. Chiocchetti A, Zhou J, Zhu H, Karl T, Haubenreisser O, Rinnerthaler M, Heeren G, Oender K, Bauer J, Hintner H, Breitenbach M, Breitenbach-Koller L. 2007. Ribosomal proteins Rpl10 and Rps6 are potent regulators of yeast replicative life span. *Exp Gerontol* 42: 275-86

384. Luce MC, Bunn CL. 1989. Decreased accuracy of protein synthesis in extracts from aging human diploid fibroblasts. *Exp Gerontol* 24: 113-25
385. Yokoyama K, Fukumoto K, Murakami T, Harada S, Hosono R, Wadhwa R, Mitsui Y, Ohkuma S. 2002. Extended longevity of Caenorhabditis elegans by knocking in extra copies of hsp70F, a homolog of mot-2 (mortalin)/mthsp70/Grp75. *FEBS Lett* 516: 53-7
386. Hsu AL, Murphy CT, Kenyon C. 2003. Regulation of aging and age-related disease by DAF-16 and heat-shock factor. *Science* 300: 1142-5
387. Spriggs KA, Bushell M, Willis AE. 2010. Translational regulation of gene expression during conditions of cell stress. *Mol Cell* 40: 228-37
388. Wortel IMN, van der Meer LT, Kilberg MS, van Leeuwen FN. 2017. Surviving Stress: Modulation of ATF4-Mediated Stress Responses in Normal and Malignant Cells. *Trends Endocrinol Metab* 28: 794-806
389. Li W, Li X, Miller RA. 2014. ATF4 activity: a common feature shared by many kinds of slow-aging mice. *Aging Cell* 13: 1012-8
390. Li W, Miller RA. 2015. Elevated ATF4 function in fibroblasts and liver of slow-aging mutant mice. *J Gerontol A Biol Sci Med Sci* 70: 263-72
391. Hussain SG, Ramaiah KV. 2007. Reduced eIF2alpha phosphorylation and increased proapoptotic proteins in aging. *Biochem Biophys Res Commun* 355: 365-70
392. Bertolo RF, Burrin DG. 2008. Comparative aspects of tissue glutamine and proline metabolism. *J Nutr* 138: 2032S-9S
393. Wu G, Bazer FW, Hu J, Johnson GA, Spencer TE. 2005. Polyamine synthesis from proline in the developing porcine placenta. *Biol Reprod* 72: 842-50
394. Wu G, Bazer FW, Datta S, Johnson GA, Li P, Satterfield MC, Spencer TE. 2008. Proline metabolism in the conceptus: implications for fetal growth and development. *Amino Acids* 35: 691-702
395. Wu G, Flynn NE, Knabe DA. 2000. Enhanced intestinal synthesis of polyamines from proline in cortisol-treated piglets. *Am J Physiol Endocrinol Metab* 279: E395-402
396. Shah P, Ding Y, Niemczyk M, Kudla G, Plotkin JB. 2013. Rate-limiting steps in yeast protein translation. *Cell* 153: 1589-601

397. Szymanska P, Martin KR, MacKeigan JP, Hlavacek WS, Lipniacki T. 2015. Computational analysis of an autophagy/translation switch based on mutual inhibition of MTORC1 and ULK1. *PLoS One* 10: e0116550
398. Yu L, McPhee CK, Zheng L, Mardones GA, Rong Y, Peng J, Mi N, Zhao Y, Liu Z, Wan F, Hailey DW, Oorschot V, Klumperman J, Baehrecke EH, Lenardo MJ. 2010. Termination of autophagy and reformation of lysosomes regulated by mTOR. *Nature* 465: 942-6
399. Menzies FM, Fleming A, Rubinsztein DC. 2015. Compromised autophagy and neurodegenerative diseases. *Nat Rev Neurosci* 16: 345-57
400. Ravikumar B, Vacher C, Berger Z, Davies JE, Luo S, Oroz LG, Scaravilli F, Easton DF, Duden R, O'Kane CJ, Rubinsztein DC. 2004. Inhibition of mTOR induces autophagy and reduces toxicity of polyglutamine expansions in fly and mouse models of Huntington disease. *Nat Genet* 36: 585-95
401. Menzies FM, Huebener J, Renna M, Bonin M, Riess O, Rubinsztein DC. 2010. Autophagy induction reduces mutant ataxin-3 levels and toxicity in a mouse model of spinocerebellar ataxia type 3. *Brain* 133: 93-104
402. Jiang T, Yu JT, Zhu XC, Tan MS, Wang HF, Cao L, Zhang QQ, Shi JQ, Gao L, Qin H, Zhang YD, Tan L. 2014. Temsirolimus promotes autophagic clearance of amyloid-beta and provides protective effects in cellular and animal models of Alzheimer's disease. *Pharmacol Res* 81: 54-63
403. Vanneman M, Dranoff G. 2012. Combining immunotherapy and targeted therapies in cancer treatment. *Nat Rev Cancer* 12: 237-51
404. Nishimura K, Shiina R, Kashiwagi K, Igarashi K. 2006. Decrease in polyamines with aging and their ingestion from food and drink. *J Biochem* 139: 81-90
405. Sugiyama Y, Nara M, Sakanaka M, Gotoh A, Kitakata A, Okuda S, Kurihara S. 2017. Comprehensive analysis of polyamine transport and biosynthesis in the dominant human gut bacteria: Potential presence of novel polyamine metabolism and transport genes. *Int J Biochem Cell Biol* 93: 52-61
406. Abdulhussein AA, Wallace HM. 2014. Polyamines and membrane transporters. *Amino Acids* 46: 655-60
407. Park MH, Igarashi K. 2013. Polyamines and Their Metabolites as Diagnostic Markers of Human Diseases. *Biomol Ther (Seoul)* 21: 1-9

408. Newman JC, Milman S, Hashmi SK, Austad SN, Kirkland JL, Halter JB, Barzilai N. 2016. Strategies and Challenges in Clinical Trials Targeting Human Aging. *J Gerontol A Biol Sci Med Sci* 71: 1424-34